ADVERTIMENT. La consulta d'aquesta tesi queda condicionada a l'acceptació de les següents condicions d'ús: La difusió d'aquesta tesi per mitjà del servei TDX (www.tesisenxarxa.net) ha estat autoritzada pels titulars dels drets de propietat intel·lectual únicament per a usos privats emmarcats en activitats d'investigació i docència. No s'autoritza la seva reproducció amb finalitats de lucre ni la seva difusió i posada a disposició des d'un lloc aliè al servei TDX. No s'autoritza la presentació del seu contingut en una finestra o marc aliè a TDX (framing). Aquesta reserva de drets afecta tant al resum de presentació de la tesi com als seus continguts. En la utilització o cita de parts de la tesi és obligat indicar el nom de la persona autora.

ADVERTENCIA. La consulta de esta tesis queda condicionada a la aceptación de las siguientes condiciones de uso: La difusión de esta tesis por medio del servicio TDR (www.tesisenred.net) ha sido autorizada por los titulares de los derechos de propiedad intelectual únicamente para usos privados enmarcados en actividades de investigación y docencia. No se autoriza su reproducción con finalidades de lucro ni su difusión y puesta a disposición desde un sitio ajeno al servicio TDR. No se autoriza la presentación de su contenido en una ventana o marco ajeno a TDR (framing). Esta reserva de derechos afecta tanto al resumen de presentación de la tesis como a sus contenidos. En la utilización o cita de partes de la tesis es obligado indicar el nombre de la persona autora.

WARNING. On having consulted this thesis you're accepting the following use conditions: Spreading this thesis by the TDX (www.tesisenxarxa.net) service has been authorized by the titular of the intellectual property rights only for private uses placed in investigation and teaching activities. Reproduction with lucrative aims is not authorized neither its spreading and availability from a site foreign to the TDX service. Introducing its content in a window or frame foreign to the TDX service is not authorized (framing). This rights affect to the presentation summary of the thesis as well as to its contents. In the using or citation of parts of the thesis it's obliged to indicate the name of the author

UNIVERSITAT POLITÈNICA DE CATALUNYA

Some approaches to improve the ventilation system in underground potash mines

By

Marc Bascompta Massanés

Director: Dr.Lluís Sanmiquel Pera

Manresa, Spain

2015

Thesis for the Doctor of Philosophy Degree at the Polytechnic University of Catalonia within Doctoral Program of Natural Resources and Environment

ABSTRACT

Mine ventilation is a crucial factor for the sake of underground operations. Not only does it affect efficiency and effectiveness rates, but it also influence the health and safety of the employees. Despite it is a topic thoroughly analysed, every mine has its particularities and there is not much specific information concerning potash mines currently.

This thesis investigates the main characteristics of the ventilation system in two potash mines, using a room and pillar method, with the idea to analyse their specific behaviour in terms of airway particularities, heat exchange and gas concentrations. Data regarding subsurface ventilation conditions have been collected from 2008 to 2015.

First, it has been necessary to create a system able to manage such quantity of different parameters related to ventilation and obtain results from short to long term. For this purpose, it has been used a geographical information system (GIS), being able to model the behaviour of the environmental conditions as well as establish a methodology for other types of mines or underground infrastructures. This system has allowed to determine the weaknesses of the ventilation systems and where the investigations regarding efficiency and health and safety should be focused on. Part of the data managed by the GIS has been used to determine the friction factors of the airways and heat inputs of both mines.

The airways of the cases studied have a particular roughness due to the exploitation method and intrinsic characteristics of evaporitic minerals. The results achieved have given standard friction factors in potash mining applicable to other similar mines for modelling the ventilation system and know the airflow behaviour.

The investigations have also been focused on calculating the heat load of the system and proposing some approaches to reduce temperatures and gas concentrations in underground environments. Based on the friction factor results and the GIS created, the characteristic heat factors in the case study have been determined as well as the different heat inputs, comparing the variation in heat generation using diesel and electrical equipment. The outcomes display an important reduction in heat generation and subsequently a potential increasing improvement in the workplace conditions.

Keywords:

Mine ventilation; Geographic information system (GIS); Health and safety; Friction factor; Heat; Underground environment.

ACKNOWLEDGMENTS

I would like to express my gratitude to my doctoral thesis supervisor Dr. Lluís Sanmiquel Pera for his guidance and support, as well as the staff of Iberpotash S.A. for their willingness and high commitment to improve the ventilation conditions of the mine.

I must also acknowledge the postgraduate students A. Galera and D. Flores for helping me during the creation of the geographical information system. Thanks also to J. Castany, H. F. Anticoi and E. De Pablo for their contribution in the data obtaining process.

Finally, I would like to thank the Department of Mining Engineering and Natural Resources from the Polytechnic University of Catalonia and Iberpotash Chair in mining sustainability without which this thesis would not have been possible.

TABLE OF CONTENTS

NOMENCLATURE

A	Cross section area of the airway/tunnel (m^2)
A_B	Area of the obstacle (m^2)
α	Thermal diffusivity (m^2/s)
C	Specific heat (J/KgºC)
c	Combustible (l/s)
C_D	Shape correction obstacle factor (dimensionless)
DFA	Daily face advance (m)
Dh	Hydraulic diameter (m)
E	Efficiency of machine (%)
Ec	Combustion efficiency (%)
e	Height of the roughening (m)
f	Coefficient of friction (dimensionless)
g	Gravity force (m/s^2)
H	Enthalpy (J/Kg)
K	Thermal conductivity (W/mºC)
k	Atkinson friction factor (kg/m^3)
k_x	Angle compensation of the airway bend (dimensionless)
L	Length of the airway/tunnel (m)
Leq	Equivalent length (m)
λw	Water latent vaporization heat (kJ/kg)
m	Mass flow (Kg/s)
NVP	Natural ventilation pressure (Pa)
θ	Temperature (ºC)
P	Pressure (Pa)
PC	Combustible calorific value (kJ/l)

Pn	Nominal power (W)
Per	Perimeter (m)
ρ	Air density (kg/m^3)
Q	Airflow (m^3/s)
q	Heat flow (W)
q_{sen}	Sensible heat flow (W)
ql	Latent heat flow (W)
R	Atkinson's resistance (Ns^2/m^8)
r	Rate of liquid equivalent
Re	Reynolds number
η	Fan efficiency (%)
u	Velocity of the air (m/s)
μ	Viscosity (Ns/m^2)
VRT	Virgin rock temperature (ºC)
W	Water generated (l)
X	Shock loss factor (dimensionless)
Z	Depth relative (m)

LIST OF FIGURES

LIST OF TABLES

CHAPTER 1

INTRODUCTION
OBJECTIVES
HYPOTHESIS AND METHODOLOGY

"You must be the change you wish to see in the world." —Gandhi

INTRODUCTION

Mine ventilation is an important matter since the earliest underground mines started to exploit natural resources, appearing the first book that treats ventilation issues in the Middle Ages, called “De Re Metallica” by Georgius Agricola. However, it does not become crucial until the first and second Industrial Revolutions due to the increase of coal demand. In this period, it is when engineers and technicians start to concern about the necessity of airflow supply in workshops and initial handbooks are published, such as “On the theory of the ventilation of mines” by John Job Atkinson.

The aim of an underground ventilation system is to provide clean air to the parts of the mine where people are working, either permanently or sporadically, in order to ensure health and safety conditions. Despite what is understood by acceptable underground conditions differs among countries in terms of allowable temperature, airflow, dust or gas concentrations, this difference is gradually converging and it has similar requirements nowadays.

The intrinsic characteristics of a mine and the method used to exploit the mineral determine the underground environmental conditions together with the requirements established under the national and international legislation, which influence its operational capacity in terms of costs and efficiency. Hence, improving the ventilation system has become so important during the lifetime of mines.

In spite of a large amount of information –surveys and studies related to mine ventilation– each mine has its own particular conditions and requires specific solutions. Here it is where the idea of this thesis arises, trying to improve the ventilation conditions in two case studies. Investigations have been focused on two mines called Vilafruns and Cabanasses, which belong to ICL Iberia, and they are currently exploiting potassium and salt from the Catalan basin. The Polytechnic University of Catalonia (UPC) and the company have an agreement to make research in the fields of underground ventilation and subsidence through the Iberpotash Chair in Mining Sustainability.

Although both mines are exploiting the same resource with the same theoretical method, the geological conditions and mine planning are different. These differences will have an influence on the weaknesses of their ventilation systems and therefore the approaches to solve the problems will be different as well. Despite they fulfil the Spanish legal requirements, as it is seen along this thesis, Vilafruns has more difficulties for managing gas concentrations, while Cabanasses suffers more problems related to temperatures in workshops.

The dissertation is focused on analysing the natural factors of the mines and the design of the ventilation system. The following aspects have been studied:

- Layout of the ventilation circuit
- Airway characteristics
- Mining method
- Mining equipment
- Characteristics of the mineral exploited

1.1 Regional geology

The characteristic of the deposit will determine the mine planning and consequently mine ventilation will be influenced by the geology as well. In addition, other factors such as strata heat conditions the operational functioning of the mine as it will be seen in subsequent sections of the dissertation.

Catalan basin was formed due to convergence movement of the Eurasian and Iberian Plates between upper Cretaceous and lower Miocene, creating an evaporation deposit formed by anhydrite, halite and potash with a variable strata sequence, overcoming thickness of 300 meters. Deposits from Sallent and Súria, location of Vilafruns and Cabanasses respectively, are placed within this basin (Del Santo et al., 2000; Cendón et al., 2003). The geological repository displays a typical sequence of manganese-sulphate divided in four units (Cendón et al, 2003).

- BAU, basal Anhydrite Unit
- LHU, lower Halite Unit
- PU, potash Unit, a base formed by sylvinite-halite and upper carnalite-halite
- UHU, upper Halite Unit

These layers were subsequently covered by sedimentary materials such as conglomerates, sandstone and lutites. Afterwards, tectonic movements affected the evaporitic deposits, folding and placing part of the evaporitic minerals near the surface (Cendón et al., 2003).

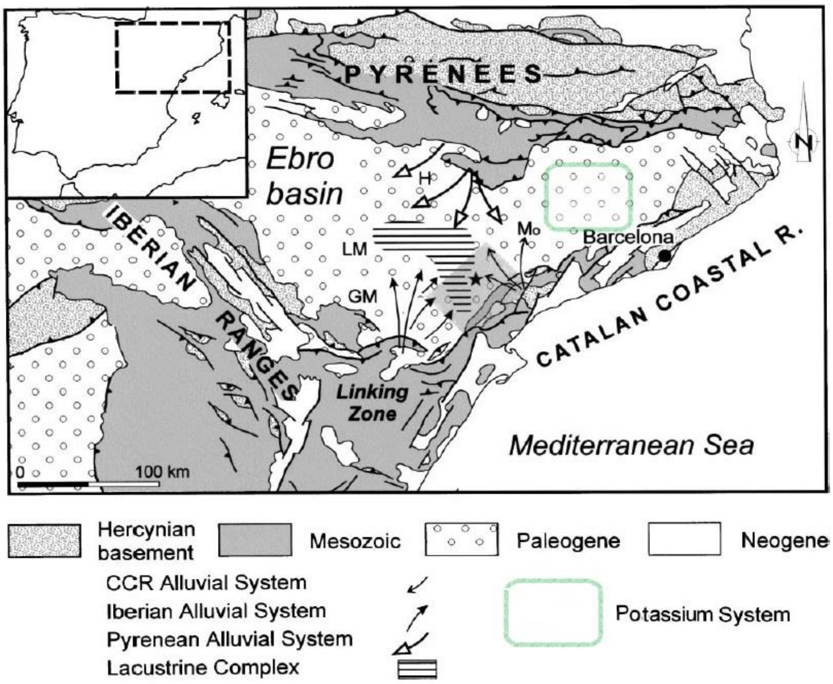

Figure 1. Catalan Basin with the place of the potassium system pointed in green (Cabrera et al, 2002).

1.2 Facilities

As it has been said, the operational functioning of both mines is slightly different due to the deposit configuration and facilities available. Cabanasses uses a two shaft system for the connection surface-underground, while Vilafruns has a shaft for the personal entry and a ramp to carry the mineral to the surface.

These differences are going to determine, in part, the ventilation system configuration and underground environmental conditions as it will be seen along the thesis.

1.2.1. Exploitation method

The resource is exploited between 500 and 900 metres below the surface, depending if it is Vilafruns (shallower) or Cabanasses (deeper), by means of an irregular room and pillar system. Figure 2 displays a theoretical system in a horizontal layer and working faces in two different levels.

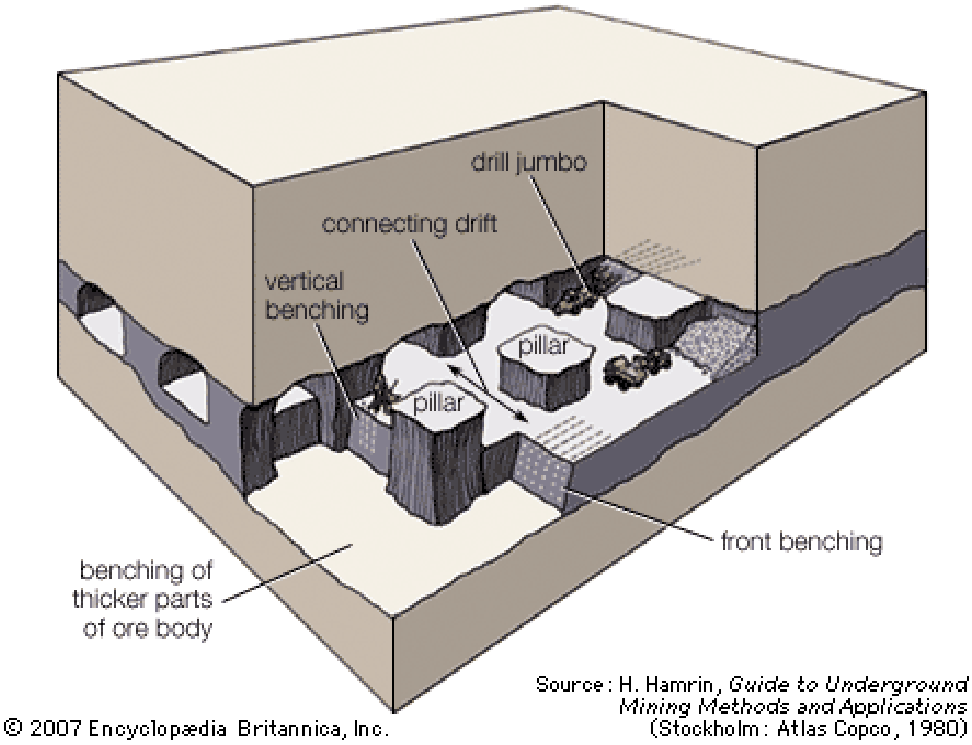

Figure 2. Scheme of the room and pillar method (Hamrin, 1980).

Normally, the underground tunnels are placed in two different levels. The exploitation zone, working faces and workshops, are placed in the upper levels. Meanwhile the service tunnels are in a lower level, which are used to connect the different parts of the mine and a conveyor belt system that carries the mineral to the shaft or directly to the surface through a ramp. The mineral transmission between exploitation and service levels is done by vertical downholes with a length of approximately 30 meters. Their diameter will be proportional to the particles size in order to avoid any blockage.

Figure 3. Image of some pillars in a potash mine (Source: ICL Iberia).

The exploitation is done using continuous mining machines, also known as miners, in both mines. They are usually equipped with a radial head, digging and transmitting the mineral into a truck that carries the burden to the downholes connection levels. Commonly, a loader is used to achieve a better mineral transmission between both levels, while there is a transmission system formed by a crusher and a continuous haulage machine attached to the conveyor belt system in the service level. Figures 4 and 5 show two types of miners with different head, radial and axial, respectively.

Figure 4. Radial miner. (Source: Potash Corporation).

Figure 5. Axial continuous mining machine (Source: Mineral resources of Saskatchewan).

On the other hand, service tunnel maintenance is done by smaller miners, obtaining less roughness. This feature will be very important so as to achieve the lowest possible friction factors and therefore better conditions for air to flow.

With regard to energy sources, miners and conveyor systems use electricity, whereas trucks, loaders and other auxiliary machinery are equipped with internal combustion engines. These conditions are important concerning heat inputs to the ventilation system in terms of sensible and latent heat as will be seen in following sections.

1.3. Ventilation system

The system in both mines has some similarities. They have the main fans located at the beginning of the ventilation circuit forcing the air and an additional fan in the upcast shaft in the case of Cabanasses. All the fans are placed in the underground facilities.

The air is led to the workshops using intermediate booster fans as well as temporary stoppings, curtains and doors, with the following characteristics:

- Door: Double door system capable of mitigate airflow leakages. When a vehicle wants to cross the door system, it has to pass the first one, wait in an intermediate space until it is closed and then the second door can be opened.
- Curtain: It is used to partially guide the airflow, varying its length and weight depending on the quantity of air wanted to redirection.

On the other hand, the auxiliary circuit provides clean air, removes the pollutants and the heat generated in every working face through a duct system, using an exhausting system with a fan placed in an intermediate location. Sometimes it is necessary a connexion of several fans in series or an overlap forcing-exhausting system when the circuit exceeds a certain length.

Despite the similarities stated above, their ventilation layouts are quite different because of distinct mine planning approach and geological characteristics of the mineral deposit. Following subsections give insight of their singularities.

1.3.1. Vilafruns mine

Potash is exploited around 500 metres below surface and the connection surface-underground is done by a shaft for the intake and a ramp for the return. Distance between entry and exit is around 4 kilometres. Figure 6 details the ventilation system of the mine and the parts in colours: the intake sea blue, the return red, the leakage sky blue and the auxiliary ventilation pink. Airflow direction has also been indicated.

Air from the intake is partially led to the first workshop and then mixed with the clean air forward. Subsequently, this mixture goes to the second and third workshop consecutively. Finally, it flows through the return to the ramp and then to the surface. The layout showed in Figure 6 varies as mine workings spread out. However, the ventilation circuit concept remains the same.

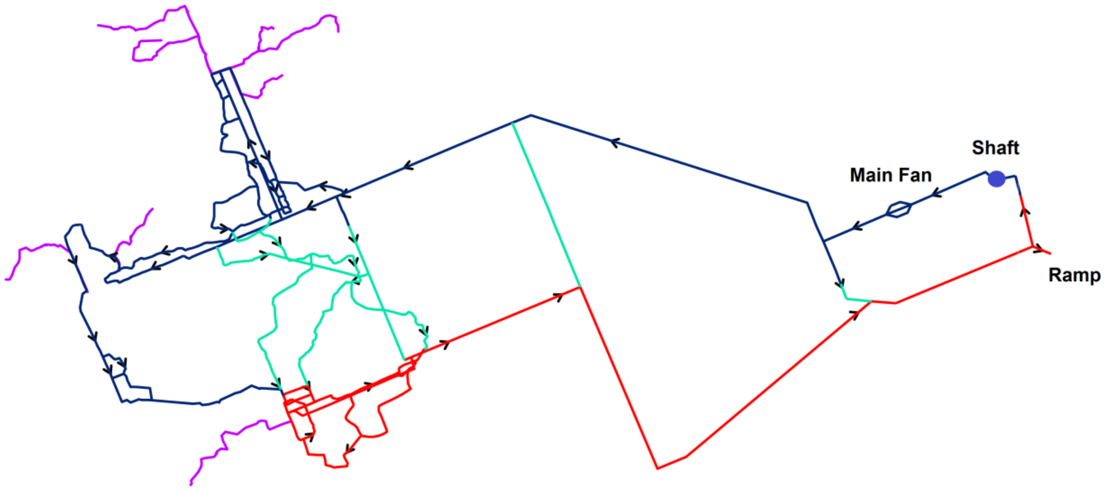

Figure 6. Scheme of Vilafruns mine.

1.3.2. Cabanasses

The depth of the mine varies between 700 and 900 meters below the surface approximately. Having a U-shape circuit provided with two shafts separated around 100 meters. As it can be seen in Figure 7, there are two main sections in the principal ventilation circuit, either for the intake or the return, commonly called north zone and south zone. In addition, Cabanasses is equipped with an exhausting main fan at the bottom of the upcast shaft.

In both sections, the circuit follows the same pattern. There is a main airway intake deepen as it is further from downcast, while the return is a parallel airway with air flowing in the opposite direction. When air reaches the workshop levels, clean air is taken from the intake and then it goes directly to the return after refreshing the working faces. Perpendiculars airways displayed in Figure 7 are used to connect the intake with the return and the auxiliary circuit in each workshop.

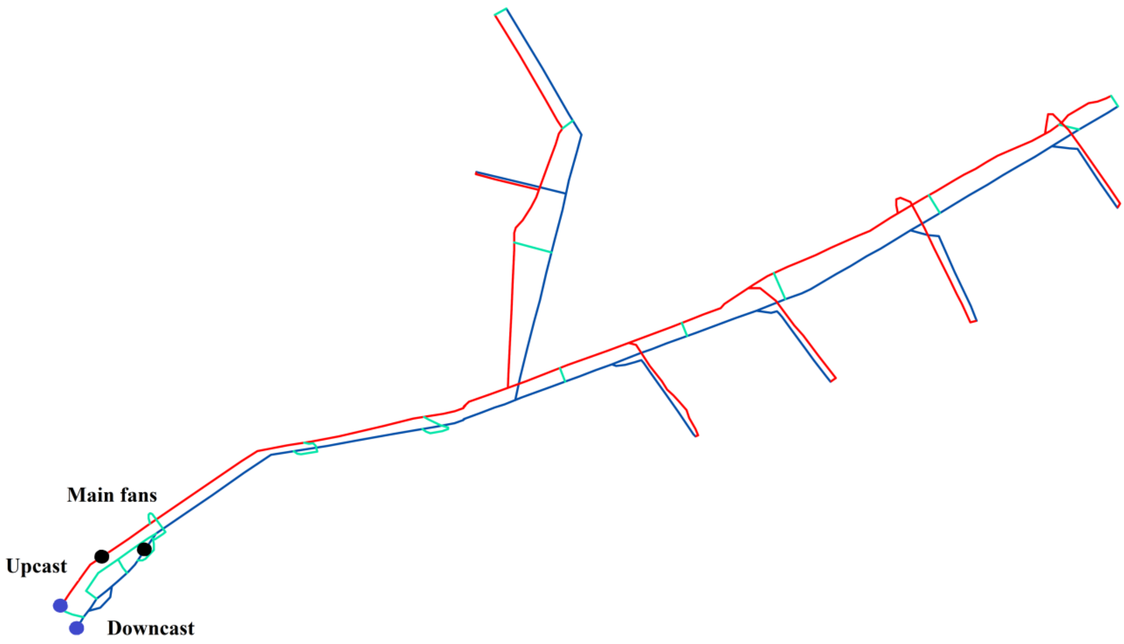

Figure 7. Scheme of the Cabanasses mine.

Schemes of Cabanasses and Vilafruns follow the same distinctive colours to differentiate the main parts of the ventilation system. Their creation have been done by means of a geographic information system, which is used later to accomplish some objectives of this dissertation.

OBJECTIVES

1.4. General objective

The aim is to assess and study the natural factors inherent of underground potash mines and intrinsic of the zone where they are placed, as well as determine the influence of mining design factors to the ventilation conditions in order to find out better alternatives in terms of health and safety and efficiency improvements.

1.5. Specific objectives

Several specific goals have been stablished for such purpose. However, each one requires a particular methodology and approach. The objectives are:

i. Determine a method able to collect all data from the ventilation circuit in a long term, taking into account the time when measures were done and their spatial reference, likewise having the possibility to obtain results and extract conclusions.
ii. Find out the characteristic friction factors of potash mines using a room and pillar exploitation method and continuous miners.
iii. Assess the heat generated by the strata and mining equipment used in underground mines with a system of electrical continuous miners and diesel trucks and loaders in order to estimate the difference heat inputs to the ventilation circuit using electrical machinery instead of diesel.
iv. Evaluate the underground environmental conditions in the principal and auxiliary ventilation systems and their variation depending on the layout of the circuit. Comparing the behaviour of gas concentrations and temperatures between both mines and finding out trends for future modelling and simulations.

HYPOTHESIS AND METHODOLOGY

Hypothesis 1:

The creation of a system able to manage all the ventilation data will give solutions and improvements to the environmental working conditions in terms of gases concentration and temperatures.

Two databases regarding the main ventilation features from Cabanasses and Vilafruns, –collected between 2008 and 2015– will be created by means of a geographic information system (GIS). This system will stand for the situation in the principal and auxiliary ventilation circuits in a long and short term.

The GIS will allow to assess the underground environmental conditions and extracting conclusions and trends from two case studies, likewise creating a suitable tool to control the characteristics of any other underground space.

Hypothesis 2:

The ventilation layout is the main factor that influences the concentration of gases in working faces, workshops and the principal circuit in a system with airflow recirculation.

Ventilation layouts of Vilafruns and Cabanasses are going to be thoroughly analysed by means of in situ data from the principal and auxiliary ventilation circuit. This information –through the GIS created– will give the possibility to know the conditions in the working faces, intake and return taking into account the airflow recirculation and the variations in the ventilation layouts along the years and how this influences the temperature and gas concentrations levels.

Hypothesis 3:

The variation and evolution of underground environmental conditions in each mine can be modelled.

These variations will be modelled by means of in situ measures taken in some chosen points that stand for the ventilation conditions of the mine. Modelling equations will give the possibility to know the conditions of the mine in future workshops.

Hypothesis 4:

Mines exploiting potash by means of continuous mining machines in a room and pillar system have their specific friction factors.

Several key points that represent the conditions of the principal ventilation circuit in terms of airways characteristics are going to be measured every month in order to obtain the representative friction factor values of the mines.

Hypothesis 5:

The main factor that affects air temperature, in a potash mine with a middle depth, is diesel machinery, being possible a huge reduction of heat input to the system using electrical equipment.

First, characteristics from strata heat and mining equipment are going to be either collected or calculated by means of theoretical equations and modelling software. Subsequently, heat input from all factors (strata, machinery and fragmented rock) will be determined regarding sensible and latent heat. Finally, the results will be compared with a possible change of the current diesel loaders and trucks to electrical ones and how it would vary the heat transferred to the airways because of that.

CHAPTER 2

LITERATURE REVIEW
FUNDAMENTALS OF MINE VENTILATION

"You can't connect the dots looking forward; you can only connect them looking backwards." —Steve Jobs

LITERATURE REVIEW

The review of the literature has been focused on three areas. The first one is an overview of the underground environmental conditions and their management to know and improve the workplace conditions. Next, it is focused on the current friction factor values in different underground mines. The last one discusses the subsurface heat sources, either endogenous of the zone or exogenous, and their influence to wet and dry temperatures.

2.1. Underground environmental conditions

The mining sector have one of the toughest working conditions and for this reason environmental factors such as effective temperature, gases concentration or airflow –all of them related to the ventilation system– have to be controlled and kept within an acceptable range. Otherwise, occupational hazards and operating cost rise exponentially either by legal restrictions or by a reduction in the worker's performance due to inappropriate working conditions (Sanmiquel et al., 2012; Sanmiquel et al., 2015).

Thus, a ventilation management system is necessary in underground spaces and a proper one should deal with efficiency and health and safety questions at the same time. Both concepts are crucial issues, but sometimes this important connection is overlooked. According to Reddy (2009), up to 60% of the mining operating cost is attributable to mine ventilation, while the relationship among accidents, worker's efficiency and hygienic conditions such as effective temperature, airflow or gas concentration has been previously mentioned by Payne and Mitra (2008) and García-Herrero et al. (2012).

Many investigations have been focused on occupational health and safety as well as efficiency (Allen and Keen, 2008; Kurnia et al., 2014a; Mahdevari et al., 2014; Sanmiquel et al., 2014), and they used many times a software to get a better understanding of the ventilation, modelling and optimising different parts of the system (Brunner, 1995; Hargreaves and Lowndes, 2007; Szmyd et al., 2013; Toraño et al., 2011; Torno et al., 2013). Figure 8 displays an example of modelling using a CFD software.

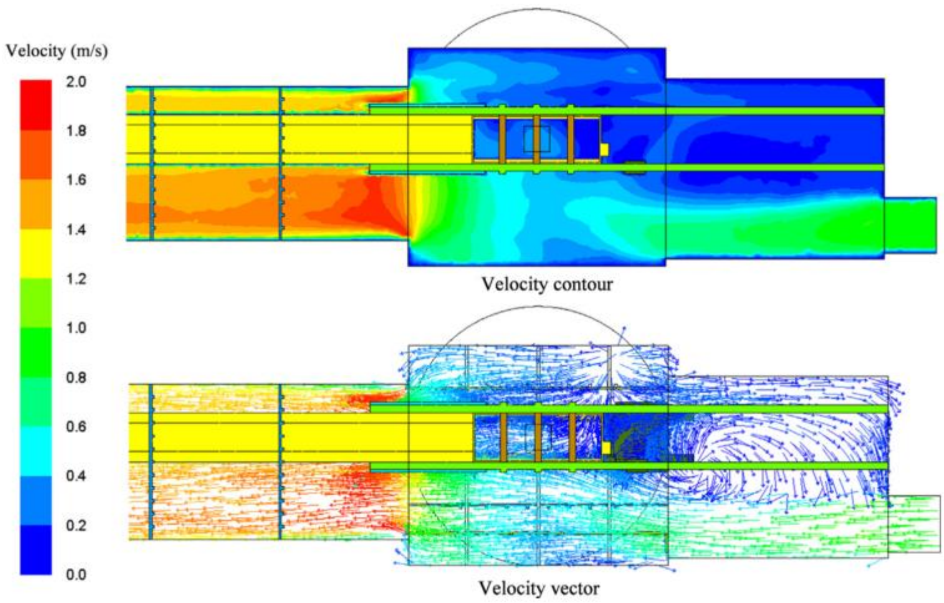

Figure 8. Velocity distribution at worker's breathing level in a conveyor belt system using CFD modelling software (Ren et al., 2014).

The usage of a GIS for purposes related to mining is quite frequent due to majority of the data generated have some sort of spatial component that can be represented or linked in a map form. There is a wide range of possibilities with this software, varying from mineral exploration (Harris et al., 2000) to management (Bahuguna and Kumar, 2006; Dheeraj, 2010), pollutants emission (Puliafito et al., 2002), subsidence (Kim et al., 2006) or underground ventilation (Likar and Čadež, 2000; Düzgün et al., 2011; Cheng and S. Yang, 2012). However, it is rarely used for the management of ventilation issues (Liu and D. Yang, 2004; Salp et al., 2009) and the concept of efficiency is not even mentioned.

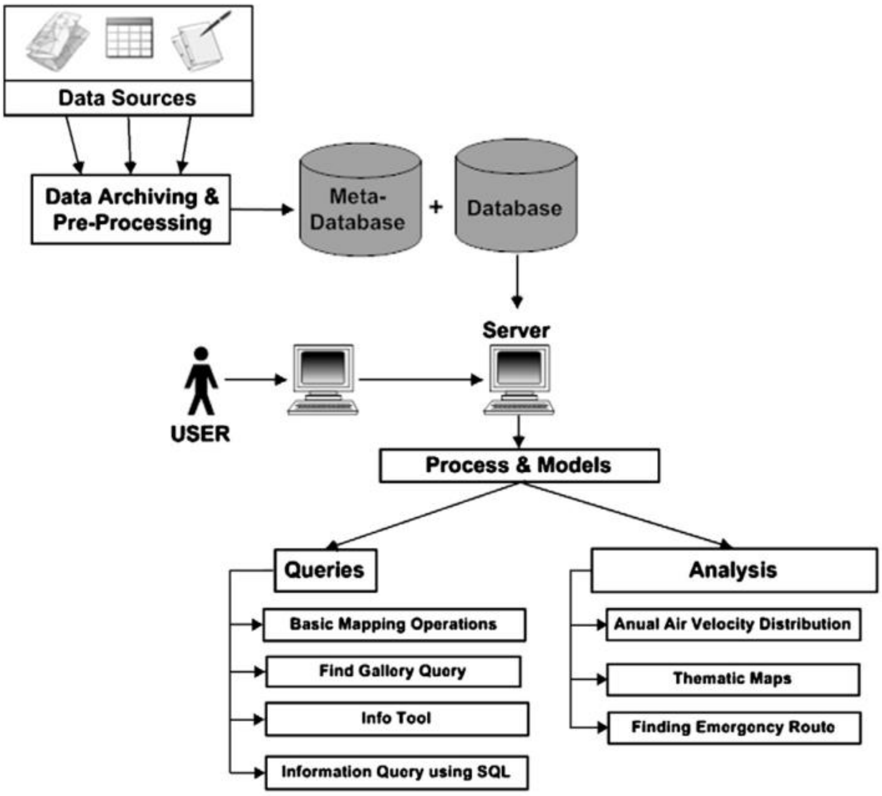

Figure 9. GIS usage scheme for safety issues in underground coal mining (Salp et al., 2009).

Despite that, a geographic information system is able to provide tools, frameworks and understanding of the real situation inside the mine (Saleh and Cummings, 2011) so programs and procedures can be implemented to ensure occupational health and safety objectives (Akcil, 2006) through a database collected from underground environment features such as airflow, gases or air pressure drop, among others.

The fulfilment of these objectives can contribute to improve the working conditions and the efficiency of the whole mine in from short to long term.

Specifically, these problems are mainly because of high temperatures (dry and wet temperatures), gas concentrations (CO, CO_2, NO_x…) and not enough airflow provided to the workshops. Similar problems have been deeply studied taking different approaches, such as controlling the airflow leakages (Widiatmojo, et al., 2014), focused on underground gases and finding out more efficient ventilation designs (Kurnia et al., 2014b) or improving the underground environment conditions in coal mines reducing the level of dust and methane (Xi et al., 2014; Zhang et al., 2014; Zhang et al., 2015).

Unfortunately, dilute gases and removing heat becomes more difficult as the mine spreads out and the ventilation circuit gain complexity. Hence, it is important to find methodologies to predict the future operating conditions of the mine (Kocsis et al., 2008). In spite of a large quantity of studies carried out is this field, there is little information focused on non-metallic mines and more specifically potash exploitations.

For achieving such purpose, the characteristics of the mine need to be determined, either as a consequence of natural conditions or created by the resource exploitation conditions. The origin of gases and temperature levels in a mine can be consequence of the mineralization or the exploitation method used (mining equipment, blasting, etc.). In some special cases, potash mines placed in a zone that has previously suffered volcanism, carbon monoxide and dioxide can be spontaneously released in huge quantities (Carrasco et al., 2011).

The importance of controlling their concentration levels is because they affect employees health in short and long term, being toxics and some of them even cancerous (Attfield et al., 2012; Silverman et al., 2012). Several investigations have been carried out, especially in coal mining (Noack, 1998; Sasmito et al., 2013; Cheng et al., 2015), to determine if the airflow supplied to the working faces is enough. Figure 10 show an analysis of the underground environment in several auxiliary configurations in a working face.

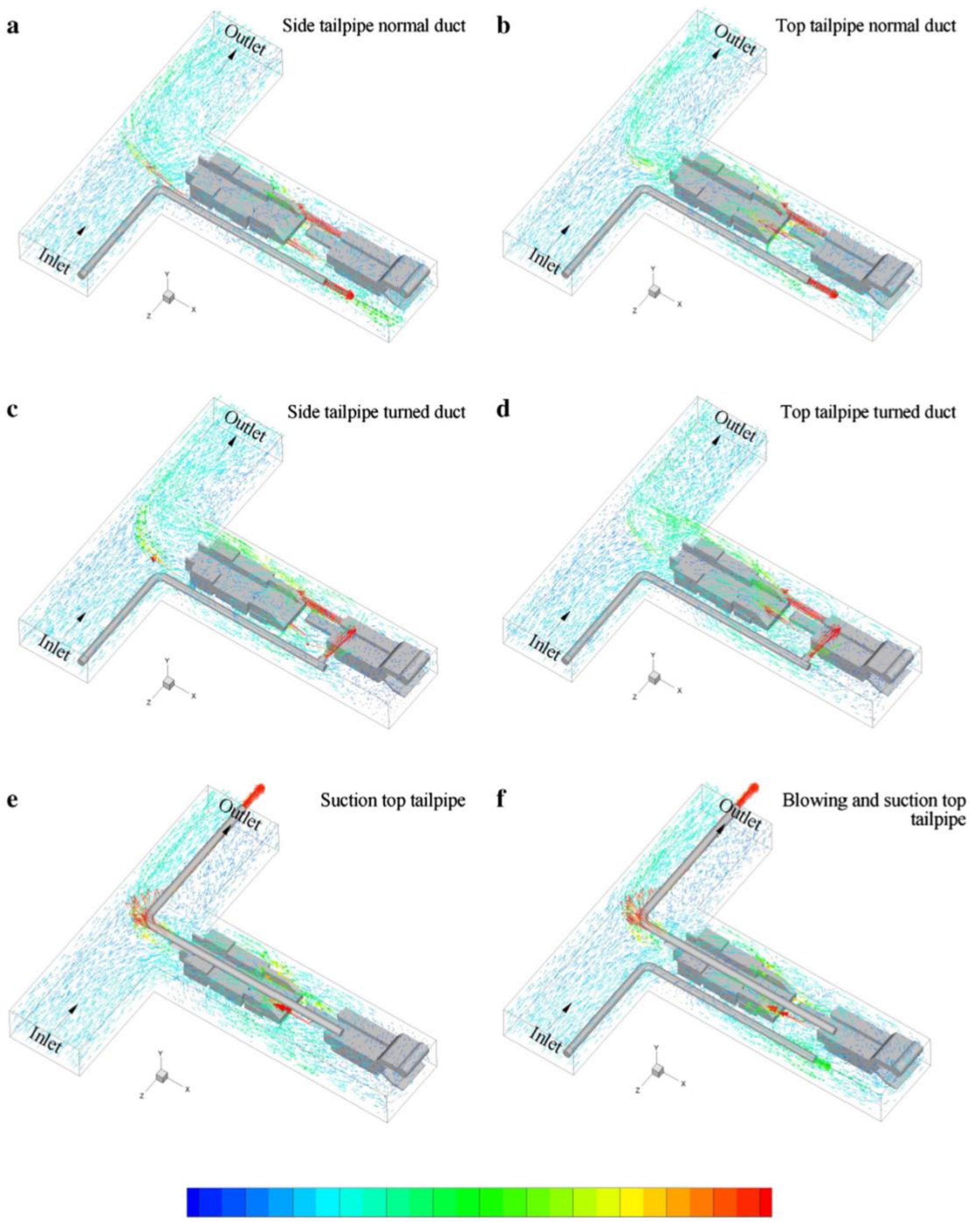

Figure 10. Air velocity profile using different auxiliary systems (Kurnia et al., 2014a).

However, the relationship between ventilation layout and the trend of gases and temperature has not already been studied. This condition will be very important to know the underground conditions in future workings.

2.2. Friction factors

Friction factors define the behaviour of the ventilation system in a mine and their determination will be necessary for modelling the circuit (Shalimov, 2011), having a huge influence to the resistance against the flow of the air through the airways (Alymenko, 2012). This parameter will be basically affected by the exploitation method, geometric characteristics of the tunnels and physic conditions of the mine (Duckworth and Prosser, 1998).

A part from the resistance of the airways due to obstacles like conveyor belts, roughness will determine the friction factor value. In this respect, potash mines have some special characteristics because of the properties of evaporitic minerals. This kind of mines is very deformable due to pressure of the surrounding rock, producing a considerable roughness in the surface of the tunnels. Besides, changes in conditions such as temperature or humidity affect their values as well.

One of the first studies concerning friction factors in mining was done by McElroy (1935), which was based on data of the pressure loss gauged in several coal and metal mines. Table 1 displays the friction factor values depending on the airways characteristics at the time. These values have been used for a long time (Hartman, 1997), introducing only some changes in coal mining by Kharkar et al. (1974), who pointed out the influence of support and lining to friction factors.

Table 1. Friction factor references according to McElroy (1935).

Type of airway	Irregularities of surfaces, areas and alignment	Values of $10^{10}\cdot k$[1]											
		Straight			Sinuous or curved								
					Slightly			Moderately			High degree		
		Clean (basic values)	Slightly obstructed	Moderately obstructed	Clean	Slightly obstructed	Moderately obstructed	Clean	Slightly obstructed	Moderately obstructed	Clean	Slightly obstructed	Moderately obstructed
Smooth-lined	Minimum	10	15	25	20	25	35	25	30	40	35	40	50
	Average	15	20	30	25	30	40	30	35	45	40	45	55
	Maximum	20	25	35	30	35	45	35	40	50	45	50	60
Sedimentary rock (or coal)	Minimum	30	35	45	40	45	55	45	50	60	55	60	70
	Average	55	60	70	65	70	80	70	75	85	80	85	95
	Maximum	70	75	85	80	85	95	85	95	100	95	100	110
Timbered	Minimum	80	85	95	90	95	105	95	100	110	105	110	120
	Average	95	100	110	105	110	120	110	115	125	120	125	135
	Maximum	105	110	120	115	120	130	120	125	135	130	135	145
Igneous rock	Minimum	90	95	105	100	105	115	105	110	120	115	120	130
	Average	145	150	160	155	160	165	160	165	175	170	175	195
	Maximum	195	200	210	205	210	220	210	215	225	220	225	235

[1] 10 in the table is equivalent to 0,0000000010; 100 to 0,0000000100. All values are for air weighing 0,075 pound per cubic foot.

The problem of values released by McElroy is that current openings are much larger and the equipment used is completely different, a fact that makes varying these values. For this reason, several studies have been undertaken in metal and long wall coal mines to obtain new friction factors more suitable with the current situation (Wala, 1991; Duckworth and Prosser, 1998; Prosser and Wallace, 1998; Prosser and Wallace, 2002; Duckworth et al., 2012; Hurtado et al., 2014). Some of these values are displayed in the following tables.

Table 2. Friction factors in coal mining long wall (Duckworth and Prosser, 1998).

Description of airway	**Atkinson friction factor (kg/m^3)**				
	Very poor	**Poor**	**Average**	**Good**	**Very good**
Headgate	0,0088	0,0072	0,0056	0,0046	0,0036
Tailgate	0,1808	0,1475	0,1142	0,0934	0,0726

Table 3. Friction factors for metal mines in kg/m^3 (Prosser and Wallace, 1998).

	Level drift	**Ramp**	**Alimak raise**	**Bored raise**	**Beltway**	**TBM drift**
Average value	0,00879	0,01158	0,01126	0,00466	0,01399	0,0044
Maximum value	0,01284	0,01739	0,01579	0,00698	0,01664	0,0056
Minimum value	0,00468	0,00698	0,00874	0,0023	0,001228	0,00341
Standard deviation	0,00239	0,0031	0,0033	0,00152	0,00184	0,00111
Number of measurements	40	20	5	10	5	3

Table 4. Friction factors in coal mines (Prosser and Wallace, 1998)

	Intake drift	**Return drift**	**Belt drift**	**Cribbed drift**
Average value	0,00753	0,00872	0,01058	0,06781
Maximum value	0,01148	0,01133	0,01757	0,14409
Minimum value	0,00482	0,00566	0,00459	0,04522
Standard deviation	0,00219	0,00176	0,00636	0,02516
Number of measurements	23	15	5	7

Prosser and Wallace (1998) also gathered the friction factor values in the United States, comparing different bibliographic sources of the moment.

Table 5. Comparison of friction factors (kg/m^3) from published data (Prosser and Wallace, 1998).

Airway type	Mean MVS measured data	Suggested MVS value	McPherson (2009)	Hartman et al. (1997)
Rectangular airway – Clean airway (coal or soft rock with bolts limited mesh)	0,0075	0,0075	0,009	0,008
Rectangular airway – Some irregularities (coal or soft rock with bolts limited mesh)	0,0087	0,0087	0,009	0,0091
Metal mine drift (arched and bolted with limited mesh)	0,0088	0,01	0,012	0,0269
Metal mine ramp (arched and bolted with limited mesh)	0,0116	0,013	-	0,0297
Metal mine beltway (large area, rock bolted with mesh)	0,014	0,015	-	-
Bored circular raise (with entry/exit loss)	0,0047	0,005	0,004	0,0028
Rectangular alimark raise	0,01126	0,0129	0,014	-
TBM drift (rock bolts with mesh)	0,0044	0,005	0,0055	0,0037

Meanwhile, a doctoral thesis done by Meyer (1998) also determined some friction factors in coal mining. The main difference compared to previous bibliography is the fact that these values were determined for a room and pillar method using continuous miners, which suits with the method used in the case studies of the dissertation.

Table 6. Friction factors for conventional room and pillar mining (Meyer, 1998).

Low seam mining (< 2,0 metres)	**Ns^2/m^4**
Intake airways	0.01107
Return airways	0.01210
Medium seam mining (2,0 to 4,0 metres)	**Ns^2/m^4**
Intake airways	0.01334
Return airways	0.01467
High seam mining (> 4,0 metres)	**Ns^2/m^4**
Intake airways	0.01482
Return airways	0.01584

Table 7. Friction factors for mechanical room and pillar mining (Meyer, 1998).

Low seam mining (< 2,0 metres)	**Ns^2/m^4**
Intake airways	0.00950
Return airways	0.01040
Medium seam mining (2,0 to 4,0 metres)	**Ns^2/m^4**
Intake airways	0.00990
Return airways	0.01090
High seam mining (> 4,0 metres)	**Ns^2/m^4**
Intake airways	0.01060
Return airways	0.01170

Another study takes into account the geometric characteristics and the roughness of the walls in metal mining (Fytas and Gagnon, 2008).

Table 8. Friction factor in metal mines, Quebec (Fytas and Gagnon, 2008).

Type of airways	Wall roughness	Mean k $(Kg/m^3)\cdot 10^{-4}$
Regular airways	Very smooth	44
	Smooth	85
	Normal	117
	Typical k	107
Small airways	Smooth to normal	97
		69
Inclined haulage drifts	Smooth to normal	96
		52
Spiral ramp	Smooth to normal	221
		167

In addition, Carrasco Galán et al. (2011) in the handbook called “Manual de ventilación de minas y obras subterráneas” details many empirical equations to calculate friction factors and other possible resistances of the airways.

Information regarding friction factors in coal and metallic mining is far more extensive, being able to find values for specific situations in such type of mines. However, there is a lack of information in non-metallic mines, including potash mining.

2.3. Heat sources

Underground temperatures are function of the heat inputs, generated either naturally or due to the exploitation process. Nowadays, it is a matter of great concern because it conditions the running of the mine (Hardcastle and Butler, 2008; Aminossadati et al., 2010), affecting safety issues and efficiency rates. Thus, climatic conditions in subsurface environments are very important aspects to pay attention, especially as underground workings go deeper and there is a more intense use of mechanization (Hardcastle et al., 2008; Zhongpeng, 2012). The four major heat sources according to Kocsis et al. (2008) are:

- Conversion of potential energy into thermal energy as air descends vertical airways (auto-compression).
- Mining machinery. Using diesel or electricity
- Strata (geothermal gradient).
- Pressure generators. Primary, booster and auxiliary fans.

In addition, there are other possible factors like ground water or fragmented rock carried along the airways that can also have a significant contribution. Depending on the mine, the input of each part varies due to its specific characteristics. Figure 11 shows a graph of the heat inputs percentage contribution in a case study.

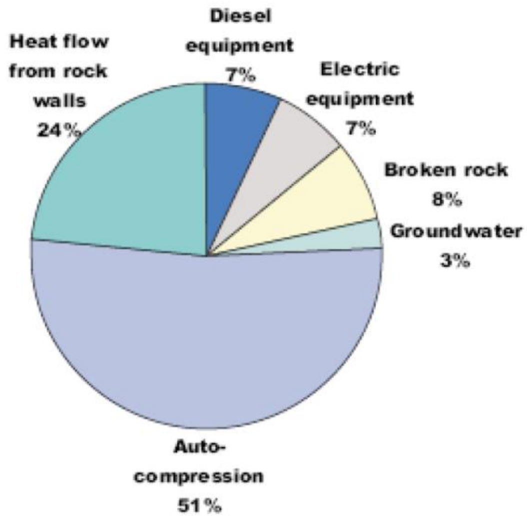

Figure 11. Heat contributor in a metal mine, case study (Payne and Mitra, 2008).

However, the quantification of these heat sources needs some fundamental parameters that have to be previously determined. Without them, it will not be possible to achieve a prediction model of the ventilation circuit (Zhou et al., 2011). Strata heat characteristics can be obtained from bibliographic information (McPherson, 2009), but the values can vary considerably from real conditions of the mine. Thus, it is necessary to take in situ measures and apply laboratory essays to determine these values (Mousset-Jones and McPherson, 1984; Krishnaiah et al., 2004; Sundberg et al., 2005). However, it is not always possible to obtain results this way and it has to be done by means of equations and modelling software, being able to achieve outcomes with accuracy enough for mine ventilation surveys (McPherson, 2009).

The reduction of heat flow in underground mines is usually focused on optimising the efficiency of the refrigeration system and cutting down its operating costs (Del Castillo, 1988; Swart, 2003; He et al., 2010; Vosloo et al., 2012; Edgar et al., 2013). Recently, a different approach has come out with the idea of improving the efficiency of the mine through reducing power consumption of the ventilation system and providing the necessary airflow to the workshops and workplaces monitoring the underground conditions, commonly called ventilation on demand method or simply VOD (Hardcastle et al., 2006; Li et al., 2011; Kazakov et al., 2013). Despite that, none of them have considered the benefits in ventilation conditions of changing part of the mining equipment using diesel to electrical ones, comparing the contribution difference of heat input to the airways in both situations.

Apart from the type of energy sources of the mines, there are other important factors that affect the underground air temperature such as: the outer climate, geological factors of the zone and mineral exploitation method (Xiaojie et al., 2011). All of them should be taken into account for any accurate survey.

FUNDAMENTALS OF MINE VENTILATION

Main expressions used along the dissertation are detailed in the following subsections. It is also the basis to understand subsurface ventilation and the principals of the specialized software.

2.4. General ventilation theory

2.4.1. Airflow behaviour

The square law and Atkinson equation are the basic expressions to know airflow behaviour in underground mines (Hall, 1981; Meyer, 1998; McPherson, 2009; Diego et al, 2011). The first one relates the concepts of pressure, airflow and resistance to pass the air through an airway.

$$\Delta P = R \cdot Q^2 \tag{1}$$

Where:

ΔP – Pressure or difference pressure (Pa);

R – Atkinson resistance (Ns^2/m^8);

Q – Amount of airflow (m^3/s).

Pressure difference in an airway will be function of the resistance, characteristics of the tunnel, obstacles and quantity of air flowing through the airway. This difference is a crucial factor to determine in mine ventilation and it can be calculated by means of two different methods.

1. Direct methods: There are two additional alternatives, obtaining more accurate values with the gauge and tube method, but being more difficult to apply (Prosser and Loome, 2004).

    - Gauge and tube: System formed by a manometer and a tube with a certain length. The orientation of the tube will have to face the airflow direction. Figure 12 displays the system.

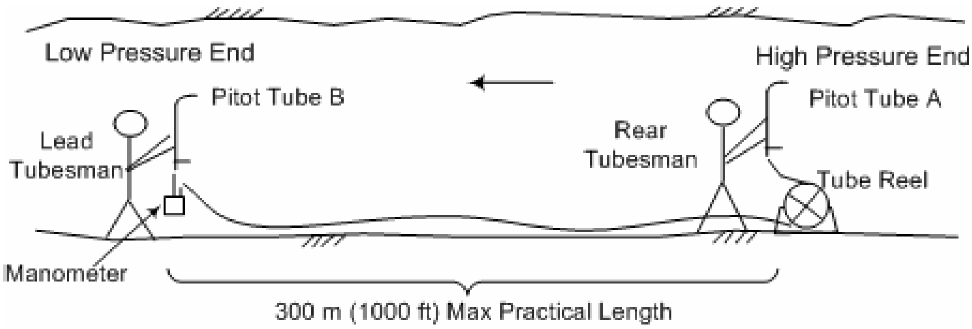

Figure 12. Gauge and tube technique (Prosser and Loomis, 2004).

    - Barometer survey: It determines the relative pressure in a certain part of the ventilation circuit. It is only necessary to measure the representative points of the circuit.

2. Indirect method: When it is not possible to use a direct method, the pressure difference can be achieved measuring the airflow and characteristics of the airways. Equations (8-9) detail this procedure.

Square law (1) is used for turbulent flows. If it felt to a transitional or laminar regime, corresponding values of resistance would vary. In such case, the square expression should change as it follows.

$$P = R \cdot Q^n \tag{2}$$

Where:

n – It is a value that would vary in a range between 1 from laminar regimes to 2,05 for fully turbulent ones (dimensionless).

While airways are always within a turbulent flow, laminar and transitional regimes can be found when air flows through stoppings, doors or old workings (McPherson, 2009). The way to know the regime of the fluid is calculating the Reynolds number.

$$Re = \frac{\rho \cdot u \cdot Dh}{\mu} \tag{3}$$

Where:
Re – Reynolds number (dimensionless);
ρ – Air density (kg/m^3);
Dh – Hydraulic diameter, Dh = 4A/per (m);
u – Velocity of the airflow (m/s);
μ – Viscosity (Ns/m^2).

The flow will be in a laminar regime when the Reynolds number is below 2000, being in a transition zone between 2000 and 3000 and in a turbulent regime when the value is above 3000 (McPherson, 2009).

One of the necessary values to determine the pressure drop or pressure difference is the resistance factor. The Atkinson resistance of the airway included in the formula (1) can be obtained by means of the following equation (Atkinson equation).

$$R = k \cdot L \cdot \frac{Per \cdot \rho}{A^3 \cdot 1{,}2} \tag{4}$$

Where:
R – Atkinson resistance (Ns^2/m^8);
k – Atkinson friction factor (kg/m^3);
per – Perimeter (m);
L – Length of the tunnel (m);
ρ – Air density (kg/m^3);
A – Section of the tunnel (m^2).

Usually, the airways have dimensional and directional variations or obstacles such as airway bends or conveyors that influence the flow of the air. All these elements are independent of roughness and are not included in the friction factor. However, these variations add resistance to the ventilation circuit and have also to be taken into account. Carrasco Galán et al. (2011) contain many empirical equations for variations in the tunnels, using some of them along the thesis. Once the shock loss is obtained, it has to be added to the Atkinson's equation as an equivalent length. The shock loss factor, X, is experimentally determined (McElroy, 1935; Hartman et al., 1997; Montecinos and Wallace, 2010), adding an equivalent increase in the length of the tunnel where air flows (Meyer, 1998). The length increase (equivalent length) will vary depending on the type of obstacle (Carrasco, 2011), obtaining a corrected Atkinson equation. Its determination is achieved using a relationship between equivalent length and shock loss factor.

$$Leq = \frac{\rho \cdot X}{8 \cdot \mathrm{k}} \cdot Dh \qquad (5)$$

Where:

X – Shock loss factor (dimensionless);

Dh – Hydraulic mean diameter (m).

The most typical shock losses in airways are gathered in the following Figures (13-16). Figures 13 and 14 are used to calculate the loss due to bends. First it is calculated the shock loss, X, for an angle of 90º through the radius and hydraulic diameter.

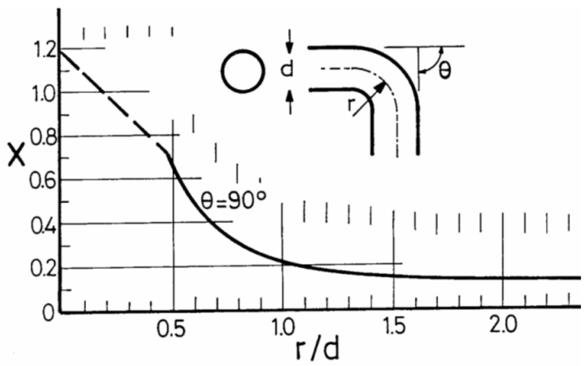

Figure 13. Shock loss factor in an equivalent circular cross section with an angle of 90º (McPherson, 2009).

Once it is known the X value, it has to be applied the next expression (6) to correct the value taking into account the airway bend angle through Figure 14.

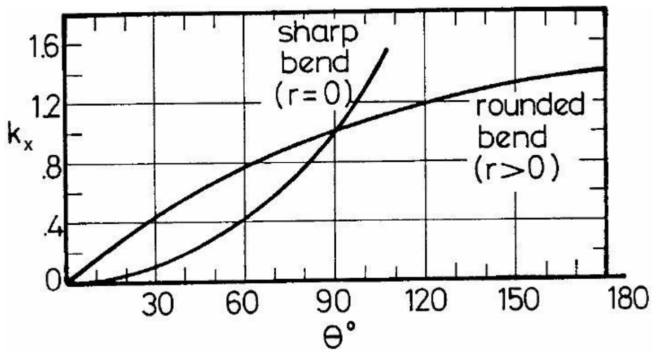

Figure 14. Bend correction depending on the airway angle (McPherson, 2009).

k_x factor from Figure 14 varies the value from Figure 13, considering if the bend is sharp or rounded. The final value from equation (6) is used in equation (5) to know the equivalent length of each bend.

$$X_o = X_{90} \cdot k_x \tag{6}$$

Where:

Xo – Shock loss factor with the real angle (dimensionless);

X_{90} – Shock loss factor with an angle of 90º (dimensionless);

k_x – Angle compensation depending on the shape of the airway (dimensionless).

Shock loss can also be consequence of cross section areas changes and linear obstructions as it is seen in Figures 15 and 16.

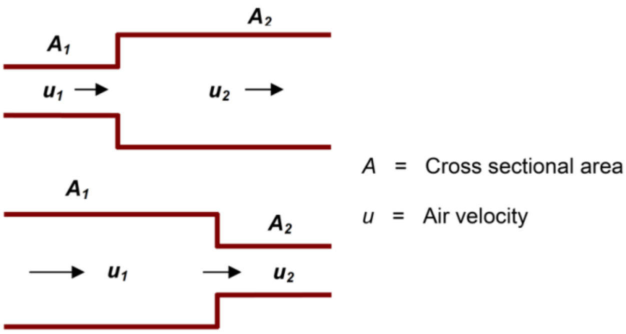

Figure 15. Shock loss due to changes in cross section (McPherson, 2009).

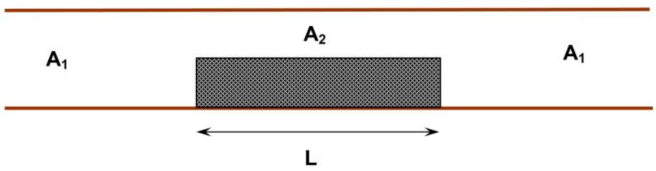

Figure 16. Linear obstructions (McPherson, 2009).

Linear obstructions will be very important in the two case studies because the conveyor belt system is mainly placed in the intake. Its value will be calculated with the following expression.

$$X = C_D \cdot \frac{A_B}{A} \tag{7}$$

Where:

X – Linear shock loss factor (dimensionless);

C_D – Shape correction obstacle factor (dimensionless);

A_B – Area of the obstacle (m^2);

A – Area of the airway (m^2).

The value called C_D depends on the shape of the obstacle. Figure 17 display such relationship. This figure is also used to determine the resistance generated by obstacles in the shafts.

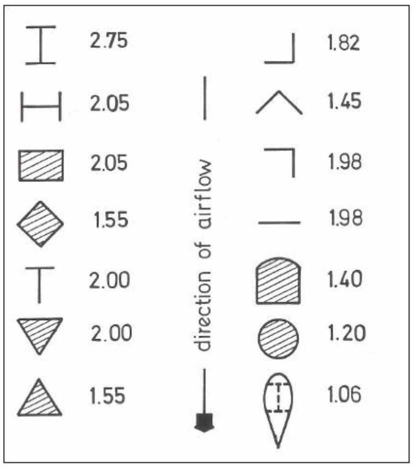

Figure 17. Resistance factor of shape depending on the obstacle (Bromilow, 1960).

The following expression shows how the equivalent length calculated is included within the Atkinson equation.

$$R = k \cdot (L + Leq) \cdot \frac{Per \cdot \rho}{A^3 \cdot 1{,}2} \tag{8}$$

Where:
Leq – Equivalent length (m).

In addition, Carrasco et al. (2011) expose several resistance values for doors, brattices and curtains.

On the other hand, the resistance determination depends on the friction factor as well, which at the same time is function of the coefficient of friction, f, and roughness of the airways, e. Friction factors can be obtained by means of values determined in previous studies, tables that gather standard values or determining in situ using the next equation.

$$f = \frac{2k}{\rho} = \frac{1}{4 \cdot \left[2 \cdot \log_{10}\left(\frac{Dh}{e}\right) + 1.14\right]^2} \tag{9}$$

Where:
Dh – Hydraulic mean diameter of the gallery (m);
e – Height of the roughening (m);
f – Coefficient of friction (dimensionless).

The values needed to measure in situ are roughness, perimeter and section of the airways, being able to obtain the coefficient of friction. Its relationship with the friction factor used in the Atkinson equation is done through air density, which influences its value and subsequently the resistance of the airways. Air density will vary with the depth and its flow through the workings, changing pressures and temperatures. However, it can be considered as incompressible, because this variation will not have significance for the calculations (McPherson, 2009).

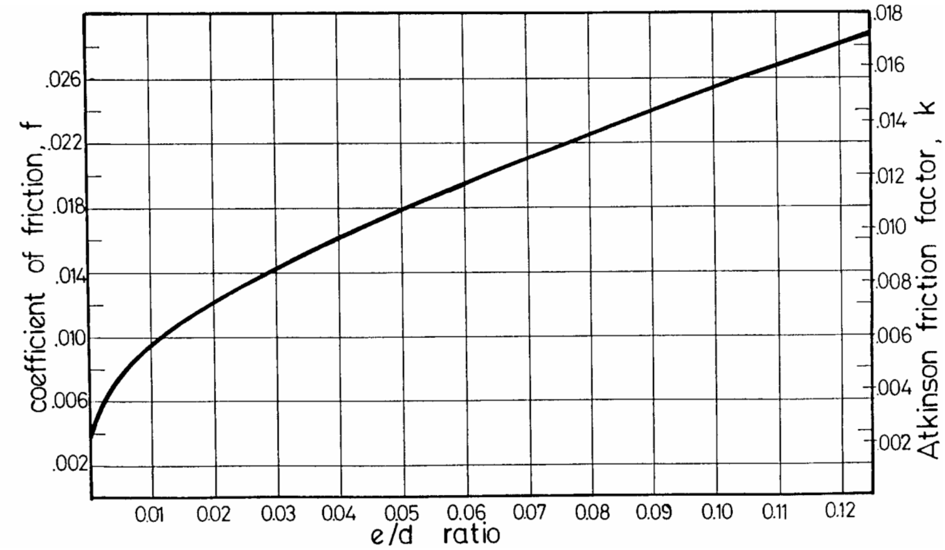

Figure 18. Variation of the coefficient of friction and friction factor depending on the roughness and hydraulic mean diameter (McPherson, 2009).

Apart from friction factor and potential obstacles, the airway resistance is also function of the airway characteristics (McPherson, 2009):

1. Size: As it can be seen in the expression (4), resistance is proportional to the perimeter and section, per/A^3.
2. Shape: Perimeter and section factors determine the shape of the airway, being the circular one the most favourable and the rectangular the most adverse.

Besides, in terms of resistance, the shafts are the most difficult parts to assess and determine the value. Actually, it is one of the ventilation circuit parts that contribute more due to high velocities and elements complicating the flowing of the air. The principal resistance elements are:

3. Shaft walls: Function of the friction factors
4. Pipes, cables, ropes, etc.
5. Skips or cages
6. Loading and unloading points

The resistance from whole circuit of the mine is needed to know the size of the main fans. This value can be achieved by means of the Kirchhoff's laws, which are also applicable to fluid networks. In order to simplify the survey, those zones with small leakages and dead heading do not need to be taken into account for representing the network.

The problem of applying the Kirchhoff's equations directly to full mine circuits is that it can give several hundred equations. For this reason, it is necessary to use analytical methods to simplify the ventilation circuit, obtaining the equivalent resistance, or through numerical methods, applying the Hardy Cross technique. Currently, these outcomes are achieved by means of computer packages.

2.4.2. Fans

The objective of fans is to provide an increasing of pressure that allows to flow the air through airways and workings. Equation (10) gives the pressure of the fan.

$$Pn = \frac{Q \cdot p}{\eta} \quad (10)$$

Where:

Pn – Nominal power of the fan (W);

Q – Cabal (m^3/s);

p – Increasing pressure generated by the fan (Pa);

η – Fan efficiency (%).

There are three types of fans in subsurface mine ventilation, accomplishing different objectives within the ventilation circuit:

1. Main fans
2. Booster fans
3. Auxiliary fans

Main fans are used to lead air through airways and they can be placed underground or on the surface just before the shaft. Depending on their position in the ventilation circuit, they are forcing or exhausting and if it is required they can be connected in series or parallel, Figures 19 and 20. The selection of a mine fan is established by several duty points based on the airflow and pressure required along the life of the mine (Gamble et al., 2009).

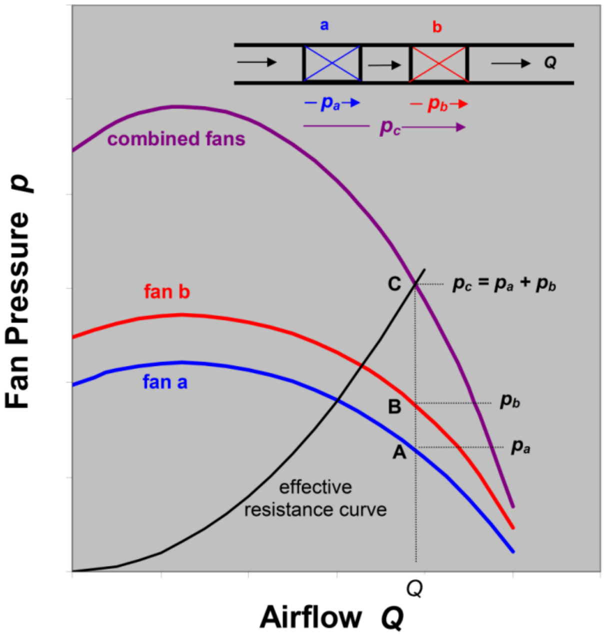

Figure 19. Mine resistance curve and two fans connected in series (McPherson, 2009).

Connection from Figure 19 gives more pressure to the system than only one fan. However, it is necessary that both have the same or very similar power. Otherwise, the weaker one becomes an obstacle to the system. On the other hand, the connection in parallel provides more airflow to the system, Figure 20.

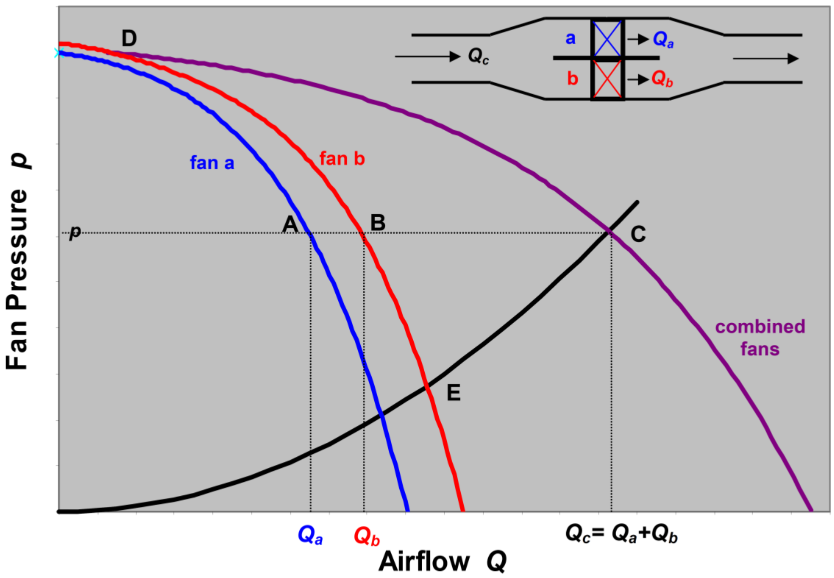

Figure 20. Mine resistance curve and two fans connected in parallel (McPherson, 2009).

The idea of both connections is to provide enough pressure to overcome the resistance of the mine generated by the elements described in the previous section and placed in the principal circuit. However, it is not always possible to achieve it or it is too expensive and then it is necessary to use one or more booster fans that can reduce the pressure required from the main fan and decrease leakages (Martikainen and Taylor, 2010). Figure 21 display a basic situation where it would be necessary a booster fan.

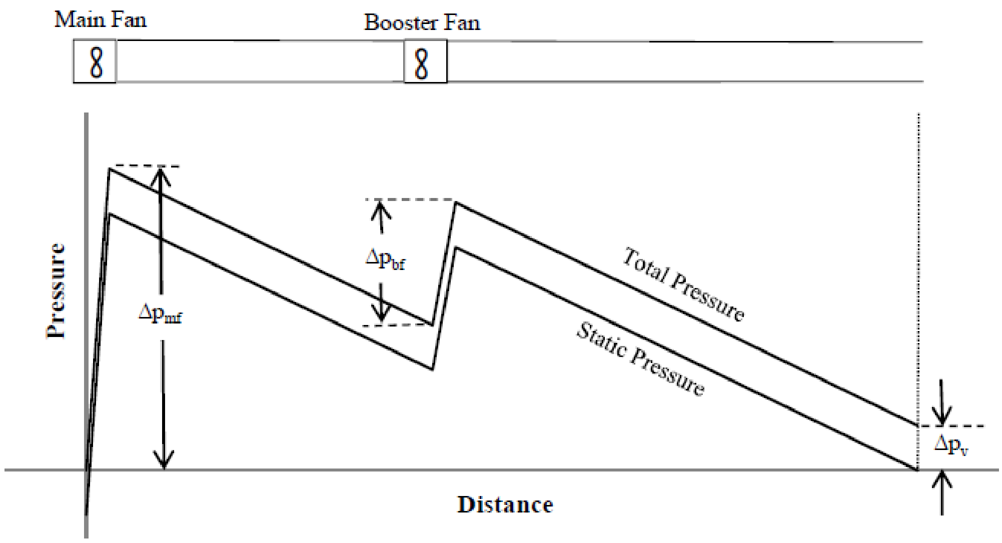

Figure 21. Pressure profile using a booster fan (Hartman et al., 1997).

Many times, the airflow from the principal circuit does not reach the working faces and workshops, being necessary an auxiliary system formed by one or more fans and a duct line. Figure 22 shows two simplified examples of what it could be an auxiliary system.

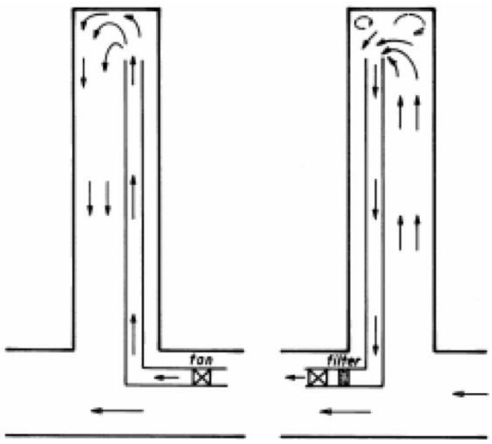

Figure 22. Scheme of two types of auxiliary systems (McPherson, 2009)

Together with the fans, the air is led through a system of doors, curtains and brattices that intercept or split the airflow circulation. Sometimes a portion of the air from the return is directed to the intake again. This recirculation can increase the air velocity near the production areas (Marks, 1989). Unfortunately, there are also uncontrolled recirculation situations, creating a potential risk for the employees in terms of heat, dust and pollutants.

2.4.3. Natural ventilation pressure

Once the air enters to the shaft and goes down, its pressure increases due to more weight in the air column. This phenomenon is called auto-compression and it increases the air temperature apart from modifying the air density. In addition, the temperature can also vary because of the strata heat exchange, increasing or decreasing the airflow temperature, and the friction through the shaft. These conditions could vary depending on hour, day or season because of different atmospheric conditions. This circumstance is called flywheel and was discovered by Stroh (1979), the heat from the air is transferred to the strata during the day and receive heat during the night.

Other important factor is the natural ventilation pressure (NVP). Depending on the ventilation system and the thermodynamic conditions it can go to the same direction as the artificial ventilation or against (in dip workings, natural ventilation energy, NVE, is summarized to the applied ventilation energy while in rise working the NVE subtracts from the artificial ventilation energy, AVE, the added pressure). Heat exchange in underground workings is the cause of the NVP movement. Figures 23 and 24 display the PV (pressure-volume) and TS (temperature-entropy) diagrams, respectively, for an underground mine using an exhausting fan at the top of the upcast shaft. Point 4 is the inlet of the fan at a sub-atmospheric pressure and when air passes through the fan it goes back to atmospheric pressure.

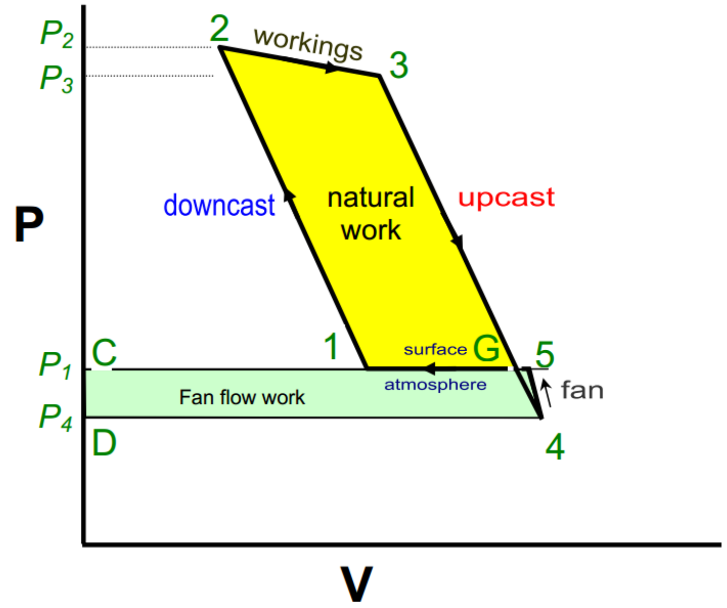

Figure 23. PV diagram in a mine with an exhausting fan (McPherson, 2009).

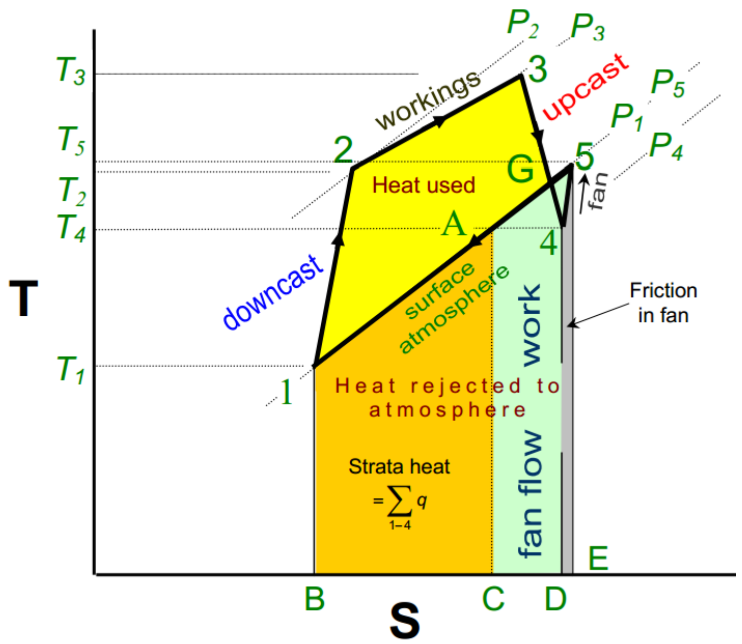

Figure 24. TS diagram with an exhausting fan (McPherson, 2009).

Observing previous Figures, heat exchange is produced in the downcast and working areas. However in the cases studied the downcast part does not have an influence to the temperatures as large as workings.

$$NVP = g \cdot (Z_1 - Z_2) \cdot (\rho_{md} - \rho_{mu}) \quad (11)$$

Where:

NVP – Natural ventilation pressure (Pa);

g – Gravity force (m/s^2);

Z – Depth relative (m);

ρ_{mu} – Mean air density at the inlet (kg/m^3);

ρ_{md} – Mean air density at the outlet (kg/m^3).

2.5. Subsurface climatic conditions

Climatic conditions in underground spaces are function of endogenous and exogenous factors. Strata heat, mining equipment and fragmented rock are the main heat load factors, but there are also others such as explosives, oxidation or water flow that could have some influence depending on the mining method and conditions.

2.5.1. Strata heat

There is a large amount of variables that have to be taken into account for determining the strata heat load.

- Length and geometry of the opening
- Depth below surface and inclination of the airway
- Mining method
- Wetness of the airway surfaces
- Roughness of the airway surfaces
- Rock breaking
- Time elapsed since the airway was driven
- Volume flow of air
- Barometric pressure
- Wet and dry temperatures
- Virgin rock temperature
- Distance of the workings from downcast shafts

- Geothermic step or geothermic gradient
- Thermal properties of the rock
- Machinery and cooling plants

The amount of heat transmitted decrease over the time, being the working faces the places with more transmission. Its quantification is usually done by means of computer simulations, but some of the parameters described above have small influence and a heat flow approximation can be achieved with simple equations. Another possible option would be using data from other similar mines in order to determine the strata heat load, although the results cannot have the expected accuracy (McPherson, 2009). As there is no information from similar mines, empirical equations and modelling software will be used. Figures 25 and 26 show the strata heat behaviour.

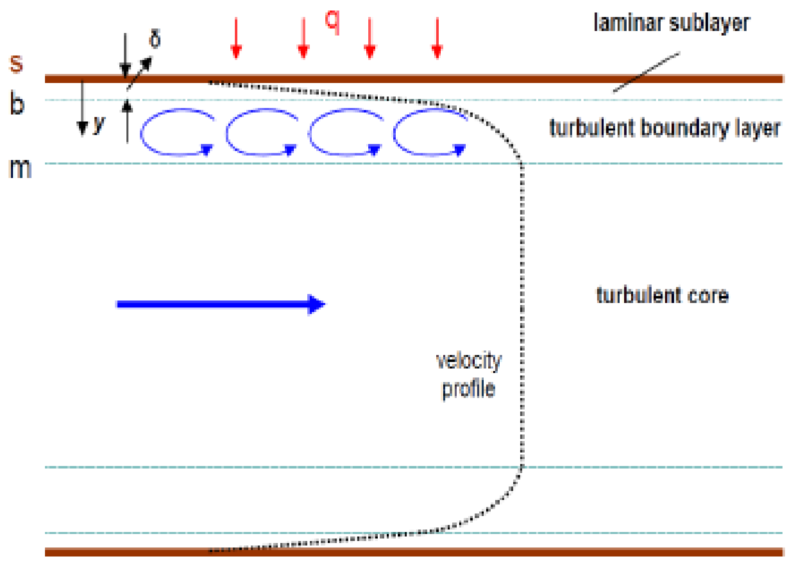

Figure 25. Strata heat flow and airflow behaviour (McPherson, 2009)

Heat flow displayed in Figure 26 can be positive or negative, depending on temperatures of the air and rock. The presence of water evaporation/condensation will influence the heat balance and therefore sensible heat, q_{sen}, and latent heat, q_l. Both types of heat are explained below in the section regarding the equipment.

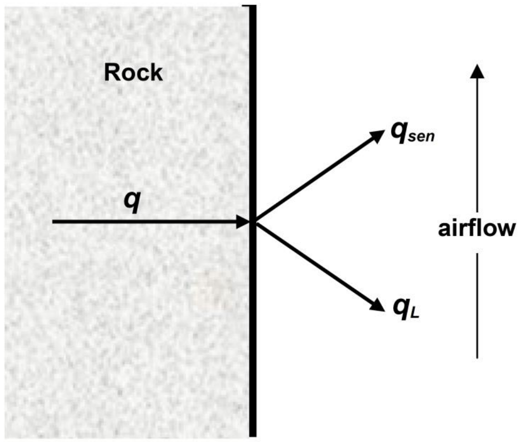

Figure 26. Heat exchange between the strata and the air (McPherson, 2009).

The specific software used for modelling are called ClimSim and VnetPro+, which allow simulating airflow and heat flow behaviours. Their functioning is also explained in a subsequent section.

The method by means of simple equations distinguishes between established tunnels and advancing end of a heading. In both cases the radial heat flow is obtained but it requires different data.

2.5.1.1. Established tunnels

$$q = 3{,}35 \cdot L \cdot K^{0{,}854} \cdot (VRT - \theta d) \quad (12)$$

Where:
q – Heat flow from strata (W);
L – Length of the tunnel (m);
K – Thermal conductivity of the rock (W/m·ºC);
VRT – Virgin rock temperature (ºC);
θd – Average dry temperature (ºC).

In well stablished return airways, it can occur an equilibrium of temperatures between surrounding rock and air. In these cases there is no heat transfer, having an adiabatic and isothermal process. Despite that decompression produce a fall in temperature, the frictional heat generates a very similar rate of heat, maintaining the equilibrium. When air returns to the surface through a shafts or ramp, there is a decompression, increasing the specific volume despite a decrease in temperature. Comparing the heat exchange between downcast and upcast shafts, the last one is less susceptible to heat exchange.

2.5.1.2. Advancing end of a heading

$$q = 6 \cdot K \cdot (L + (4 \cdot DFA)) \cdot (VRT - \theta d) \tag{13}$$

Where:
L – Length of the advancing in the previous month (m);
DFA – Daily face advance (m).

Tunnels with more than 1 month are considered as established tunnels and subsequently, equation 12 has to be used instead of 13 one. The main problem of the equations detailed above is the mean dry temperature, which has to be estimated. For this reason, climate simulation software is necessary to achieve more accurate values. In this case it has been used ClimSim.

Some parameters included in equations 12 and 13 have to be described in order to get a better understanding of the heat behaviour. Temperature of the rock depends mainly of the depth of the rock (Sundberg et al., 2009), which is a function of the geothermic gradient (m/ºC) and the rock virgin temperature (ºC).

The rock virgin temperature (VRT) increases at the same time of the depth due to the heat of the Earth’s core. The presence of groundwater or radioactivity could modify its value. The most precise method to determine it is by means of down-holes and laboratory analysis (Sundberg et al., 2009). Despite that, there is an alternative method, when there is no such information, using the fragmented rock from working faces as equivalent value (McPherson, 2009).

With respect to geothermic gradient, it takes into account the temperature increasing as depth increase, varying with the type of mineralogy. Its determination also needs samples and laboratory tests (Krishnaiah et al., 2004; Sundberg et al., 2005; Di Sipio et al., 2013), but there is extensive information, particularly in the zone studied (www.igc.cat).

Regarding rock thermal conductivity (W/mºC), it is a factor that determines the capacity to transmit heat into the tunnel. The higher the value is, the easier the heat transference from the strata is. This parameter is mostly based on its mineralization and density, while temperature of the rock and mechanic stress have less influence. When high precision is needed, rock thermal conductivity has to be obtained from samples analysed in laboratory, although aspects like groundwater and rock fracture can modify the results (Mousset-Jones and McPherson, 1984; Krishnaiah et al., 2004; Sundberg et al., 2005). Rock conductivity and heat flow are related by means of the Fourier's Law.

$$q = -K \cdot A \cdot \left(\frac{d\theta}{dx}\right) \tag{14}$$

Where:
K – Thermal conductivity (W/mºC);
A – Section (m^2);
θ – Temperature (ºC);
x – Distance (m).

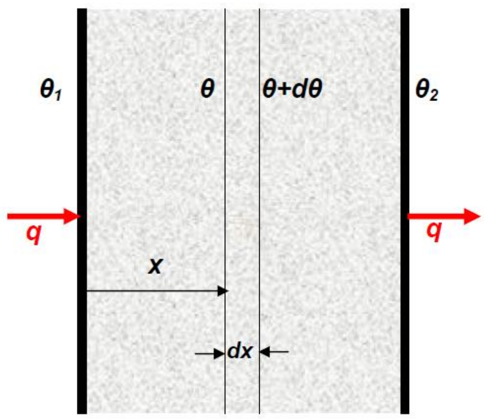

Figure 27. Heat conduction (McPherson, 2009).

In addition, rock thermal conductivity, together with the specific heat and density, determine the cooling velocity of the rock exposed to the airways, known simply as rock thermal diffusivity (m^2/s).

$$\alpha = \frac{Kr}{\rho r \cdot Cr} \qquad (15)$$

Where:

α – Thermal diffusivity (m^2/s);

Kr – Rock thermal conductivity (W/mºC);

ρr – Density of the rock (J/Kg·ºC);

Cr – Specific heat of the rock (J/KgºC).

Finally, the geothermal step (m/ºC) is obtained by the next expression and data collected in the zone.

$$\text{Geothermal step} = \frac{dD}{d\theta} \qquad (16)$$

2.5.2. Equipment

The obtaining procedure for the mining equipment heat load is different if the power source is electricity or diesel. Besides, heat load composition of both types will be different. In the case of diesel equipment there will be sensible and latent heat, while electrical equipment only produces sensible heat

Latent heat is the energy of a system during a constant temperature process, such as a change of state of matter, evaporating liquid water into the airway. In mine ventilation it is a very important factor linked to the wetness factor and humidity. It has also influence for calculating the effective temperature. On the other hand, sensible heat is the heat exchanged by a system. Strata or machinery heat generated is added to the ventilation circuit, increasing its temperature.

2.5.2.1. Electrical equipment

Figure 28 displays the methodology followed in different steps to obtain the sensible heat produced and added to the airways.

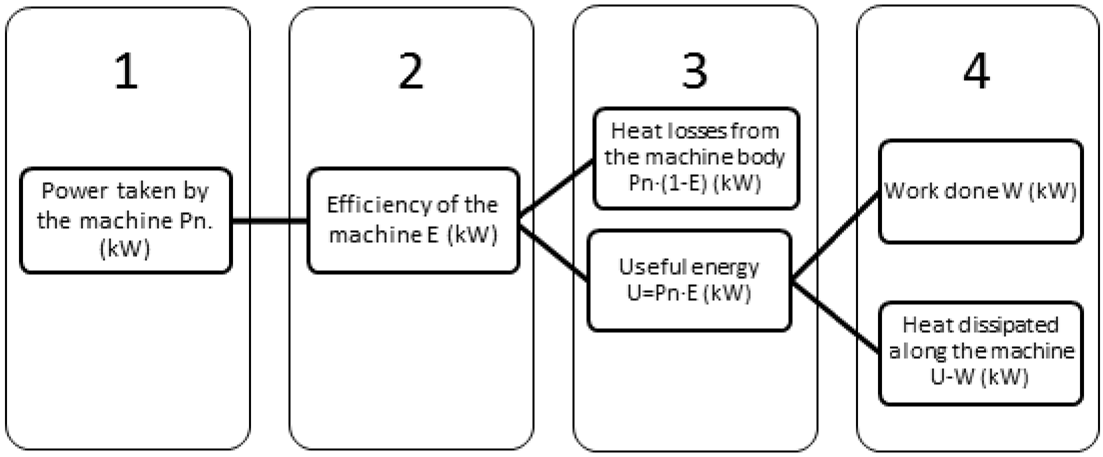

Figure 28. Electrical equipment heat load generation.

2.5.2.2. Diesel equipment

They have an efficiency of approximately 1/3 compared to the electrical equipment. In addition, they produce sensible and latent heat. The main sources, in a similar proportion, are:

- Radiator and machine body.
- Exhaust gases generated by intern combustion.
- Frictional processes of the machine doing their task.

The relationship electrical-diesel equipment can be done with a rate of 0,3 litres of diesel per 1 kW per hour with a calorific value of 34000 kJ/litre. Giving as heat emitted to the airways 2,83 kW for each kilowatt of mechanical output (McPherson, 2009).

$$\left(\frac{0{,}3}{60\cdot 60}\right)\cdot 34000 = 2{,}83\,\frac{kJ}{s}\ o\ kW \tag{17}$$

In order to know the heat produced, it is necessary to determine the diesel consumption per shift or the average rate of machine utilization.

On the other hand, latent heat generated can be calculated using a ratio of 1,1 litres of water per litre of fuel consumed (Kibble, 1978). However, in situ measures have reported from 3 to 10 litres of water per litre of fuel, depending on the engine power and maintenance (McPherson, 1986). The equation below explains the reaction generated when fuel is consumed.

$$C_nH_n + O_s = H_2O + CO_2 \tag{18}$$

Apart from heat generated and a certain quantity of water and CO_2, the combustion produce other gases and pollutants that affect the workplace environment and increase mine ventilation costs.

2.5.3. Fragmented rock

When the mineral exploited is exposed to the airways, there is a temperature difference between air and rock, generating heat transference. These conditions are found in working faces and the conveyor belt system in the cases studied. The amount of heat can be determined by the next equation.

$$q_{fr} = m \cdot C \cdot (\theta_1 - \theta_2) \tag{19}$$

Where:

qfr – Heat load generated by the broken rock (kW);

m – Mass flow of rock (Kg/s);

C – Specific heat of rock (kJ/kgºC);

θ_1 – Temperature of the rock after the fragmentation (ºC);

θ_2 – Temperature of the rock at the end of the ventilation system (ºC).

Rock temperature at working faces is slightly below the VRT, but the friction applied for digging the mineral increases its value to a similar temperature. So, temperature θ_1 can be considered equal to the VRT (McPherson, 2009).

2.5.4. Auto-compression

Flowing of the air downward increases its pressure and internal energy. Therefore, temperature of the air will do the same.

$$(H_2 - H_1) = (Z_1 - Z_2) \cdot g + q_{12} \tag{20}$$

Where:

H – Enthalpy (J/Kg);

Z – Height from the surface (m);

g – Gravity force (m/s^2);

q – Heat added/extracted from surroundings (J/Kg).

2.6. Safety issues

Underground environmental conditions are bound to health and safety issues. Gas concentrations, temperatures and humidity will affect working conditions, but the majority of these situations can be improved providing the proper airflow. All these factors are regulated by the Spanish legislation and detailed in the RGNBSM.

2.6.1. Subsurface gases

Airflow has to be enough to evacuate the strata gas, dust, diesel exhaust fumes and heat according to the legal requirements and with the aim of providing health and safety workplaces. These factors will be conditioned by the airflow quantity and air velocity limit at the same time.

Air from the surface, theoretically, is composed of 78% nitrogen, 21% oxygen and 1% of other gases. This initial mixture changes as air flows through the underground mine due to strata gas such as methane, carbon dioxide, chemical reactions, the usage of explosives, machinery, etc.

All of them can generate hazardous situations to the employees because of their explosive and/or toxic characteristics for short duration exposures. Moreover, some of them can also be cancerous in long term exposures.

The admissible pollutant and gas concentrations are limited by the threshold limit values (TLV). Three different types of TLV have to be distinguished; the time-weighted average (TWA) which is the average concentration per 8 hours shift and 40 hours per week, the short-term exposure limit (STEL) for no more than 15 minutes and the ceiling (C) which cannot be exceeded at any time. There are several organizations, such as NIOSH, INSHT or OSHA that release their threshold limit values. Tables 9 and 10 have gathered the TLV of the present gases in the potash mines studied according to the most representative organizations.

Table 9. TLV depending on the organization.

Gas	**PEL (OSHA)**	**MAC**	**REL (NIOSH)**	
			TWA	**STEAL**
CO (ppm)	50	30	35	-
CO_2 (ppm)	5000	5000	5000	30000
SO_2 (ppm)	5	2	2	5
SH_2 (ppm)	20	10	-	10
NO (ppm)	25	-	25	35
NO_2 (ppm)	1	-	-	1

Table 10. TLV depending on the organization.

Gas	**TLV (ACGIH)**		**TLV (INSHT)**	
	TWA	**STEAL**	**TWA**	**STEAL**
CO (ppm)	25	400	25	-
CO_2 (ppm)	5000	30000	5000	-
SO_2 (ppm)	2	5	2	5
SH_2 (ppm)	10	15	10	15
NO (ppm)	25	35	25	-
NO_2 (ppm)	3	5	3	5

According to the Spanish law, apart from individual analysis, values of NO and NO_2 have to be summarised (RGNBSM, ITC 04.7.02) to analyse the fulfilment of the legislation. It is very important to involve all the managers and employees to identify hazards in their workplace environments with the aim to manage them (Bahn, 2013).

As underground mining presents an environment with several gases and pollutants, it is necessary to analyse the situation taking into account a gas mixture when they affect the same part of the body. The following expression has to be used to determine the threshold limit values.

$$\sum \frac{E_i}{TLV_i} \tag{21}$$

Where:

Ei – Different chemical agent exposure;

TLVi – Threshold limit value.

When the result is above 1, the threshold limit value is considered as overcome and measures to reduce gas concentrations have to be applied (Carrasco et al., 2011).

Gases generated can be a consequence of the mineralization exploited or the exploitation method (mining equipment, blasting, etc.). In potash mining, carbon monoxide and dioxide can be spontaneously released (Carrasco et al., 2011; Hedlund, 2012). However, natural CO_2 generation is not a problem in the mines studied since there is no geologic information about volcanic CO_2 inclusions to the evaporitic layers. Being diesel combustion the main factor, producing carbon monoxide and dioxide, sulphur dioxide, nitric oxide, nitrous oxide and aldehydes such as benzene, formaldehyde and hydrocarbons (Rundell et al., 1996). All these gases are hazardous since they are toxics or cancerous:

- Toxic gases: NOx, sulphur dioxide and carbon monoxide.
- Cancerous gases: benzene and hydrocarbons.

In addition, the ingestion of combustion particles (DPM) increases lung cancer mortality (Attfield et al., 2012; Silverman et al., 2012). DPM is composed by soot and unburned diesel components. The main problem is that this particles can have a size of less than 0,1 µm and combined with other elements from fuel, can remain within the lungs in a long term. It is believed these particles may cause different type of cancers among other symptoms (Noll et al., 2007). Table 11 shows the hazards and origin of potential gases produced in underground potash mines.

Table 11. Origin and effects of the gases (Carrasco et al., 2011).

Gas	Physical risk	Hygienic risk	Principal origin
CO	Explosive Inflammable	Asphyxiating Toxic	Engine combustion Strata emissions
CO_2		Asphyxiating	Engine combustion Strata emissions
SO_2		Irritant Toxic	Engine combustion
NO_x		Toxic	Engine combustion
SH_2		Asphyxiating Toxic	Engine combustion
Benzene		Cancerous	Engine combustion
Hydrocarbons		Cancerous	Engine combustion
H_2	Explosive Inflammable	Asphyxiating	Electrical engines and batteries

Gas concentration can be reduced using filters, catalytic converters or diesel with low percentage of sulphur. Ventilation can also be used to reduce or eliminate the hazardous gases in some cases.

2.6.2. Temperature

Underground conditions suffered by employees can produce an unbalanced metabolic heat situation and for this reason it has to be controlled. One of the main parameters is the effective temperature obtained by the following equation, according to the Spanish law (Royal Decree 863/1985).

$$te = 0{,}9 \cdot tw + 0{,}1 \cdot td \qquad (22)$$

Where:

te – Effective temperature (ºC);

tw – Wet temperature (ºC);

td – Dry temperature (ºC).

Cold and hot environments can create problems when the body cannot regulate heat load, appearing problems with mental and manual work. Moreover, the productivity rate decrease and safety levels are reduced. If the situation is extended for a long time risks such as heat fainting, exhaustion or cramps can arise, causing even heat strokes if the core temperature rises above 41 ºC. This risk can be reduced by means of an acclimatization process in hot environments.

Figure 29 displays the influence of effective temperature to the worker performance. According to McPherason (2009), it can be considered that when cooling power of the airstream decreases below 300 W/m2 in hot workings, psychological and physiological effects can arise.

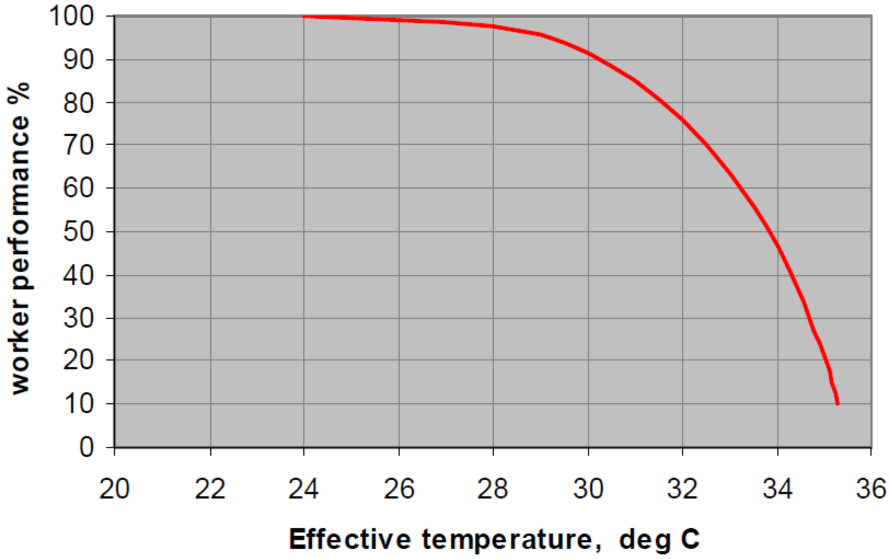

Figure 29. Relationship effective temperature – worker performance (Poulton, 1970).

2.6.3. Dust and aerosols

The hazard of dust exposure depends on the size of the particle and the potential effects. When particles are greater than 10 µm they are not able to accumulate within the organism. In the case of potash mining, as potassium and salt are soluble lung problems are highly reduced.

CHAPTER 3

APPROACHES IN THE CASES STUDY

"I have not failed. I've just found 10,000 ways that won't work." —Thomas A. Edison

APPROACHES IN THE CASES STUDY

3.1. Data collection

Initial data used along the dissertation have been obtained from in situ measures and bibliographical values when the first option has been impossible. The same procedure is applied in Cabanasses and Vilafruns.

As it is not possible to take measures along all the airways, places standing for the ventilation system have to be found, either in the principal or the auxiliary ventilation system. Characteristics taken into account for such purpose are:

- Principal ventilation system: Key points from the intake and return, taking into account features such as split airways, the presence of doors and curtains or significant cross section and shape changes.
- Auxiliary system: Each working face is a point of measure in the auxiliary circuit.

All points are measured monthly and then the information is gathered in a database created for such purpose. The factors measured are: Air velocity, temperatures, carbon monoxide (CO), carbon dioxide (CO_2), nitric oxide (NO), nitrogen dioxide (NO_2), oxygen (O_2), section (m^2) and other relevant information such as pipeline length, position of the miners and points, wall roughness, etc. All the data collected is explained in the following three sections.

Usually, control points are in fixed places, but the evolution of the workings varies the position of some control points along the time, having fewer measures recorded in some of them. For this reason, the data analysis has been done merging some points when their characteristics were similar.

3.2. Geographic information system creation

As both mines, Cabanasses and Vilafruns, have a lot of data linked to the ventilation conditions, a geographic information system (GIS) of each mine has been created, giving the possibility to study the conditions separately or mixing data from both mines. For such purpose it has been used the software ArcMap 9.3.

This software is a good choice for managing information from the ventilation system due to its user friendliness and capability to deal with huge quantity of interconnected spatially referenced information, monitoring and analysing the ventilation parameters and finally extracting conclusions in maps, tables and even converting the information to other software files. The possibility to display and query historic data can give insight to the current situation of the mine and how it would react in the future if any variable change. Moreover, this system can also be applied in any other underground infrastructure following a similar pattern.

Its creation gives a new usefulness for a GIS, fitting perfectly with what is demanded for a place like a mine that is spreading out every day and generating a huge quantity of information coming from monitoring a dynamic environment (Gibert et al., 2006). Figures 30 and 31 are a scheme of the ventilation system of Cabanasses and Vilafruns created by means of the GIS. The return is coloured with red, the intake with sea blue and the leakages with sky blue.

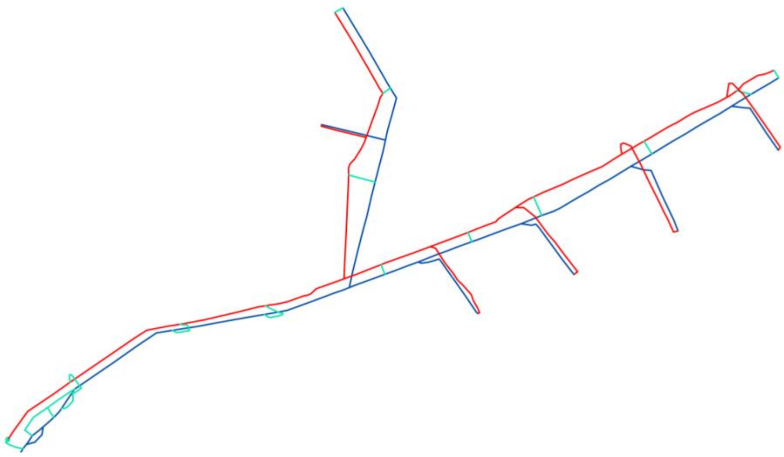

Figure 30. Scheme of the principal ventilation circuit in Cabanasses, created by means of GIS.

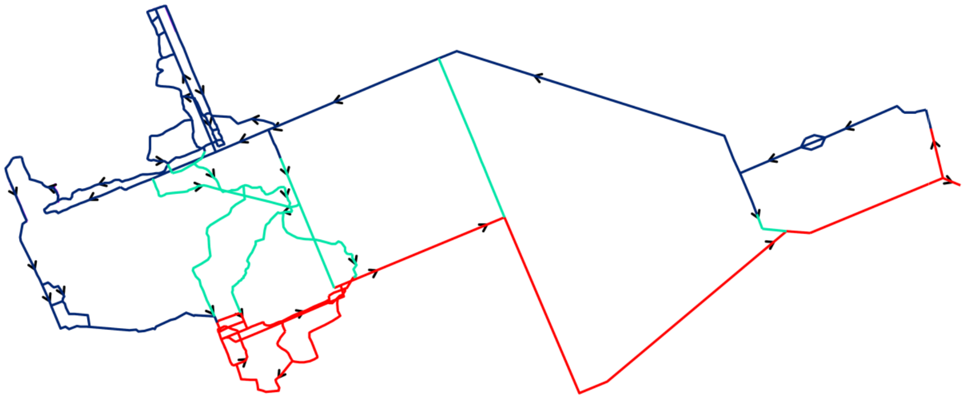

Figure 31. Scheme of the principal ventilation circuit in Vilafruns, created by means of GIS.

As it can be seen in previous Figures, each mine has a different ventilation circuit and therefore the individual analysis will be distinct as well as the data processing and results achieved.

3.2.1. GIS construction and database management

Collection data

First of all, the placement of the points registered was chosen in order to stand for the situation of the ventilation system according to the rules described in the previous section.

The parameters were obtained in situ and they were measured by conventional methods, taking them during two consecutive days every month, one day for the principal ventilation circuit and the other one for the auxiliary. All the measures were always taken during the same period of time, from 7 am to 1 pm.

978 points have been measured in Vilafruns since April 2008 until October 2015, belonging 725 points to the principal ventilation system and 253 to the auxiliary system. Meanwhile in Cabanasses were 481, 336 in the principal and 145 in the auxiliary within the same period.

The validity of the analysis depends on the reliability of the method used to obtain the data. The lower the reliability of the outcome is, the more difficult it is to detect the effects of an intervention (Cook et al., 1990; Lipsey, 1990). Low reliability of measures can occur because of instability in what is being measured and variations in the measure instrument (Shannon et al., 1999). For this reason, the equipment is calibrated regularly in order to keep its accuracy and measures are taken twice. In addition, if there is any measure with an abnormal value, it is taken again and the equipment has to be tested additionally when two values do not gauge consistent values.

Data format and characteristics

Initially, the information consisted of several maps and the collected database. Maps were in dxf (AutoCad) format and contained the layout of the mine, while the database was in xls (Excel) and contained the ventilation features. Both files were merged and transformed to a shape file through ArcMap software. The reference system used has been the Universal Transverse Mercator projection (UTM), based on the European Datum 1950 in the zone 31 N.

Pre-processing

For the construction of the GIS file, data from maps and ventilation characteristics have been divided in different layers as of two conditions: principal or auxiliary ventilation and depending on the layout of the ventilation system. This division is necessary because each one has different features and makes the management of the database easier. Next step was to store the information of the database that belongs to each point, taking into account the division described. Once the database of the GIS has been created, some parameters have been used to calculate important features such as airflow or effective temperature, while the others are used directly as a characteristic of the ventilation behaviour.

3.2.1.1. Ventilation parameters description

Parameters described below are either measured in situ or calculated by means of the initial data. There are 16 parameters concerning the principal ventilation layer and 20 in the auxiliary. Each parameter means a column in the GIS file.

Principal ventilation

1. Point: Identification number.
2. Coordinates (UTM): Position of the point within the ventilation circuit (m).
3. Date of the measure: The day, month and year of the taken measure.
4. Hour: Time when the measure has been taken during the day.
5. Air velocity (m/s): Measured with a rotating vane anemometer.
6. Dry temperature (ºC): Measured with a sling psychrometer.
7. Wet temperature (ºC): Measured with a sling psychrometer.
8. Carbon monoxide (CO): in parts per million, ppm. Measured with a gas detector.
9. Carbon dioxide (CO_2): in ppm. Measured with a gas detector.
10. Nitric oxide (NO): in ppm. Measured with a gas detector.
11. Nitrogen dioxide (NO_2): in ppm. Measured with a gas detector.
12. Oxygen (O_2): Expressed as a percentage. Measured with a gas detector.
13. Section (m^2): It is calculated regularly with a laser distance measurer.
14. Airflow (m^3/s): Knowing the air velocity and the section, it can be calculated using the formula Airflow = Air velocity x Section.
15. Effective temperature (ºC): It is calculated through equation (16)
16. NO_x (ppm): The nitrous gases (NO and NO_2) have to be summarised as the Spanish law explained previously requires.

Auxiliary ventilation

1. Continuous miner: Identification number.
2. Miner state: If it is working or in standby while taking the measures.
3. Coordinates (UTM): Position of the miner (m).
4. Date of the measure
5. Hour
6. Air velocity (m/s)
7. Section (m^2): It is provided by the supplier.
8. Dry wet temperature (ºC)
9. Wet temperature (ºC)
10. Effective temperature (ºC):
11. Carbon monoxide (CO)
12. Carbon dioxide (CO_2)
13. Nitric oxide (NO)

14. Nitrogen dioxide (NO_2)
15. Oxygen (O_2)
16. Airflow pipeline entry (m^3/s): Knowing the Air velocity and the section, it can be calculated using the formula Airflow = Air velocity x Section.
17. Airflow pipeline exit (m^3/s)
18. Distance between the working face and the pipeline entry (m): Using a laser distance measurer.
19. Type of fan: If it is exhausting, forcing or an overlap system exhausting-forcing.
20. Other information: Any incident or remarkable situation taking the measures.

All the parameters without procedure explanation have been calculated or measured following the same approach applied in the previous subsection.

3.2.1.2. Database design and management

After the database has been correctly introduced into ArcMap and calculations are done, the information is properly organized. Figure 32 shows different configurations that refer the ventilation layout depending on the evolution of the mine workings. Within each configuration, there are two different files that represent the principal and the auxiliary ventilation, having the database stored inside. The principal includes the points where measures have been taken and intake, return and leakage airflows. This distinction is created by 3 different layers in colours, allowing either individual or group analysis. On the other hand, the auxiliary contains the position of the continuous miner and the pipeline that provides airflow.

In addition, the mine workings layer stand for all the galleries exploited until now and it helps to get a better understanding of the reality and the layout configuration of the ventilation system.

Figure 32. Structure of the geographic information system file created.

The information within each configuration is thoroughly detailed in Figure 33. Data from the principal and auxiliary ventilation circuit are stored in the points called P_Principal and Miner.

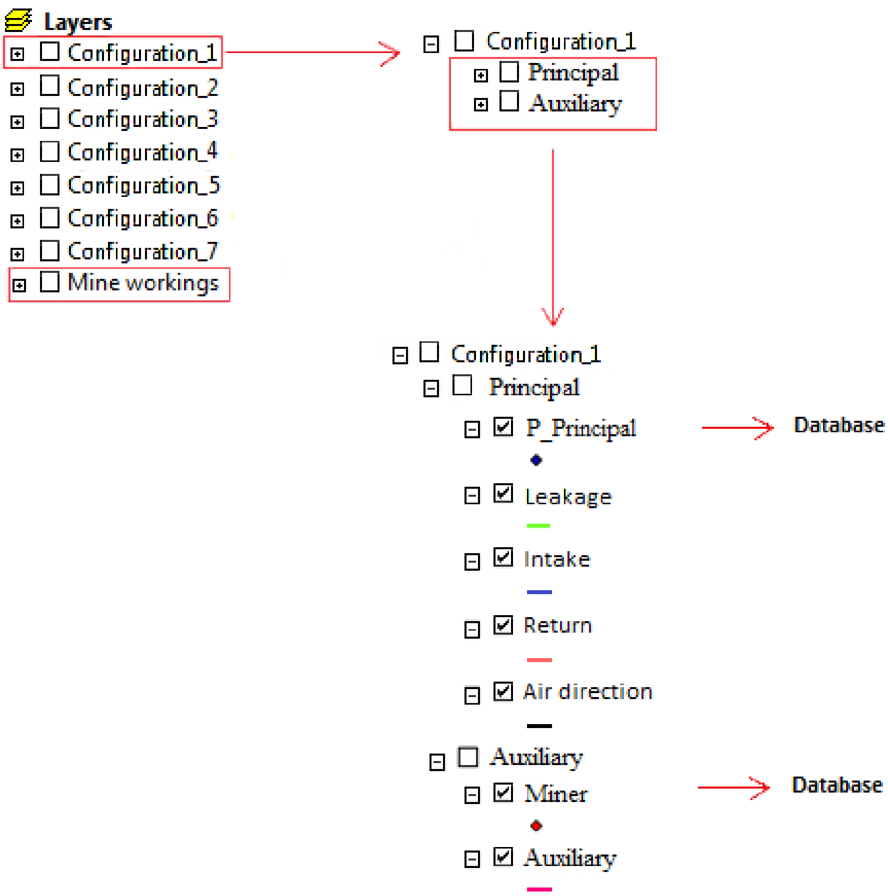

Figure 33. Internal organization scheme of the GIS created.

Figure 34 illustrates the steps followed to create the GIS file described above. The layer called "mine workings" has not been included in the scheme, following the stages 1, 2 and 3 for its creation.

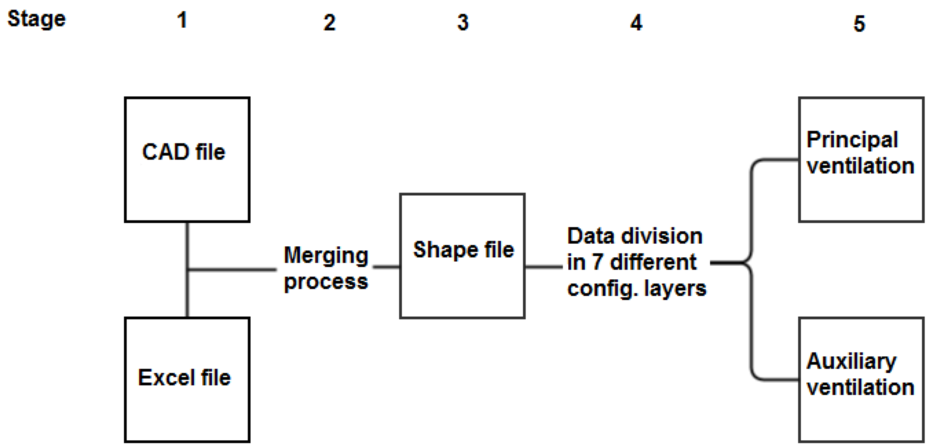

Figure 34. Scheme of the process followed to create the GIS file.

Figure 35 represents one of the configurations, in different colours to achieve a better visual understanding (sea blue for the intake, red the return, blue sky for the leakages and pink the auxiliary ventilation system). In addition, there are the points that represent those places where measures are taken. Points called "Mxx" are continuous miners while numbers "xx" are key points of the principal circuit.

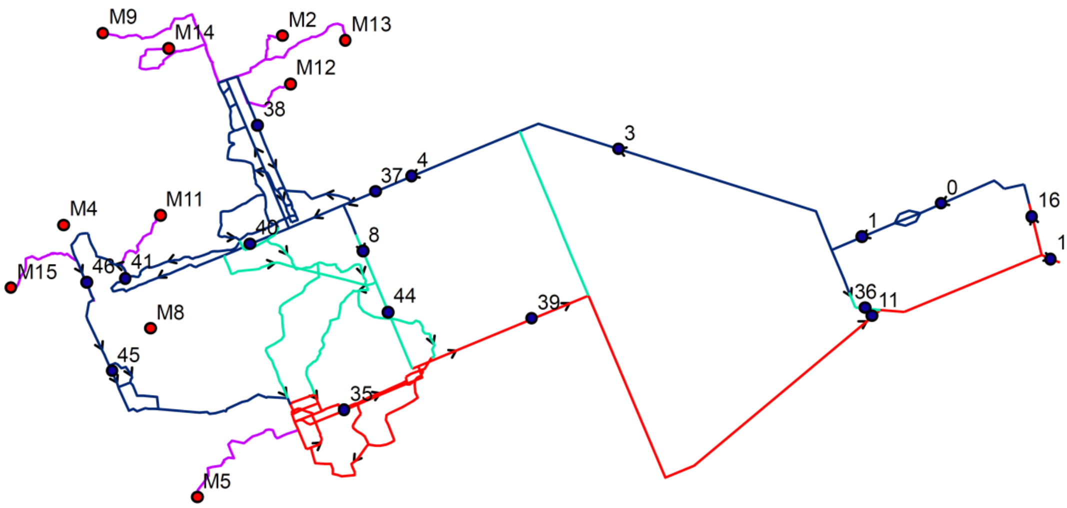

Figure 35. Image of the configuration 7.

Figure 36 is an image regarding part of the ventilation circuit and mine workings. Both layers, displayed at the same time, are useful to understand the ventilation circuit and figure out any possible variation in the airflow route.

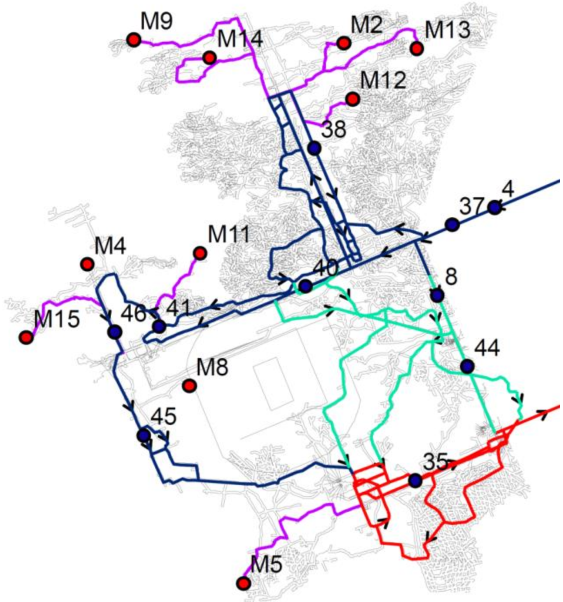

Figure 36. Part of a ventilation circuit in detail with the mine workings layer activated.

Data stored inside the points are divided in columns, standing for each column a representative parameter of the mine ventilation, either measured or calculated previously. Table 12 shows part of the data stored and how is organized inside the GIS.

Table 12. Partial data from the principal ventilation system in the configuration 4.

Point	X	Y	Velocity	Section	Cabal	Td	Tw
0	406644,520	4632795,437	4,52	40,00	180,80	16	13
1	406299,020	4632649,864	5,30	34,54	183,06	22	17
36	406312,822	4632339,316	1,20	31,84	38,21	24	17
3	405239,806	4633032,355	4,30	34,04	146,37	22	17
4	404338,413	4632913,879	4,25	27,86	118,41	27	18
37	404179,622	4632847,245	0,40	34,80	13,92	28	23
34	404875,824	4632946,927	0,60	28,37	17,02	27	21
7	405059,097	4632507,499	0,41	23,86	9,78	31	23
8	404125,445	4632587,232	0,41	31,54	12,93	35	22
38	403666,696	4633134,300	1,37	32,29	44,24	31	20

35	404044,481	4631896,851	3,96	27,83	110,21	38	28
39	404861,197	4632294,199	5,08	26,89	136,60	37	25
11	406344,243	4632305,139	6,18	24,36	150,54	32	25
13	407122,589	4632553,472	4,90	35,96	176,20	33	24
16	407039,769	4632738,951	0,45	21,61	9,72	34	24
40	403634,961	4632619,300	1,52	31,33	47,62	32	21

Once the database has been stored and linked to the graphical information, the system can be inquired and extract results using the tools of the GIS software.

3.2.2. Results

The following results are part of the possibilities to analyse the ventilation conditions of an underground mine. These outcomes could vary depending on the necessities of the technicians and the parameters collected. If it was necessary the system created could be adapted to any other type of underground infrastructure. Results from Vilafruns and Cabanasses have been achieved.

3.2.2.1. Vilafruns mine

The principal and auxiliary ventilation system are analysed in the following subsections regarding the underground environment, assessing the parameters measured and calculated in the GIS.

3.2.2.1.1. Principal ventilation system

Air velocity

It is a key parameter either for health and safety or operation costs. Air velocity is also important for modelling the airflow necessities of the principal and auxiliary ventilation circuit considering the number of people working there, the gases produced by diesel engines, the necessity to remove excessive temperature due to strata heat or machines and the maximum velocity of the air permitted by law. Gas concentrations and temperatures increase rapidly without an adequate air supply, worsening the environmental conditions of the workers as well as their efficiency.

The system proposed gives insight in a long term airflow analysis, comparing the air velocities depending on the ventilation layout variations. Figure 37 displays an analysis of the air velocity in three different chosen points from the ventilation system.

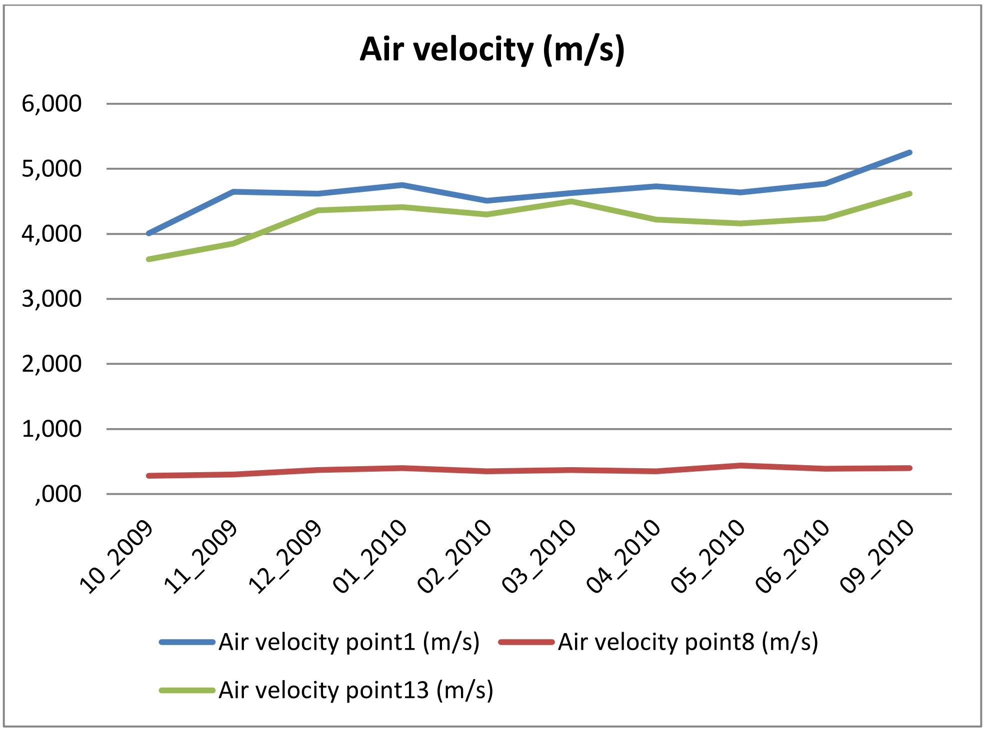

Figure 37. Air velocity in points 1, 8, and 13 from configuration 2.

Point number 1 is the first place where a measure is taken in the ventilation system after the airflow has passed through the downcast and main fan, while 13 is at the beginning of the ramp, the last one before the airflow in the return flows to the surface. On the other hand, point 8 is placed in an intermediate position.

Gases

Points 1 and 13 have been used once more to compare the gases. Table 13 shows how the first one doesn't have any concentration, while their values in the return airflow have significantly increased. However, they remain always under the TLV specified by the Spanish law, RGNBSM ITC 04.7.02, about the maximum gas concentrations allowed.

Table 13. Comparison between gas concentrations from points 1 and 13.

Point 1						
Month	**Year**	**Day**	**NO (ppm)**	**NO_2 (ppm)**	**CO (ppm)**	**CO_2 (ppm)**
October	2009	23	0,00	0,00	0,00	0,00
November	2009	26	0,00	0,00	0,00	0,00
December	2009	1	0,00	0,00	0,00	0,00
January	2010	11	0,00	0,00	0,00	0,00
February	2010	25	0,00	0,00	0,00	0,00
March	2010	24	0,00	0,00	0,00	0,00
April	2010	4	0,00	0,00	0,00	0,00
May	2010	17	0,00	0,00	0,00	0,00
June	2010	18	0,00	0,00	0,00	0,00
September	2010	20	0,00	0,00	0,00	0,00
Point 13						
Month	**Year**	**Day**	**NO (ppm)**	**NO_2 (ppm)**	**CO (ppm)**	**CO_2 (ppm)**
October	2009	23	5,00	0,20	8,00	2500,00
November	2009	26	5,00	0,20	8,00	2800,00
December	2009	1	5,00	0,20	9,00	3000,00
January	2010	11	1,00	0,00	0,00	500,00
February	2010	25	2,00	0,00	4,00	1900,00
March	2010	24	0,00	0,00	1,00	1500,00
April	2010	4	0,00	0,20	0,00	800,00
May	2010	17	6,00	0,10	4,00	2100,00
June	2010	18	0,00	0,10	7,00	400,00
September	2010	20	4,00	0,00	0,00	100,00

Its comparison, together with the visualization of the ventilation system from Figure 38, illustrates the evolution of the gases in the airflow from the principal ventilation system between the entry and the exit. These points are important because they are permanent regardless any possible variation in the ventilation circuit.

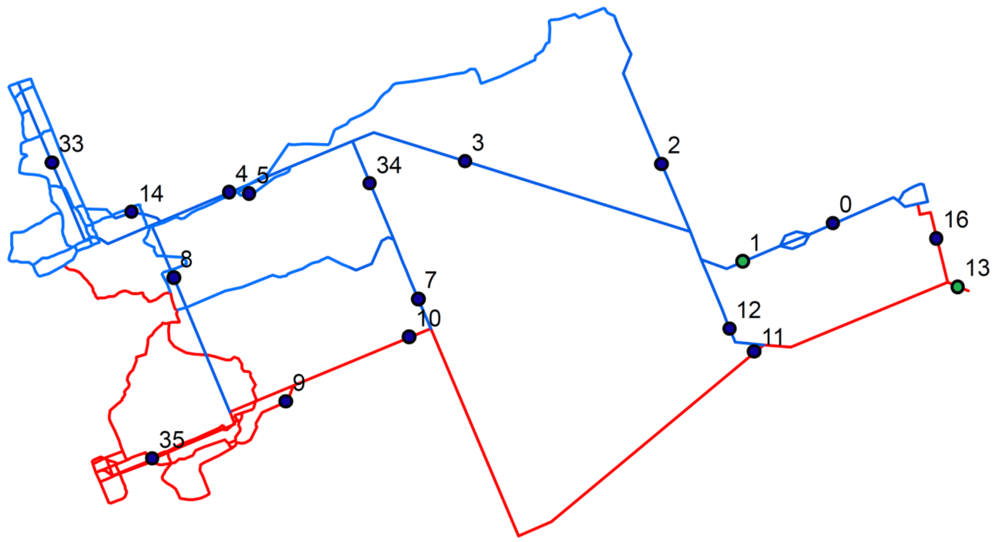

Figure 38. Principal ventilation layout of configuration 2 with points 1 and 13 selected in green.

3.2.2.1.2. Auxiliary ventilation system

Effective temperature

Not only does it show whether the temperature is below the maximum permitted by law, but figures can also be used to compare the real situation of the mine after changing some characteristics of the ventilation system. Having the temperature below a certain value improves the efficiency of the mine because employees are able to stay in the working faces more time and their degree of mental concentration increases when the workplace remains within an acceptable temperature range (García-Herrero et al. 2012). Table 14 comprises a selection, using GIS tools, of the measures in working faces that have been over 30 ºC during 2012, while Figure 39 displays the location of those miners.

Table 14. Selection of the measures over 30ºC during 2012.

Miner	X	Y	Month	Year	Day	E. temp. (ºC)
M5	403584,3210	4631491,2930	February	2012	21	34,40
M5	403501,3440	4631512,6890	April	2012	21	32,10
M11	403192,3100	4632604,5000	April	2012	21	31,00
M15	402635,8200	4632536,1770	April	2012	21	30,20
M7	403423,8600	4631908,2440	May	2012	23	30,00
M11	403198,0640	4632596,1310	May	2012	23	31,00
M14	403016,5470	4633352,8320	October	2012	19	30,80
M2	404010,7660	4633606,8540	October	2012	19	32,00
M12	403802,5090	4633316,2760	October	2012	19	32,50
M6	404061,2650	4631677,4540	October	2012	19	31,80
M5	403500,6710	4631509,1540	October	2012	19	33,80
M7	403521,0480	4631717,8980	October	2012	19	30,00
M5	403403,1010	4631515,7260	November	2012	22	30,00
M11	403243,7040	4632742,6100	November	2012	22	31,10

As it can be seen, only 14 in 156 measures from 2012 have exceeded the conditions imposed. Using the GIS, it is possible to detect adverse conditions more easily and quickly. Knowing when it has happened, how many times and which parts are the most negative with regard to health and safety.

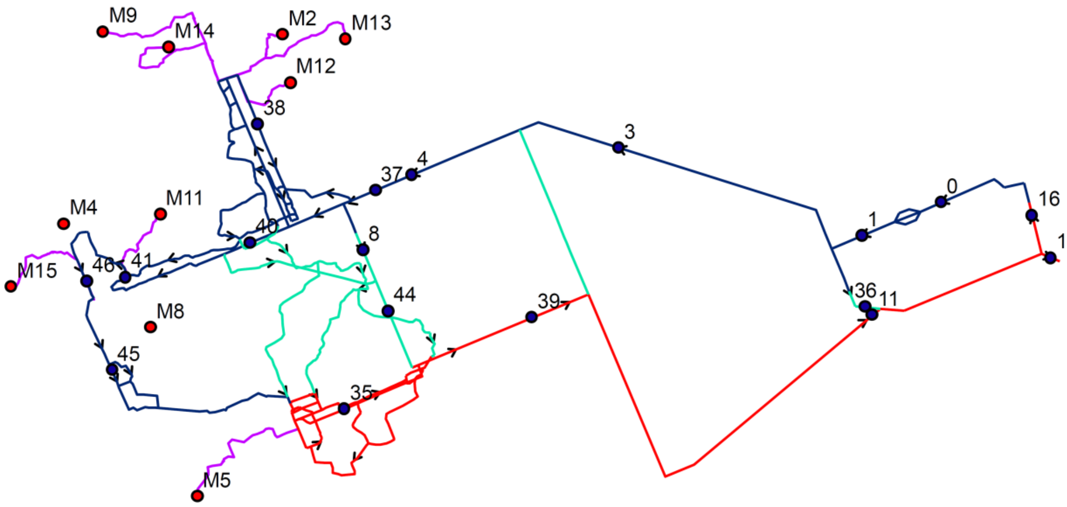

Figure 39. Principal and auxiliary ventilation system from configuration 7 with the placement of the key points and miners.

<u>Relationship temperature-gases-airflow</u>

Several features can also be studied together. Figure 40 relates all the data collected concerning temperature, gases and airflow from the auxiliary circuit (159 measures in total). Unfortunately, there is a short period without CO and airflow measures. The concentration of the CO_2 (in ppm) has been divided per 100 to get a more visual chart.

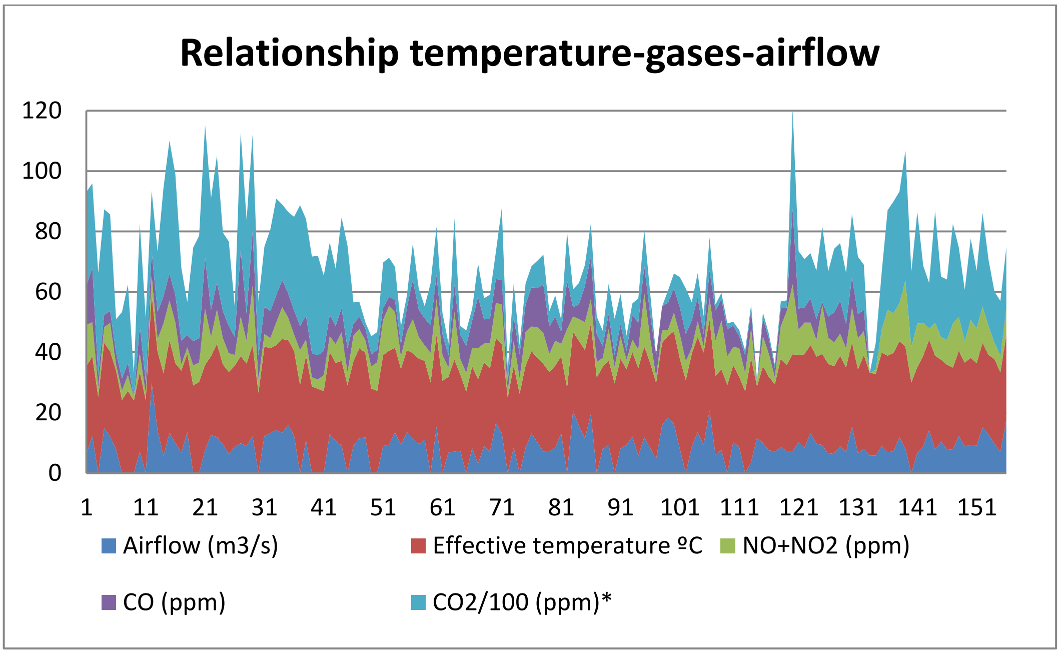

Figure 40. Measures of temperature, gases and airflow of the auxiliary ventilation system.

As it can be seen, there is a correlation between temperature, gases and airflow. The larger the airflow is, the higher the temperature and the gases concentration are. The air, supposedly clean, flows from a working face to another, carrying part of the gases from the previous miner and so on. This approach can be useful to assess any change in the auxiliary system and to find unwanted local airflow recirculation. This important issue is deeply studied in the following subsection.

3.2.2.1.3. Underground environmental analysis

In this part the environmental conditions in the principal and auxiliary circuit are assessed in order to determine the gas concentrations and temperatures behaviour pointed out in Figure 40.

Auxiliary ventilation system

Gas concentrations are a crucial matter in Vilafruns. The mine uses a partial recirculation ventilation system in which a controlled fraction of the air returning from a working face goes back into the intake. This method has the advantage of be more economical, but the airflow has to be monitored to control that gas concentrations are below a certain value in a short term. The GIS has allowed determining three groups in terms of air clearness arriving to the working faces (auxiliary system). Each group have different environmental conditions.

- Group 1: Working faces provided with clean air.
- Group 2: Working faces partially provided with clean air.
- Group 3: Working faces mainly provided with recirculated air.

Figure 41 details the groups created using the data collected and the visual information by means of the geographic information system.

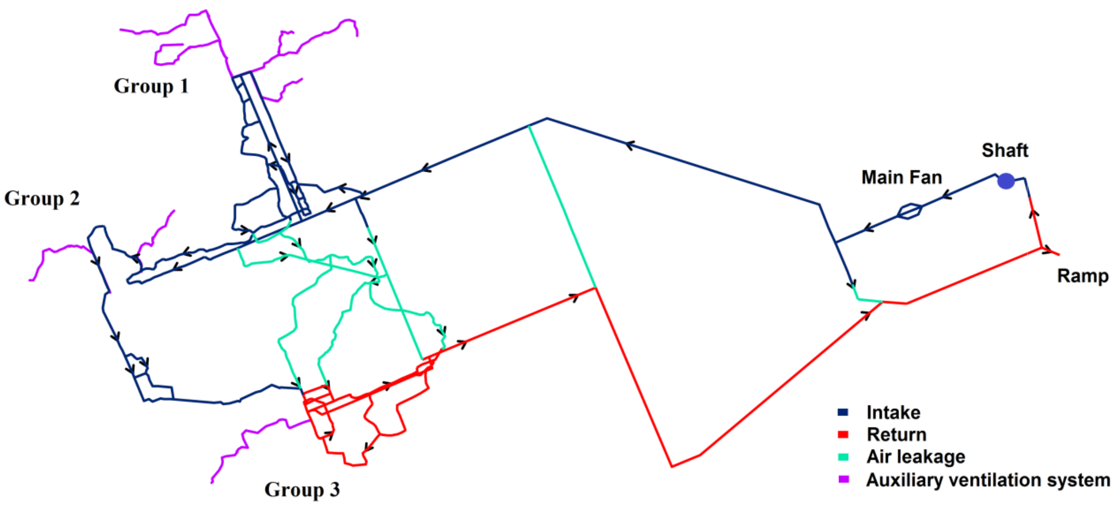

Figure 41. Vilafruns mine scheme.

Data have been analysed by group and individually by continuous miner. All measures have been split in three groups, having each group 123, 67 and 63 measurements respectively. Afterwards, means of airflow, effective temperature, CO, CO_2, NO and NO_2 from each group and continuous miner have been calculated.

The possibility of combining spatial referenced continuous miners with the information of gases and airflow has permitted to split the information in three groups using all the information. In addition, as miners move from one place to another, the GIS provides a simple tool to distinguish the information depending on the group. Figure 42 shows an example of one of the workplaces, called M8, and the evolution of its position between April 2009 and September 2010, changing from group 1 to group 2, thus this variation has to be taken into account to analyse the environment conditions, moving from a clean air to a partially recirculated situation.

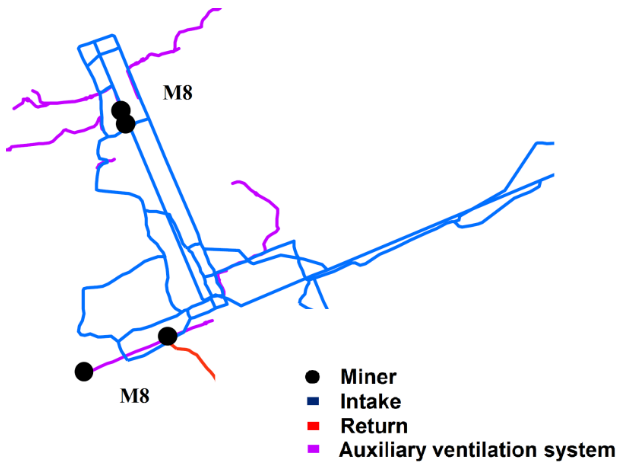

Figure 42. Position evolution of the continuous miner M8.

Without the usage of the GIS it would have been more difficult to discriminate this information in the three groups proposed. Especially when the data collected is from a long time ago.

Mean values of airflow, effective temperature, CO, CO_2 and NO_x from all the data are gathered in Table 15. While Table 16 compares the percentage variation in the different underground conditions.

Table 15. Mean values of the different environment groups.

	Airflow (m^3/s)	**Effective temperature (ºC)**	**CO (ppm)**	**CO_2 (ppm)**	**NO_x (ppm)**
Group 1	10,59	27,99	6,18	1819,27	7,974
Group 2	10,03	28,17	5,81	1641,62	8,28
Group 3	11,32	29,19	8,43	1883,53	9,306

Table 16. Percentage variation using Group 1 as a reference.

	Airflow (%)	Effective temperature (%)	CO (%)	CO_2 (%)	NO_x (%)
Group 1	0,00	0,00	0,00	0,00	0,00
Group 2	-5,29	0,64	-5,99	-9,76	3,84
Group 3	6,89	4,29	36,41	3,53	16,70

As it can be seen from the tables above, there is an increasing of gas concentrations and effective temperature with a similar amount of airflow comparing groups 1 and 3, especially regarding CO and NO_x parameters. However, the comparison between groups 1 and 2 provides mixed outcomes; probably because there is air recirculation within the same group (group 1) as it can be seen examining the position of the miners and the ventilation layout.

The individual analysis by miner is displayed in the next Tables and Figures, where each miner stands for a row in Table 17 and a bar in Figures 43 to 47. However, the same miner has changed from one group to another in some cases, such as miners 2 and 3 from group 1, which are physically the same as miners 2 and 3 from group 2, because at some point they were changed to another part of the mine. Therefore, they are considered as different miners for the study of the environmental factors. However, their identification names will be very important for managing the database in the GIS. In addition, Table 18 compares the minimum and maximum values of the parameters analysed among the miners.

Table 17. Name and number of measures from each miner.

	Name of the miner	Number of measures
Group 1	1	21
	2	15
	3	17
	4	27
	5	21
	6	23
Group 2	1	17
	2	21
	3	14
	4	18
Group 3	1	24
	2	27
	3	18

The percentage variation of the conditions showed in Table 18 has been linked to the information from Table 17 by the last column, called Group-miner, which identify the group and then the miner having the maximum and minimum value of each condition respectively.

Table 18. Difference between maximum and minimum values in the working faces.

	Maximum Value	Minimum value	Difference (%)	Group-miner
Airflow (m^3/s)	12,92	9,74	32,65	3.2-2.4
Effective temperature (ºC)	29,75	26,74	11,26	3.1-1.1
CO (ppm)	8,96	5,60	60,00	3.2-2.2
CO_2 (ppm)	2400,00	1291,88	85,78	1.3-2.1
NO_x (ppm)	10,94	7,39	48,04	3.1-1.1

Meanwhile, Figures 43 to 47 show the individual mean values of each miner, distinguishing the three groups in different coloured bars depending on the airflow conditions: clean air, partially recirculated or recirculated. As it can be seen, the quantity of continuous miners per group is different; having groups 1, 2 and 3 a quantity of 6, 4 and 3 miners respectively. The difference in the number of miners is just a matter of mine planning.

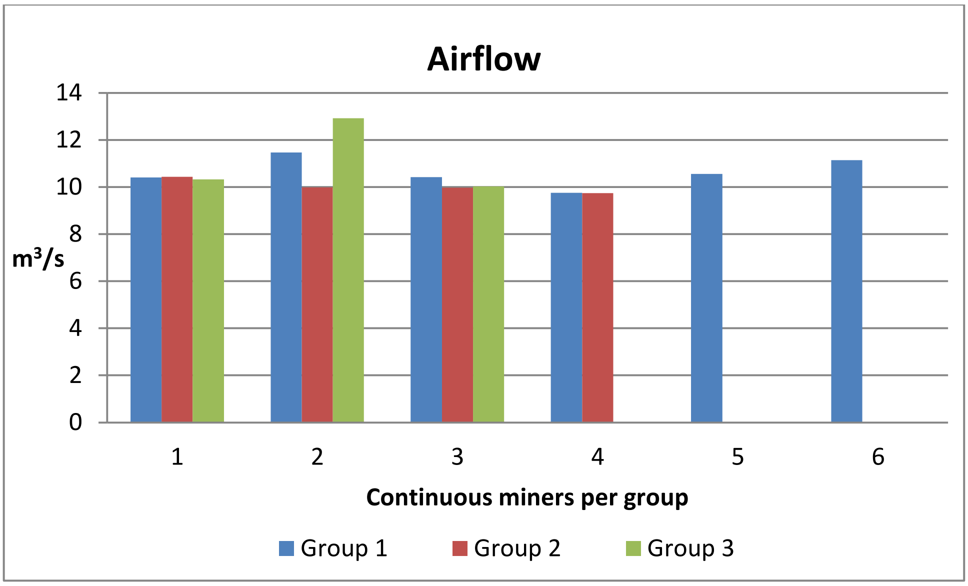

Figure 43. Amount of airflow per continuous miner, distinguishing each group.

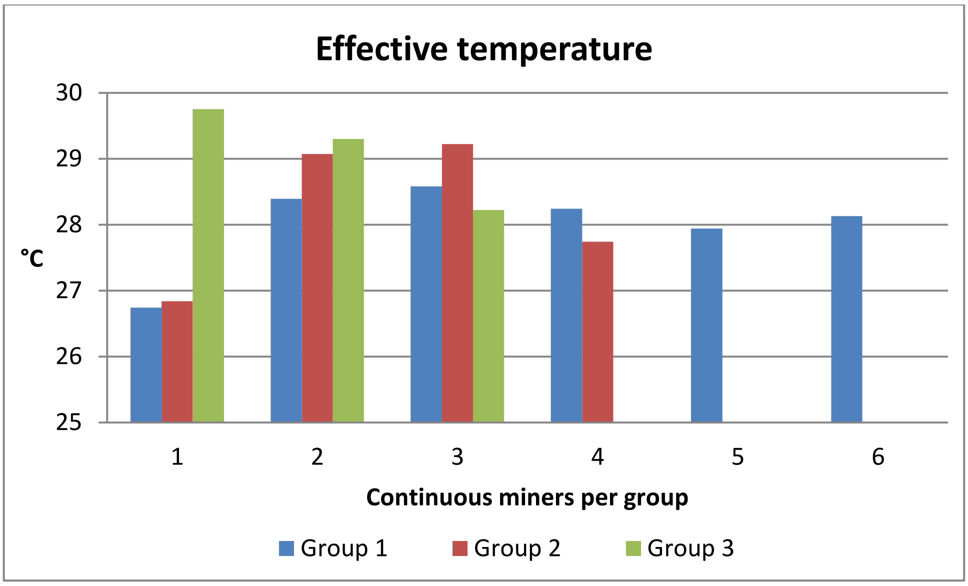

Figure 44. Effective temperature in each continuous miner.

The airflow per continuous miner fluctuates around 10 m^3/s. All miners have a similar quantity of air regardless the ventilation layout and the presence of recirculation. Therefore, the variation in the workplace conditions is not caused by the airflow supply.

Analysing the effective temperature, all the mean values are between almost 27 and 30 ºC, having the highest difference, 11,26%, between miner 1 from Group 1 and miner 1 from Group 3 according to Table 18. In accordance with the groups of clean and recirculated airflow respectively. In addition, when both miners are individually examined with the GIS, it can be appreciated that the one with the lowest effective temperature is placed very close to the service tunnels, having less heat input to the ventilation system than the other miners.

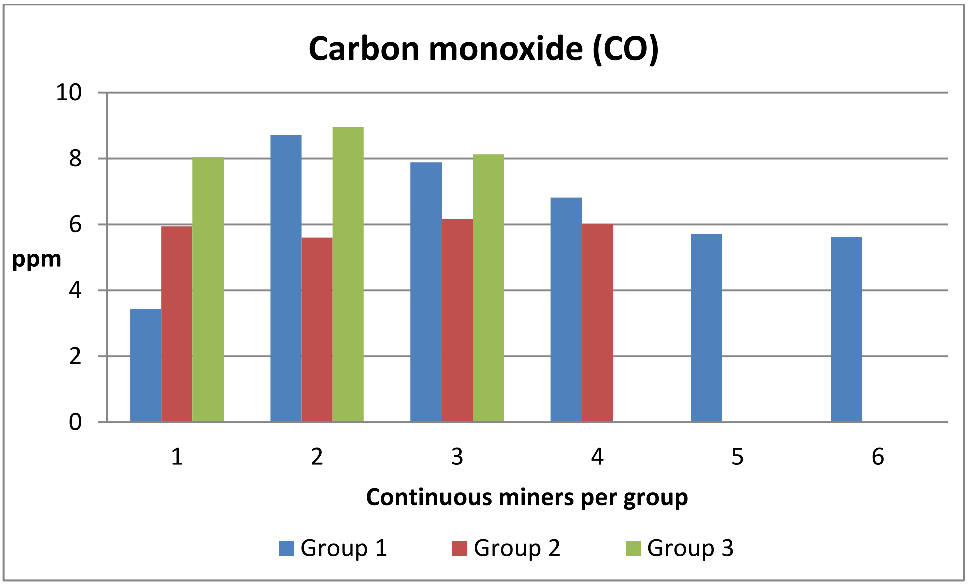

Figure 45. Carbon monoxide concentration per continuous miner.

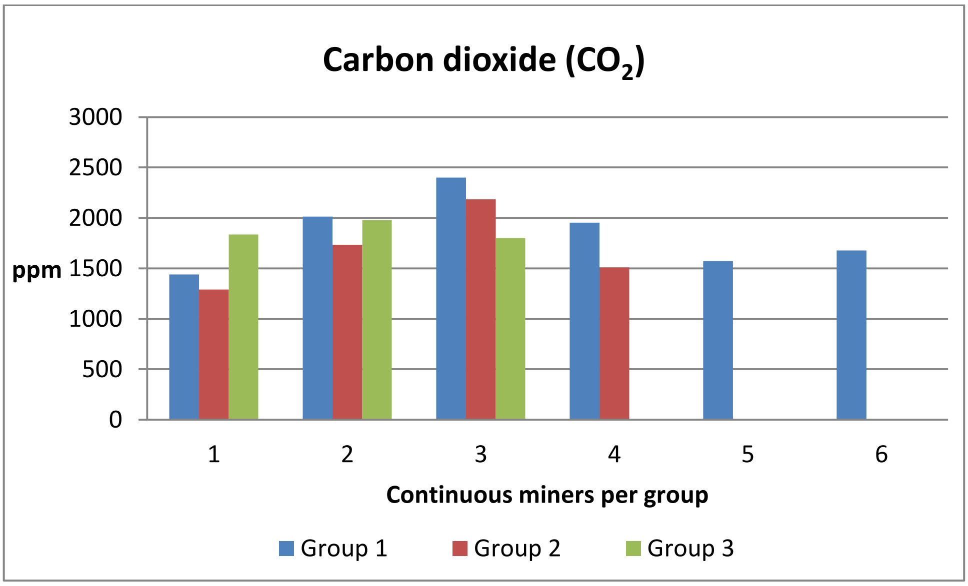

Figure 46. Carbon dioxide concentration per continuous miner.

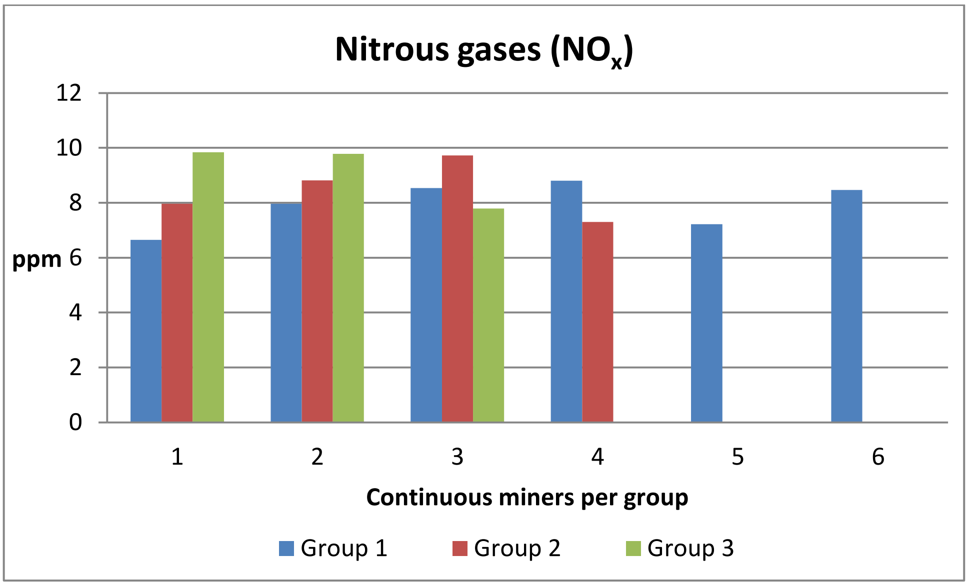

Figure 47. Nitrous gases concentration per continuous miner.

Carbon monoxide values from Group 3 show a trend of higher concentrations. However, there is not any clear variation in CO levels between group 1 and 2. Moreover, there is an important difference between the highest and lowest concentration level within group 1, reaching a variation of 56,47%.

In the case of carbon dioxide, the trend is not clear either. This parameter should be analysed thoroughly because it cannot be obtained any conclusion from individual and group values. Regarding nitrous gases, group 3 displays higher concentrations, but the trend is not as clear as the mean values.

If graphs are analysed together, it can be pointed out that the environmental conditions vary considerably despite having the same airflow within each group. However, if the ventilation circuit is assessed it does not explain this phenomenon, which is probably caused by local uncontrolled airflow recirculation due to an unappropriated auxiliary circuit.

The mine uses an exhausting system to renew the air in the working faces, leading the pollutants and heat throw a duct to the main circuit. Information related to these ducts should be included in the GIS such as position, leakages, layout of the auxiliary fans and distance from the entry of the duct and the working face. In addition, information regarding the discharge zone of the duct should also be included, so that tunnels with potential recirculation can be taken into account.

Principal ventilation system

Regarding the principal ventilation system and taking into account the 3 groups from the auxiliary system, there will also be 3 different groups.

- Group 1: Clean air provided by the intake
- Group 2: Air partially clean.
- Group 3: Recirculated air.

Group 1 does not have any concentration level of gas due to it is clean air from the downcast. Meanwhile the other 2 groups will show a certain quantity of pollutants. Tables 19 and 20 show the control points concerning Groups 2 and 3 and their means, respectively.

Table 19. Control points from group 2.

Control point	**Effective temperature (ºC)**	**CO (%)**	**CO_2 (%)**	**NO_x (%)**	**Number of measures**
6	27,00	5,40	1240,00	4,60	12
7	26,99	6,20	1157,14	5,74	14
Mean	26,99	5,80	1191,67	5,25	26

Table 20. Control points from group 3.

Control point	**Effective temperature (ºC)**	**CO (%)**	**CO_2 (%)**	**NO_x (%)**	**Number of measures**
10	28,68	8,00	1500,00	7,97	13
12	27,60	6,17	1450,00	7,66	10
13	25,82	6,00	1300,00	6,36	10
14	26,30	6,00	1362,50	6,03	14
Mean	27,26	6,65	1413,89	7,10	47

Group 3 has higher effective temperatures and gas concentrations than Group 2. These values are in accordance with the analysis of the auxiliary ventilation system previously done.

3.2.2.2. Cabanasses mine

As the ventilation layout of Cabanasses is different compared to Vilafruns, the analysis will need another approach. The intake and return do not need a distinction per groups, because the employees that are working in those parts do not have a permanent workplace, moving from one part to another such as electricians, mechanics, conveyor maintenance, auxiliary workings, etc. Therefore, the most important are the environmental mean values in the intake and return. On the other hand, continuous miners in workshops and working faces receive clean air without any recirculation.

In this mine, the main problems come from the gases generated individually in each working face and temperature levels. There are two main exploitation zones, thus the database has been managed according to this characteristic. From now on the control points will be referred as north and south zones as it is indicated in Figure 48.

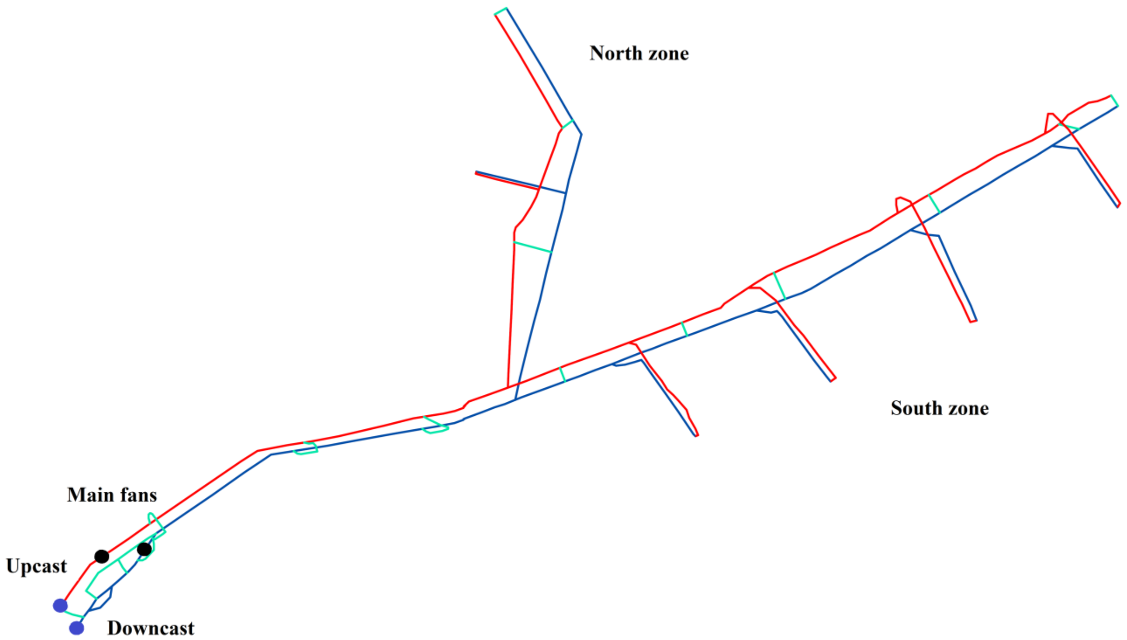

Figure 48. Cabanasses mine scheme with both zones.

3.2.2.2.1. Principal ventilation system

Tables 21 and 22 display the mean values of the environmental conditions from measures taken in the north and south zones regarding the intake.

Table 21. Environmental parameters measured in the south zone.

Control point	Effective temperature (ºC)	CO (%)	CO_2 (%)	NO_x (%)	Number of measures
1	19,03	0	375	0,25	14
2	20,58	0	466,67	0,17	14
3	22,61	0	533,33	0,83	14
4	21,8	0	475	0,75	14
5	23,14	0,5	575	1,13	14
6	23,51	3	520	0,8	15
7	26,36	0	666,67	0,83	17
8	26,63	0	825	1,25	13
9	28,05	3	1000	1,63	13
10	29,63	2,5	1008,33	2	17
11	30,65	4	1150	2,25	12

Table 22. Environmental parameters measured in the north zone.

Control point	Effective temperature (ºC)	CO (%)	CO_2 (%)	NO_x (%)	Number of measures
12	24,21	0	575	0,88	14
13	25,54	0	625	1,13	13
14	28,43	1,5	768,33	1,83	17

The number of measures in each control point varies depending on the availability of the place at the moment planned to take them.

Figures 49 to 51 display the visual information from Table 21. Meanwhile values from Table 22 have not been plotted because there are too few control points to obtain a clear trend. When the north zone spread and there are more ventilation control points, an environmental conditions tendency will also be possible.

In addition, CO values from south zone are neither plotted due to the wide disparity of the values.

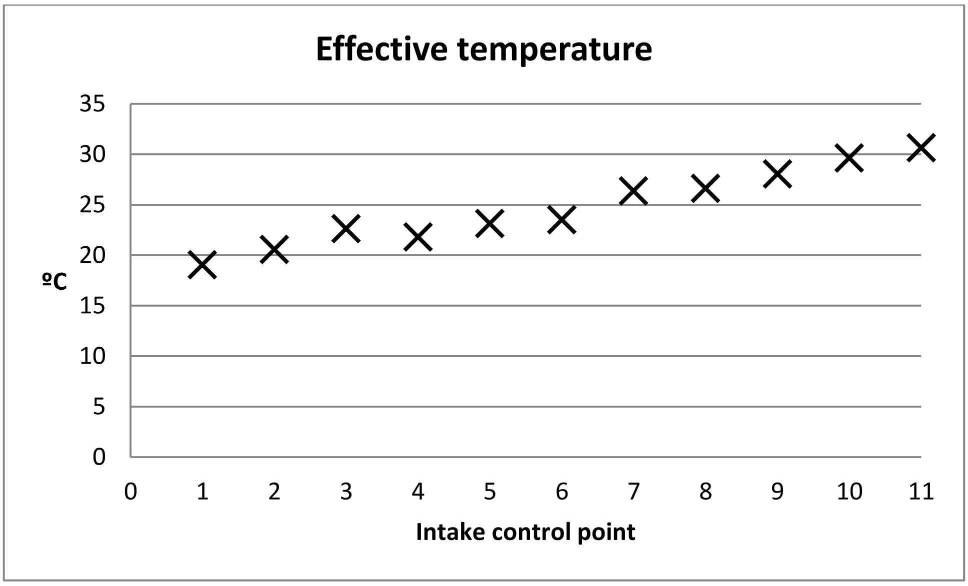

Figure 49. Effective temperature from the intake in the south zone.

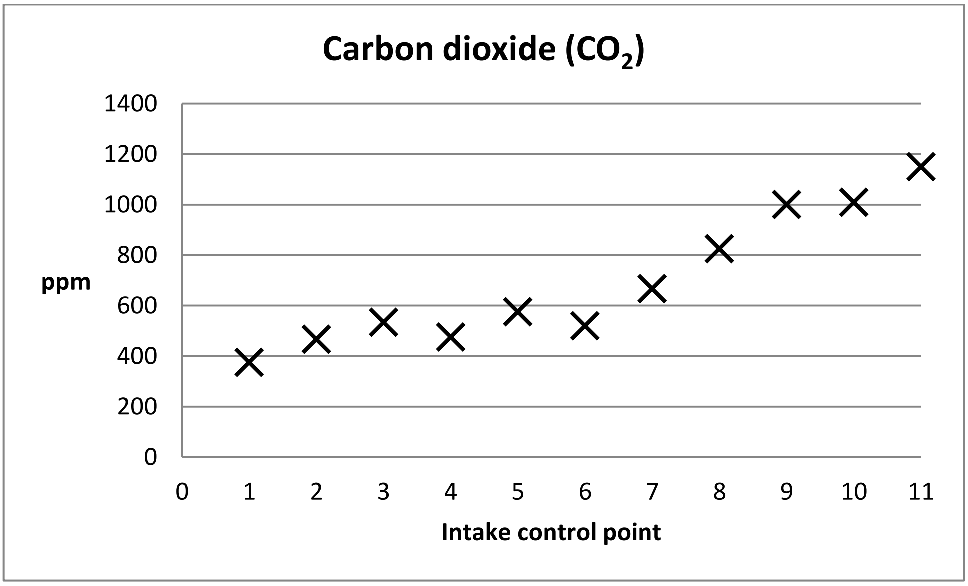

Figure 50. Carbon dioxide behaviour from the intake in the south zone.

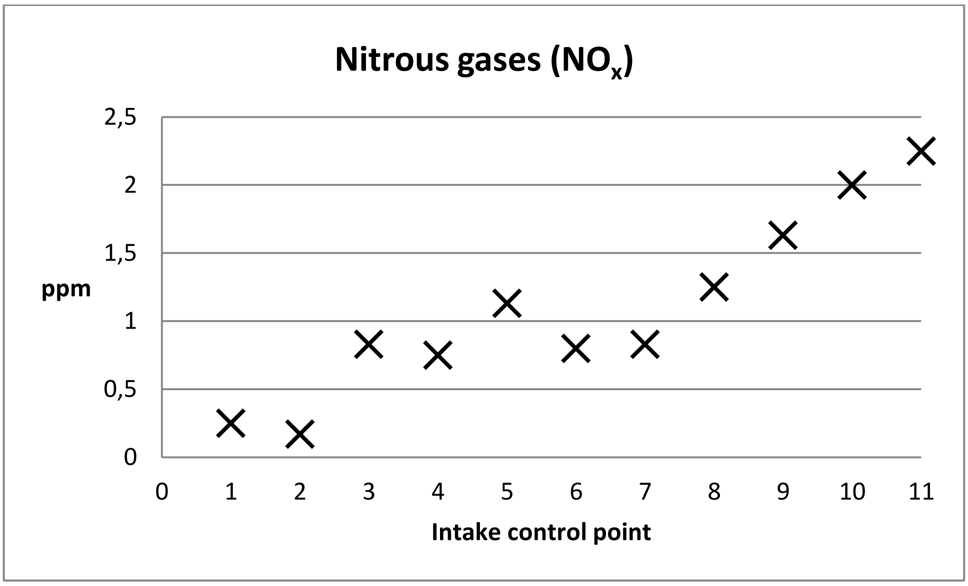

Figure 51. Nitrous gas behaviour from the intake in the south zone.

It can be seen that there is an increasing trend of gas concentrations and effective temperatures as the control point is further from the intake shaft. However, points are not equally separated among them. Table 23 indicates the actual distance of each control point from the downcast. This information is needed for modelling the behaviour of the mine in the intake.

Table 23. Actual distance of each control point from the downcast.

Control point	Horizontal distance (m)
1	60
2	454
3	530
4	714
5	2109
6	2319
7	3569
8	4064
9	4344
10	4494
11	4714

These values can be useful to predict the environmental conditions in new openings. Mean values from each point are linked to their actual distance from the downcast. Figures 52 to 54 display the tendency of the intake in the south zone. As it was previously stated, the north zone and CO values have not been plotted due to lack of information.

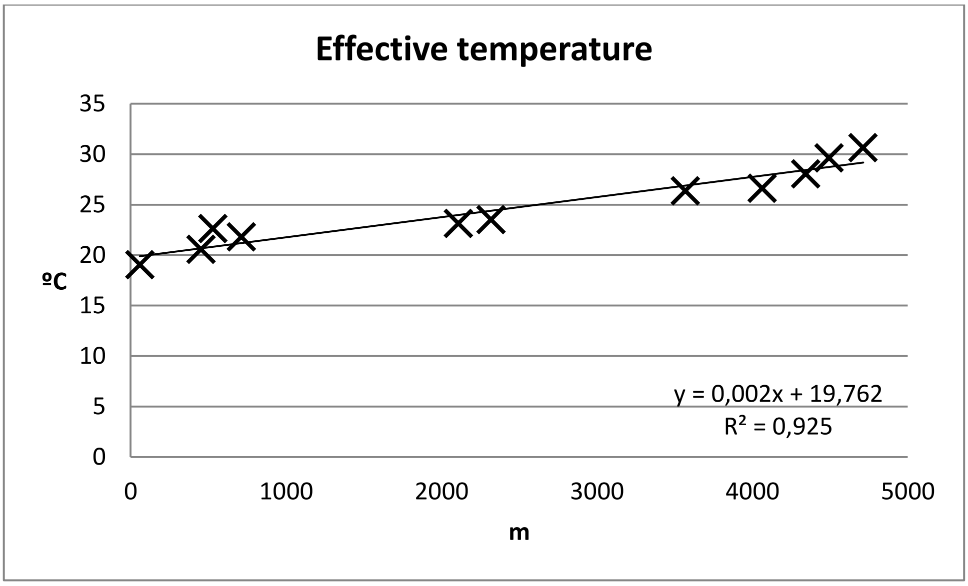

Figure 52. Effective temperature trend in the intake, south zone.

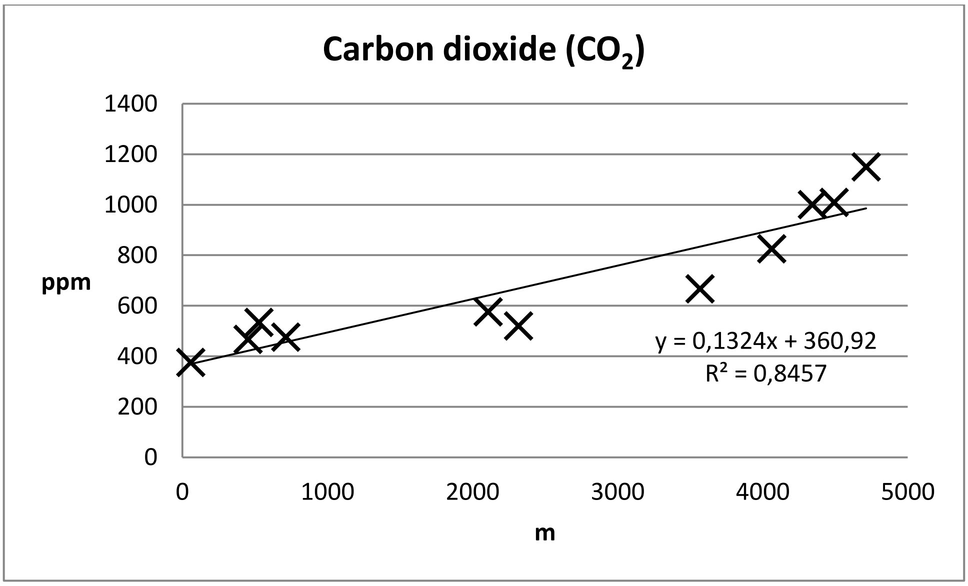

Figure 53. Carbon dioxide trend in the intake, south zone.

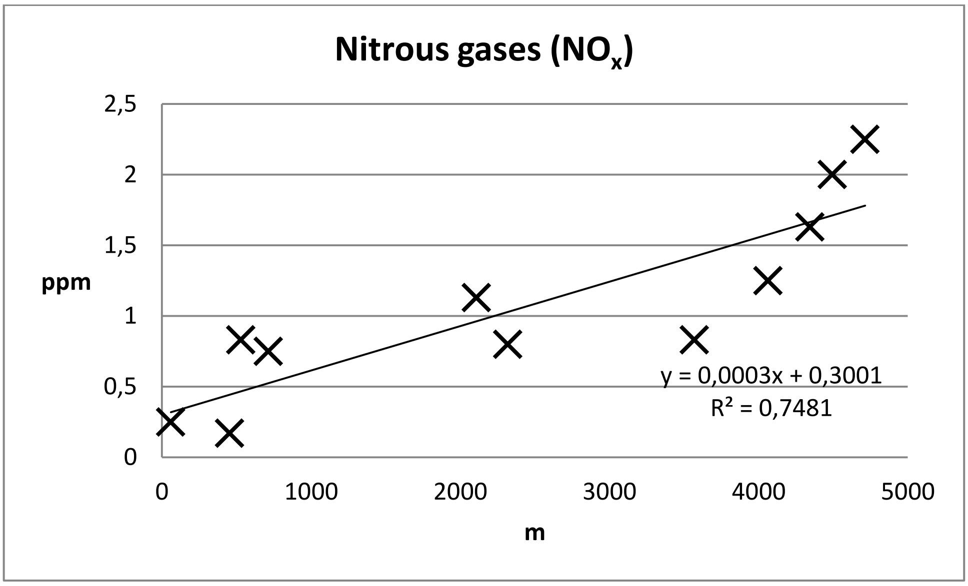

Figure 54. Nitrous gases trend in the intake, south zone.

Previous Figures display a trend to increase the effective temperature, CO and NO_x, but it is not until last control points that the increment is clear, probably due to it is where new openings are placed and there are the majority of the mining equipment. Figures 55 to 57 gather the information regarding the last four points (points 8, 9, 10 and 11).

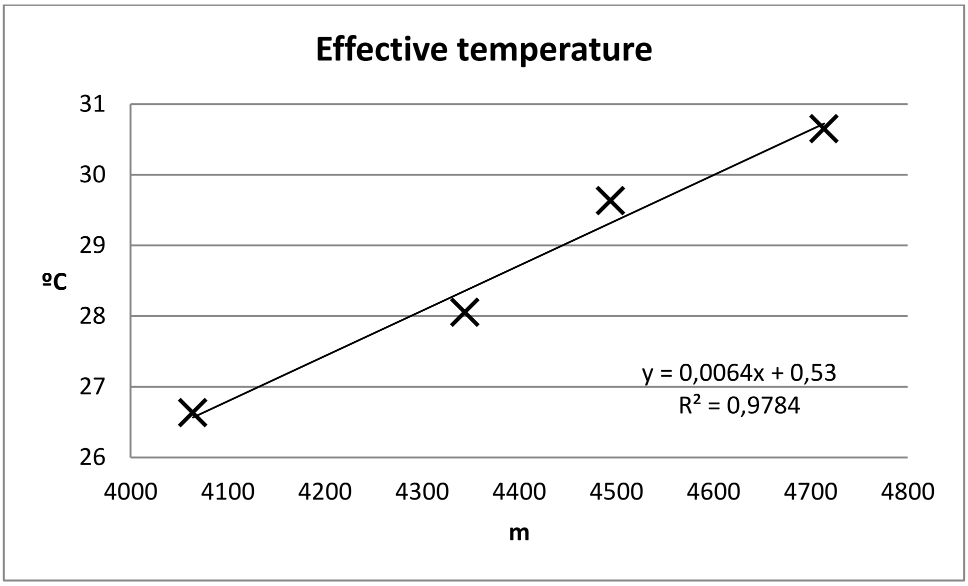

Figure 55. Mean effective temperatures of the last four control points.

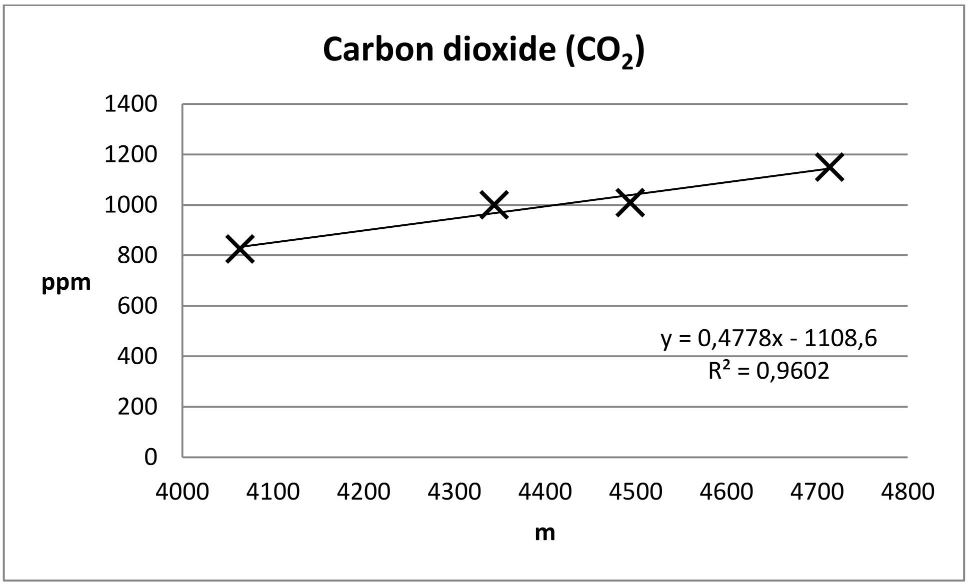

Figure 56. Mean carbon dioxide values of the last four control points.

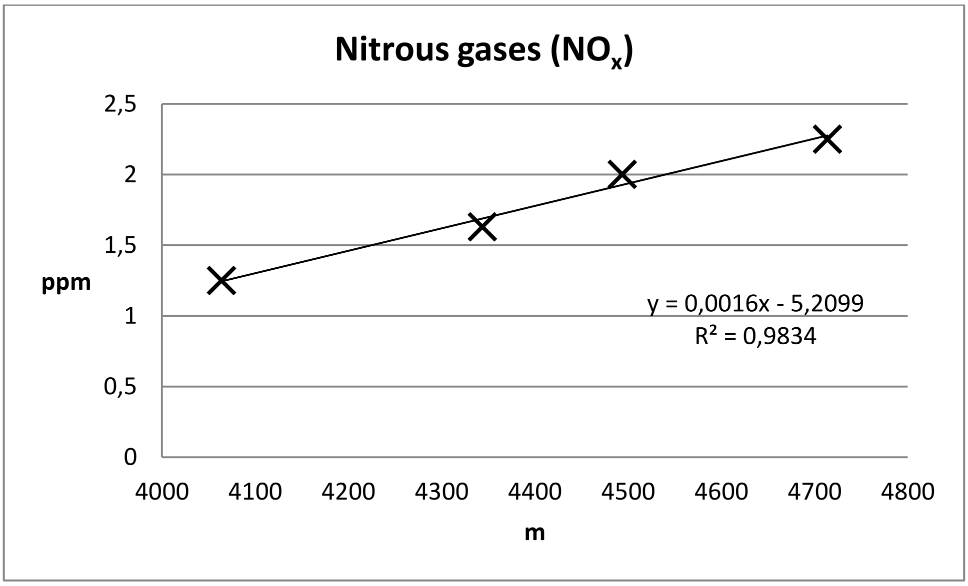

Figure 57. Mean nitrous gas values of the last four control points.

Last three Figures give a clear approach of the future conditions in hypothetical new openings in the south zone. Giving the possibility to calculate the CO, NO_x and effective temperatures through equations exposed in the graphs. Still, more intermediate points should be stablished to achieve results with higher representativeness.

The equations below and their coefficient of determination display the future behaviour of effective temperatures, CO_2 and NO_x in the south zone as well as the adjustment of the possible results.

Effective temperature:

$$y = 0{,}0064 \cdot X - 0{,}53 \qquad (23)$$
$$R^2 = 0{,}9784$$

Carbon dioxide (CO_2):

$$y = 0{,}4778 \cdot X - 1108{,}6 \qquad (24)$$
$$R^2 = 0{,}9602$$

Nitrous gases (NO_x):

$$y = 0{,}0016 \cdot X - 5{,}2099 \qquad (25)$$
$$R^2 = 0{,}9834$$

On the other hand, Table 24 shows the mean environmental conditions from the return. Individual values of each point are not relevant for the conditions of the employees in this zone of the mine, as it has been previously explained.

Table 24. Mean environmental conditions in the return, Cabanasses.

	Mean value	**Number of measures**
Effective temperature (ºC)	27,3	106
CO (ppm)	5	64
CO_2 (ppm)	1036,8	135
NO_x (ppm)	4,1	135

3.2.2.2.2. Auxiliary ventilation system

The auxiliary ventilation system has been analysed globally and individually. Table 25 exposes the mean values per miner (working face), while Figures 58 to 62 compares each factor among all miners.

Table 25. Mean values of the environmental factors in the working faces.

Miner	Cabal (m^3/s)	Ef. temperature (ºC)	CO (ppm)	CO_2 (ppm)	NO_x (ppm)	Number of measures
1	9,17	27,94	7,67	1214,29	6,29	12
2	9,15	29,13	9,57	1725,00	9,91	15
3	7,68	29,84	7,33	1675,00	8,06	12
4	11,56	29,45	8,64	1463,64	7,35	11
5	10,50	28,83	6,71	1183,33	5,00	12
6	10,54	27,76	6,44	1090,00	4,48	10
7	10,92	29,55	6,33	1254,55	7,15	12
8	8,49	30,25	5,08	1310,91	4,77	9
9	6,74	30,60	3,00	1833,33	6,05	9
10	16,57	27,65	6,00	1175,00	6,25	9
11	11,96	27,49	7,14	945,45	3,89	12
12	5,82	31,27	3,00	1133,33	2,47	9
13	7,13	30,19	9,43	1585,71	6,69	8
14	9,11	31,90	3,00	1400,00	3,48	5
Mean	9,54	29,18	7,05	1340,19	6,12	145

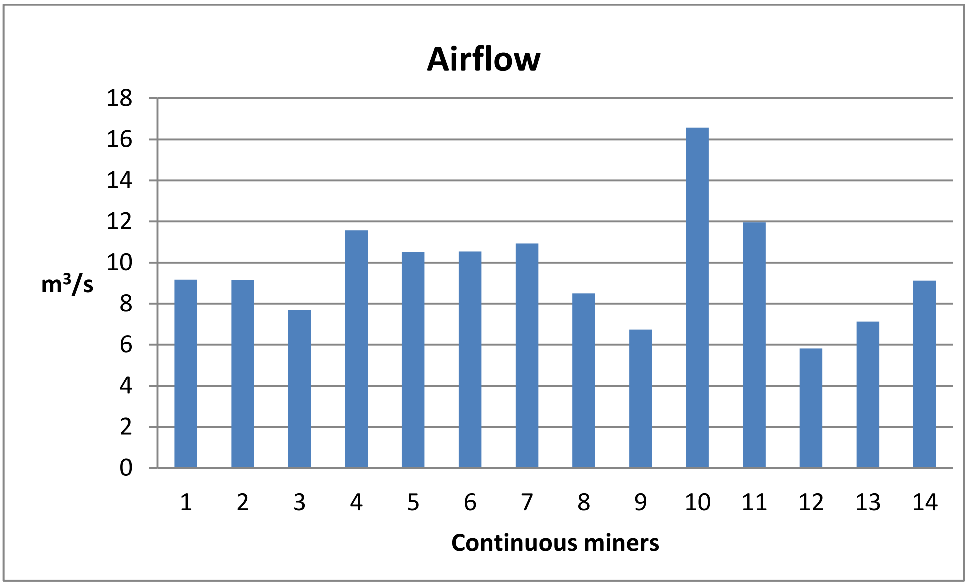

Figure 58. Amount of airflow per continuous miner.

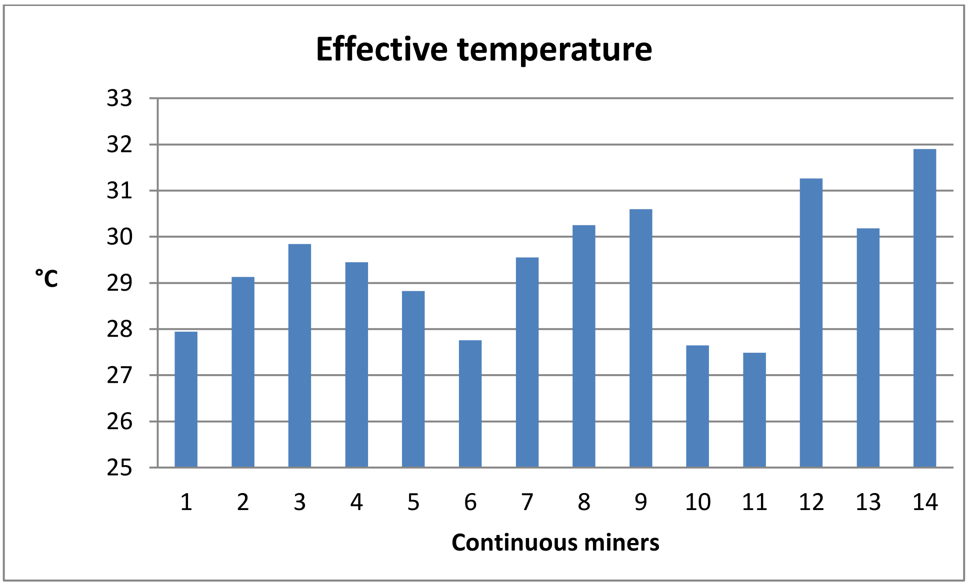

Figure 59. Effective temperature per continuous miner.

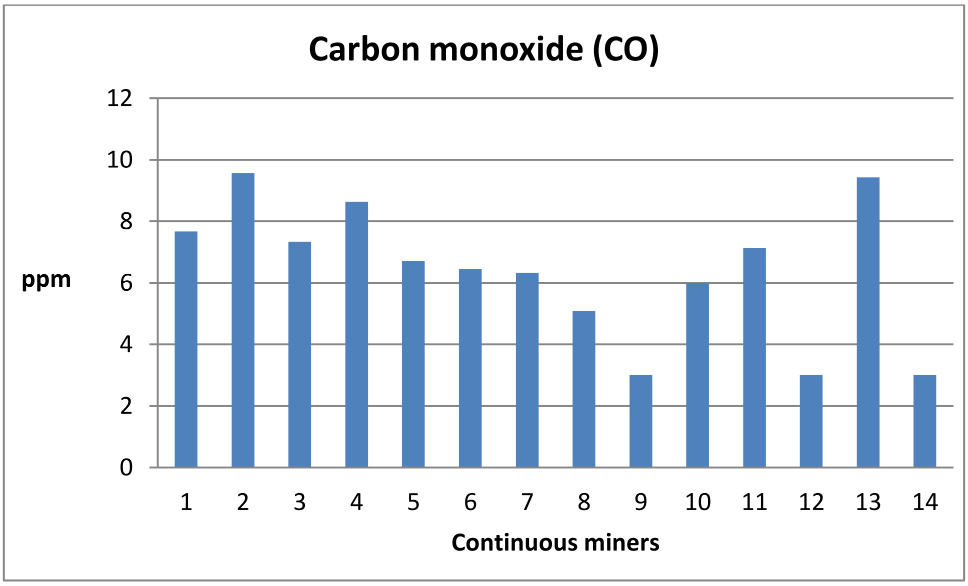

Figure 60. CO concentration per continuous miner.

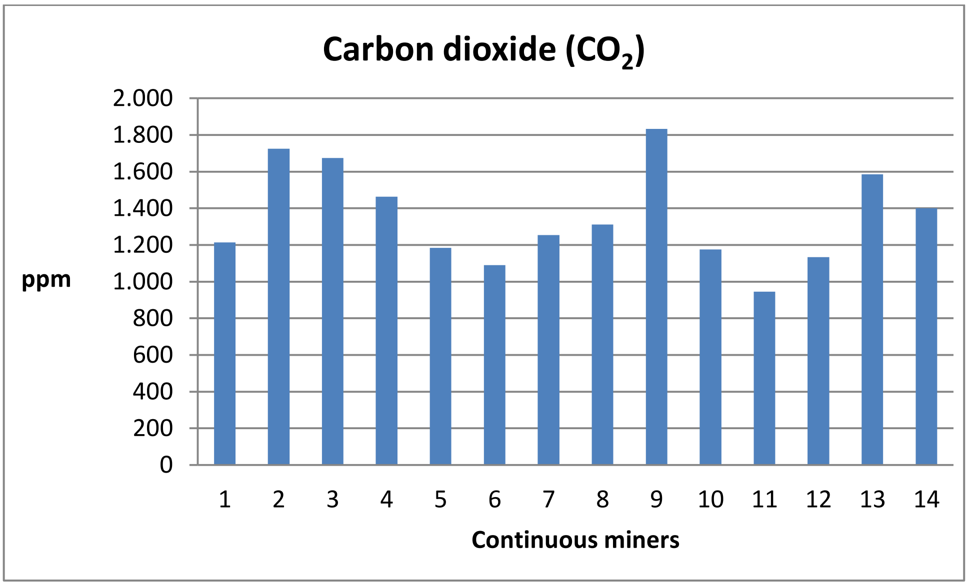

Figure 61. CO_2 concentration per continuous miner.

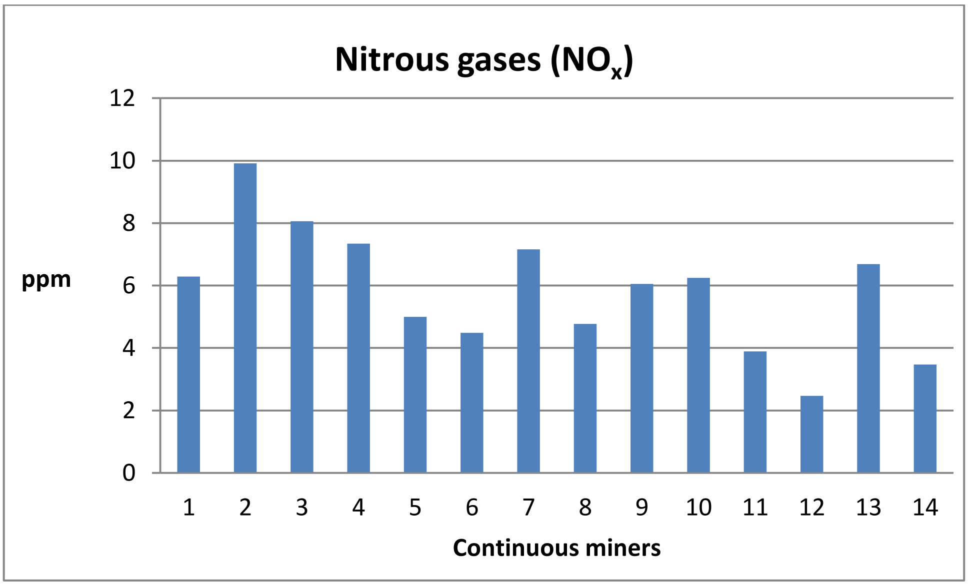

Figure 62. NO_x concentration per continuous miner.

Individual analysis and mean values have considerable differences among them in gas concentrations, airflow and effective temperatures. Probably, the contrast is because of local factors from each working face or workshop. The auxiliary ventilation system of each one should be assessed to know if the circuit it is properly set up and the effectiveness of it.

3.2.2.3. Other outcomes

The system can also be used to complement other software or feed them with the correct data. It can give a selection of the data for further processing.

In this case, the GIS has been used to provide data to VnetPro+ and ClimSim (see the software functioning in section 9). Figure 63 exposes the temperature evolution when the air from the leakages returns to the intake though the doors.

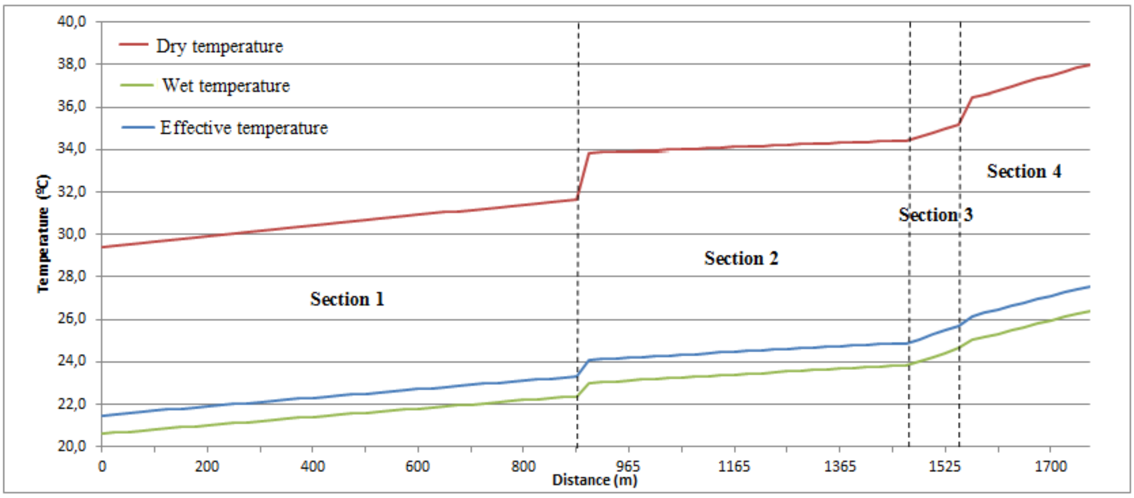

Figure 63. ClimSim modelling of the temperature along the intake in Cabanasses.

3.3. Friction factor determination

Friction factor is a key issue to model the ventilation circuit in any underground mine and know the air behaviour. It effects and determines the airflow supply along the mine and therefore the viability of mine operations. This parameter depends on the exploitation method, natural characteristic of the geological layers and any other specific condition of the mine. Actually, it can vary from one part to another within the same exploitation as well. Hence, the obtaining of these factors will be very important.

As it has been previously stated, there is a lack of information about friction factors in potash mining. For this reason, they have been determined following the steps described in the paragraphs below. The study has been carried out in both mines.

3.3.1. Methodology

According to the section "fundamentals of mine ventilation" from this dissertation, friction factors can be obtained using the expression detailed below, which is a form of the Cherzy-Darcy equation and it can be obtained combining equations 1, 4 and 9.

$$\mathrm{p} = f\mathrm{L}\frac{\mathrm{Per}}{\mathrm{A}}\rho\frac{u^2}{2} \tag{26}$$

Where:

f – Coefficient of friction (dimensionless);

p – Pressure loss (Pa);

Per – Airway perimeter (m);

A – Area (m^2);

ρ – Air density (kg/m^3);

u – Air velocity (m/s);

L – Length of the airway (m).

Later on, it was adapted to the well-known Atkinson's equation, expressed in frictional pressure drop, where all the variables have been previously described.

$$R = \frac{p}{Q^2} = kL\frac{Per}{A^3}\frac{\rho}{1.2} \qquad (27)$$

The Von Kármán equation gives a relationship with the friction factor of the Atkinson equation for turbulent flows. It is applicable to circular and non-circular airways, by means of the hydraulic mean diameter, following the relationship Dh=4A/Per, which is used to adapt noncircular diameters to the next equation.

$$f = \frac{2k}{\rho} = \frac{1}{4\cdot\left[2\cdot\log_{10}\left(\frac{Dh}{e}\right)+1.14\right]^2} \qquad (9)$$

Once the coefficient of friction is calculated through roughness in situ measures, friction factor can be obtained and subsequently the resistance of the airways and the whole mine using equation (8). The equivalent length factor, Leq, is used for obstructions in the airways.

$$R = k(L + Leq)\frac{per}{A^3}\frac{\rho}{1.2} \qquad (8)$$

Apart from roughness measures, it is necessary to determine air velocities, sections and perimeters. Air density is considered as 1,2 kg/m^3 due to its small influence in such calculations.

3.3.2. Roughness determination

First, the ventilation system have been analysed in order to know where are the places that could stand for the specific conditions of each mine and how many control points are needed. For their selection it has been taken into account that each one must be representative of the permanent features in the mine, avoiding temporary conditions, such as machines or material stacked in a certain place.

According to the conditions of the mines, 18 and 19 key points have been considered in Vilafruns and Cabanasses, respectively. Roughness of each point has been measured once every month during a year. It is important to take measures in different periods of the year because potash mines are influenced by the outer climatic conditions (pressure, temperature and humidity), affecting walls and roof of the tunnels and producing fractures and the fall of small rocks into the airways. Roughness is measured with a tape, five times in each point, and then the average is taken as the monthly value. Figure 64 displays an example of the points used to obtain the friction factors, detailing their specific characteristics. The rest are attached in the appendix.

Control point	**1**
Description: Point after the main fan, which propels the airflow to the tunnels and workings.	Coordinates: X: 406366 Y: 4632678

Data:

Section	34,54 m^2
Perimeter	24,09 m
Mean roughness	0,149 m
Friction factor k	0,00826 kg/m^3

Theoretical frame

Real frame

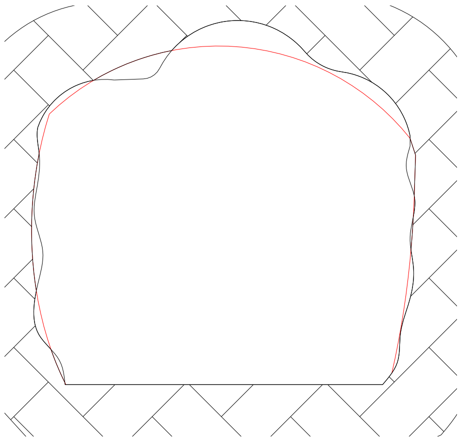

Figure 64. Control point description.

3.3.3. Results

Data collected from both mines have been processed separately, Vilafruns and Cabanasses, and then the outcomes are compared between them and with other types of mining.

3.3.3.1. Vilafruns

Table 26 shows the mean values used to calculate the friction factors, taking special relevance the coefficient of friction (*f*), which is function of the other data from the table. They have been measured in situ or calculated using the data collected and the equations previously detailed.

Table 26. Mean parameters used to calculate the friction factors.

Point	A (m^2)	Per (m)	Dh (m)	e (m)	*f*
0	40,00	24,60	6,50	0,36300	0,01880
1	34,54	24,09	5,74	0,14900	0,01345
2	31,84	22,60	5,64	0,14390	0,01336
3	34,04	23,22	5,86	0,13260	0,01273
4	27,86	21,85	5,10	0,11000	0,01250
5	34,80	23,24	5,99	0,14170	0,01296
6	28,37	21,50	5,28	0,23330	0,01687
7	23,86	17,50	5,45	0,23750	0,01676
8	31,54	25,00	5,05	0,11910	0,01295
9	32,29	23,09	5,59	0,30000	0,01845
10	27,83	22,03	5,05	0,18240	0,01543
11	26,89	20,73	5,19	0,11440	0,01261
12	24,36	18,00	5,41	0,10000	0,01178
13	35,96	26,28	5,47	0,12000	0,01258
14	21,61	20,00	4,32	0,17480	0,01622
15	31,33	19,34	6,48	0,17480	0,01366
A	29,82	21,89	5,45	0,30000	0,01868
D	33,40	23,00	5,81	0,23750	0,01630
Mean				0,18522	

Values displayed in Table 27 correspond to the mean friction factors per season and the global value per point, taking into account the four season values in each key point, as well as their corresponding standard deviation (Box et al., 2005).

Table 27. Mean friction factors and standard deviation from each point.

Point	**Spring k (kg/m^3)**	**Summer k (kg/m^3)**	**Autumn k (kg/m^3)**	**Winter k (kg/m^3)**	**General value k (kg/m^3)**	**Standard deviation**
0	0.01163	0.01134	0.01168	0.01184	0.01162	0.00021
1	0.00821	0.00801	0.00822	0.00838	0.00820	0.00015
2	0.00835	0.00848	0.00835	0.00853	0.00843	0.00009
3	0.00794	0.00778	0.00787	0.00802	0.00790	0.00010
4	0.00781	0.00796	0.00781	0.00796	0.00788	0.00009
5	0.00743	0.00701	0.00750	0.00739	0.00733	0.00022
6	0.00876	0.00872	0.00875	0.00933	0.00889	0.00029
7	0.00860	0.00856	0.00857	0.00856	0.00857	0.00002
8	0.00894	0.01014	0.00900	0.00940	0.00937	0.00055
9	0.00947	0.00787	0.00952	0.00900	0.00896	0.00077
10	0.00890	0.00890	0.00900	0.00893	0.00893	0.00005
11	0.00735	0.00729	0.00738	0.00732	0.00733	0.00004
12	0.00690	0.00686	0.00677	0.00677	0.00682	0.00007
13	0.00798	0.00855	0.00803	0.00821	0.00819	0.00026
14	0.00956	0.00956	0.00963	0.00956	0.00958	0.00003
15	0.00758	0.00694	0.00821	0.00759	0.00758	0.00052
A	0.01081	-	0.01207	0.01088	0.01125	0.00071
D	0.00956	-	0.00972	0.00960	0.00963	0.00009

It has to be pointed out that there are no results in the points called A and D during summer, because the ventilation circuit was partially modified.

3.3.3.2. Cabanasses

Tables 28 and 29 detail the coefficient of friction, friction factors per season and other parameters needed to calculate the global friction factor from each point.

Table 28. Mean parameters used to calculate the friction factors.

Point	A (m^2)	Per (m)	Dh (m)	e (m)	*f*
A	40,03	27,49	5,82	0,09000	0,01102
1	30,29	21,83	5,55	0,10600	0,01193
B	25,47	21,17	4,81	0,06200	0,01033
C	25,60	20,93	4,89	0,05600	0,00991
D	34,50	26,23	5,26	0,04800	0,00918
4	20,79	18,37	4,53	0,05500	0,01012
I	31,02	22,97	5,40	0,06300	0,00999
G	38,28	27,44	5,58	0,05200	0,00924
R	32,83	22,62	5,81	0,10600	0,01173
H	49,45	29,66	6,67	0,11400	0,01144
11	27,37	20,72	5,28	0,12000	0,01275
12	34,91	23,95	5,83	0,11700	0,01214
V	19,49	17,84	4,37	0,09500	0,01254
K	28,64	20,92	5,48	0,15800	0,01402
L	32,84	27,81	4,72	0,06600	0,01063
M	30,85	21,67	5,69	0,16300	0,01401
N	47,80	29,47	6,49	0,15300	0,01293
9	29,98	23,13	5,18	0,16200	0,01450
8	26,32	20,92	5,03	0,21000	0,01644
Mean				0,10505	

Table 29. Mean friction factors and standard deviation from each point.

Point	**Spring k (kg/m^3)**	**Summer k (kg/m^3)**	**Autumn k (kg/m^3)**	**Winter k (kg/m^3)**	**General value k (kg/m^3)**	**Standard deviation**
A	0,00655	0,00665	0,00664	0,00661	0,00661	0,00005
1	0,00709	0,00686	0,00720	0,00716	0,00708	0,00015
B	0,00614	0,00594	0,00623	0,00620	0,00613	0,00013
C	0,00589	0,00570	0,00598	0,00595	0,00588	0,00012
D	0,00546	0,00555	0,00554	0,00551	0,00551	0,00004
4	0,00601	0,00582	0,00610	0,00607	0,00600	0,00013
I	0,00594	0,00633	0,00603	0,00600	0,00607	0,00017
G	0,00549	0,00531	0,00557	0,00554	0,00548	0,00012
R	0,00697	0,00675	0,00708	0,00704	0,00696	0,00015
H	0,00680	0,00658	0,00690	0,00687	0,00679	0,00014
11	0,00758	0,00733	0,00769	0,00765	0,00756	0,00016
12	0,00794	0,00699	0,00733	0,00729	0,00739	0,00040
V	0,00745	0,00721	0,00756	0,00752	0,00743	0,00016
K	0,00833	0,00806	0,00845	0,00841	0,00831	0,00018
L	0,00632	0,00611	0,00641	0,00638	0,00631	0,00013
M	0,00832	0,00805	0,00844	0,00840	0,00830	0,00018
N	0,00769	0,00744	0,00776	0,00776	0,00766	0,00015
9	0,00862	0,00834	0,00874	0,00870	0,00860	0,00018
8	0,00978	0,00946	0,00992	0,00987	0,00976	0,00021

3.3.3.3. Results comparison

Once friction factors are determined, a comparison between both mines and the current bibliography is useful to know the margin variation and concordance of the outcomes. Table 30 compares the mean friction factor from all the points depending on the season in Vilafruns and Cabanasses.

Table 30. Comparison of the friction factors per season.

	Spring k (kg/m^3)	Summer k (kg/m^3)	Autumn k (kg/m^3)	Winter k (kg/m^3)	General value k (kg/m^3)	Standard deviation
Vilafruns	0,00865	0,00837	0,00878	0,00874	0,00869	0,00024
Cabanasses	0,00707	0,00687	0,00714	0,00710	0,00704	0,00016
Dif. (%)	22,4	21,9	23,1	23,0	23,4	52,4

Although values are quite similar, friction factors from Cabanasses are lower in all seasons than in Vilafruns, having a difference of 23,4% between both mines. Thus, Cabanasses will offer better conditions for the air to flow. However, there are other features that influence this flow, as it has been stated in previous sections.

Figure 65 show a graph comparing the friction factors in both mines and their evolution along the seasons. As it can be seen, their trends are quite similar, having higher values in spring and autumn than in winter and summer. This relation could be because the zone where mines are placed spring and autumn have important variations in climate and humidity conditions, affecting the air going down through the downcast and therefore the stability of roofs and walls in the airways suffer, increasing the roughness a subsequently the friction factor values.

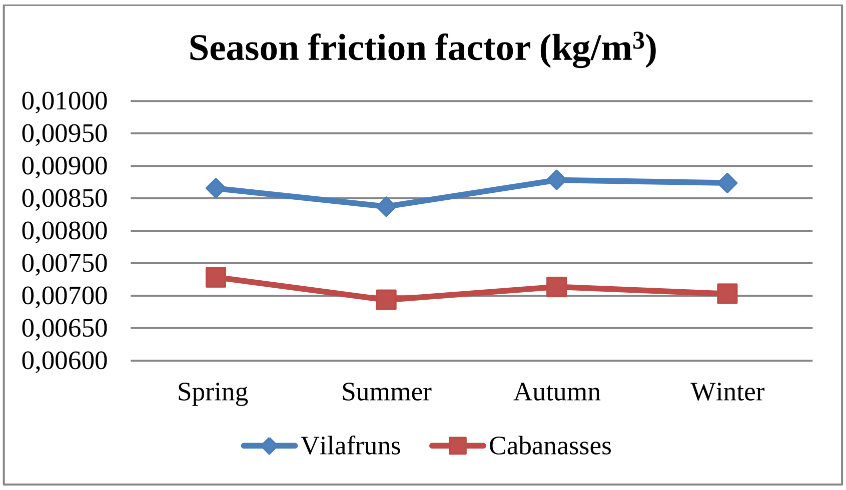

Figure 65. Graph of the friction factor per season

As there are no bibliographical values from potash mines, the comparison is done with friction factors from coal and metal mines. Tables 31 and 32 compare the results with published data.

Table 31. Comparison between published data and the values obtained.

Airway type	Prosser and Wallace (2002)	McPherson (2009)	Hartman et al. (1997)	Potash mine values
Rectangular Airway – Clean Airway (Coal and soft rocks)	0,0076	0,0075	0,009	0,008
Rectangular Airway – Some Irregularities (Coal and soft rocks)	0,0076	0,0087	0,009	0,0091
Metal Mine Drift	0,0122	0,0088	0,012	0,0269
Metal Mine Ramp	0,0082	0,0116	-	0,0297

The comparison from the ramp airway type has only been done with values from Vilafruns, because there is no ramp in Cabanasses. The other values are obtained using data from both mines, regarding the information collected in the control points included in the appendix and matching the points with more similarities to the airway type according to the bibliographical information. In addition, Table 32 analyse the percentage difference from values gathered in Table 31.

Table 32. Percentage difference between the values obtained and the bibliography values.

Airway type	Potash mine values	Difference (%)		
		Prosser and Wallace (2002)	McPherson (2009)	Hartman et al. (1997)
Rectangular Airway – Clean Airway	0,0076	-1,32	18,42	5,26
Rectangular Airway – Some Irregularities	0,00762	14,17	18,11	19,42
Mine Drift	0,01215	-27,57	-1,23	121,40
Mine Ramp	0,00823	40,95	-	260,87

It can be summarised that friction factors from potash mining are quite similar to values from coal and metal mines. Despite the results are usually higher than in other types of mining, outcomes from the ramp part are significantly different, perhaps due to fewer data available.

3.3.4. Validation

The friction factors obtained have been used to model both mines with ventilation software, VnetPro+, and subsequently a comparison between the airflow modelled and the in situ measures have been done, either in Cabanasses or Vilafruns.

3.3.4.1. Vilafruns

Four different models, corresponding to the four season of the year with their friction factors, have been carried out in the case of Vilafruns (see appendix II) and the results are consistent. Table 33 gathers the airflow variation in Vilafruns regarding the in situ measures and modelling outcomes. Taking into account the mean friction factor values and airflow of the whole year.

Table 33. Comparison between the measures and the modelling results in Vilafruns.

Control point	Percentage variation (%)	Absolute variation (m^3/s)	Description
0	0,79	1,41	Beginning of the ventilation circuit
1	0,67	1,18	Intake after the main fan
2	2,99	1,03	Leakage 1
3	2,17	3,03	Intake intermediate position
4	1,31	1,51	Leakage 2
5	17,62	2,68	Entry workshop 1
6	5,55	1,50	Leakage 3
7	22,34	3,50	Leakage 4
8	27,38	3,45	Leakage 5
9	2,85	2,65	workshop north zone
10	6,34	7,06	Intake south zone
11	2,37	2,96	intake south zone intermediate
12	1,51	2,14	Return
13	2,53	4,29	Ramp
14	26,88	2,29	Leakage 6
A	9,61	6,76	Recirculation workshops north and 1
D	15,16	3,47	Leakage 7

The modelling outcomes are satisfactory, having only appreciable variations in some leakages in terms of percentage.

3.3.4.2. Cabanasses

Following the same procedure of the previous subsection, Table 34 gathers the airflow percentage variation between the control point measures and the ventilation circuit modelled. As the different configurations depending on the season did not show a significant variation, it has only been done a modelling with the mean values in the case of Cabanasses.

Table 34. Comparison between the measures and the modelling results in Cabanasses.

Control point	Percentage variation (%)	Absolute variation (m^3/s)	Description
A	8,83	18,40	Begin. of the ventilation circuit
B	9,69	1,51	Leakage 1
C	3,36	1,81	Storage connection
D	0,63	1,21	Main intake
G	8,62	6,13	Beginning of the north zone
H	3,30	2,44	Intermediate north zone
I	4,55	4,06	Beginning of the east zone
K	6,45	2,22	Entry workshop 1
L	6,33	5,19	Intermediate east zone
M	4,19	1,00	Entry workshop 2 a
N	13,60	8,59	Entry workshop 2 b
R	296,50	8,48	Leakage 2
1	11,62	2,45	Leakage 3
4	5,29	8,34	Return connexion zones
8	0,58	0,62	Return workshop 1
9	5,79	6,21	Return workshop 2
11	3,97	2,94	Return north zone ending
12	3,75	2,67	Return north zone intermediate
V	2,45	5,11	Exit

Except the values from one of the leakages, where the percentage variation is important but not the airflow quantity, the other results display a strong similarity.

3.4. Heat sources study

Environmental conditions inside an underground mine are highly influenced by heat exchanges with strata and machinery due to the geological characteristics of the repository and the exploitation method. As it has been mentioned in the literature review, auto-compression in vertical shafts and fans also increase the temperature of the air.

This part is focused on determining the heat load from machinery and strata in potash mines using a room and pillar method. Afterwards it is proposed a change of the diesel equipment to electrical one because of fewer heat input produced and higher efficiency.

Internal combustion engines from diesel equipment have an overall efficiency only about one third of the one achieved by electrical units. Hence, the usage of diesel will produce approximately three times as much heat as electrical equipment for the same mechanical work output (McPherson, 2009). Obviously, this hypothetical change cannot be applied to all machines, but the aim would be to reduce it as much as possible within the possibilities of the mine.

Heat analysis has been backed by theoretical equations and two modelling software: VnetPro+, used to determine the air pressure drop and airway resistances, and ClimSim, which provides predicted values of the variation in psychometric and thermodynamic properties of the air regarding heat inputs from strata and machinery. For such purpose, data collected from 2009 to 2015 has been used, as well as bibliographic information when the first option was not possible. In addition, ClimSim has been used to determine some parameters impossible to obtain in situ without affecting the mine operations. The study is focused on Vilafruns because of the huge quantity of data available. Overall, the sequence followed to determine the climate parameters and make the comparison is:

1. Gather and select the necessary data for modelling and apply theoretical equations, with the aid of the GIS created.
2. Modelling the ventilation circuit by means of VnetPro+ with the information collected in situ and the friction factors determined in the previous section.

3. Determine the rock thermal conductivity and diffusivity of the mine using ClimSim.
4. Calculate the current heat load from the strata and machinery, diesel and electrical, using ClimSim and theoretical equations.
5. Make a proposal of changing the diesel equipment for electrical one and determine the heat input variation to the ventilation circuit.

3.4.1. Data used

Data needed to determine the heat inputs have been either collected in situ, provided by the staff of the mine, calculated or found in previous publications.

- Airway dimensions: Cross section, length and perimeter measured in situ.
- Friction factors: Calculated in the previous section.
- Airflow: Measured in situ.
- Stopping, doors and any possible obstacle in the airways through field inspections. Resistance of doors and curtains to let the air pass through them is obtained from Carrasco et al. (2011).
- Fans characteristics: Provided by the staff of the mine.
- Temperatures: Dry and wet bulb temperatures measured in situ.
- Virgin rock temperature: Temperature of the rock immediately after being dug by a continuous miner.
- Depth of the tunnels and airways: Consulting the historical planning data in CAD format.
- Wetness factor: Obtained from bibliographical information (McPherson, 2009).
- Age of the tunnels: Consulting the historical planning data in CAD format.
- Geothermal gradient: It has been obtained from the “Institut Cartogràfic de Catalunya” (www.icc.cat), where there is a compilation of the geothermal gradients along Catalonia.
- Rock conductivity and diffusivity have been obtained from bibliographic references (McPherson, 2009) and afterwards the initial values have been adjusted by means of iterations using ClimSim.
- Daily face advance of the stopes where there are continuous miners working: Information provided by the staff of the mine.

- Electrical and diesel equipment characteristics: Nominal power, consumption, efficiency, number of machines, etc. The information has been obtained from the staff of the mine and commercial catalogues.
- Rate of water per litre of fuel: Obtained from McPherson (2009).

Age and depth of the tunnel are two factors from the list that have not been explained in the section “fundamentals of mine ventilation” because are specific parameters required for modelling by ClimSim. Within the software are called “age in”, “age out”, “depth in” and “depth out”. Factors “depth in” and “depth out” stand for the depth at the beginning and end of the airway modelled. On the other hand, the terms “age in” and age out” describe the time (in days) since beginning and end of the airways were opened.

3.4.1.1. Mining equipment

Tables 35-37 display a list of the current mining equipment in the mine before the change proposed and their features needed to determine the heat input.

Table 35. Current equipment of the mine.

Electrical machines	Diesel machines
Continuous miners	Underground trucks
Conveyors	Underground loaders
Continuous haulage machines	Jumbo drillings
	Auxiliary equipment
	Cars

Table 36. Diesel equipment characteristics.

Type	Quantity	N. Power (CV)	N. Power (kW)	Consumption (l/h)	Model
Truck	22	400	294	67	MT 436
Loader	12	300	221	58	ST 1030
Car	64	100	74	14	Iveco massif
Jumbo	3	90	66	14	-
Auxiliary equipment	6	88	65	14	-

The equipment detailed in Table 37 has been used together with their positions and lengths.

Table 37. Electrical equipment characteristics.

Type	Nominal power (kW)	Quantity
Continuous haulage machine	165	1
	180	1
	220	5
Conveyors	56	2
	110	1
	180	1
	200	2
	400	3
	600	6
Continuous miner	529	10

3.4.2. Determination of the fundamental heat parameters

3.4.2.1. VnetPro+ modelling

Before determining the heat parameters, airways pressure drop needs to be calculated since they are part of the parameters required by ClimSim.

First, the ventilation circuit has been imported in dxf format, which contain the X, Y and Z coordinates of the tunnels, into the VnetPro+. Figure 66 displays the modelling, distinguishing intake and return in different colours. Information of all the branches is attached in the appendix.

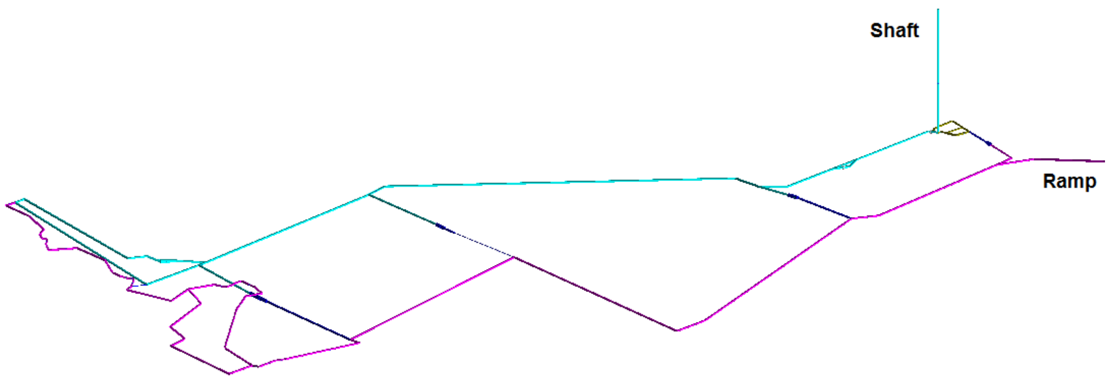

Figure 66. Principal ventilation circuit from Vilafruns modelled by means of VnetPro+.

Equations (1) and (4) are the basis of VnetPro+ internal functioning in terms of airflow behaviour. All variables involved have been previously explained.

$$\Delta P = R \cdot Q^2 \quad (1)$$

$$R = k \cdot L \cdot \frac{Per \cdot \rho}{A^3 \cdot 1{,}2} \quad (4)$$

As airways have different characteristics along the ventilation circuit, the software allows introducing the features of each branch. Figure 67 shows all the parameters needed to determinate or measure to model the ventilation circuit.

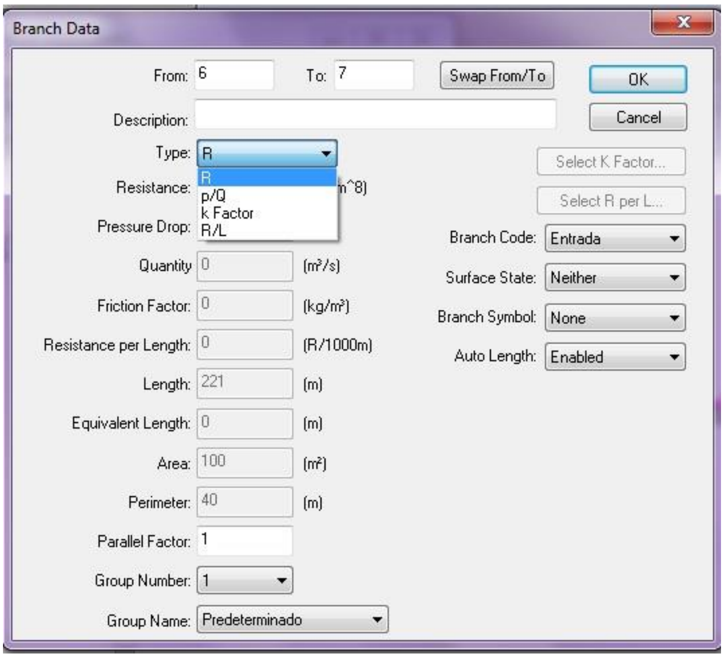

Figure 67. VnetPro+ branch characteristics.

Once the airways are defined, it is only necessary to know the position and curve of the main fans and boosters to model the ventilation. Subsequently, results of pressure drop and airflow can be plotted. Figures 68 and 69 show part of the modelling achieved.

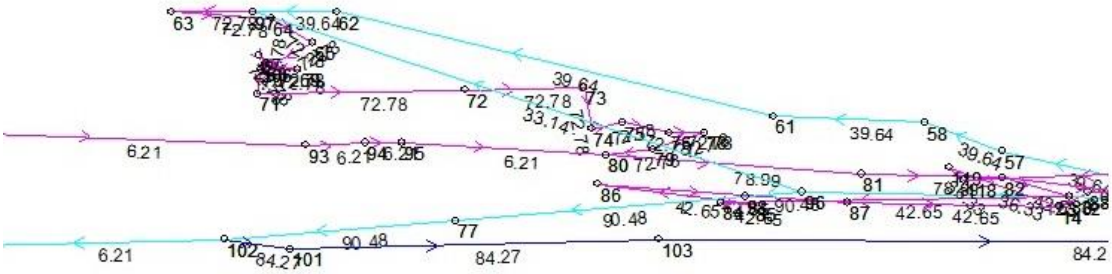

Figure 68. Scheme of Vilafruns and its ventilation characteristics.

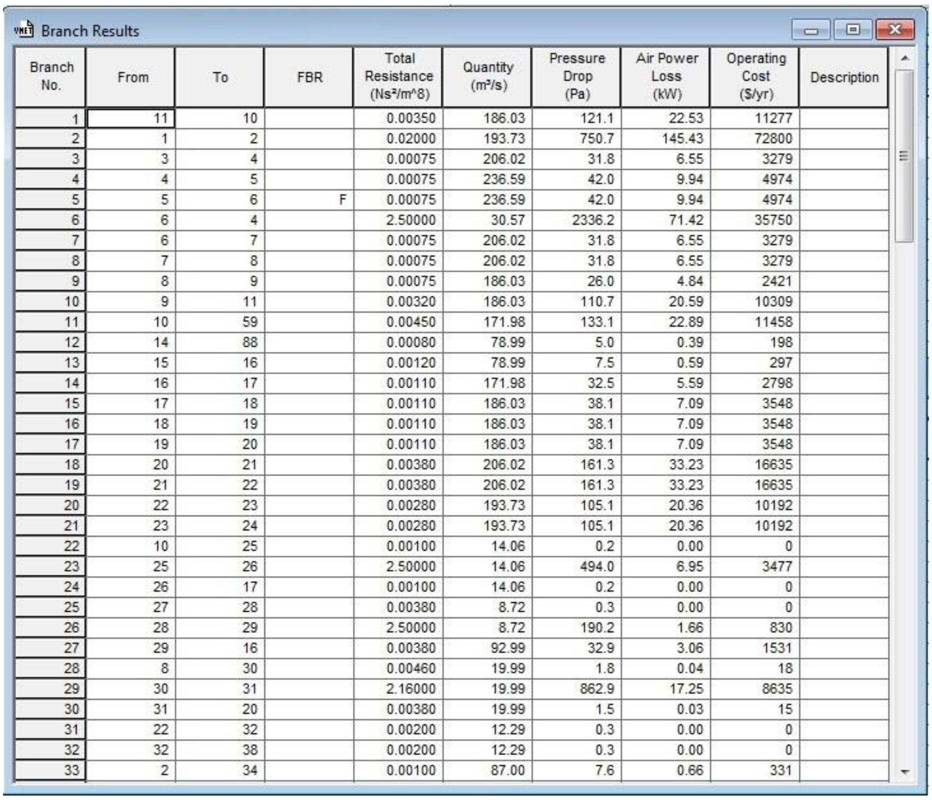

Branch Results

Branch No.	From	To	FBR	Total Resistance (Ns²/m^8)	Quantity (m³/s)	Pressure Drop (Pa)	Air Power Loss (kW)	Operating Cost ($/yr)	Description
1	11	10		0.00350	186.03	121.1	22.53	11277	
2	1	2		0.02000	193.73	750.7	145.43	72800	
3	3	4		0.00075	206.02	31.8	6.55	3279	
4	4	5		0.00075	236.59	42.0	9.94	4974	
5	5	6	F	0.00075	236.59	42.0	9.94	4974	
6	6	4		2.50000	30.57	2336.2	71.42	35750	
7	6	7		0.00075	206.02	31.8	6.55	3279	
8	7	8		0.00075	206.02	31.8	6.55	3279	
9	8	9		0.00075	186.03	26.0	4.84	2421	
10	9	11		0.00320	186.03	110.7	20.59	10309	
11	10	59		0.00450	171.98	133.1	22.89	11458	
12	14	88		0.00080	78.99	5.0	0.39	198	
13	15	16		0.00120	78.99	7.5	0.59	297	
14	16	17		0.00110	171.98	32.5	5.59	2798	
15	17	18		0.00110	186.03	38.1	7.09	3548	
16	18	19		0.00110	186.03	38.1	7.09	3548	
17	19	20		0.00110	186.03	38.1	7.09	3548	
18	20	21		0.00380	206.02	161.3	33.23	16635	
19	21	22		0.00380	206.02	161.3	33.23	16635	
20	22	23		0.00280	193.73	105.1	20.36	10192	
21	23	24		0.00280	193.73	105.1	20.36	10192	
22	10	25		0.00100	14.06	0.2	0.00	0	
23	25	26		2.50000	14.06	494.0	6.95	3477	
24	26	17		0.00100	14.06	0.2	0.00	0	
25	27	28		0.00380	8.72	0.3	0.00	0	
26	28	29		2.50000	8.72	190.2	1.66	830	
27	29	16		0.00380	92.99	32.9	3.06	1531	
28	8	30		0.00460	19.99	1.8	0.04	18	
29	30	31		2.16000	19.99	862.9	17.25	8635	
30	31	20		0.00380	19.99	1.5	0.03	15	
31	22	32		0.00200	12.29	0.3	0.00	0	
32	32	38		0.00200	12.29	0.3	0.00	0	
33	2	34		0.00100	87.00	7.6	0.66	331	

Figure 69. Collection of the internal information from each branch.

Once the circuit has been modelled, pressure drop results have been compared to theoretical validation to ensure its reliability. It is very important to know the pressure drop in the zones where ClimSim will be used.

The validation has not been done in whole ventilation circuit, it has only done in two stretches, between points 1-3 and 3-4 as it can be seen in Figure 70. The reason is because it will be used the same part of the circuit to determine some of the fundamental parameters from the strata heat of the mine. This specific part has been chosen because of the small interference of mining equipment as it is advised by the ClimSim user's manual.

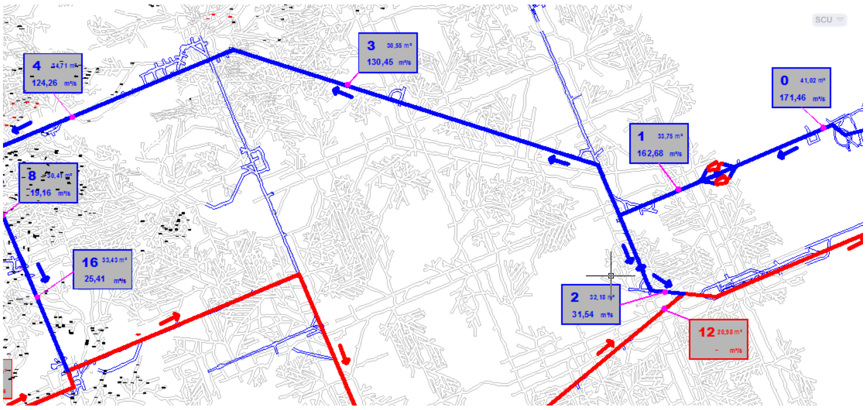

Figure 70. Ventilation circuit, detailing the airflow direction and airways in colours. The intake in blue and the return in red.

Pressure drop has been calculated using equations (1) and (3) and two methods: the procedure explained in Figures 13 and 14 (McPherson, 2009) and some empirical expressions regarding the airway variations from Carrasco Galán et al. (2011), exposed below. Its determination can be obtained with the following expressions and the planning information of the mine.

$$\varepsilon_k = 0{,}2 \cdot \frac{\delta}{90} + \left(\frac{\delta}{90}\right)^2 \qquad (28)$$

Where:

ε_k – Increasing resistance factor (dimensionless);

$\boldsymbol{\delta}$ – Rotation angle of the airway.

$$R_k = 0{,}61 \cdot \frac{\varepsilon_k}{A^2} \qquad (29)$$

Where:
R_k – Resistance added to the airway (Ns^2/m^8);
A – Airway section (m^2).

Table 38 displays the theoretical and modelled pressure drop results in the stretches analysed using both methods.

Table 38. Comparison of the theoretical and modelled pressure drop results.

Stretch	**VnetPro +**	**Theoretical**
1-3	140,57	142,22
3-4	93,98	99,26

There is a difference of 1,2% between theoretical and modelled values in the stretch 1-3 and 5,6% in the stretch 3-4. This difference has been considered as acceptable for a system with a very adverse environment in terms of measuring the conditions and where it is difficult to achieve accurate values. Therefore, the VnetPro+ modelling of the mine is confirmed as reliable concerning the geometrical characteristics of the airways as well as the pressure drop.

3.4.2.2. ClimSim modelling

Stretches displayed in Figure 70 are used to obtain the strata heat characteristics by means of ClimSim iterations from initial data, bibliographical values in this case. The adjustment of these values has to be done in a place as free as possible of equipment, specially of diesel machines, with the aim of avoiding any possible alteration in the moment of determine the strata heat parameters (M.V.S., 2013).

Following these conditions, parts chosen are at the beginning of the ventilation circuit. The survey has been done in two stretches instead of only one in order to achieve a higher accuracy. First stretch is from point 1 to 3 and the other one from point 3 to 4, Figure 70. It is the zone with the least possible disturbances in the airway and with a stable geometry along the time. Moreover, there are ventilation data in each point, which will be very important to run simulations. The only downside is the presence of a conveyor belt carrying mineral exploited along the part analysed.

The software takes into account the heat flow transferred to the air by radiation and convection methods. Determining the heat flow of a circular tunnel for a certain homogenous rock as Figure 71 describes.

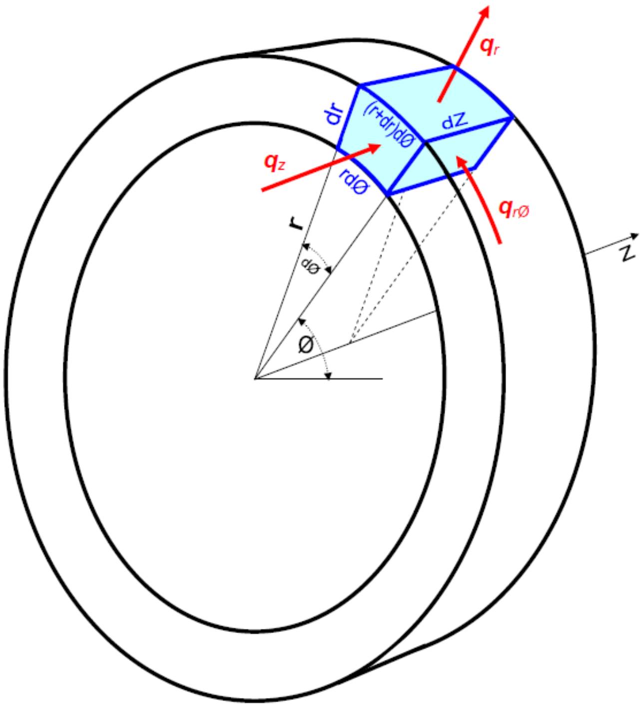

Figure 71. Heat flow in a hypothetical circular airway (McPherson, 2009).

The heat flow determination using ClimSim is based on radial heat conduction equations –expressed in polar cylindrical coordinates– detailed below. Equations (30) and (31) display two different forms of the same equation.

$$\frac{k}{\rho\cdot C}\left[\frac{\partial^2\theta}{\partial r^2}+\frac{1}{r}\left(\frac{\partial\theta}{dr}\right)+\frac{1}{r^2}\left(\frac{\partial^2\theta}{\partial\emptyset^2}\right)+\frac{\partial^2\theta}{\partial z^2}\right]=\frac{\partial\theta}{\partial t} \quad \text{ºC/s} \tag{30}$$

Or

$$k\left[\frac{r\partial^2\theta}{\partial r^2}+\left(\frac{\partial\theta}{dr}\right)+\frac{1}{r}\left(\frac{\partial^2\theta}{\partial\emptyset^2}\right)+r\frac{\partial^2\theta}{\partial z^2}\right]=r\rho C\frac{\partial\theta}{\partial t} \text{ W/m}^2 \tag{31}$$

Figure 72 is a simplified scheme of the ClimSim functioning based on the information from the user's manual.

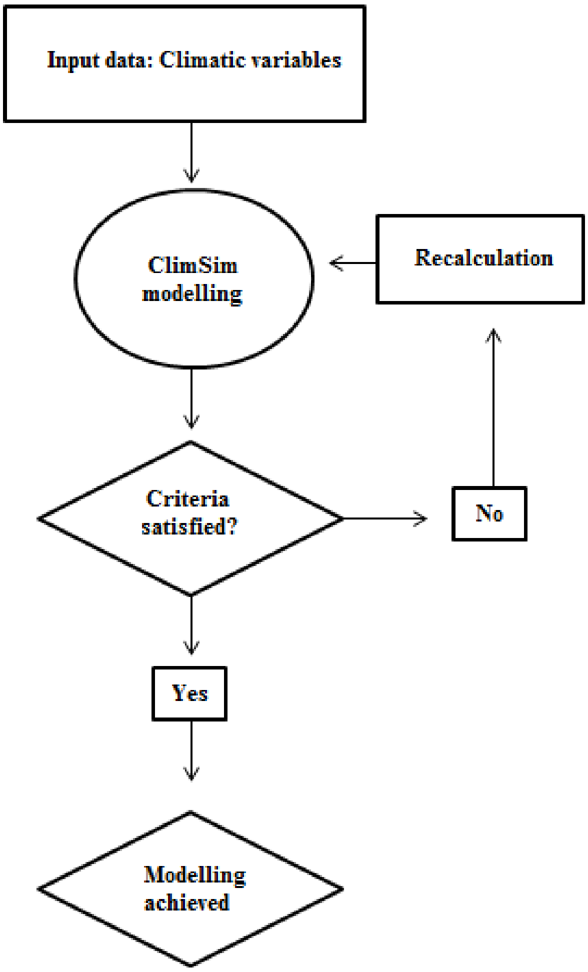

Figure 72. Scheme of the ClimSim functioning.

Computer modelling needs some previously determined parameters and characteristics of the stretches analysed. Parameters stated below have been either calculated or measured following the methodology explained in the section "fundamentals of mine ventilation" and in the "heat sources study, data obtaining". These required data are listed below.

- Dry bulb at inlet (ºC)
- Wet bulb inlet (ºC)
- Pressure at inlet (kPa)
- Airflow (m^3/s)
- Length (m)

- Depth in (m)
- Depth out (m)
- Cross section area (m^2)
- Perimeter (m)
- Friction factor (kg/m^3)
- Wetness factor
- Age in (days)
- Age out (days)
- VRT (ºC)
- Geothermal step (m/ºC)
- Rock conductivity (W/m·ºC)
- Rock diffusivity (m^2/s·10^{-6})

Figure 73 shows part of the data already introduced into the software. It is possible to connect more than one tunnel to model them at the same time.

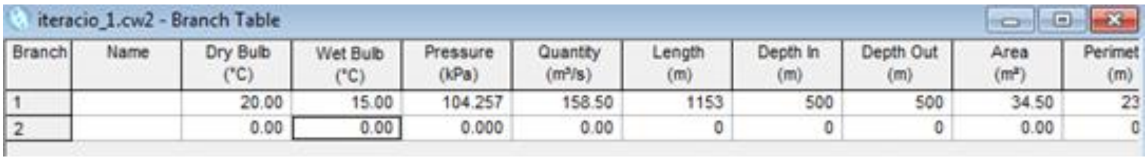
iteracio_1.cw2 - Branch Table

Branch	Name	Dry Bulb (°C)	Wet Bulb (°C)	Pressure (kPa)	Quantity (m³/s)	Length (m)	Depth In (m)	Depth Out (m)	Area (m²)	Perimet (m)
1		20.00	15.00	104.257	158.50	1153	500	500	34.50	23
2		0.00	0.00	0.000	0.00	0	0	0	0.00	0

Figure 73. Some of the parameters introduced to ClimSim for running the software.

Once all the parameters have been introduced to the software, the sources of heat due to conveyors, continuous haulage machines and fragmented rock have to be introduced. The program allows spot and linear sources of heat. In this case there is a conveyor system carrying the mineral all the length of the stretches. Hence, sources of heat have been considered as linear. Figure 74 details the heat contribution of fragmented rock and the sum of conveyors and continuous haulage machines as linear heat sources within the stretches analysed.

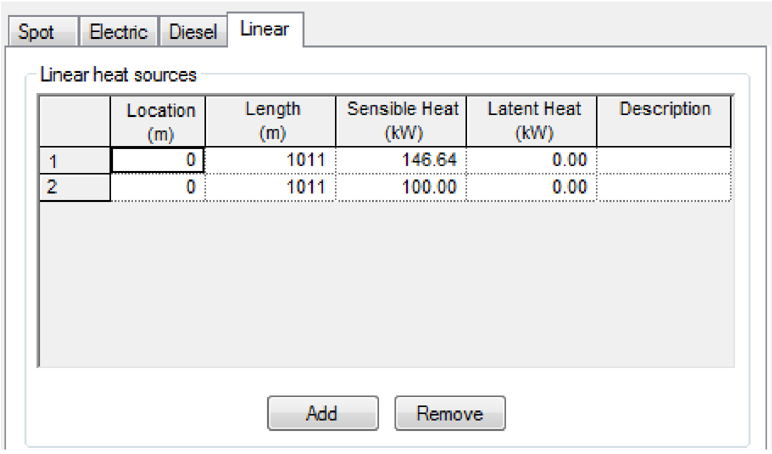

Figure 74. Linear heat sources.

Either the conveyor system or the fragmented only generate sensible heat in contrast to diesel machines. The power taken by the machine that is not transformed to work is dissipated, producing sensible heat. In the case of broken rock, heat exchange is due to higher temperature of the rock than the air from the airways. The obtaining of their values is achieved by means of equation (19) and the next expression (32).

Regarding the part analysed, there is system formed by conveyor belts and continuous haulage machines. Despite that, they can be considered as only one item at the moment of calculating the heat generation because they are always set up together and in both cases they use electricity as energy source.

$$q = Pn \cdot (100 - E) \tag{32}$$

Where:

q – Heat generated by the head (kW);

Pn – Nominal power (kW);

E – Efficiency of machine (%).

The efficiency of the machines is based on values provided by the staff of the mine. Meanwhile the heat generated by lights and the Joule effect produced by the electrical cables have not been taken into account because of their small contribution to the overall heat generation (McPherson, 2009).

When rock is fragmented by continuous mining machines, a temperature difference is created between rock and air of the tunnel, generating heat transference to the ventilation circuit. These conditions can be found in workshops and conveyors carrying mineral. Its determination is done using the following expression.

$$q_{fr} = m \cdot C \cdot (\theta_1 - \theta_2) \tag{19}$$

Next step after introducing the initial parameters is to produce outcomes by means of iterations so that correct values of rock diffusivity and conductivity can be determined. The value is considered acceptable when simulations give the same dry and wet bulb temperature measured in situ with an acceptable range variation of ±1 ºC at the end of the stretch, points 3 and 4 from Figure 70 in this case. Temperatures comparison has been done with the mean wet and dry bulb temperature from data between 2009 and 2014.

Figure 75 shows part of the results from iterations. The program gives results every certain distance between the beginning and end of the stretch, normally every 20 meters, even though this distance can be modified at the discretion of the technician. Full results are attached in the appendix.

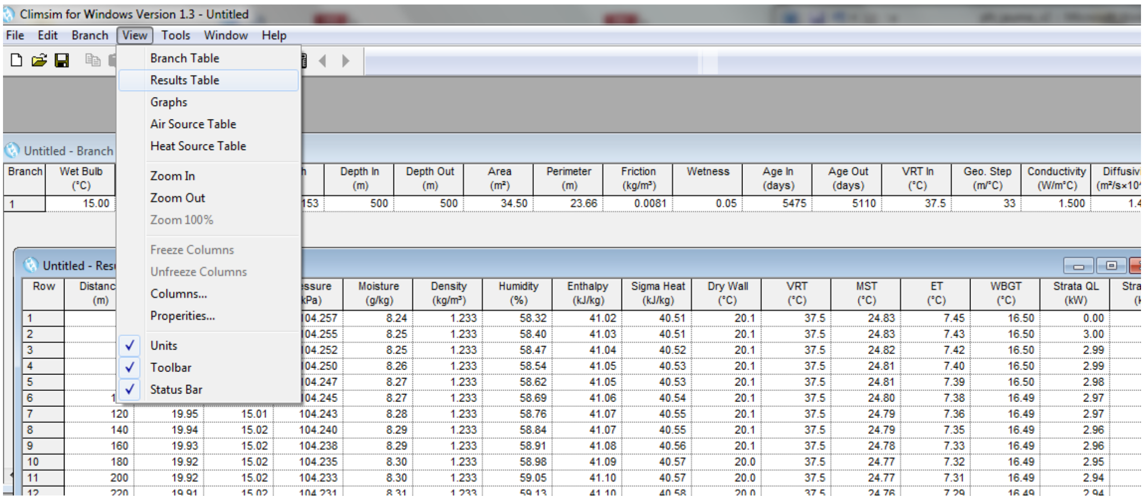

Figure 75. Part of iteration results using ClimSim.

Once rock conductivity and diffusivity are adjusted in stretches 1-3 and 3-4, they have been evaluated using data from different seasons of the year in order to validate the results. In this case four months have been chosen to stand for the four seasons (June, October, January and April), using the mean airflow as well as wet and dry bulb temperature from each month. After several iterations, the values adjusted are the following.

- Rock thermal conductivity: 6 W/mºC.
- Rock thermal diffusivity: 5,55 $m^2/s \cdot 10^{-6}$.

Hence, they can be considered as the characteristic values to model despite it can be some variations along the mine. Tables 39 and 40 display the comparison of airways modelling climatic conditions, dry and wet bulb temperatures, with the mean temperatures measured in situ and using the values of rock thermal conductivity and diffusivity obtained by means of ClimSim iterations in the first case.

Table 39. Comparison of the modelling climatic conditions in the stretch 1-3.

	Point 3					
	Dry bulb temperature (ºC)			**Wet bulb temperature (ºC)**		
	Measured	**ClimSim**	**Difference**	**Measured**	**ClimSim**	**Difference**
Overall	24	21,62	2,38	17	15,96	1,04
January	19	17,6	1,4	11	12,07	-1,07
April	25	23,07	1,93	18	15,87	2,13
June	30	27,8	2,2	22	20,65	1,35
October	27	24,95	2,05	19	17,77	1,23

Table 40. Comparison of the modelling climatic conditions in the stretch 3-4.

	Point 4					
	Dry bulb temperature (ºC)			**Wet bulb temperature (ºC)**		
	Measured	**ClimSim**	**Difference**	**Measured**	**ClimSim**	**Difference**
Overall	26	25,45	0,55	17	17,93	-0,93
January	26	20,9	5,1	14	12,4	1,6
April	28	26,2	1,8	18	18,81	-0,81
June	31	30,7	0,3	23	22,62	0,38
October	31	27,95	3,05	21	19,75	1,25

The comparison has given an acceptable range according to mean dry and wet bulb temperature from points 3 and 4 except in dry bulb temperature between point 1 and 3 in October and January. Probably due to remaining deviations of water evaporation or condensation caused by air from the surface, which varies considerably its moisture fraction in these months. Wetness factor should also be thoroughly assessed and then check if there is any difference respect to the value used.

On the other hand, Figure 76 expose the outcomes from Tables 39 and 40 with their corresponding effective temperatures, calculated according to the Spanish law (RGNBSM, itc 04.7.02), te = 0,9·tw + 0,1·td, where te is effective temperature, tw wet temperature and td dry temperature.

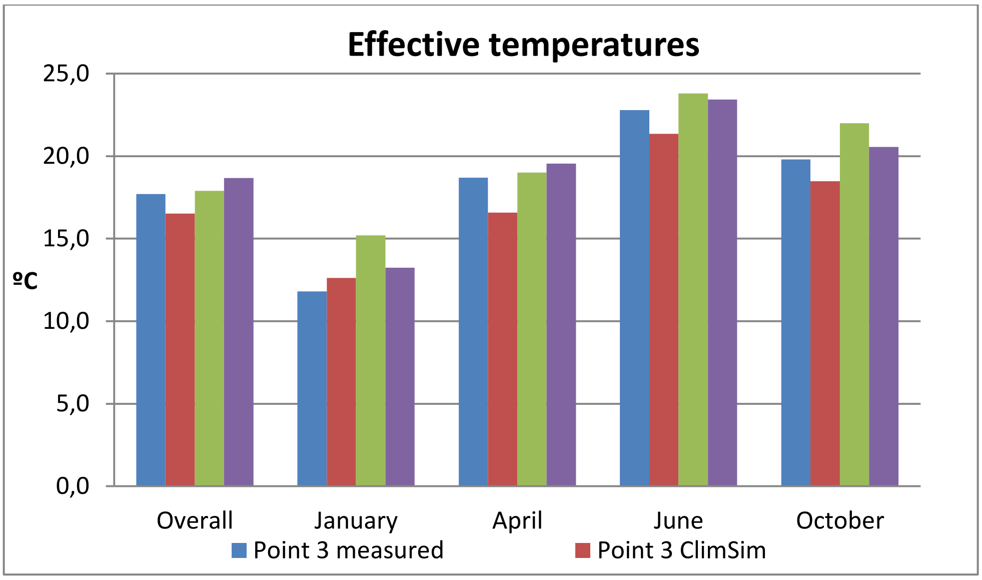

Figure 76. Comparison of the effective temperatures modelled and measured in situ.

3.4.3. Heat input determination

3.4.3.1. Strata heat

As there is no information from other similar mines, strata heat needs to be calculated by means of equations and ClimSim. When the tunnel studied has been opened for more than 30 days, equation (12) has been used to determine the radial heat flow into established tunnels.

$$q = 3{,}35 \cdot L \cdot k^{0{,}854} \cdot (VRT - \theta d) \qquad (12)$$

While in the case of the advancing done in less than 30 days, equation (13) has been applied.

$$q = 6 \cdot k \cdot (L + (4 \cdot DFA)) \cdot (VRT - \theta d) \qquad (13)$$

Mean dry bulb temperature has been determined using data measured in situ between 2009 and 2014, meanwhile rock thermal conductivity and virgin rock temperature have been calculated in previous paragraphs. The main problem of equation (12) is to know the time that strata transfer heat to the air until thermal equilibrium is achieved. This setback has been solved modelling the strata behaviour using ClimSim.

Parameters that take into account time since the tunnel analysed was opened are “age in” and “age out”. The program computes the age of each section of the airway by interpolating linearly between ages of two points. These two factors have been used to determine the heat contribution to the airways along the time. Table 41 gathers the initial values of the zone studied, which will be a new opening.

Table 41. Initial values used for modelling.

Parameter	**Value**
Dry bulb temperature (ºC)	36,68
Wet bulb temperature (ºC)	26,37
Initial pressure (kPa)	103,824
Cabal (m^3/s)	15
Length (m)	500
Depth in (m)	500
Depth out (m)	500
Cross section (m^2)	30
Perimeter (m)	25
Friction factor (kg/m^3)	0,01136
Wetness factor	0,25
Age in (days)	50
Age out (days)	1
VRT (ºC)	40
Geothermal step (m/ºC)	33
Rock thermal conductivity (W/mºC)	6
Rock thermal diffusivity ($m^2/s \cdot 10^{-6}$)	5,55

Once the table is filled, it has given a fix value for the length (500 meters), which is the average monthly face advance, and changing the values “age in” and “age out” in several iterations the sensible heat has reached a value of zero. After that, it has been calculated by means of theoretical equations the sensible heat of one month face advance to corroborate the modelling values, equation (13).

Table 42 and Figure 77 detail the behaviour of strata heat (sensible and latent) using ClimSim. Results have been used to know the length of the tunnel giving heat to the airways based on the monthly advance of the miners.

Table 42. Behaviour of the strata modelled by ClimSim.

Age in (days)	Age out (days)	Sensible heat (kW)	Latent heat (kW)	Months since the tunnel was opened
30	0	17,93	33,72	1
90	60	6	27,28	3
182	152	2,64	25,97	6
365	335	0,13	25,08	12
730	700	-1,85	24,43	24

The contribution of sensible heat to the airways is near zero after one year since the airway was opened. This value has been used to know the strata heat input. After this period, rock receives heat from the airways until it reaches a thermal equilibrium.

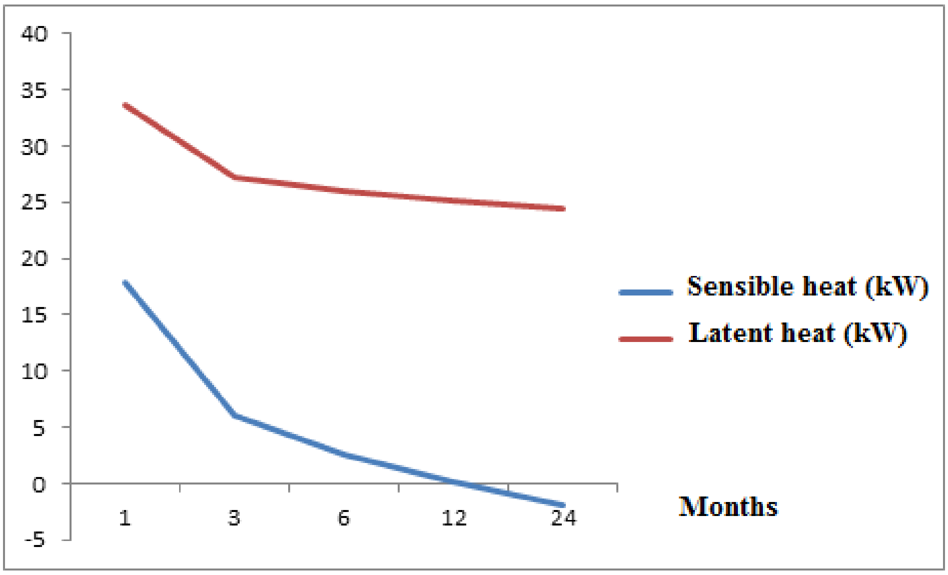

Figure 77. Graphical behaviour of the strata heat.

Modelling results compared to theoretical equations have given a percentage variation of 9,97%, reaching an acceptable accuracy for an environment with such degree of uncertainty.

3.4.3.2. Mechanized equipment

The exploitation method determines its influence to the heat load. The equipment in the case study uses diesel or electrical energy for their functioning. However, there is an important difference in terms of heat generation between both types.

The determination of heat generated by electrical equipment has been done following the scheme in Figure 28. On the other hand, diesel machines heat load has been calculated using bibliographic values according to McPherson (2009).

Conveyors, continuous haulage machines and continuous miners

In this case, the main part that generates heat is the power head, calculated by the following expression.

$$q = Pn \cdot (100 - E) \qquad (32)$$

The efficiency of the machines is based on values provided by the staff of the mine. In the case of continuous miners, it has to be taken into account that they are equipped with several motors: The cutter, the hydraulic power pack and the loader.

Diesel machines

The following equation determines the total heat generated, which comprises latent and sensible heat.

$$qc = c \cdot \frac{Ec}{100} \cdot PC \qquad (33)$$

Where:

qc – Heat emitted by the combustion (kW);

c – Combustible (l/s);

Ec – Combustion efficiency (%);

PC – Combustible calorific value (kJ/l);

McPherson (2009) gives some references used in this dissertation for the combustion efficiency, 95%, combustible calorific value, 34000 kJ per litre, and the rate of liquid equivalent per litre of fuel, 5. The last parameter is necessary to calculate the quantity of water generated by the combustion.

$$W = c \cdot \frac{Ec}{100} \cdot r \tag{34}$$

Where:
W – Water generated (l);
r – Rate of liquid equivalent.

After determining the water generated, latent heat is calculated taking into account a standard value of the water latent vaporization heat, 2450 kJ/kg, and an equivalency 1:1 litre-kilogram of water.

$$ql = \lambda\mathrm{w} \cdot W \tag{35}$$

Where:
ql – Latent heat (kW);
λw – Water latent vaporization heat (kJ/kg).

Finally, sensible heat can be obtained deducting latent heat from the result of equation (33). The comparison between electrical and diesel equipment has been done using the information supplied by the manufacturer, which states that electrical trucks and loaders generate 80% and 40% less heat respectively, producing only sensible heat. These values take as a reference the whole heat generated by the machines. The information of the electrical mining equipment used in the calculations has been extracted from AtlasCopco website (http://www.thenewgreenline.com). Trucks and loaders chosen are from the branch called *green line*.

3.4.3.3. Fragmented rock

These conditions are found in the working faces, workshops and conveyors. The next equation is used to calculate its value. Specific heat of the rock, C, has been obtained from bibliographical information (McPherson, 2009), while the mass flow of rock, m, was provided by the staff of the mine.

$$q_{fr} = m \cdot C \cdot (\theta_1 - \theta_2) \tag{19}$$

3.4.4. Changing equipment proposal

The change of electrical machinery instead of the diesel equipment currently employed is detailed in Tables 43 and 44. As it can be seen, either the proposal machines or the current ones have very similar characteristics, matching perfectly with the requirements of the current exploitation method.

Table 43. Comparison of the underground loaders.

	Current diesel equip.	**Electrical equip. chosen**
Model	Scooptram ST1030	Scooptram EST1030
Capacity (metric tonnes)	10	10
Nominal power (kW)	186	132
Width (mm)	2490	2352
Height (mm)	2355	2548
Turning radius (º)	42,5	42,5

Table 44. Comparison of the underground trucks.

	Current diesel equip.	**Electrical equip. chosen**
Model	MT 436B	EMT35
Capacity (metric tonnes)	32,6	35
Nominal power (kW)	298	400
Width (mm)	3065	3246
Height (mm)	2680	3177 - 3789
Turning radius (º)	42,5	42

In spite of the similarities, there are some differences that should be pointed out. The operational functioning is less flexible in the case of electrical ones, because loaders use a cable as power source, being limited by its extension. Meanwhile trucks have a small diesel engine, but they need a trolley line set up in their habitual route.

3.4.5. Results

Heat input factors described in previous subsections are gathered in Tables 45 and 46 in terms of latent and sensible heat contribution from each source as well as the percentage contribution to the whole heat added into the system using internal combustion engine or using electrical ones.

Table 45. Heat input using diesel trucks and loaders.

Source of heat	Sensible heat(kW)	Latent heat (kW)	(%)
Machines	11093	6248	73,8
Conveyors	1072		4,6
Continuous haulage machine	145		0,6
Miners	1455		6,2
Fragmented rock	297		1,3
Strata	1102	2072	13,5
Total	**15163**	**8320**	**100,0**

Table 46. Heat input using electrical trucks and loaders.

Source of heat	Sensible heat (kW)	Latent heat (kW)	(%)
Machines	5609	987	51,8
Conveyors	1072		8,4
Continuous haulage machine	145		1,1
Miners	1455		11,4
Fragmented rock	297		2,3
Strata	1102	2072	24,9
Total	**9679**	**3059**	**100,0**

As it can be deduced from tables above and Figure 78, the main source of heat is due to the machinery with regard to sensible or latent heat. Overall, the change of the loaders and trucks would reduce the contribution of the mining equipment by 23%, meanwhile assessing the sensible and latent heat, they would decrease about 36% and 63% respectively.

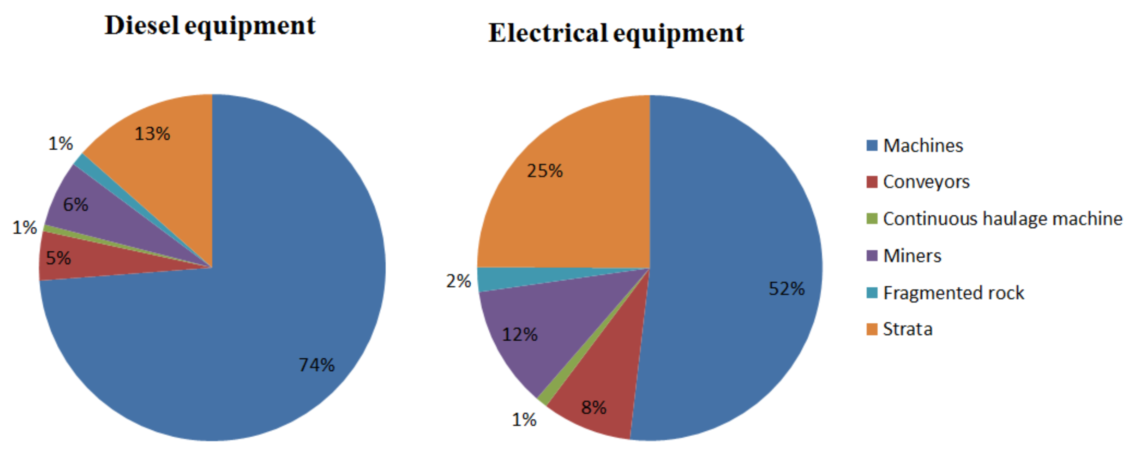

Figure 78. Percentage variation of the different heat inputs using electrical or diesel equipment.

Table 47. Summary of heat generated by the vehicles.

Type	Unit heat (kW)		Total sensible heat (kW)		Difference sensible heat (%)	Total latent heat (kW)		Difference latent heat (%)
	Dies.	Elec.	Dies.	Elec.		Dies.	Elec.	
Truck	450,9	90	6345	1984	68,7	3574	0	-
Loader	390,3	156	2996	1873	37,5	1687	0	-
Car	39,3	-	1607	[1]	-	905	[2]	-
Jumbo	25,1	-	48	[1]	-	27	[2]	-
Auxiliary equipment	25,1	-	96	[1]	-	54	[2]	-
TOTAL			**11093**	**5608**	**49,4**	**6248**	**986**	**84,2**

[1]Only loaders and trucks are changed. Thus, other equipment using diesel is added to the total sensible heat after applying the proposal.

[2]Electrical equipment does not produce sensible heat, so only the other equipment is added.

The unit heat per machine is considerably reduced using the electrical equipment. Results above show a huge difference in terms of heat generation. Besides, as consumption of fuel would be cut down, the generation of pollutants such as NOx, CO or CO2 would also decrease. Taking a ratio of 1:1 quantity of pollutants-litres of diesel burned, the generation would be minimized by 88% based on the data used.

CHAPTER 4

MAIN FINDINGS AND DISCUSSION

CONCLUSIONS

REFERENCES

"The real voyage of discovery consists not in seeking new lands but seeing with new eyes." —Marcel Proust

MAIN FINDINGS AND DISCUSSION

4.1. Findings and hypothesis fulfilment

4.1.1. Creation of a GIS database

The system proposed to manage the environmental conditions of an underground mine, a GIS, has been proved as a reliable option to manage any possible factor involved with ventilation issues in a long term and it is able to improve health and safety conditions as well as efficiency matters. Therefore, **the first hypothesis stated has been fulfilled.**

The methodology exposed to create the GIS, which splits the information between principal and auxiliary circuits depending on the evolution of the ventilation layout, gives a simple system to extract results from the database. The ventilation characteristics such as air velocity, effective temperature, airflows and gas concentrations have been studied regarding different conditions proposed to the system.

Results have allowed to control the TLV and temperatures in a long term and how the ventilation layout evolution along the time influences the underground conditions. In addition, adverse situations like leakages and airflow recirculation have been located and analysed, determining its influence to the workshops and working faces. In the mine called Vilafruns, 3 groups concerning different zones with airflow recirculation have been located: the first group with no recirculation, the second one with partial recirculation and the third one with fully recirculated airflow. These conditions create adverse workplaces in terms of effective temperatures, CO, CO_2 and NO_x. However, this comparison does not give clear results about the contribution of the layout to these conditions. For this reason, **the second hypothesis is only partially arisen.**

Finally, some expression of the gasses and temperature behaviour are proposed in order to model the mine for future openings taking into account their special geological characteristics and exploitation conditions. This model has been achieved in the mine called Cabanasses, which presents a very interesting relationship between control points and workings. As it has few interferences in the intake airways, the evolution of the mine workings can be linked with gas concentrations and effective temperatures. On the other hand, Vilafruns has a ventilation system quite complicated, being difficult to obtain a conclusion with the data collected in this regard. Hence, **the third hypothesis is also partially accomplished.**

4.1.2. Friction factor determination

The fourth hypothesis has been fulfilled, obtaining the characteristic friction factors of 2 underground potash mines using continuous miners in a room and pillar system. Roughness of the airways from Vilafruns and Cabanasses varies depending on the ventilation circuit zone. In addition, consistent difference of the friction factors along the year are found in both mines, but these differences are small enough to not influence the ventilation circuit modelling. In both cases the models have matched the measured airflows with a variation below 10%.

Moreover, the comparison made with bibliographical friction factors from metal and coal mines shows similar order of magnitude values, Table 48 displays these outcomes.

Table 48. Potash mine friction factors.

Airway type	Potash mine values
Rectangular Airway – Clean Airway	0,0076
Rectangular Airway – Some Irregularities	0,0076
Mine Drift	0,0122
Mine Ramp	0,0082

Thus, values are considered as acceptable. However, more investigations should be undertaken, in both mines, to confirm the validity and accuracy of these results along the time.

4.1.3. Heat sources study

After obtaining the rock thermal conductivity and diffusivity, 6 W/mºC and 5,55 $m^2/s \cdot 10^{-6}$ respectively through several iterations with the software ClimSim, the heat input of each part has been determined.

The diesel equipment represents almost a 52% of all the heat generated (taking into account all the equipment, strata and fragmented rock). Besides, sensible and latent heat difference between diesel equipment and the change proposed would be reduced about 63% and 36% respectively. Therefore, **the fifth hypothesis is fulfilled.**

The change proposed would cut down the dependence of the company to oil prices variation and therefore its degree of uncertainty at the moment of making any decision. Nowadays, health and safety legislation in Europe and Spain has a clear trend to improve the environmental working conditions of the employees, which means more restrictive TLV and in conclusion, it leads to efficiency reductions and an increase of the exploitation costs if no changes are implemented.

Table 49. Advantages and disadvantages of using diesel and electrical equipment.

	Advantages	**Disadvantages**
Diesel equipment	- Very flexible to undertake different tasks.	- Low energy efficiency, which generates an important heat load to the ventilation system. - Increase of the humidity rate due to the combustion process. - Production of gases and pollutants that affects the underground environment. - Higher airflow requirements
Electrical equipment	- High energy efficiency. - Lower humidity rates, latent heat and sensible heat load to the ventilation system. - Non-existent gases and pollutants generation. - Lower airflow requirements, either the principal or the auxiliary ventilation system.	- Less flexibility to take different tasks. It depends on the electric cable.

As it can be deduced from Table 49, the usage of electrical equipment also reduces the energy consumption due to the lower ventilation requirements and more efficient machinery. Obviously there are other possible alternatives to improve the ventilation conditions, such as implementing a VOD system, increasing the airflow or installing a heat exchanger, but none of them is able to fulfil both conditions.

4.2. Implication of the findings, further research and improvements

The study gives some approaches to manage health and safety conditions as well as presents some characteristic values and expressions for modelling the ventilation system and the underground environment conditions. These findings based on two case studies can also be used as reference values for other potash mines with similar exploitation features.

In spite of the results achieved, it would be necessary to improve the models and make further research to back the current outcomes and widen the research scope in terms of better working conditions and more efficient ventilation system. The following paragraphs explain about the weaknesses, possible improvements and further needed research.

4.2.1. Creation of a GIS database

The system could be automatized instead of taking the measures in situ manually, providing real time operating data, which would help to improve safety aspects and efficiency of the whole mine (Michell et al., 1986). Currently, there are several softwares able to simulate the environmental conditions of a mine, but the feedback between simulation and the real situation is quite new. Although some underground facilities start to use modelling software, monitor the conditions and provide the system with collected data to give feedback between the simulation and the real situation (Ruckman and Prosser, 2010), the GIS could be an intermediate step between the data collected and the simulation, because it is more efficient discriminating the information by means of knowledge and necessities of the technicians.

On the other hand, there are some pollutants not measured in the cases studied that would be important to control because their origins come from diesel combustion according to Carrasco et al. (2011) and Attfield et al. (2012).

- Sulphur dioxide (SO_2): It is toxic, irritating and it creates problems in the respiratory system.
- Hydrogen sulphide (SH_2): Irritation of the eyes and respiratory system.

- Aldehydes and polycyclic aromatic hydrocarbons (PAH): Their health effects vary depending on the PAH, but they are all related to cancer diseases.
- DPM: Small particles are able to get to the respiratory system and cause cancer diseases according to some studies.

Moreover, the working faces analysis in Vilafruns does not show a very clear trend. In the first case, the comparison between CO and CO_2 mean values from the first group (clean airflow) and the second one (partially recirculated airflow), taking the first as a reference, gives a decreasing level of almost 6% in CO and 10% in CO_2, even though it should give higher concentrations in the second group. Analysing in detail each working face, some miners display higher CO and CO_2 concentrations in the first group. As there is no historical volcanic activity known in the zone that could explain this difference, the problem must come from the auxiliary ventilation system. Further investigation should be undertaken to determine if there is local recirculation within the same group or if the duct circuit is properly installed.

Regarding Cabanasses, the expressions obtained in the principal ventilation system would need more data from each point to achieve better accuracy. Besides, it would be necessary to take more control points –especially in the north zone– to get the trend of the underground environmental conditions. Also, workshops give quite different gas concentrations despite there is a very different layout in contrast to the situation in Vilafruns and the airflow is clean in all the situations. Therefore, the auxiliary ventilation system should be thoroughly analysed as well. The air in the working faces is led by a duct to the main circuit. Information related to these ducts should be included in the GIS, such as position, leakages, layout of the auxiliary fans or distance between the entry of the duct and the working face. In addition, data regarding the discharge zone of the duct would be important as well, so that tunnels with potential recirculation could be taken into account.

4.2.2. Friction factor determination

In order to reach more reliable values, it would be necessary to follow the same process described to continue measuring the roughness of the airways. It would also be advisable to study other potash mines using a similar exploitation method and compare their friction factors.

4.2.3. Heat sources study

Rock thermal conductivity and diffusivity used to model the heat load in Vilafruns should be thoroughly studied in order to reach more accurate values with the software ClimSim. As the main deviations are produced by the dry bulb temperature, all possible sources of water evaporation and condensation must be analysed. Besides, the same study should be carried out in Cabanasses to determine its fundamental conditions and know if there are some local differences in terms of heat from the strata and machinery.

CONCLUSIONS

The main conclusions obtained from this study are the following:

- It is confirmed that the GIS created is a useful tool to provide a healthier and safer work environment as well as to improve the efficiency of the ventilation system. The possibility of improving the GIS and complement it with any other software gives an enormous flexibility in order to control an environment that is evolving every day and where the requirements could change anytime, either by legal issues, new factors to take into account or the evolution of the mine and the ventilation system. It could also be adapted to any other type of underground facility.
- The GIS is able to analyse information in long and mid-term periods and discriminate temporary abnormal conditions labelled by monitoring systems as unacceptable, which are quite common in underground mining.
- The most sensitive parts of the mine in terms of gases, temperature, air velocity and airflow have been located in the principal and auxiliary circuit. All these factors have been analysed individual and collectively.
- CO and NO_x concentrations in working faces from Vilafruns –where the majority of the air has been previously recirculated– comply with the current Spanish legislation, but more restrictive regulation in the future would cause operating difficulties. In addition, a reduction in the level of gases would improve the workplace conditions and increase the productivity of the mine. It would be advisable to partially change the ventilation layout of the working faces from the group 3, so that part of the airflow was not previously recirculated.
- Working faces in both mines show problems in the auxiliary ventilation system, varying their working conditions in similar theoretical situations.
- The characteristic friction factors in potash mines using a room and pillar method have been determined. Despite each mine has its own parameters, it has been achieved a framework for future studies related to mine ventilation in this type of exploitations.

- The airways roughness in potash mining is due to, basically, the exploitation method and the nature of the deposit, which has certain deformable properties that define the shape of the tunnels. At the same time, roughness is affected by the climatic conditions of the air from the surface.
- Some approaches to determine the rock conductivity and diffusivity using modelling software instead of laboratory analysis have been exposed.
- The usage of electrical loaders and trucks decrease the sensible heat generation by almost 50% and latent heat around 84%. Overall, the contribution of heat from the machines plummeted from 73,8% to 51,85. Moreover, the model has permitted to know the behaviour of the strata heat in a potash mine, finding out the trend of sensible and latent heat in Vilafruns.
- It would be advisable to combine electrical and diesel equipment with the idea of keeping the same operational flexibility.
- The decrease in heat load would allow higher energy efficiency due to lower ventilation requirements and better workplace environment, which at the same time would improve worker's efficiency owing to lower effective temperature and combustion gases generation. Hence, the number stops when temperature or gases exceed the maximum values according to the law could be reduced.
- The geological characteristics of the deposit, such as thickness and morphology of the seams or depth of the deposit determine the mine planning and therefore, the section of the airways and tunnels. These factors will influence the strata heat input, machinery used and behaviour of the airflow.
- The usage of electrical equipment can help to reduce the uncertainty of the mining activity in terms of oil price variations, fight more restrictive legal values and get a better vision from the society towards mining activities.

REFERENCES

Akcil, A. (2006). Managing cyanide: health, safety and risk management practices at Turkey's Ovacik gold–silver mine. *Journal of Cleaner Production*, *14*(8), 727–735.

Allen, C., Inco, V., Keen, B. (2008). Ventilation on demand (VOD) project – Vale Inco Ltd. Coleman Mine. *12th North American Mine Ventilation Symposium*, 45–50.

Alymenko, N. I. (2012). Aerodynamic parameters of ventilating passages joined-up with the main mine fan. *Journal of Mining Science*, 47(6), 814–823.

Aminossadati, S. M., Mohammed, N. M., Shemshad, J. (2010). Distributed temperature measurements using optical fibre technology in an underground mine environment. *Tunnelling and Underground Space Technology*, 25(3), 220–229.

Attfield, M. D., Schleiff, P. L., Lubin, J. H., Blair, A., Stewart, P., Vermeulen, R., Silverman, D. T. (2012). The Diesel Exhaust in Miners study: a cohort mortality study with emphasis on lung cancer. *Journal of the National Cancer Institute*, 104(11), 869–83.

Bahn, S. (2013). Workplace hazard identification and management: The case of an underground mining operation. *Safety Science*, 57, 129–137.

Bahuguna, P. P., Kumar, D. (2006). Application of Geographical Information System (GIS) for opencast coal mines. *Proceedings of the Indian Conference on Mine Surveying*, 125-132.

Box, G. E. P., Hunter J. S., Hunter, W. G. (2005). Statistics for experiments. Design, innovation and discovery, *Wiley & Sons*.

Bromilow, J. G. (1960). The Estimation and Reduction of the Aerodynamic Resistance of Mine Shafts. *Transactions of the American Institute of Mining Engineers*, 119, 449-465.

Brunner, D. J. (1995). Examples of the application of computational fluid dynamics simulations to mine and tunnel ventilation. *7th U.S. Mine Ventilation Symposium*.

Cabrera, L., Cabrera, M., Gorchs, R., De las Heras, F. X. C. (2001). Lacustrine basin dynamics and organosulphur compound origin in a carbonate-rich lacustrine system (Late Oligocene Mequinenza Formation, SE Ebro Basin, NE Spain). *Sedimentary geology*, 148, 289-317.

Carrasco Galán, J., Alarcón Rojas, D., Albuerne Pérez, J., Fernández Bustillo, E., Fernández Vilas, E., García García, L., Madera García, J. (2011). *Manual de ventilación de minas y obras subterráneas*. Aitemin Centro Tecnológico, Madrid, Spain, ISBN 978-84-615-0941-6.

Cendón, D., Ayora, C., Pueyo, J., Taberner, C. (2003). The geochemical evolution of the Catalan potash subbasin, South Pyrenean foreland basin (Spain). *Chemical geology*, 200, 339-257.

Cheng, J., Wu, Y., Xu, H., Liu, J., Yang, Y., Deng, H., Wang, Y. (2015). Comprehensive and Integrated Mine Ventilation Consultation Model – CIMVCM. *Tunnelling and Underground Space Technology*, 45, 166–180.

Cheng, J., Yang, S. (2012). Data mining applications in evaluating mine ventilation system. *Safety Science*, *50*(4), 918–922.

Cook, T. D., Campbell, D. T., Peracchio L. (1990). *Quasi experimentation*. Handbook of Industrial and Organizational Psychology. Consulting Psychologists Press, 491-576. Palo Alto, California.

Del Castillo, D. (1988). Air cycle refrigeration system for cooling deep mines. *International journal of refrigeration*, 11(2), 87–91.

Del Santo, G., Gracía-Sansegundo, J., Sarasa, L., Torrebadella, J. (2000). Estratigrafía y estructura del terciario en el sector oriental de la cuenca del Ebro entre Solsona y Manresa (NE de España). *Revista sociedad geológica de España*, 265-278.

Dheeraj, K. (2010). *Emerging tools and techniques for mine safety and disaster management. Natural and Anthropogenic Disasters: Vulnerability, Preparedness and Mitigation*. Springer, 356-363. Dordrecht, Netherlands. ISBN: 9789048124985.

Di Sipio E., Chiesa S., Destro E., Galgaro A., Giaretta A., Gola G., Manzella A. (2013). Rock thermal conductivity as key parameter for geothermal numerical models. *Energy Procedia*, 40, 87–94.

Diego, I., Torno, S., Toraño, J., Menéndez, M., and Gent, M. (2011). A practical use of CDF for ventilation of underground Works. *Tunnelling and underground space technology*, 26(1), 189-200.

Duckworth, I. J., Loomis, I., Prosser, B. (2012). Fifteen years of resistance data collected at Freeport Indonesia, *14th U.S./North American Mine Ventilation Symposium*, 161–166.

Duckworth, I., Prosser, B. (1997). Analysis of the data obtained from ventilation studies of longwall panels. *6th International mine ventilation congress*, 223-229.

Düzgün, Ş., Künzer, C., Özgen Karacan, C. (2011). Applications of remote sensing and GIS for monitoring of coal fires, mine subsidence, environmental impacts of coal-mine closure and reclamation. *International Journal of Coal Geology, 86*(1), 1–2.

Edgar, G., Plessis, D., Liebenberg, L., Mathews, E. H., Nicolaas, J. (2013). A versatile energy management system for large integrated cooling systems. *Energy Conversion and Management*, 66, 312–325.

Fytas, K., Gagnon, C. (2008). A database of ventilation friction factors for Quebec underground mines, *12th U.S./North American Mine Ventilation Symposium*, 615-622.

Gamble, G. A., Ray, R. E., Americas, P. B. and York, N. (2009). Differences In Design Considerations For Tunnel vs. Mine Ventilation Fan Systems, *SME Annual Meeting*.

Garcia-Herrero, S., Mariscal, M. A., García-Rodríguez, J., Ritzel, D. O. (2012). Working conditions psychological physical symptoms and occupational accidents. Bayesian network models. *Safety Science*, 50, 1760-1774.

Gibert, K., Sànchez-Marrè, M., Rodríguez-Roda, I. (2006). GESCONDA: An intelligent data analysis system for knowledge discovery and management in environmental databases. *Environmental Modelling & Software*, 21(1), 115–120.

Hall, C.J. (1981). *Mine Ventilation Engineering*. The Society for Mining, Metallurgy and Exploration Inc., 62-72.

Hamrin, H. (1980). *Guide to Underground Mining Methods and Applications*. Atlas Copco, Stockholm, Sweden.

Hardcastle S., Kocsis C., Li G., Hortin K. (2008). Analysing Ventilation Requirements And The Utilization Efficiency Of The Kidd Creek Mine Ventilation System. *12th U.S. North American Mine Ventilation Symposium*, 27-36.

Hardcastle, S., Butler, K. (2008). A comparison of globe, wet and dry temperature and humidity measuring devices available for heat stress assessment. *12th US/North American Mine Ventilation Symposium*, 181–190.

Hargreaves, D. M., Lowndes, I. S. (2007). The computational modelling of the ventilation flows within a rapid development drivage. *Tunnelling and Underground Space Technology*, *22*, 150–160.

Harris, J. R., Wilkinson, L., Grunsky, E. C. (2000). Effective use and interpretation of lithogeochemical data in regional mineral exploration programs : application of Geographic Information Systems (GIS) technology. *Ore geology reviews*, *16*, 107–143.

Hartman, H., Mutmansky, J., Ramani, R., Wang, Y. (1997). Mine ventilation and air conditioning, *John Wiley and sons*, 3º edition, Vancouver, ISBN 0-471-11635-1.

He, M., Cao, X., Xie, Q., Yang, J., Qi, P., Yang, Q., Chen, X. (2010). Principles and technology for stepwise utilization of resources for mitigating deep mine heat hazards. *Mining Science and Technology (China)*, 20(1), 20–27.

Hedlund, F. H. (2012). The extreme carbon dioxide outburst at the Menzengraben potash mine 7 July 1953. *Safety Science*, *50*(3), 537–553.

Hurtado, J.P., Díaz, N., Acuña, E.I., and Fernández, J. (2014). Shock losses characterization of ventilation circuits for block caving production levels. *Tunnelling and Underground Space Technology*, 41, 88–94.

Kazakov, B. P., Shalimov, A. V., Kiryakov, A. S. (2013). Energy-Saving Mine Ventilation. *Journal of Mining Science*, 49(3), 475–481.

Kharkar, R., Stefanko, R., and Ramani, R.V. (1974). *Analysis of Leakage and Friction Factors in Coal Mine Ventilation Systems*. Special Research Report Number SR-99, Pennsylvania Department of Commerce.

Kibble, J.D. (1978). Some notes on mining diesels. *Mining Technology,* 393-400.

Kim, K. D., Lee, S., Oh, H. J., Choi, J. K., Won, J. S. (2006). Assessment of ground subsidence hazard near an abandoned underground coal mine using GIS. *Environmental Geology*, 50(8), 1183–1191.

Kocsis C., Hardcastle S., Keen B. (2008*)*. A heat study and the modelling of future climatic conditions at Vale Inco's Coleman McCreedy East Mine. *12th U.S. North American Mine Ventilation Symposium*, 203–210.

Krishnaiah, S., Singh, D., Jadhav, G. N. (2004). A methodology for determining thermal properties of rocks. *International Journal of Rock Mechanics and Mining Sciences,* 41, 877–882.

Kurnia, J. C., Sasmito, A. P., Mujumdar, A. S. (2014a). Simulation of a novel intermittent ventilation system for underground mines. *Tunnelling and Underground Space Technology,* 42, 206–215.

Kurnia, J. C., Sasmito, A. P., Wong, W. Y., Mujumdar, A. S. (2014b). Prediction and innovative control strategies for oxygen and hazardous gases from diesel emission in underground mines. *The Science of the total environment*, 481, 317–334.

Li, G., Kocsis, C., Hardcastle, S. (2011). Sensitivity analysis on parameter changes in underground mine ventilation systems. *Journal of Coal Science and Engineering (China)*, 17(3), 251–255.

Likar, J., Čadež, J. (2000). Ventilation Design of Enclosed Underground Structures. *Tunnelling and Underground Space Technology*, 15(4), 477–480.

Lipsey, M.W. (1990). *Design Sensitivity*. Sage Publications, Newbury Park, California.

Liu, H., Yang, D., City, H. (2004). GIS-Based Mine Ventilation Network and Safety Analysis. *IEEE International Geoscience and Remote Sensing Symposium Proceedings*, 5, 2945–2948.

M.V.S. (2013). *ClimSim user's manual and general theory*. Mine Ventilation Servicies Inc., 4946 Yale Ave., Fresno, California, USA.

Mahdevari, S., Shahriar, K., Esfahanipour, A. (2014). Human health and safety risks management in underground coal mines using fuzzy TOPSIS. *The Science of the total environment*, 488-489, 85–99.

Marks, J. R. (1989). Rationale and Methodology in Designing Controlled Recirculation Ventilation Systems. *American Mining Congress*.

Martikainen, A. L., Taylor, C. D. (2010). Breaking the Ice on the Booster Fan Dilemma in US Underground Coal Mines. *Mining Engineering*, 62(10), 47-53.

McElroy, G. (1935). *Engineering factors in the ventilation of metal mines*. Bureau of mines, U.S. Department of interior, Washington.

McPherson, M. J. (1986). The analysis and simulation of heat flow into underground airways. *International Journal of Mining and Geological Engineering*, 4, 165-196.

McPherson, M. J. (2009). *Subsurface Ventilation and Environmental Engineering*. California, USA, ISBN: 978-0-692.00024-3.

Meyer, C. (1998). *Determining the friction factors for underground colliery board and pillar working*. Safety in mines research advisory committee, 14-34.

Ministerio de industria y energía (1994). *Reglamento General de Normas Básicas de Seguridad Minera*. Centro de publicaciones, Madrid, ISBN: 8474747481.

Mitchell, J., Eros, L., King, R. (1986). Deserado Mine Computer Monitoring and Control System. *Proceedings of the Eighth WVU Mining Electro Technology Conference*.

Montecinos, C., Wallace, K. (2010). Equivalent roughness for pressure drop calculations in mine ventilation. *13th U.S./north American mine ventilation symposium*, 225-230.

Mousset-Jones, P., McPherson, M. J. (1984). Measurement of in-situ thermal parameters in an underground mine. *Proceedings 2nd Annual Workshop*, Generic Mineral Technology Centre, USA, 113-131.

Noack, K. (1998). Control of gas emissions in underground coal mines. *International Journal of Coal Geology*, 35, 57–82.

Noll, J. D., Bugarski, A. D., Patts, L. D., Mischler, S. E., McWilliams, L. (2007). Relationship between Elemental Carbon, Total Carbon and Diesel Particulate Matter in Several Underground Metal/Non-metal Mines. *Environmental science and technology*, 41(3), 710–716.

Payne, T., Mitra, R. (2008). A review of heat issues in underground metalliferous mines. *12th U.S./North American Mine Ventilation Symposium*, 197–202.

Poulton, E. C. (1970). Environment and human efficiency. *C.C. Thomas*, Springfield, Illinois, U.S.A.

Prosser, B. S., Loomis, I. M. (2004). Measurement of Frictional Pressure Differentials during a Ventilation Survey. *10th US/North American Mine Ventilation Symposium*.

Prosser, B. S., Wallace, K. G. (1999). Practical Values of Friction Factors, *8th US Mine Ventilation Symposium*, 691-696.

Prosser, B. S., Wallace, K. G. (2002). Practical values of friction factors, *Mine ventilation service, Inc*., California, USA.

Puliafito, E., Guevara, M., Puliafito C. (2002). Characterization of urban air quality using GIS as a management system. *Environmental Pollution*.

Reddy, A. C. (2009). *Development of a Coal Reserve GIS Model and Estimation of the Recoverability and Extraction Costs*. Master of Science Thesis, Department of Mining Engineering, West Virginia University.

Ren, T., Wang, Z., Cooper, G. (2014). CFD modelling of ventilation and dust flow behaviour above an underground bin and the design of an innovative dust mitigation system. *Tunnelling and Underground Space Technology*, 41, 241–254.

Royal Decree 863/1985, de 2 de abril, por el que se aprueba el Reglamento General de Normas Básicas de Seguridad Minera (RGNBSM).

Ruckman, R., Prosser, B. (2010). Integrating ventilation monitoring sensor data with ventilation computer simulation software at the Waste Isolation Pilot Plant facility. *13th United States/North American Mine Ventilation Symposium*, 237–242.

Rundell, B., Ledin, M. C., Hammarström, U., Stjernberg, N., Lundback, B., Sandstrom, T. (1996). Effects on symptoms and lung function in humans experimentally exposed to diesel exhaust. *Occupational Environmental Medicine*, 53, 658-662.

Şalap, S., Karslıoğlu, M. O., Demirel, N. (2009). Development of a GIS-based monitoring and management system for underground coal mining safety. *International Journal of Coal Geology*, 80(2), 105–112.

Saleh, J. H., Cummings, A. M. (2011). Safety in the mining industry and the unfinished legacy of mining accidents: Safety levers and defence-in-depth for addressing mining hazards. *Safety Science*, *49*(6), 764–777.

Sanmiquel L., Rossell J.M., Vintró, C., Freijo, M. (2014). Influence of occupational safety management on the incidence rate of occupational accidents in the

Spanish industrial and ornamental stone mining, *WORK: a journal of prevention, assessment and rehabilitation*, 49, 307–314.

Sanmiquel Pera, L., Vintro Sanchez, C., Freijo Álvarez, M. (2012). Characteristics of the 3 most common types of occupational accident in Spanish sub-surface and surface mining, from 2003–2008. *Dyna*, 79(172), 118-125.

Sanmiquel, L., Rossell, J. M., Vintró, C. (2015). Study of Spanish mining accidents using data mining techniques. *Safety Science*, 75, 49–55.

Sasmito, A. P., Birgersson, E., Ly, H. C., Mujumdar, A. S. (2013). Some approaches to improve ventilation system in underground coal mines environment – A computational fluid dynamic study. *Tunnelling and Underground Space Technology*, 34, 82–95.

Shalimov, A. V. (2011). Numerical Modelling of Air Flows in Mines under Emergency State Ventilation. *Journal of Mining Science,* 47(6), 807–813.

Shannon, H. S., Robson, L. S., Guastello, S. J. (1999). Methodological criteria for evaluating occupational safety intervention research. *Safety Science*, 31, 161–179.

Silverman, D. T., Samanic, C. M., Lubin, J. H., Blair, A. E., Stewart, P., Vermeulen, R., Attfield, M. D. (2012). The Diesel Exhaust in Miners study: A nested case-control study of lung cancer and diesel exhaust. *Journal of the National Cancer Institute*, 104(11), 855–68.

Stroh. R. (1979). A note on the downcast shaft as a thermal flywheel. *Journal of the mine ventilation society of South Africa*, 32, 77-80.

Sundberg, J., Back, P. E., Christiansson, R., Hökmark, H., Ländell, M., Wrafter, J. (2009). Modelling of thermal rock mass properties at the potential sites of a Swedish nuclear waste repository. *International Journal of Rock Mechanics and Mining Sciences*, 46(6), 1042–1054.

Sundberg, J., Back, P. E., Hellström, G. (2005). *Scale dependence and estimation of rock thermal conductivity. Analysis of upscaling, inverse thermal* *modelling and value of information with the Äspö HRL prototype repository*. Report SKB R-05-82, Stockholm.

Swart, C. (2003). *Optimising the operation of underground mine refrigeration plants and ventilation fans for minimum electricity cost*. PhD thesis, Department of Mechanical Engineering, North-West University, USA.

Szmyd, J., Branny, M., Karch, M., Wodziak, W., Jaszczur, M., Nowak, R. (2013). Experimental and Numerical Analysis of the air Flow in T-Shape Channel Flow. *Archives of Mining Sciences*, 58(2), 333–348.

Toraño, J., Torno, S., Menéndez, M., Gent, M. (2011). Auxiliary ventilation in mining roadways driven with roadheaders : Validated CFD modelling of dust behaviour. *Tunnelling and Underground Space Technology*, 26, 201–210.

Torno, S., Toraño, J., Ulecia, M., Allende, C. (2013). Conventional and numerical models of blasting gas behaviour in auxiliary ventilation of mining headings. *Tunnelling and Underground Space Technology*, 34, 73–81.

Vosloo, J., Liebenberg, L., Velleman, D. (2012). Case study: Energy savings for a deep-mine water reticulation system. *Applied Energy*, 92, 328–35.

Wala, A. M. (1991). Studies of Friction Factor for Kentucky's Coal Mines, *5th U.S. Mine Ventilation Symposium*, 675- 684.

Widiatmojo, A., Sasaki, K., Sugai, Y., Suzuki, Y., Tanaka, H., Uchida, K., Matsumoto, H. (2015). Assessment of air dispersion characteristic in underground mine ventilation: Field measurement and numerical evaluation. *Process Safety and Environmental Protection*, 93, 173–181.

Xi, Z., Jiang, M., Yang, J., Tu, X. (2014). Experimental study on advantages of foam–sol in coal dust control. *Process Safety and Environmental Protection*, 92(6), 637–644.

Xiaojie, Y., Qiaoyun, H., Jiewen, P., Xiaowei, S., Dinggui, H., Chao, L. (2011). Progress of heat-hazard treatment in deep mines. *Mining Science and Technology (China)*, 21(2), 295–299.

Zhang, H., Sanmiquel, L., Vintró, C., Zhao, Y. (2014). Applied Research of U-Shape Ventilation Network in Underground Mine. *Archives of Mining Sciences*, 59(2), 381–394.

Zhang, H., Sanmiquel, L., Zhao, Y., Vintró, C. (2015). Researches and applications on geostatistical simulation and laboratory modelling of mine ventilation network and gas drainage zone. *Process Safety and Environmental Protection*, 94, 55–64.

Zhongpeng, X. (2012). Distribution Law of High Temperature Mine’s Thermal Environment Parameters and Study of Heat Damage's Causes. *Procedia Engineering*, 43, 588–593.

Zhou G., Cheng, W., Nie, W., Xun, J., Xie, J., Cui, Q. (2011). Prediction and study of air thermal parameters in unexploited mine regions based on temperature prediction model in whole ventilation network. *First International Symposium on Mine Safety Science and Engineering Prediction*, 26, 751–758.

APPENDICES

5.1. Appendix I: Friction factor control points

The following points correspond to the control points where all the data are gauged.

5.1.1. Vilafruns

Control point	**0**
Description: Point after the downcast shaft and before the main fan.	Coordinates: X: 406847 Y: 4632883

Data:

Section	40 m^2
Perimeter	24,6 ,m
Mean roughness	0,363 m
Friction factor k	0,01170 kg/m^3

Theoretical frame

Real frame

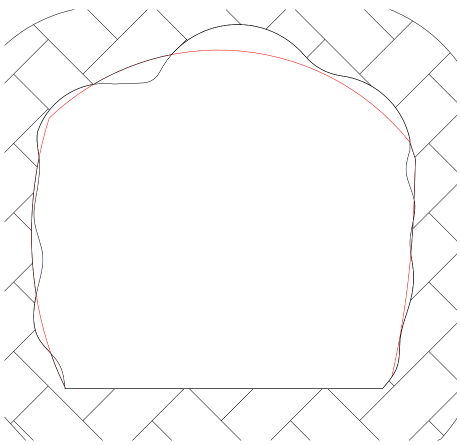

Control point	**1**
Description: Point after the main fan, which propels the airflow to the tunnels and workings.	Coordinates: X: 406366 Y: 4632678

Data:

Section	34,54 m^2
Perimeter	24,09 m
Mean roughness	0,149 m
Friction factor k	0,00826 kg/m^3

Theoretical frame

Real frame

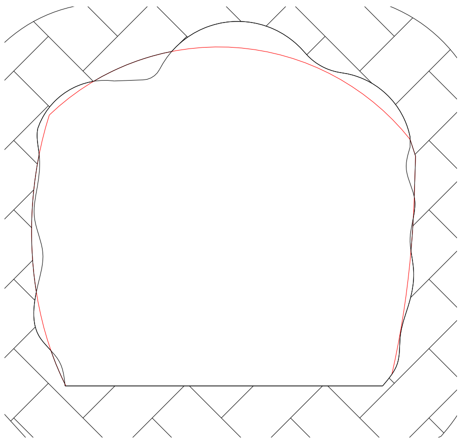

Control point	**2**
Description: Leakages control point in the door called S-4	Coordinates: X: 406320 Y: 4632339

Data:

Section	31,84 m^2
Perimeter	22,6 m
Mean roughness	0,1439 m
Friction factor k	0,00847 kg/m^3

Theoretical frame

Real frame

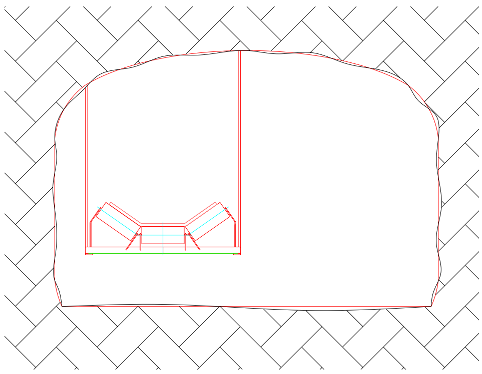

Control point	3
Description: Airway called diagonal.	Coordinates: X: 405268 Y: 4633026

Data:

Section	34,04 m^2
Perimeter	23,22 m
Mean roughness	0,1326 m
Friction factor k	0,00794 kg/m^3

Theoretical frame

Real frame

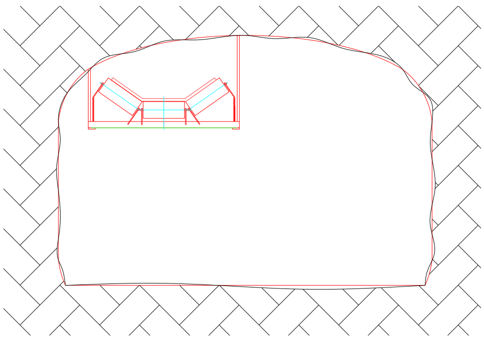

Control point	4
Description: Point before the door S – 16.	Coordinates: X: 404352 Y: 4632920

Data:

Section	27,86 m^2
Perimeter	21,85 m
Mean roughness	0,11 m
Friction factor k	0,00791 kg/m^3

Theoretical frame

Real frame

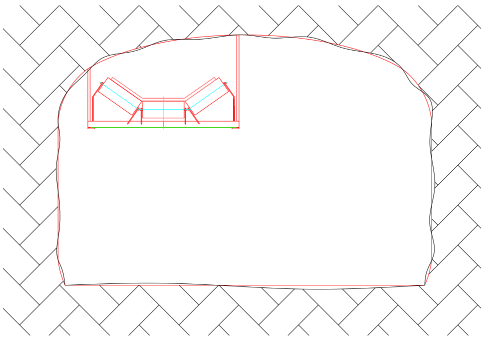

Control point	**5**
Description: Point after the first airflow split to the group 1.	Coordinates: X: 404048 Y: 4632821

Data:

Section	34,8 m^2
Perimeter	23,24 m
Mean roughness	0,1417 m
Friction factor k	0,00733 kg/m^3

Theoretical frame

Real frame

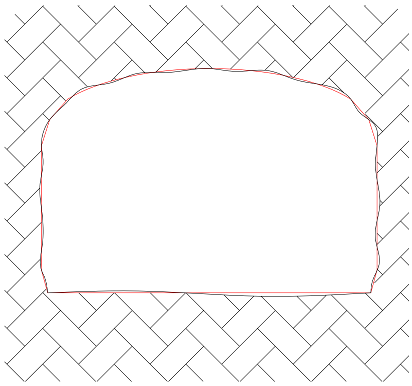

Control point	**6**
Description: Point after the door S -16	Coordinates: X: 404908 Y: 4632872

Data:

Section	28,37 m^2
Perimeter	21 5 m
Mean roughness	0,2333 m
Friction factor k	0,00892 kg/m^3

Theoretical frame

Real frame

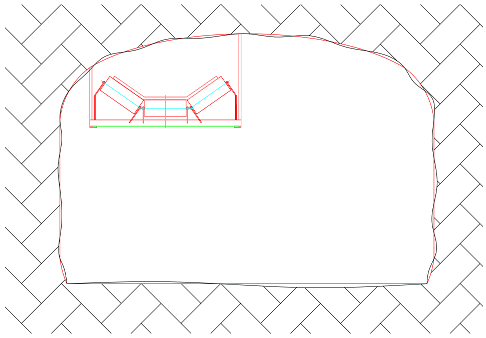

Control point	**7**
Description: Point control after the airway of the point 6.	Coordinates: X: 405066 Y: 4632494

Data:

Section	23,86 m^2
Perimeter	17,5 m
Mean roughness	0,2375 m
Friction factor k	0,00858 kg/m^3

Theoretical frame

Real frame

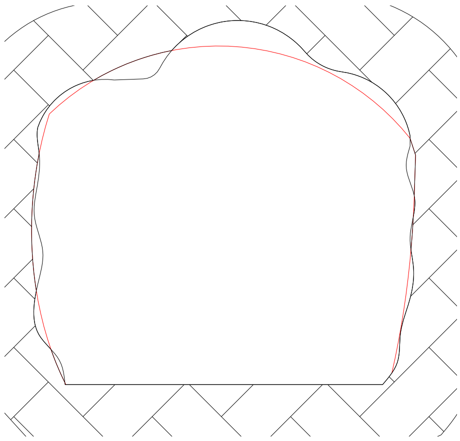

Control point	**8**
Description: Control point before the door S – 14.	Coordinates: X: 404123 Y: 4632593

Data:

Section	31,54 m^2
Perimeter	25 m
Mean roughness	0,233 m
Friction factor k	0,00943 kg/m^3

Theoretical frame

Real frame

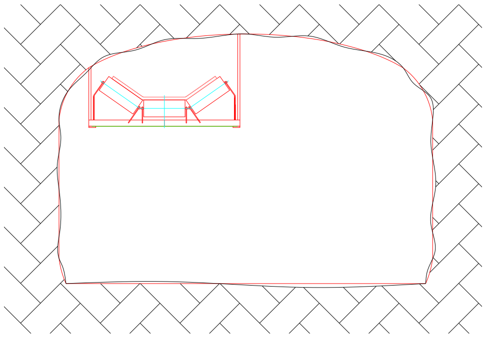

Control point	9
Description: Control point north zone.	Coordinates: X: 403603 Y: 4633593

Data:

Section	32,29 m^2
Perimeter	23 09 m
Mean roughness	0,146 m
Friction factor k	0,00898 kg/m^3

Theoretical frame

Real frame

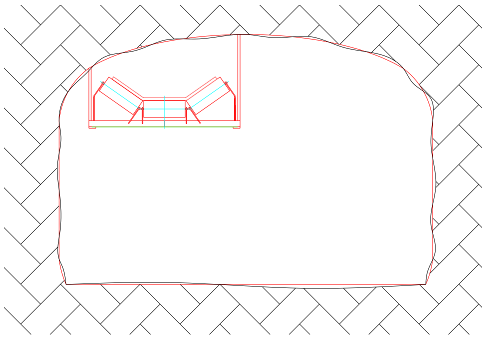

Control point	10
Description: Control point south zone.	Coordinates: X: 403955 Y: 4631859

Data:

Section	27,83 m^2
Perimeter	22,03 m
Mean roughness	0,1824 m
Friction factor k	0,00894 kg/m^3

Theoretical frame

Real frame

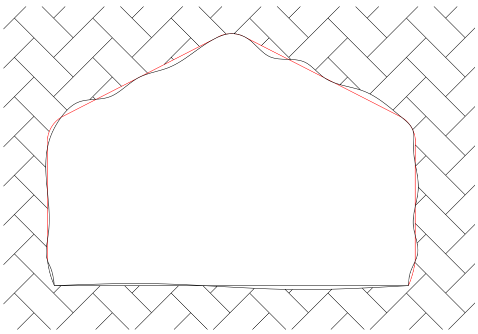

Control point	**11**
Description: Point in the south zone after the door S- 14.	Coordinates: X: 407465 Y: 4632256

Data:

Section	26,89 m^2
Perimeter	20,73 m
Mean roughness	0,1144 m
Friction factor k	0,00734 kg/m^3

Theoretical frame

Real frame

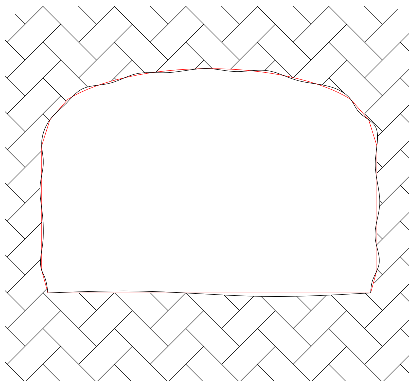

Control point	**12**
Description: Airflow control point at the return.	Coordinates: X: 406320 Y: 4632283

Data:

Section	24,36 m^2
Perimeter	18 m
Mean roughness	0,1 m
Friction factor k	0,00678 kg/m^3

Theoretical frame (red line)

Real frame (black line)

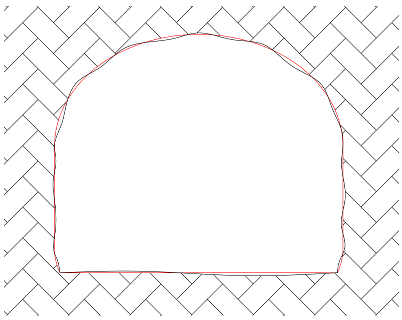

Control point	13
Description: Point at the end of the return.	Coordinates: X: 407177 Y: 4632530

Data:

Section	35,96 m^2
Perimeter	26,28 m
Mean roughness	0,12 m
Friction factor k	0,00823 kg/m^3

Theoretical frame

Real frame

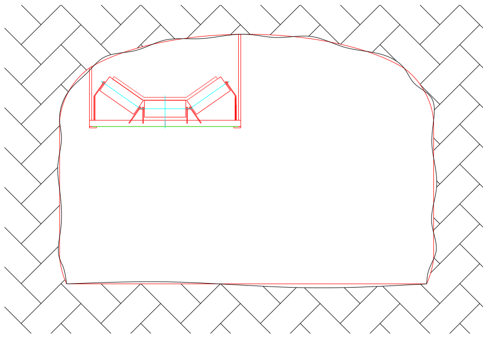

Control point	**14**
Description: Leakages from the downcast shaft	Coordinates: X: 407062 Y: 4632657

Data:

Section	21,61 m^2
Perimeter	20 m
Mean roughness	0,1748 m
Friction factor k	0,00958 kg/m^3

Theoretical frame

Real frame

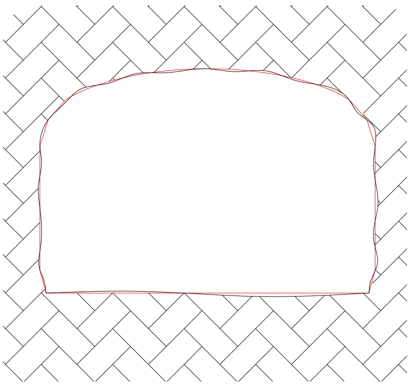

Control point	**15**
Description: Point at the beginning of the intake at the group 2.	Coordinates: X: 403637 Y: 4632620

Data

Section	31,33 m^2
Perimeter	19,34 m
Mean roughness	0,1 m
Friction factor k	0,00758 kg/m^3

Theoretical frame

Real frame

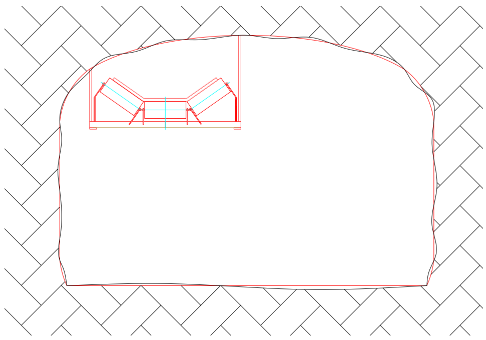

Control point	**A**
Description: Airflow recirculation in the north part.	Coordinates: X: 403093 Y: 4632470

Data:

Section	29,82 m^2
Perimeter	21,89 m
Mean roughness	0,3 m
Friction factor k	0,01136 kg/m^3

Theoretical frame

Real frame

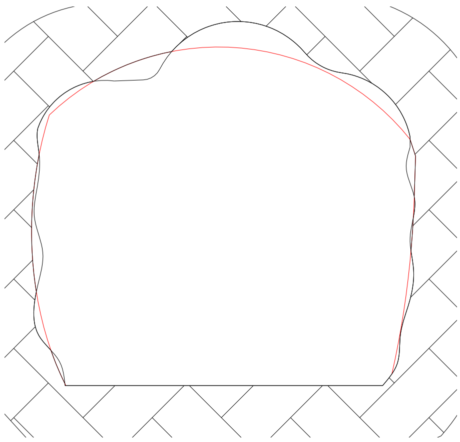

Control point	**D**
Description: Leakage control after the door S – 18.	Coordinates: X: 404237 Y: 4632321

Data:

Section	33,4 m^2
Perimeter	23 m
Mean roughness	0,2375 m
Friction factor k	0,00960 kg/m^3

Theoretical frame

Real frame

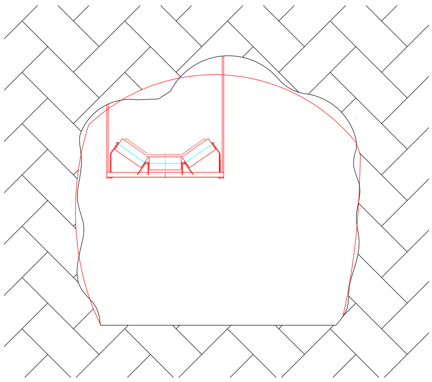

5.1.2. Cabanasses

Control point	**1**
Description: First door between intake and return	Coordinates: X: 396482 Y: 4633081

Data:

Section	30,29 m^2
Perimeter	21,83 m
Mean roughness	0,106 m
Friction factor k	0,00716 kg/m^3

Theoretical frame

Real frame

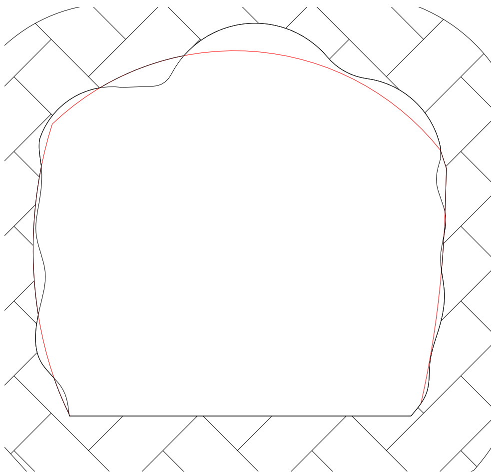

Control point	**4**
Description: Next to the maintenance workshop	Coordinates: X: 398389 Y: 4634010

Data:

Section	20,79 m^2
Perimeter	18,37 m
Mean roughness	0,055 m
Friction factor k	0,00607 kg/m^3

Theoretical frame

Real frame

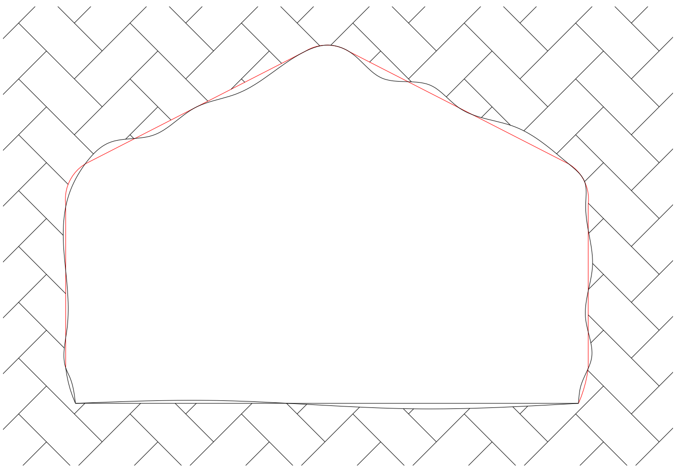

Control point	**8**
Description: Return, exit from T-13. Zone south.	Coordinates: X: 400072 Y: 4634744

Data:

Section	26,32 m^2
Perimeter	20,92 m
Mean roughness	0,210 m
Friction factor k	0,00987 kg/m^3

Theoretical frame

Real frame

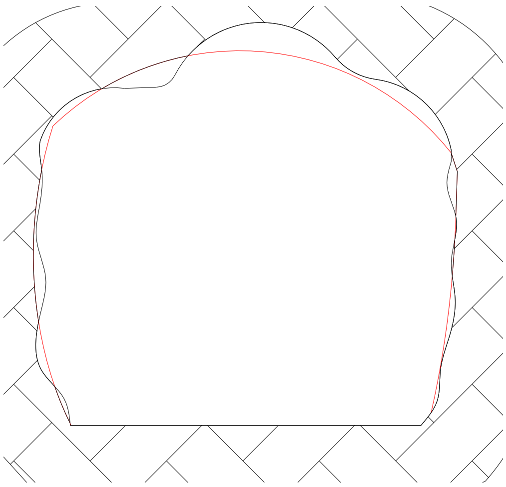

Control point	**9**
Description: Return, exit from T-14. Zone south.	Coordinates: X: 400659 Y: 4635066

Data:

Section	29,98 m^2
Perimeter	23,13 m
Mean roughness	0,162 m
Friction factor k	0,00870 kg/m^3

Theoretical frame

Real frame real

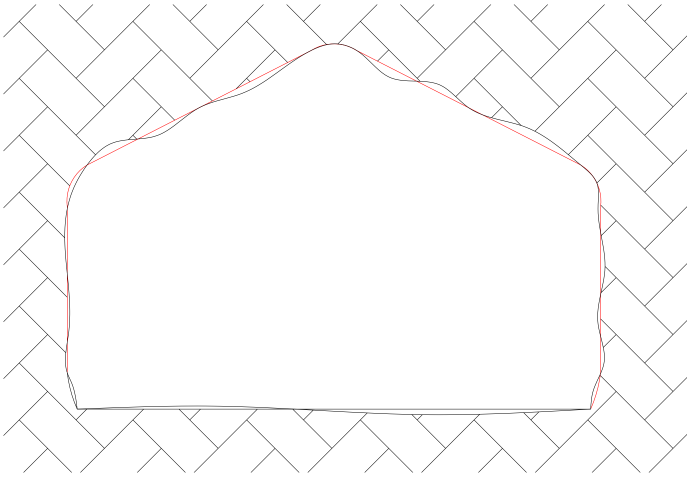

Control point	**11**
Description: Return, south zone.	Coordinates: X: 398689 Y: 4635481

Data:

Section	27,37 m^2
Perimeter	20,72 m
Mean roughness	0,120 m
Friction factor k	0,00765 kg/m^3

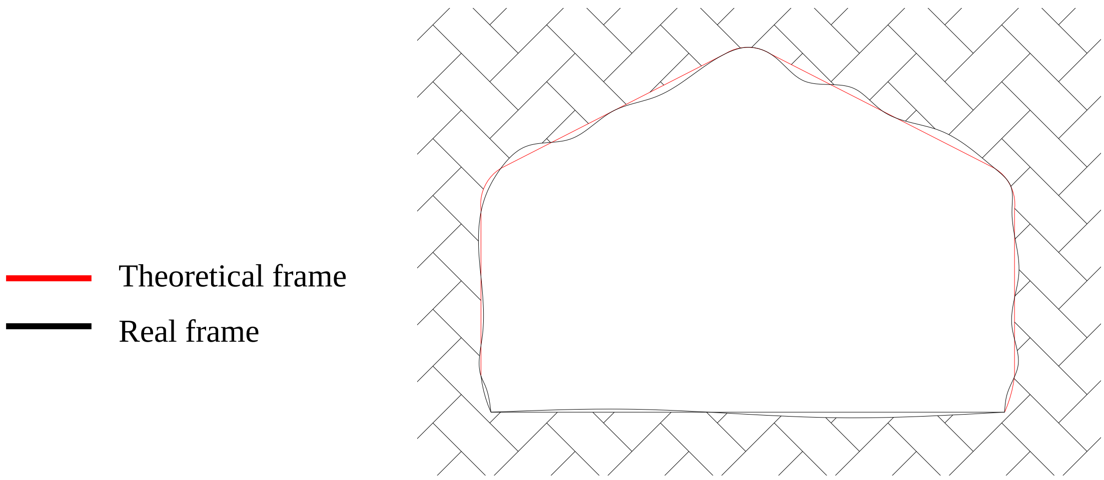

Control point	**12**
Description: Return, south zone, intermediate control point.	Coordinates: X: 398811 Y: 4634856

Data:

Section	34,91 m^2
Perimeter	23,95 m
Mean roughness	0,117 m
Friction factor k	0,00729 kg/m^3

Theoretical frame

Real frame

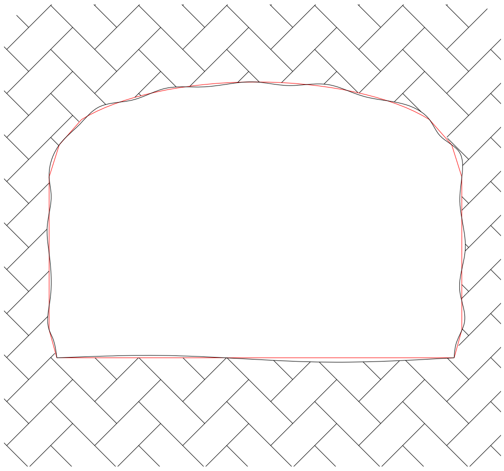

Control point	**A**
Description: Intake, beginning of the ventilation circuit.	Coordinates: X: 396537 Y: 4633089

Data:

Section	40,03 m^2
Perimeter	27,49 m
Mean roughness	0,090 m
Friction factor k	0,00661 kg/m^3

Theoretical frame

Real frame

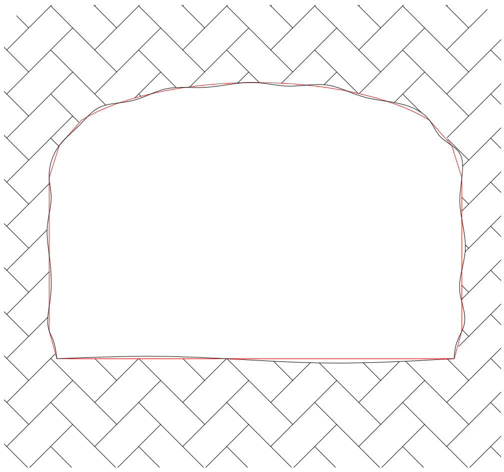

Control point	B
Description: Leakage after the main forcing fan, intake.	Coordinates: X: 396809 Y: 4633375

Data:

Section	25,47 m^2
Perimeter	21,17 m
Mean roughness	0,062 m
Friction factor k	0,00620 kg/m^3

Theoretical frame

Real frame

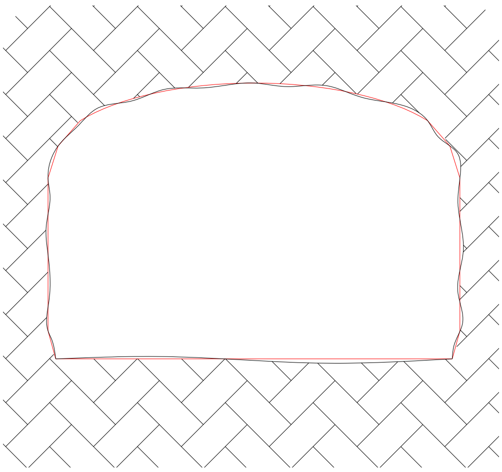

Control point	**C**
Description: Leakage conveyor belt system, next to the main forcing fan.	Coordinates: X: 396716 Y: 4633332

Data:

Section	25,60 m^2
Perimeter	20,93 m
Mean roughness	0,056 m
Friction factor k	0,00595 kg/m^3

Theoretical frame

Real frame

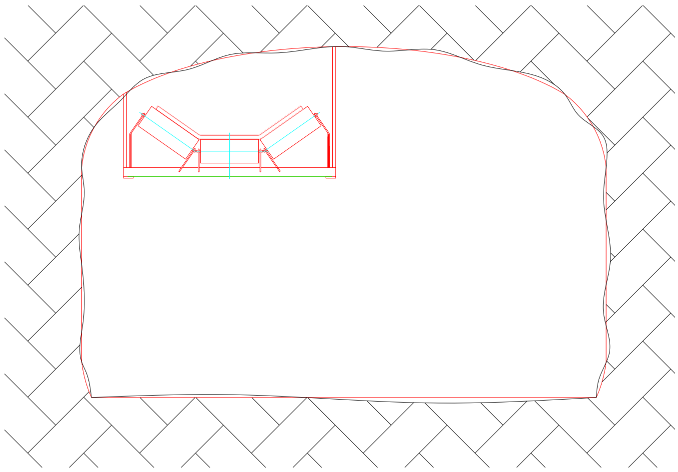

Control point	D
Description: Intake, after the main forcing fan	Coordinates: X: 396985 Y: 4633515

Data:

Section	34,50 m^2
Perimeter	26,23 m
Mean roughness	0,048 m
Friction factor k	0,00551 kg/m^3

Theoretical frame

Real frame

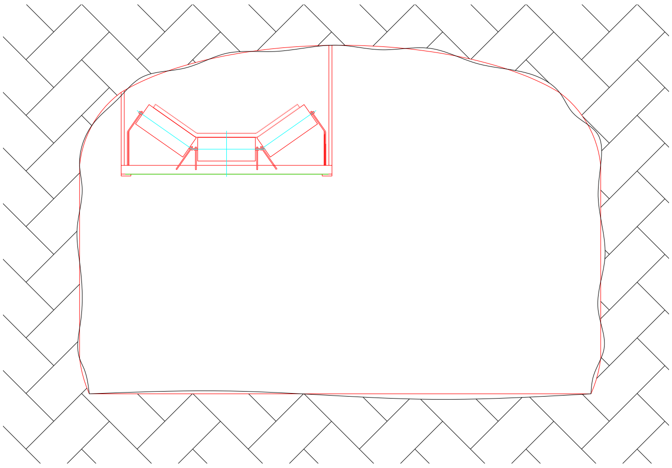

Control point	**G**
Description: Intake, beginning north zone	Coordinates: X: 398769 Y: 4634262

Data:

Section	38,28 m^2
Perimeter	27,44 m
Mean roughness	0,052 m
Friction factor k	0,00554 kg/m^3

Theoretical frame

Real frame

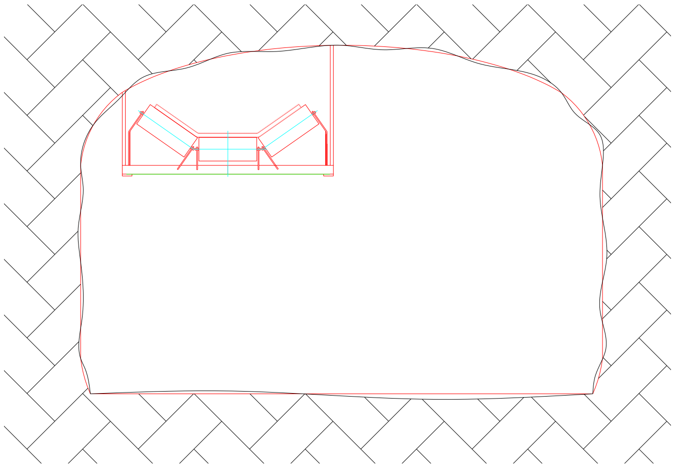

Control point	**H**
Description: Intake, end of the north zone	Coordinates: X: 398923 Y: 4635177

Data:

Section	49,45 m^2
Perimeter	29,66 m
Mean roughness	0,114 m
Friction factor k	0,00687 kg/m^3

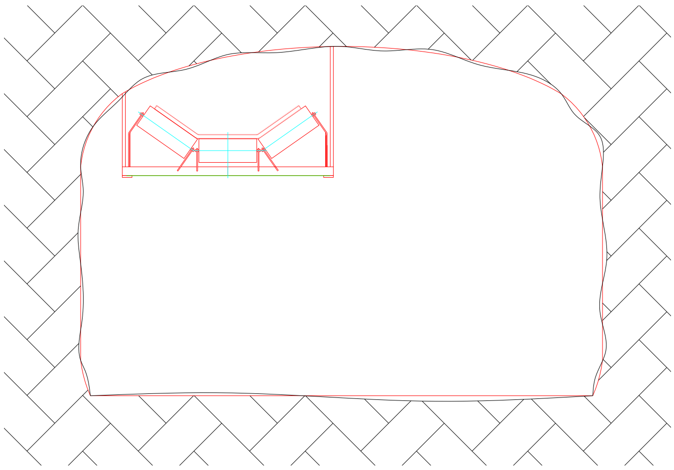

Theoretical frame

Real frame

Control point	**I**
Description: Intake, beginning of the south zone	Coordinates: X: 399009 Y: 4634201

Data:

Section	31,02 m^2
Perimeter	22,97 m
Mean roughness	0,063 m
Friction factor k	0,00600 kg/m^3

Theoretical frame

Real frame

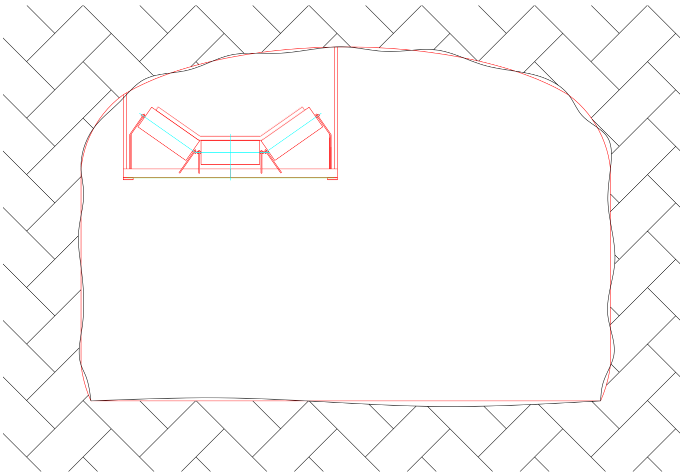

Control point	**K**
Description: Intake, entry of T-13	Coordinates: X: 400264 Y: 4634735

Data:

Section	28,64 m^2
Perimeter	20,92 m
Mean roughness	0,158 m
Friction factor k	0,00841 kg/m^3

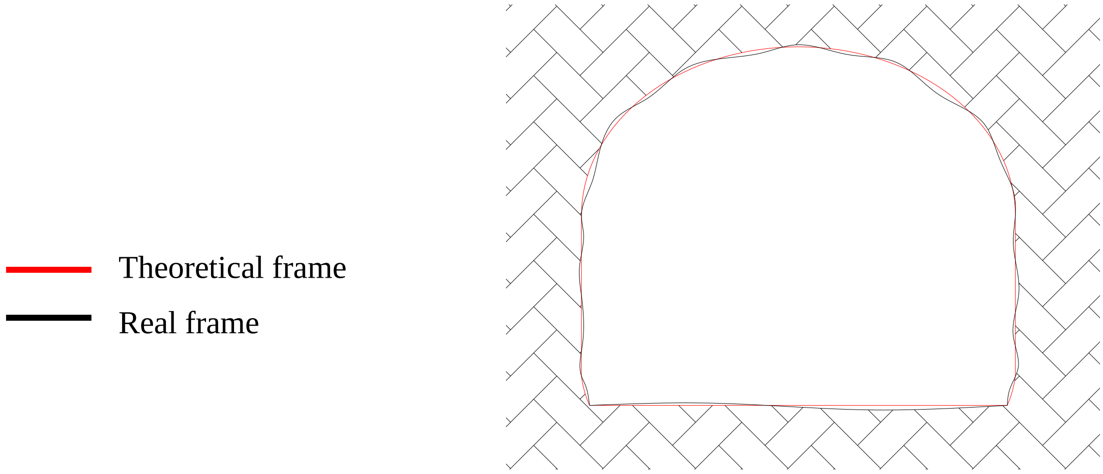

Control point	L
Description: Intake, between T-13 and T-14	Coordinates: X: 400505 Y: 4634909

Data:

Section	32,84 m^2
Perimeter	27,81 m
Mean roughness	0,066 m
Friction factor k	0,00638 kg/m^3

Theoretical frame

Real frame

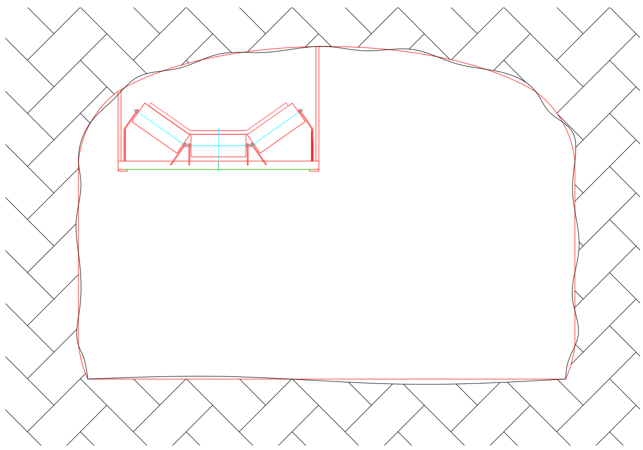

Control point	**M**
Description: Intake, entry of T-14	Coordinates: X: 400747 Y: 4634989

Data:

Section	30,85 m^2
Perimeter	21,67 m
Mean roughness	0,163 m
Friction factor k	0,00840 kg/m^3

Theoretical frame

Real frame

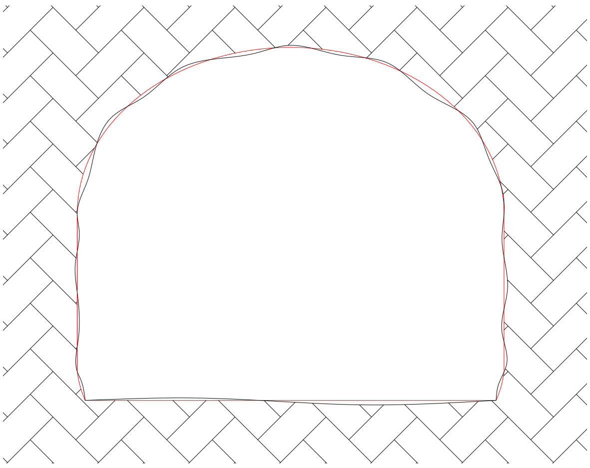

Control point	**R**
Description: Intake, intermediate point in the north zone	Coordinates: X: 398820 Y: 4634705

Data:

Section	32,83 m^2
Perimeter	22,62 m
Mean roughness	0,106 m
Friction factor k	0,00704 kg/m^3

Theoretical frame

Real frame

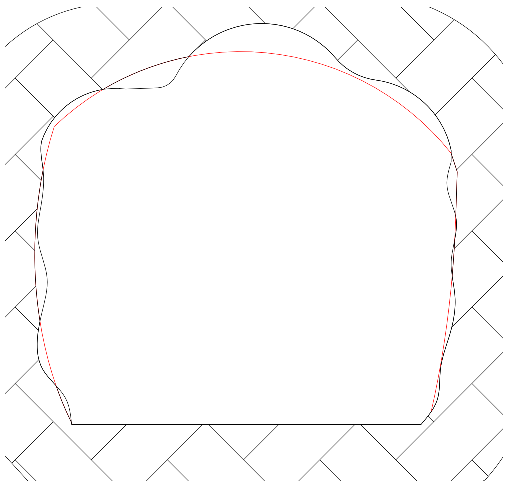

Control point	**V**
Description: Return, before the main exhausting fan.	Coordinates: X: 396522 Y: 4633232

Data:

Section	19,49 m^2
Perimeter	17,84 m
Mean roughness	0,095 m
Friction factor k	0,00752 kg/m^3

Theoretical frame

Real frame

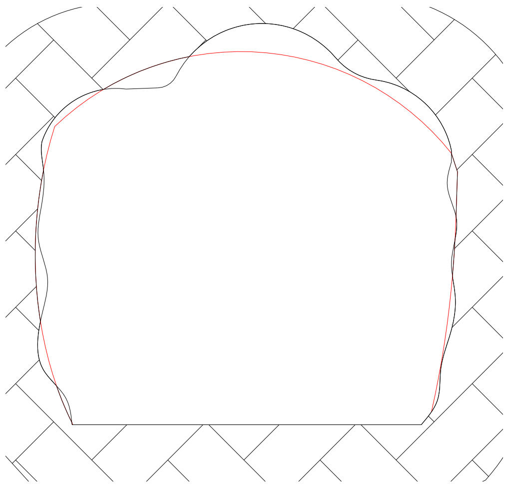

5.2. Appendix II: VnetPro+ modelling

As the friction factors change along the year, several simulations have been done, corresponding to each ventilation circuit, in order to verify the adequacy of the values obtained in Vilafruns.

On the other hand, as the mean values of the whole year have given a very good match with the real airflows it has only been carried out 1 model with the mean values in the case of Cabanasses, giving similar values between the model and the reality.

5.2.1. Fan characteristics

The modelling have been done using the main and booster fans described in Tables 50-52. Each fan has several operating positions. All these data have been introduced in the software.

Table 50. Booster fan positions, type 1.

Position 1				
Point	**Airflow (m^3/s)**	**Pressure (kPa)**	**Efficiency (%)**	**Effective power (kW)**
1	29	1,81	76	69
2	33	1,67	78	71
3	43	1,32	79	72
4	50	1,03	78	66
5	56	0,67	76	49
6	62	0,35	70	31
Position 2				
Point	**Airflow (m^3/s)**	**Pressure (kPa)**	**Efficiency (%)**	**Effective power (kW)**
1	40	2,16	77	112
2	45	2,01	78	116
3	50,5	1,79	80	113
4	61	1,33	80	101
5	67	1,01	78	87
6	76	0,39	70	42

Position 3				
Point	**Airflow (m^3/s)**	**Pressure (kPa)**	**Efficiency (%)**	**Effective power (kW)**
1	51	2,21	78	145
2	57	2,03	80	145
3	61	1,93	84	140
4	72	1,52	84	130
5	75	1,37	80	128
6	80	1,10	78	113
7	92	0,42	70	55
Position 4 (ηmax = 78%)				
Point	**Airflow (m^3/s)**	**Pressure (kPa)**	**Efficiency (%)**	**Effective power (kW)**
1	63	2,40	78	194
2	72	2,20	84	189
3	89	1,66	84	176
4	97	1,27	78	158
5	106	0,88	75	124
6	114	0,48	70	78
Position 5 (ηmax = 75%)				
Point	**Airflow (m^3/s)**	**Pressure (kPa)**	**Efficiency (%)**	**Effective power (kW)**
1	73	2,58	78	241
2	100	1,90	84	226
3	125	0,85	74	144
4	134	0,53	70	101
Position 6 (ηmax = 72%)				
Point	**Airflow (m^3/s)**	**Pressure (kPa)**	**Efficiency (%)**	**Effective power (kW)**
1	86	2,64	78	291
2	112	2,21	80	309
3	138	1,10	74	205
4	156	0,59	70	131

Table 51. Booster fan positions, type 2.

Position 1				
Point	**Airflow (m^3/s)**	**Pressure (kPa)**	**Efficiency (%)**	**Effective power (kW)**
1	29	1,81	76	69
2	33	1,67	78	71
3	43	1,32	79	72
4	50	1,03	78	66
5	56	0,67	76	49
6	62	0,35	70	31
Position 2				
Point	**Airflow (m^3/s)**	**Pressure (kPa)**	**Efficiency (%)**	**Effective power (kW)**
1	40	2,16	77	112
2	45	2,01	78	116
3	50,5	1,79	80	113
4	61	1,33	80	101
5	67	1,01	78	87
6	76	0,39	70	42
Position 3				
Point	**Airflow (m^3/s)**	**Pressure (kPa)**	**Efficiency (%)**	**Effective power (kW)**
1	51	2,21	78	145
2	57	2,03	80	145
3	61	1,93	84	140
4	72	1,52	84	130
5	75	1,37	80	128
6	80	1,10	78	113
7	92	0,42	70	55
Position 4				
Point	**Airflow (m^3/s)**	**Pressure (kPa)**	**Efficiency (%)**	**Effective power (kW)**
1	63	2,40	78	194
2	72	2,20	84	189
3	89	1,66	84	176
4	97	1,27	78	158

Point	Airflow (m^3/s)	Pressure (kPa)	Efficiency (%)	Effective power (kW)
5	106	0,88	75	124
6	114	0,48	70	78
Position 5 (ηmàx = 77%)				
Point	**Airflow (m^3/s)**	**Pressure (kPa)**	**Efficiency (%)**	**Effective power (kW)**
1	73	2,58	78	241
2	100	1,90	84	226
3	125	0,85	74	144
4	134	0,53	70	101
Position 6 (ηmax = 74%)				
Point	**Airflow (m^3/s)**	**Pressure (kPa)**	**Efficiency (%)**	**Effective power (kW)**
1	86	2,64	78	291
2	112	2,21	80	309
3	138	1,10	74	205
4	156	0,59	70	131

Table 52. Main fan positions.

Blade angle -8º				
Point	**Airflow (m^3/s)**	**Pressure (kPa)**	**Efficiency (%)**	**Effective power (kW)**
1	120	2,45	77	382
2	130	2,28	81	366
3	147	2,07	82	371
4	165	1,77	79	370
5	185	1,42	76	346
6	200	1,08	70	309
Blade angle -6º				
Point	**Airflow (m^3/s)**	**Pressure (kPa)**	**Efficiency (%)**	**Effective power (kW)**
1	125	2,53	79	400
2	143	2,38	82	415
3	170	2,01	81	422
4	191	1,65	78	404

Point	Airflow (m^3/s)	Pressure (kPa)	Efficiency (%)	Effective power (kW)
5	223	1,08	70	344
Blade angle -4º				
Point	**Airflow (m^3/s)**	**Pressure (kPa)**	**Efficiency (%)**	**Effective power (kW)**
1	143	2,60	80	465
2	153	2,50	82	466
3	177	2,23	82	481
4	204	1,83	79	473
5	222	1,55	76	453
6	238	1,18	70	401
Blade angle -2º				
Point	**Airflow (m^3/s)**	**Pressure (kPa)**	**Efficiency (%)**	**Effective power (kW)**
1	155	2,70	80	523
2	166	2,60	82	526
3	190	2,35	82	545
4	222	1,91	79	537
5	240	1,57	75	502
6	254	1,27	70	461
Blade angle 0º				
Point	**Airflow (m^3/s)**	**Pressure (kPa)**	**Efficiency (%)**	**Effective power (kW)**
1	170	2,75	80	584
2	179	2,70	82	589
3	212	2,36	81	618
4	230	2,11	79	614
5	250	1,77	76	582
6	268	1,42	70	544
Blade angle +2º				
Point	**Airflow (m^3/s)**	**Pressure (kPa)**	**Efficiency (%)**	**Effective power (kW)**
1	182	2,79	80	635
2	208	2,61	81	670
3	232	2,28	79	670

Point	Airflow (m^3/s)	Pressure (kPa)	Efficiency (%)	Effective power (kW)
4	255	2,02	77	669
5	283	1,56	70	631

5.2.2. Vilafruns

5.2.2.1. First configuration

Table 53. Initial data of the first configuration.

Branches		Description	Section (m^2)	Perimeter (m)
11	10	Control room	35	22,66
1	2	Shaft		
3	4	Cross section change	40	24,6
4	5	Inlet main fan	34,54	24,092
5	6	Main forcing fan	34,5	24,092
6	4	Double door	34	23,25
6	7	Bend 120º	34,8	24,09
7	8	Bend 140º	35	24,09
8	9	Conveyor belt	34,5	23,216
9	11	Conveyor belt	34,04	23,216
10	59	Conveyor belt and cross section change	34,04	21,85
14	88	No obstacles	28	19,50
15	16	No obstacles	29	19,50
16	17	No obstacles	29	19,50
17	18	No obstacles	29	19,50
18	19	No obstacles	29	19,50
19	20	Bend 120º	29	18,00
20	21	Conveyor belt	31,84	22,60
21	22	Conveyor belt	31,84	22,60
22	23	Bend 125º	31,84	22,66
23	24	Conveyor belt	35,96	26,28
10	25	No obstacles	28,37	20,00
25	26	Double door	28,37	20,00
26	17	No obstacles	28,37	20,00

Branches		Description	Section (m^2)	Perimeter (m)
27	28	Conveyor belt	31,54	22,66
28	29	Double door	31,54	22,46
29	16	Conveyor belt	33,4	25,00
8	30	Conveyor belt	32	23,22
30	31	Double door	32	23,88
31	20	Conveyor belt	32	22,60
22	32	Conveyor belt	30	22,60
32	38	No obstacles	21,61	20,00
2	34	No obstacles	21,61	20,00
33	37	No obstacles	21,61	20,00
35	36	No obstacles	21,61	20,00
38	39	Double door	22	20,00
39	33	No obstacles	22	20,00
27	96	Conveyor belt	31,33	19,34
56	33	Bend 90º	32,3	21,00
100	56	Bend 110º	32,30	21,00
59	27	Conveyor belt	34,04	23,41
59	60	No obstacles	34,08	23,24
60	57	Curtain		
57	58	No obstacles	34,08	23,24
58	61	Bend 100º	34	23,24
61	62	Duct system	32,29	23,09
62	97	Duct system	32,29	23,09
63	64	No obstacles	31,080625	22,66
64	65	Bend 90º	31,080625	22,66
65	66	No obstacles	31,080625	22,66
66	67	No obstacles	31,080625	22,66
67	68	No obstacles	31,080625	22,66
68	69	Bend 90º	31,080625	22,66
69	70	No obstacles	31,080625	22,66
70	71	No obstacles	31,080625	22,66
71	72	Bend 120º	32,29	22,66

Branches		Description	Section (m^2)	Perimeter (m)
72	73	No obstacles	31,080625	22,66
73	74	No obstacles	31,080625	22,66
74	75	No obstacles	31,080625	22,66
75	76	No obstacles	31,080625	22,66
76	78	Bend 90º	30	22,66
78	79	No obstacles	31,080625	22,66
79	80	Bend 90º	30	22,66
80	81	No obstacles	30	22,66
81	82	Bend 110º	31,080625	22,66
82	83	Bend 90º	31,080625	22,66
83	84	Bend 110º	31,080625	22,66
84	85	Bend 110º	31,080625	22,66
85	86	Bend 100º	31,080625	22,66
86	87	Bend 90º	27,83	22,03
87	14	Bend 90º	27,83	22,03
88	89	Bend 120º	27,83	22,03
89	90	Bend 120º	27,83	22,03
90	15	Bend 90º	27,83	22,03
97	63	Bend 90º + duct system	31,08	22,66
96	97	Conveyor belt + Bend 90º	32,29	23,09
99	3	Occasional obstacles	31,081	22,66
36	99	Control room	40	24,60
37	35	Bend 90º	21,61	20,00
34	100	Bend 100º	21,61	20,00
100	37	Bend 90º	21,61	20,00
82	111	Bend 120º	31,080625	22,66
111	112	Bend 90º	31,080625	22,66
112	113	Bend 90º	31,080625	22,66
113	114	No obstacles	31,080625	22,66
114	115	Bend 80º	31,080625	22,66
115	116	No obstacles	31,080625	22,66
116	117	No obstacles	31,080625	22,66

Branches		Description	Section (m^2)	Perimeter (m)
117	118	No obstacles	31,080625	22,66
118	119	No obstacles	31,080625	22,66
119	14	No obstacles	27,83	22,03
2	99	Occasional obstacles	31,080625	22,6621875

Table 54. Friction parameters, first configuration.

Branches		Dh (m)	K (kg/m^3)	Total Leq (m)	R (Ns^2/m^8)
11	10	6,18	0,01157		
1	2		0,01020		
3	4	6,50	0,00822	1,4833	
4	5	5,73	0,00822		
5	6	5,73	0,00822		
6	4	5,85	No friction factor	R	2,5
6	7	5,78	0,00822	25,310	
7	8	5,81	0,00822	27,577	
8	9	5,94	0,00794	19,150	
9	11	5,86	0,00794	19,54	
10	59	6,23	0,00802	229,093	
14	88	5,74	0,00891		
15	16	5,95	0,00851		
16	17	5,95	0,00732		
17	18	5,95	0,00732		
18	19	5,95	0,00851		
19	20	6,44	0,00655	38,3531	
20	21	5,64	0,00860	18,514	
21	22	5,64	0,00860	18,514	
22	23	5,62	0,00851	24,756	
23	24	5,47	0,00859	14,355	
10	25	5,67	0,00851		
25	26		No friction factor	R	2,5
26	17	5,67	0,00851		
27	28	5,57	0,00851	16,832	

Branches		**Dh (m)**	**K (kg/m³)**	**Total Leq (m)**	**R (Ns²/m⁸)**
28	29		No friction factor	R	2,5
29	16	5,34	0,01015	12,882	
8	30	5,51	0,00794	19,541	
30	31		No friction factor	R	0,45
31	20	5,66	0,00860	18,514	
22	32	5,31	0,00860	18,514	
32	38	4,32	0,00959		
2	34	4,32	0,00959		
33	37	4,32	0,00959		
35	36	4,32	0,00959		
38	39		No friction factor	R	2,5
39	33	4,40	0,00959		
27	96	6,48	0,01015	16,725	
56	33	6,15	0,00959	16,038	
100	56	6,15	0,00959	3,208	
59	27	5,82	0,01015	16,3623	
59	60	5,87	0,00703		
60	57		No friction factor	R	0,45
57	58	5,87	0,00703		
58	61	5,85	0,00703	20,818	
61	62	5,59	0,00787	3,1089	
62	97	5,59	0,00787	3,1089	
63	64	5,49	0,00851		
64	65	5,49	0,00851	19,3327	
65	66	5,49	0,00851		
66	67	5,49	0,00851		
67	68	5,49	0,00851		
68	69	5,49	0,00851	19,333	
69	70	5,49	0,00851		
70	71	5,49	0,00851		
71	72	5,70	0,00851	24,102	
72	73	5,49	0,00851		

Branches		Dh (m)	K (kg/m^3)	Total Leq (m)	R (Ns^2/m^8)
73	74	5,49	0,00851		
74	75	5,49	0,00851		
75	76	5,49	0,00851		
76	78	5,30	0,00851	18,6605	
78	79	5,49	0,00851		
79	80	5,30	0,00851	18,6605	
80	81	5,30	0,00851		
81	82	5,49	0,00851	21,2660	
82	83	5,49	0,00851	19,3327	
83	84	5,49	0,00851	19,3327	
84	85	5,49	0,00851	21,2660	
85	86	5,49	0,00851	19,3327	
86	87	5,05	0,00891	17,0079	
87	14	5,05	0,00891	17,0079	
88	89	5,05	0,00891	20,4095	
89	90	5,05	0,00891	20,4095	
90	15	5,05	0,00891	17,0079	
97	63	5,49	0,00851	19,333	
96	97	5,59	0,00787	42,619	
99	3	5,49	0,00851		
36	99	6,50	0,01157	38,880	
37	35	4,32	0,00959	13,520	
34	100	4,32	0,00959	13,520	
100	37	4,32	0,00959	13,520	
82	111	5,49	0,00851	23,199	
111	112	5,49	0,00851	19,333	
112	113	5,49	0,00851	19,333	
113	114	5,49	0,00851		
114	115	5,49	0,00851	21,266	
115	116	5,49	0,00851		
116	117	5,49	0,00851		
117	118	5,49	0,00851		

Branches		Dh (m)	K (kg/m^3)	Total Leq (m)	R (Ns^2/m^8)
118	119	5,49	0,00851		
119	14	5,05	0,00891		
2	99	5,49	0,00851		

Table 55. Modelling results from first configuration.

Branches		Resistance (N·s^2/m^8)	Airflow (m^3/s)	Pressure drop (Pa)
11	10	0,00056	139,56	10,9
1	2	0	146,72	0
3	4	0,00459	168	129,5
4	5	0,00031	175,13	9,5
5	6	0,00032	175,13	9,8
6	4	250.000	7,13	127
6	7	0,00116	168	32,7
7	8	0,00061	168	17,2
8	9	0,00061	139,56	11,9
9	11	0,00599	139,56	116,7
10	59	0,00453	113,41	58,3
14	88	0	118,74	0
15	16	0	118,74	0
16	17	0	130,58	0
17	18	0	139,56	0
18	19	0	139,56	0
19	20	0,0053	139,56	103,2
20	21	0,00072	168	20,3
21	22	0,00357	168	100,8
22	23	0,00101	146,72	21,7
23	24	0,01315	146,72	283,1
10	25	0,00261	26,15	1,8
25	26	0,435	26,15	297,5
26	12	0,00038	26,15	0,3
27	28	0,00181	11,83	0,3
28	29	170.000	11,83	238

Branches		Resistance ($N \cdot s^2/m^8$)	Airflow (m^3/s)	Pressure drop (Pa)
29	16	0,00286	11,83	0,4
8	30	0,00083	28,44	0,7
30	31	0,668	28,44	540,3
31	20	0,0015	28,44	1,2
22	32	0,00071	21,28	0,3
32	38	0,00255	21,28	1,2
2	34	0,00027	7,97	0
33	37	0,00082	17,43	0,2
35	36	0,00169	29,25	1,4
38	39	0,668	21,28	302,5
39	33	0,00201	21,28	0,9
27	96	0,00176	81,03	11,6
56	33	0,00044	-3,85	0
100	56	0,00026	-3,85	0
59	27	0,0003	92,86	2,6
59	60	0,00045	20,54	0,2
60	57	0,075	20,54	31,6
57	58	0,00021	20,54	0,1
58	61	0,00039	20,54	0,2
61	62	0,00296	20,54	1,2
62	97	0,00025	20,54	0,1
63	64	0,00075	89,75	6
64	65	0,00081	89,75	6,5
65	66	0,00017	89,75	1,4
66	67	0,0001	89,75	0,8
67	68	0,00015	89,75	1,2
68	69	0,00025	89,75	2
69	70	0,00024	89,75	1,9
70	71	0,00021	89,75	1,7
71	72	0,00074	89,75	6
72	73	0,00094	89,75	7,6
73	74	0,00046	89,75	3,7

Branches		**Resistance (N·s²/m⁸)**	**Airflow (m³/s)**	**Pressure drop (Pa)**
74	75	0,00031	89,75	2,5
75	76	0,00018	89,75	1,4
76	78	0,00029	89,75	2,3
78	79	0,00028	89,75	2,3
79	80	0,00059	101,57	6,1
80	81	0,00084	101,57	8,7
81	82	0,00063	101,57	6,5
82	83	0,00057	93,12	4,9
83	84	0,00156	93,12	13,5
84	85	0,00086	93,12	7,5
85	86	0,00075	93,12	6,5
86	87	0,00291	93,12	25,2
87	14	0,00118	93,12	10,2
88	89	0,00087	118,74	12,3
89	90	0,00053	118,74	7,5
90	15	0,00343	118,74	48,4
97	63	0,0004	89,75	3,2
96	97	0,00403	69,21	19,3
99	3	0,00009	168	2,5
36	99	0,00028	29,25	0,2
37	35	0,00151	29,25	1,3
34	100	0,00064	7,97	0
100	37	0,00171	11,82	0,2
82	111	0,00081	8,45	0,1
111	112	0,00043	8,45	0
112	113	0,00062	8,45	0
113	114	0,00046	8,45	0
114	115	0,00045	8,45	0
115	116	0,00041	25,62	0,3
116	117	0,00053	25,62	0,3
117	118	0,00198	25,62	1,3
118	119	0,00019	25,62	0,1

Branches		Resistance (N·s²/m⁸)	Airflow (m³/s)	Pressure drop (Pa)
119	14	0,1	25,62	65,7
2	99	0,00017	138,75	3,3
12	17	0	8,98	0
12	115	0	17,17	0
96	79	0,5	11,82	69,9

5.2.2.2. Second configuration

Table 56. Initial data of the second configuration.

Branches		Description	Section (m²)	Perimeter (m)
11	10	Control room	35	22,66
1	2	Shaft		0,00
3	4	Cross section change	40	24,6
4	5	Inlet main fan	34,54	24,092
5	6	Main forcing fan	34,5	24,092
6	4	Double door	34	23,25
6	7	Bend 120º	34,8	24,09
7	8	Bend 140º	35	24,09
8	9	Conveyor belt	34,5	23,216
9	11	Conveyor belt	34,04	23,216
10	59	Conveyor belt and cross section change	34,04	21,85
14	88	No obstacles	28	19,50
15	16	No obstacles	29	19,50
16	17	No obstacles	29	19,50
17	18	No obstacles	29	19,50
18	19	No obstacles	29	19,50
19	20	Bend 120º	29	18,00
20	21	Conveyor belt	31,84	22,60
21	22	Conveyor belt	31,84	22,60
22	23	Bend 125º	31,84	22,66
23	24	Conveyor belt	35,96	26,28
10	25	No obstacles	28,37	20,00

Branches		Description	Section (m^2)	Perimeter (m)
25	26	Double door	28,37	20,00
26	17	No obstacles	28,37	20,00
27	28	Conveyor belt	31,54	22,66
28	29	Double door	31,54	22,46
29	16	Conveyor belt	33,4	25,00
8	30	Conveyor belt	32	23,22
30	31	Double door	32	23,88
31	20	Conveyor belt	32	22,60
22	32	Conveyor belt	30	22,60
32	38	No obstacles	21,61	20,00
2	34	No obstacles	21,61	20,00
33	37	No obstacles	21,61	20,00
35	36	No obstacles	21,61	20,00
38	39	Double door	22	20,00
39	33	No obstacles	22	20,00
40	41	No obstacles	31,33	19,34
27	96	Conveyor belt	31,33	19,34
41	42	No obstacles	31,33	19,34
42	43	No obstacles	31,33	19,34
43	44	No obstacles	31,33	19,34
54	53	No obstacles	32,3	25,82
55	54	Bend 90º	33	23,10
44	55	Bend 90º	33	23,10
56	33	Bend 90º	32,3	21,00
100	56	Bend 110º	32,30	21,00
59	27	Conveyor belt	34,04	23,41
59	60	No obstacles	34,08	23,24
60	57	Curtain		
57	58	No obstacles	34,08	23,24
58	61	Bend 100º	34	23,24
61	62	Duct system	32,29	23,09
62	97	Duct system	32,29	23,09

Branches		Description	Section (m^2)	Perimeter (m)
63	64	No obstacles	31,080625	22,66
64	65	Bend 90º	31,080625	22,66
65	66	No obstacles	31,080625	22,66
66	67	No obstacles	31,080625	22,66
67	68	No obstacles	31,080625	22,66
68	69	Bend 90º	31,080625	22,66
69	70	No obstacles	31,080625	22,66
70	71	No obstacles	31,080625	22,66
71	72	Bend 120º	32,29	22,66
72	73	No obstacles	31,080625	22,66
73	74	No obstacles	31,080625	22,66
74	75	No obstacles	31,080625	22,66
75	76	No obstacles	31,080625	22,66
77	102	Conveyor belt	31,33	22,66
76	78	Bend 90º	30	22,66
78	79	No obstacles	31,080625	22,66
79	80	Bend 90º	30	22,66
80	81	No obstacles	30	22,66
81	82	Bend 110º	31,080625	22,66
82	83	Bend 90º	31,080625	22,66
83	84	Bend 110º	31,080625	22,66
84	85	Bend 110º	31,080625	22,66
85	86	Bend 100º	31,080625	22,66
86	87	Bend 90º	27,83	22,03
87	14	Bend 90º	27,83	22,03
88	89	Bend 120º	27,83	22,03
89	90	Bend 120º	27,83	22,03
90	15	Bend 90º	27,83	22,03
53	12	Duct system	32,3	25,82
12	13	Duct system	32,3	25,82
13	91	Duct system	32,3	25,82
91	92	Duct system	32,3	25,82

Branches		Description	Section (m^2)	Perimeter (m)
92	93	Duct system	32,3	25,82
93	94	Duct system + Bend 75º	32,3	25,82
94	95	Duct system + Bend 90º	32,3	25,82
95	80	Duct system + Bend 90º	32,3	25,82
96	98	Conveyor belt	31,33	19,34
97	63	Bend 90º + duct system	31,08	22,66
96	97	Conveyor belt + Bend 90º	32,29	23,09
98	77	Conveyor belt	31,33	19,34
99	3	Occasional obstacles	31,081	22,66
36	99	Control room	40	24,60
37	35	Bend 90º	21,61	20,00
34	100	Bend 100º	21,61	20,00
100	37	Bend 90º	21,61	20,00
102	40	Conveyor belt+ Bend 120º	31,33	19,34
102	101	Bend 90º	31,080625	22,66
101	103	No obstacles	31,080625	22,66
103	104	No obstacles	31,080625	22,66
104	29	Bend 90º	31,080625	22,66
82	111	Bend 120º	31,080625	22,66
111	112	Bend 90º	31,080625	22,66
112	113	Bend 90º	31,080625	22,66
113	114	No obstacles	31,080625	22,66
114	115	Bend 80º	31,080625	22,66
115	116	No obstacles	31,080625	22,66
116	117	No obstacles	31,080625	22,66
117	118	No obstacles	31,080625	22,66
118	119	No obstacles	31,080625	22,66
119	14	No obstacles	27,83	22,03
2	99	Occasional obstacles	31,080625	22,6621875

Table 57. Friction parameters, second configuration.

Branches		Dh (m)	K (kg/m^3)	Total Leq (m)	R (Ns^2/m^8)
11	10	6,178	0,011613		
1	2		0,010200		
3	4	6,504	0,008164	1,4932	
4	5	5,735	0,008164		
5	6	5,728	0,008164		
6	4	5,849	No friction factor	R	2,5
6	7	5,778	0,008164	25,4792	
7	8	5,811	0,008164	27,7611	
8	9	5,944	0,007945	19,1272	
9	11	5,865	0,007945	19,5176	
10	59	6,233	0,008050	228,1154	
14	88	5,744	0,008904		
15	16	5,949	0,008568		
16	17	5,949	0,007322		
17	18	5,949	0,006946		
18	19	5,949	0,008568		
19	20	6,444	0,006946	36,1851	
20	21	5,635	0,008587	18,5510	
21	22	5,635	0,008587	18,5510	
22	23	5,620	0,008568	24,5976	
23	24	5,473	0,008587	14,3548	
10	25	5,674	0,008568		
25	26		No friction factor	R	2,5
26	17	5,674	0,008568		
27	28	5,567	0,008568	16,7239	
28	29		No friction factor	R	2,5
29	16	5,344	0,010178	12,8471	
8	30	5,513	0,007945	19,5176	
30	31		No friction factor	R	0,45
31	20	5,664	0,008587	18,5497	
22	32	5,310	0,008587	18,5497	

Branches		Dh (m)	K (kg/m^3)	Total Leq (m)	R (Ns^2/m^8)
32	38	4,322	0,009553		
2	34	4,322	0,009553		
33	37	4,322	0,009553		
35	36	4,322	0,009553		
38	39		No friction factor	R	2,5
39	33	4,400	0,009553		
40	41	6,480	0,006967		
27	96	6,480	0,006967	24,3680	
41	42	6,480	0,006967		
42	43	6,480	0,006967		
43	44	6,480	0,006967		
54	53	5,004	0,010880		
55	54	5,714	0,010880	13,1301	
44	55	5,714	0,010880	13,1301	
56	33	6,152	0,009553	16,1000	
100	56	6,152	0,009553	3,2200	
59	27	5,816	0,006967	23,8399	
59	60	5,866	0,007058		
60	57		No friction factor	R	0,45
57	58	5,866	0,007058		
58	61	5,852	0,007058	20,7270	
61	62	5,594	0,007917	3,0918	
62	97	5,594	0,007917	3,0918	
63	64	5,486	0,008568		
64	65	5,486	0,008568	19,2087	
65	66	5,486	0,008568		
66	67	5,486	0,008568		
67	68	5,486	0,008568		
68	69	5,486	0,008568	19,2087	
69	70	5,486	0,008568		
70	71	5,486	0,008568		
71	72	5,699	0,008568	23,9474	

Branches		Dh (m)	K (kg/m^3)	Total Leq (m)	R (Ns^2/m^8)
72	73	5,486	0,008568		
73	74	5,486	0,008568		
74	75	5,486	0,008568		
75	76	5,486	0,008568		
77	102	5,530	0,008568	18,5409	
76	78	5,295	0,008568	18,5409	
78	79	5,486	0,008568		
79	80	5,295	0,008568	18,5409	
80	81	5,295	0,008568		
81	82	5,486	0,008568	21,1296	
82	83	5,486	0,008568	19,2087	
83	84	5,486	0,008568	19,2087	
84	85	5,486	0,008568	21,1296	
85	86	5,486	0,008568	19,2087	
86	87	5,053	0,008904	17,0254	
87	14	5,053	0,008904	17,0254	
88	89	5,053	0,008904	20,4304	
89	90	5,053	0,008904	20,4304	
90	15	5,053	0,008904	17,0254	
53	12	5,004	0,010880	12,8148	
12	13	5,004	0,010880	12,8148	
13	91	5,004	0,010880	12,8148	
91	92	5,004	0,010880	12,8148	
92	93	5,004	0,010880	12,8148	
93	94	5,004	0,010880	19,3162	
94	95	5,004	0,010880	27,5946	
95	80	5,004	0,010880	27,5946	
96	98	6,480	No friction factor	R	
97	63	5,486	0,008568	19,2087	
96	97	5,593	0,007917	34,0076	
98	77	6,480	0,006967	26,7193	
99	3	5,486	0,008568		

Branches		Dh (m)	K (kg/m^3)	Total Leq (m)	R (Ns^2/m^8)
36	99	6,504	0,011613	38,7487	
37	35	4,322	0,009553	13,5721	
34	100	4,322	0,009553	13,5721	
100	37	4,322	0,009553	13,5721	
102	40	6,480	0,006967	54,6232	
102	101	5,486	0,008568		
101	103	5,486	0,008568		
103	104	5,486	0,008568		
104	29	5,486	0,008568	19,2087	
82	111	5,486	0,008568	23,0505	
111	112	5,486	0,008568	19,2087	
112	113	5,486	0,008568	19,2087	
113	114	5,486	0,008568	0,0000	
114	115	5,486	0,008568	21,1296	
115	116	5,486	0,008568		
116	117	5,486	0,008568		
117	118	5,486	0,008568		
118	119	5,486	0,008568		
119	14	5,053	0,008904		
2	99	5,486	0,008568		

Table 58. Modelling results from second configuration.

Branches		Resistance (N·s^2/m^8)	Airflow (m^3/s)	Pressure drop (Pa)
26	115	0	15,05	0
11	10	0,00055	149,18	12,2
1	2	0	165,21	0
3	4	0,00456	174	138,1
4	5	0,00031	175,32	9,5
5	6	0,00032	175,32	9,8
6	4	250.000	1,32	4,4
6	7	0,00115	174	34,8
7	8	0,0006	174	18,2

Branches		Resistance ($N \cdot s^2/m^8$)	Airflow (m^3/s)	Pressure drop (Pa)
8	9	0,00061	149,18	13,6
9	11	0,006	149,18	133,5
10	59	0,00455	124,97	71,1
14	88	0,00029	116,9	4
15	16	0,00038	116,9	5,2
16	17	0,00472	140,02	92,5
17	18	0,00478	149,18	106,4
18	19	0,0009	149,18	20
19	20	0,0056	149,18	124,6
20	21	0,00072	174	21,8
21	22	0,00356	174	107,8
22	23	0,001	165,21	27,3
23	24	0,01315	165,21	358,9
10	25	0,00257	24,22	1,5
25	26	0,56	24,22	328,4
26	17	0,00022	9,17	0
27	28	0,00178	11,15	0,2
28	29	130.000	11,15	161,8
29	16	0,00286	23,12	1,5
8	30	0,00084	24,82	0,5
30	31	120.000	24,82	738,9
31	20	0,0015	24,82	0,9
22	32	0,00071	8,79	0,1
32	38	0,00255	8,79	0,2
2	34	0,00027	20,27	0,1
33	37	0,00082	16,54	0,2
35	36	0,00169	29,06	1,4
38	39	500.000	8,79	386,2
39	33	0,00201	8,79	0,2
40	41	0,00012	36,38	0,2
27	96	0,00123	98,38	11,9
41	42	0,00135	36,38	1,8

Branches		Resistance ($N \cdot s^2/m^8$)	Airflow (m^3/s)	Pressure drop (Pa)
42	43	0,00005	36,38	0,1
43	44	0,00019	36,38	0,3
54	53	0,01598	36,38	21,1
55	54	0,00027	36,38	0,4
44	55	0,00018	36,38	0,2
56	33	0,00044	7,75	0
100	56	0,00026	7,75	0
59	27	0,00024	109,53	2,9
59	60	0,00046	15,43	0,1
60	57	0,1	15,43	23,8
57	58	0,00021	15,43	0,1
58	61	0,0004	15,43	0,1
61	62	0,00298	15,43	0,7
62	97	0,00025	15,43	0,1
63	64	0,00073	65,47	3,1
64	65	0,0008	65,47	3,4
65	66	0,00017	65,47	0,7
66	67	0,0001	65,47	0,4
67	68	0,00014	65,47	0,6
68	69	0,00025	65,47	1,1
69	70	0,00023	65,47	1
70	71	0,00021	65,47	0,9
71	72	0,00073	65,47	3,1
72	73	0,00092	65,47	3,9
73	74	0,00045	65,47	1,9
74	75	0,00031	65,47	1,3
75	76	0,00017	65,47	0,7
77	102	0,00088	48,35	2,1
76	78	0,00029	65,47	1,2
78	79	0,00028	65,47	1,2
79	80	0,00058	65,47	2,5
80	81	0,00083	101,85	8,6

Branches		Resistance ($N \cdot s^2/m^8$)	Airflow (m^3/s)	Pressure drop (Pa)
81	82	0,00058	101,85	6
82	83	0,00047	54,65	1,4
83	84	0,00153	54,65	4,6
84	85	0,00085	54,65	2,5
85	86	0,00074	54,65	2,2
86	87	0,00291	54,65	8,7
87	14	0,00118	54,65	3,5
88	89	0,00087	116,9	11,9
89	90	0,00053	116,9	7,2
90	15	0,00342	116,9	46,7
53	12	0,00051	36,38	0,7
12	13	0,00047	36,38	0,6
13	91	0,00115	36,38	1,5
91	92	0,00033	36,38	0,4
92	93	0,00127	36,38	1,7
93	94	0,00044	36,38	0,6
94	95	0,0005	36,38	0,7
95	80	0,00109	36,38	1,4
96	98	0,001	48,35	2,3
97	63	0,00039	65,47	1,7
96	97	0,00402	50,03	10,1
98	77	0,0008	48,35	1,9
99	3	0,00009	174	2,7
36	99	0,00028	29,06	0,2
37	35	0,0015	29,06	1,3
34	100	0,00064	20,27	0,3
100	37	0,0017	12,52	0,3
102	40	0,00083	36,38	1,1
102	101	100.000	11,97	143,2
101	103	0,00118	11,97	0,2
103	104	0,00263	11,97	0,4
104	29	0,00037	11,97	0,1

Branches		Resistance ($N \cdot s^2/m^8$)	Airflow (m^3/s)	Pressure drop (Pa)
82	111	0,00081	47,19	1,8
111	112	0,00042	47,19	0,9
112	113	0,00062	47,19	1,4
113	114	0,00045	47,19	1
114	115	0,00045	47,19	1
115	116	0,00041	62,24	1,6
116	117	0,00051	62,24	2
117	118	0,00195	62,24	7,6
118	119	0,00019	62,24	0,7
119	14	0,00128	62,24	5
2	99	0,00017	144,94	3,6

5.2.2.3. Third configuration

Table 59. Initial data of the third configuration.

Branches		Description	Section (m^2)	Perimeter (m)
11	10	Control room	35	22,66
1	2	Shaft		
3	4	Cross section change	40	24,6
4	5	Inlet main fan	34,54	24,092
5	6	Main forcing fan	34,5	24,092
6	4	Double door	34	23,25
6	7	Bend 120º	34,8	24,09
7	8	Bend 140º	35	24,09
8	9	Conveyor belt	34,5	23,216
9	11	Conveyor belt	34,04	23,216
10	59	Conveyor belt and cross section change	34,04	21,85
14	88	No obstacles	28	19,50
15	16	No obstacles	29	19,50
16	17	No obstacles	29	19,50
17	18	No obstacles	29	19,50
18	19	No obstacles	29	19,50

Branches		Description	Section (m^2)	Perimeter (m)
19	20	Bend 120º	29	18,00
20	21	Conveyor belt	31,84	22,60
21	22	Conveyor belt	31,84	22,60
22	23	Bend 125º	31,84	22,66
23	24	Conveyor belt	35,96	26,28
10	25	No obstacles	28,37	20,00
25	26	Double door	28,37	20,00
26	17	No obstacles	28,37	20,00
27	28	Conveyor belt	31,54	22,66
28	29	Double door	31,54	22,46
29	16	Conveyor belt	33,4	25,00
8	30	Conveyor belt	32	23,22
30	31	Double door	32	23,88
31	20	Conveyor belt	32	22,60
22	32	Conveyor belt	30	22,60
32	38	No obstacles	21,61	20,00
2	34	No obstacles	21,61	20,00
33	37	No obstacles	21,61	20,00
35	36	No obstacles	21,61	20,00
38	39	Double door	22	20,00
39	33	No obstacles	22	20,00
40	41	No obstacles	31,33	19,34
27	96	Conveyor belt	31,33	19,34
41	42	No obstacles	31,33	19,34
42	43	No obstacles	31,33	19,34
43	44	No obstacles	31,33	19,34
44	45	Duct system + Bend 90º	29,6	25,82
45	46	Duct system + Bend 110º	34	23,50
46	47	Duct system	32	21,00
47	48	Duct system + Bend 90º	33,6	21,50
48	49	Duct system + Bend 120º	34	21,40
49	50	Duct system	33	23,60

Branches		**Description**	**Section (m^2)**	**Perimeter (m)**
50	51	Duct system	32	24,00
51	52	Duct system	31	19,80
52	53	Duct system + Bend 90º	32,3	25,82
54	53	No obstacles	32,3	25,82
55	54	Bend 90º	33	23,10
44	55	Bend 90º	33	23,10
56	33	Bend 90º	32,3	21,00
100	56	Bend 110º	32,30	21,00
59	27	Conveyor belt	34,04	23,41
59	60	No obstacles	34,08	23,24
60	57	Curtain		
57	58	No obstacles	34,08	23,24
58	61	Bend 100º	34	23,24
61	62	Duct system	32,29	23,09
62	97	Duct system	32,29	23,09
63	64	No obstacles	31,081	22,66
64	65	Bend 90º	31,081	22,66
65	66	No obstacles	31,081	22,66
66	67	No obstacles	31,081	22,66
67	68	No obstacles	31,081	22,66
68	69	Bend 90º	31,081	22,66
69	70	No obstacles	31,081	22,66
70	71	No obstacles	31,081	22,66
71	72	Bend 120º	32,290	22,66
72	73	No obstacles	31,081	22,66
73	74	No obstacles	31,081	22,66
74	75	No obstacles	31,081	22,66
75	76	No obstacles	31,081	22,66
77	102	Conveyor belt	31,330	22,66
76	78	Bend 90º	30,000	22,66
78	79	No obstacles	31,081	22,66
79	80	Bend 90º	30,000	22,66

Branches		Description	Section (m^2)	Perimeter (m)
80	81	No obstacles	30	22,66
81	82	Bend 110º	31,081	22,66
82	83	Bend 90º	31,081	22,66
83	84	Bend 110º	31,081	22,66
84	85	Bend 110º	31,081	22,66
85	86	Bend 100º	31,081	22,66
86	87	Bend 90º	27,830	22,03
87	14	Bend 90º	27,830	22,03
88	89	Bend 120º	27,830	22,03
89	90	Bend 120º	27,830	22,03
90	15	Bend 90º	27,830	22,03
53	12	Duct system	32,300	25,82
12	13	Duct system	32,300	25,82
13	91	Duct system	32,300	25,82
91	92	Duct system	32,300	25,82
92	93	Duct system	32,300	25,82
93	94	Duct system + Bend 75º	32,300	25,82
94	95	Duct system + Bend 90º	32,3	25,82
95	80	Duct system + Bend 90º	32,3	25,82
96	98	Conveyor belt	31,33	19,34
97	63	Bend 90º + duct system	31,08	22,66
96	97	Conveyor belt + Bend 90º	32,29	23,09
98	77	Conveyor belt	31,33	19,34
99	3	Occasional obstacles	31,081	22,66
36	99	Control room	40	24,60
37	35	Bend 90º	21,61	20,00
34	100	Bend 100º	21,61	20,00
100	37	Bend 90º	21,61	20,00
102	40	Conveyor belt+ Bend 120º	31,33	19,34
102	101	Bend 90º	31,08	22,66
101	103	No obstacles	31,08	22,66
103	104	No obstacles	31,08	22,66

Branches		**Description**	**Section (m^2)**	**Perimeter (m)**
104	29	Bend 90º	31,08	22,66
82	111	Bend 120º	31,08	22,66
111	112	Bend 90º	31,08	22,66
112	113	Bend 90º	31,08	22,66
113	114	No obstacles	31,08	22,66
114	115	Bend 80º	31,08	22,66
115	116	No obstacles	31,08	22,66
116	117	No obstacles	31,08	22,66
117	118	No obstacles	31,08	22,66
118	119	No obstacles	31,08	22,66
119	14	No obstacles	27,83	22,03
2	99	Occasional obstacles	31,08	22,66

Table 60. Friction parameters, third configuration.

Branches		**Dh (m)**	**K (kg/m^3)**	**Total Leq (m)**	**R (Ns^2/m^8)**
11	10	6,18	0,01170		
1	2		0,01020		
3	4	6,50	0,00837	1,457	
4	5	5,73	0,00837		
5	6	5,73	0,00837		
6	4	5,85	No friction factor	No friction factor	
6	7	5,78	0,00837	24,855	
7	8	5,81	0,00837	27,081	
8	9	5,94	0,00819	18,555	
9	11	5,86	0,00819	18,934	
10	59	6,23	0,00110		
14	88	5,74	0,00895		
15	16	5,95	0,00869		
16	17	5,95	0,00732		
17	18	5,95	0,00688		
18	19	5,95	0,00869		
19	20	6,44	0,00688	36,544	

Branches		Dh (m)	K (kg/m^3)	Total Leq (m)	R (Ns^2/m^8)
20	21	5,64	0,00742	21,476	
21	22	5,64	0,00742	21,476	
22	23	5,62	0,00869	24,264	
23	24	5,47	0,00821	15,013	
10	25	5,67	0,00869		
25	26		No friction factor	No friction factor	2,5
26	17	5,67	0,00869		
27	28	5,57	0,00869	16,497	
28	29		No friction factor	No friction factor	2,5
29	16	5,34	0,01024	12,771	
8	30	5,51	0,00819	18,934	
30	31		No friction factor	No friction factor	0,45
31	20	5,66	0,00742	21,476	
22	32	5,31	0,00742	21,476	
32	38	4,32	0,00959		
2	34	4,32	0,00959		
33	37	4,32	0,00959		
35	36	4,32	0,00959		
38	39		No friction factor	No friction factor	2,5
39	33	4,40	0,00959		
40	41	6,48	0,00778		
27	96	6,48	0,00778	21,814	
41	42	6,48	0,00778		
42	43	6,48	0,00778		
43	44	6,48	0,00778		
44	45	4,59	0,01113	12,488	
45	46	5,79	0,01113	15,402	
46	47	6,10	0,01113	2,694	
47	48	6,25	0,01113	16,668	
48	49	6,36	0,01113	16,914	
49	50	5,59	0,01113	2,398	
50	51	5,33	0,01113	2,358	

Branches		Dh (m)	K (kg/m^3)	Total Leq (m)	R (Ns^2/m^8)
51	52	6,26	0,01113	2,858	
52	53	5,00	0,01113	13,427	
54	53	5,00	0,01113	0,000	
55	54	5,71	0,01113	12,831	
44	55	5,71	0,01113	12,831	
56	33	6,15	0,00959	16,034	
100	56	6,15	0,00821	3,746	
59	27	5,82	0,00778	21,342	
59	60	5,87	0,00766		
60	57		No friction factor	No friction factor	0,45
57	58	5,87	0,00766		
58	61	5,85	0,00766	19,104	
61	62	5,59	0,00797	3,070	
62	97	5,59	0,01024	2,391	
63	64	5,49	0,00869		
64	65	5,49	0,00869	18,948	
65	66	5,49	0,00869		
66	67	5,49	0,00869		
67	68	5,49	0,00869		
68	69	5,49	0,00869	18,948	
69	70	5,49	0,00869		
70	71	5,49	0,00869		
71	72	5,70	0,00869	23,622	
72	73	5,49	0,00869		
73	74	5,49	0,00869		
74	75	5,49	0,00869		
75	76	5,49	0,00869		
77	102	5,53	0,00869	18,289	
76	78	5,30	0,00869	18,289	
78	79	5,49	0,00869		
79	80	5,30	0,00869	18,289	
80	81	5,30	0,00869		

Branches		**Dh (m)**	**K (kg/m^3)**	**Total Leq (m)**	**R (Ns^2/m^8)**
81	82	5,49	0,00869	20,843	
82	83	5,49	0,00869	18,948	
83	84	5,49	0,00869	18,948	
84	85	5,49	0,00869	20,843	
85	86	5,49	0,00869	18,948	
86	87	5,05	0,00895	16,935	
87	14	5,05	0,00895	16,935	
88	89	5,05	0,00895	20,321	
89	90	5,05	0,00895	20,321	
90	15	5,05	0,00895	16,935	
53	12	5,00	0,01113	12,522	
12	13	5,00	0,01113	12,522	
13	91	5,00	0,01113	12,522	
91	92	5,00	0,01113	12,522	
92	93	5,00	0,01113	12,522	
93	94	5,00	0,01113	18,876	
94	95	5,00	0,01113	26,965	
95	80	5,00	0,01113	26,965	
96	98	6,48	No friction factor	No friction factor	
97	63	5,49	0,00880	18,710	
96	97	5,59	0,00797	33,568	
98	77	6,48	0,00778	23,919	
99	3	5,49	0,00869	0,000	
36	99	6,50	0,01198	37,561	
37	35	4,32	0,00959	13,517	
34	100	4,32	0,00959	13,517	
100	37	4,32	0,00959	13,517	
102	40	6,48	0,00778	48,899	
102	101	5,49	No friction factor	No friction factor	
101	103	5,49	0,00869		
103	104	5,49	0,00869		
104	29	5,49	0,00869	18,948	

Branches		Dh (m)	K (kg/m^3)	Total Leq (m)	R (Ns^2/m^8)
82	111	5,49	0,00869	22,738	
111	112	5,49	0,00869	18,948	
112	113	5,49	0,00869	18,948	
113	114	5,49	0,00869		
114	115	5,49	0,00869	20,843	
115	116	5,49	0,00869		
116	117	5,49	0,00869		
117	118	5,49	0,00869		
118	119	5,49	0,00869		
119	14	5,05	0,00895		
2	99	5,49	0,00869		

Table 61. Modelling results from third configuration.

Branches		Resistance (N·s^2/m^8)	Airflow (m^3/s)	Pressure drop (Pa)
11	10	0,00056	145,54	11,9
1	2	0,01127	169,07	322,2
3	4	0,00465	175,11	142,6
4	5	0,00031	175,33	9,5
5	6	0,00033	175,33	10,1
6	4	250.000	0,22	0,1
6	7	0,00117	175,11	35,9
7	8	0,00061	175,11	18,7
8	9	0,00067	145,54	14,2
9	11	0,0066	145,54	139,8
10	59	0,00462	125,86	73,2
14	88	0,00029	115,41	3,9
15	16	0,0004	115,41	5,3
16	17	0,00473	138,97	91,4
17	18	0,00474	145,54	100,4
18	19	0,00094	145,54	19,9
19	20	0,00555	145,54	117,6
20	21	0,00065	175,11	19,9

Branches		Resistance (N·s²/m⁸)	Airflow (m³/s)	Pressure drop (Pa)
21	22	0,00317	175,11	97,2
22	23	0,00103	169,07	29,4
23	24	0,01319	169,07	377
10	25	0,00268	19,67	1
25	26	0,88	19,67	340,5
26	17	0,00284	6,56	0,1
27	28	0,00185	13,99	0,4
28	29	0,88	13,99	172,2
29	16	0,00289	23,56	1,6
8	30	0,00091	29,57	0,8
30	31	0,85	29,57	743,4
31	20	0,00134	29,57	1,2
22	32	0,00065	6,04	0
32	38	0,00255	6,04	0,1
2	34	0,00027	23,47	0,1
33	37	0,00082	16,38	0,2
35	36	0,00169	29,51	1,5
38	39	2.000.000	6,04	729
39	33	0,00201	6,04	0,1
40	41	0,00012	29,71	0,1
27	96	0,00126	96,83	11,8
41	42	0,00137	29,71	1,2
42	43	0,00005	29,71	0
43	44	0,00019	29,71	0,2
44	45	0,00122	30,71	1,2
45	46	0,00189	30,71	1,8
46	47	0,00045	30,71	0,4
47	48	0,00039	30,71	0,4
48	49	0,00081	30,71	0,8
49	50	0,00047	30,71	0,4
50	51	0,0005	30,71	0,5
51	52	0,00022	30,71	0,2

Branches		Resistance ($N \cdot s^2/m^8$)	Airflow (m^3/s)	Pressure drop (Pa)
52	53	0,00048	30,71	0,5
54	53	0,00036	-1	0
55	54	0,00035	-1	0
44	55	0,00021	-1	0
56	33	0,00044	10,35	0
100	56	0,00024	10,35	0
59	27	0,00024	110,82	2,9
59	60	0,00047	15,05	0,1
60	57	0,12	15,05	27,2
57	58	0,00021	15,05	0
58	61	0,0004	15,05	0,1
61	62	0,00302	15,05	0,7
62	97	0,00033	15,05	0,1
63	64	0,00077	72,59	4,1
64	65	0,00083	72,59	4,4
65	66	0,00017	72,59	0,9
66	67	0,0001	72,59	0,5
67	68	0,00015	72,59	0,8
68	69	0,00025	72,59	1,3
69	70	0,00024	72,59	1,3
70	71	0,00021	72,59	1,1
71	72	0,00076	72,59	4
72	73	0,00096	72,59	5,1
73	74	0,00047	72,59	2,5
74	75	0,00032	72,59	1,7
75	76	0,00018	72,59	0,9
77	102	0,00091	39,28	1,4
76	78	0,00029	72,59	1,5
78	79	0,00029	72,59	1,5
79	80	0,0006	72,59	3,2
80	81	0,00086	102,3	9
81	82	0,0006	102,3	6,3

Branches		**Resistance (N·s²/m⁸)**	**Airflow (m³/s)**	**Pressure drop (Pa)**
82	83	0,00049	54,39	1,4
83	84	0,0016	54,39	4,7
84	85	0,00088	54,39	2,6
85	86	0,00077	54,39	2,3
86	87	0,00292	54,39	8,6
87	14	0,00118	54,39	3,5
88	89	0,00088	115,41	11,7
89	90	0,00053	115,41	7,1
90	15	0,00343	115,41	45,7
53	12	0,00067	29,71	0,6
12	13	0,00062	29,71	0,5
13	91	0,00158	29,71	1,4
91	92	0,00043	29,71	0,4
92	93	0,00175	29,71	1,5
93	94	0,00056	29,71	0,5
94	95	0,00061	29,71	0,5
95	80	0,00144	29,71	1,3
96	98	0,025	39,28	38,6
97	63	0,0004	72,59	2,1
96	97	0,00405	57,55	13,4
98	77	0,00081	39,28	1,2
99	3	0,00009	175,11	2,8
36	99	0,00028	29,51	0,2
37	35	0,0015	29,51	1,3
34	100	0,00064	23,47	0,4
100	37	0,0017	13,13	0,3
102	40	0,00083	29,71	0,7
102	101	130.000	9,57	119,1
101	103	0,00124	9,57	0,1
103	104	0,00274	9,57	0,3
104	29	0,00038	9,57	0
82	111	0,00084	47,92	1,9

Branches		Resistance ($N \cdot s^2/m^8$)	Airflow (m^3/s)	Pressure drop (Pa)
111	112	0,00044	47,92	1
112	113	0,00064	47,92	1,5
113	114	0,00047	47,92	1,1
114	115	0,00046	47,92	1,1
115	116	0,00042	61,03	1,6
116	117	0,00053	61,03	2
117	118	0,00204	61,03	7,6
118	119	0,00019	61,03	0,7
119	14	0,00129	61,03	4,8
2	99	0,00018	145,6	3,8
26	115	0	13,11	0

5.2.2.4. Fourth configuration

Table 62. Initial data of the fourth configuration.

Branches		Description	Section (m^2)	Perimeter (m)
108	109	New opening south zone	34,1	22,3
109	86	New opening south zone	34,1	22,3
45	105	New opening south zone	34,1	22,3
105	106	New opening south zone	34,1	22,3
108	109	New opening south zone	34,1	22,3
11	10	Control room	35	22,66
1	2	Shaft		
3	4	Cross section change	40	24,6
4	5	Inlet main fan	34,54	24,1
5	6	Main forcing fan	34,5	24,1
6	4	Double door	34	23,3
6	7	Bend 120º	34,8	24,1
7	8	Bend 140º	35	24,1
8	9	Conveyor belt	34,5	23,2
9	11	Conveyor belt	34,04	23,2
10	59	Conveyor belt and cross section change	34,04	21,8

Branches		Description	Section (m^2)	Perimeter (m)
14	88	No obstacles	28	19,5
15	16	No obstacles	29	19,5
16	17	No obstacles	29	19,5
17	18	No obstacles	29	19,5
18	19	No obstacles	29	19,5
19	20	Bend 120º	29	18,0
20	21	Conveyor belt	31,84	22,6
21	22	Conveyor belt	31,84	22,6
22	23	Bend 125º	31,84	22,7
23	24	Conveyor belt	35,96	26,3
10	25	No obstacles	28,37	20,0
25	26	Double door	28,37	20,0
26	17	No obstacles	28,37	20,0
27	28	Conveyor belt	31,54	22,7
28	29	Double door	31,54	22,5
29	16	Conveyor belt	33,4	25,0
8	30	Conveyor belt	32	23,2
30	31	Double door	32	23,9
31	20	Conveyor belt	32	22,6
22	32	Conveyor belt	30	22,6
32	38	No obstacles	21,61	20,0
2	34	No obstacles	21,61	20,0
33	37	No obstacles	21,61	20,0
35	36	No obstacles	21,61	20,0
38	39	Double door	22	20,0
39	33	No obstacles	22	20,0
40	41	No obstacles	31,33	19,3
27	96	Conveyor belt	31,33	19,3
41	42	No obstacles	31,33	19,3
42	43	No obstacles	31,33	19,3
43	44	No obstacles	31,33	19,3
44	45	Duct system + Bend 90º	29,6	25,8

Branches		Description	Section (m^2)	Perimeter (m)
45	46	Duct system + Bend 110º	34	23,5
46	47	Duct system	32	21,0
47	48	Duct system + Bend 90º	33,6	21,5
48	49	Duct system + Bend 120º	34	21,4
49	50	Duct system	33	23,6
50	51	Duct system	32	24,0
51	52	Duct system	31	19,8
52	53	Duct system + Bend 90º	32,3	25,8
54	53	No obstacles	32,3	25,8
55	54	Bend 90º	33	23,1
44	55	Bend 90º	33	23,1
56	33	Bend 90º	32,3	21,0
100	56	Bend 110º	32,30	21,0
59	27	Conveyor belt	34,04	23,4
59	60	No obstacles	34,08	23,2
60	57	Curtain		
57	58	No obstacles	34,08	23,2
58	61	Bend 100º	34	23,2
61	62	Duct system	32,29	23,1
62	97	Duct system	32,29	23,1
63	64	No obstacles	31,08	22,7
64	65	Bend 90º	31,08	22,7
65	66	No obstacles	31,08	22,7
66	67	No obstacles	31,08	22,7
67	68	No obstacles	31,08	22,7
68	69	Bend 90º	31,08	22,7
69	70	No obstacles	31,08	22,7
70	71	No obstacles	31,08	22,7
71	72	Bend 120º	32,29	22,7
72	73	No obstacles	31,08	22,7
73	74	No obstacles	31,08	22,7
74	75	No obstacles	31,08	22,7

Branches		Description	Section (m^2)	Perimeter (m)
75	76	No obstacles	31,08	22,7
77	102	Conveyor belt	31,33	22,7
76	78	Bend 90º	30,00	22,7
78	79	No obstacles	31,08	22,7
79	80	Bend 90º	30,00	22,7
80	81	No obstacles	30,00	22,7
81	82	Bend 110º	31,08	22,7
82	83	Bend 90º	31,08	22,7
83	84	Bend 110º	31,08	22,7
84	85	Bend 110º	31,08	22,7
85	86	Bend 100º	31,08	22,7
86	87	Bend 90º	27,83	22,0
87	14	Bend 90º	27,83	22,0
88	89	Bend 120º	27,83	22,0
89	90	Bend 120º	27,83	22,0
90	15	Bend 90º	27,83	22,0
53	12	Duct system	32,30	25,8
12	13	Duct system	32,30	25,8
13	91	Duct system	32,30	25,8
91	92	Duct system	32,30	25,8
92	93	Duct system	32,30	25,8
93	94	Duct system + Bend 75º	32,30	25,8
94	95	Duct system + Bend 90º	32,30	25,8
95	80	Duct system + Bend 90º	32,30	25,8
96	98	Conveyor belt	31,33	19,3
97	63	Bend 90º + duct system	31,08	22,7
96	97	Conveyor belt + Bend 90º	32,29	23,1
98	77	Conveyor belt	31,33	19,3
99	3	Occasional obstacles	31,08	22,7
36	99	Control room	40,00	24,6
37	35	Bend 90º	21,61	20,0
34	100	Bend 100º	21,61	20,0

Branches		Description	Section (m^2)	Perimeter (m)
100	37	Bend 90º	21,61	20,0
102	40	Conveyor belt+ Bend 120º	31,33	19,3
102	101	Bend 90º	31,08	22,7
101	103	No obstacles	31,08	22,7
103	104	No obstacles	31,08	22,7
104	29	Bend 90º	31,08	22,7
82	111	Bend 120º	31,08	22,7
111	112	Bend 90º	31,08	22,7
112	113	Bend 90º	31,08	22,7
113	114	No obstacles	31,08	22,7
114	115	Bend 80º	31,08	22,7
115	116	No obstacles	31,08	22,7
116	117	No obstacles	31,08	22,7
117	118	No obstacles	31,08	22,7
118	119	No obstacles	31,08	22,7
119	14	No obstacles	27,83	22,0
2	99	Occasional obstacles	31,08	22,7

Table 63. Friction parameters, fourth configuration.

Branches		K (kg/m^3)	Total Leq (m)	R (Ns^2/m^8)
108	109	0,00881	0	
109	86	0,00881	0	
45	105	0,00881	0	
105	106	0,00881	0	
108	109	0,00881	0	
11	10	0,01171	0	
1	2	0,01020	0	
3	4	0,00821	1,484	
4	5	0,00821	0	
5	6	0,00821	0	
6	4	No friction factor	No friction factor	2,5
6	7	0,00821	25,325	

Branches		K (kg/m^3)	Total Leq (m)	R (Ns^2/m^8)
7	8	0,00821	27,593	
8	9	0,00780	19,478	
9	11	0,00780	19,875	
10	59	0,00759	241,816	
14	88	0,00909	0,000	
15	16	0,00881	0,000	
16	17	0,00743	0,000	
17	18	0,00698	0,000	
18	19	0,00881	0,000	
19	20	0,00698	36,006	
20	21	0,00809	19,680	
21	22	0,00809	19,680	
22	23	0,00881	23,916	
23	24	0,00747	16,508	
10	25	0,00881	0,000	
25	26	No friction factor	No friction factor	2,5
26	17	0,00881	0,000	
27	28	0,00881	16,260	
28	29	No friction factor	No friction factor	2,5
29	16	0,00784	0,000	
8	30	0,00780	19,875	
30	31	No friction factor	No friction factor	0,45
31	20	0,00809	19,680	
22	32	0,00809	19,680	
32	38	0,00966	0,000	
2	34	0,00966	0,000	
33	37	0,00966	0,000	
35	36	0,00966	0,000	
38	39	No friction factor	No friction factor	2,5
39	33	0,00966	0,000	
40	41	0,00821	0,000	
27	96	0,00821	20,684	

Branches		K (kg/m^3)	Total Leq (m)	R (Ns^2/m^8)
41	42	0,00821	0,000	
42	43	0,00821	0,000	
43	44	0,00821	0,000	
44	45	0,01207	11,522	
45	46	0,01207	14,212	
46	47	0,01207	2,486	
47	48	0,01207	15,379	
48	49	0,01207	15,606	
49	50	0,01207	2,212	
50	51	0,01207	2,175	
51	52	0,01207	2,637	
52	53	0,01207	12,389	
54	53	0,01207	0,000	
55	54	0,01207	11,839	
44	55	0,01207	11,839	
56	33	0,00966	15,916	
100	56	0,00747	4,120	
59	27	0,00821	20,236	
59	60	0,00796	0,000	
60	57	No friction factor	No friction factor	0,45
57	58	0,00796	0,000	
58	61	0,00796	18,381	
61	62	0,01116	2,194	
62	97	0,00784	3,123	
63	64	0,00881	0,000	
64	65	0,00881	18,676	
65	66	0,00881	0,000	
66	67	0,00881	0,000	
67	68	0,00881	0,000	
68	69	0,00881	18,676	
69	70	0,00881	0,000	
70	71	0,00881	0,000	

Branches		**K (kg/m^3)**	**Total Leq (m)**	**R (Ns^2/m^8)**
71	72	0,00881	23,284	
72	73	0,00881	0,000	
73	74	0,00881	0,000	
74	75	0,00881	0,000	
75	76	0,00881	0,000	
77	102	0,00881	18,027	
76	78	0,00881	18,027	
78	79	0,00881	0,000	
79	80	0,00881	18,027	
80	81	0,00881	0,000	
81	82	0,00881	20,544	
82	83	0,00881	18,676	
83	84	0,00881	18,676	
84	85	0,00881	20,544	
85	86	0,00881	18,676	
86	87	0,00909	16,684	
87	14	0,00909	16,684	
88	89	0,00909	20,021	
89	90	0,00909	20,021	
90	15	0,00909	16,684	
53	12	0,01207	11,554	
12	13	0,01207	11,554	
13	91	0,01207	11,554	
91	92	0,01207	11,554	
92	93	0,01207	11,554	
93	94	0,01207	17,416	
94	95	0,01207	24,881	
95	80	No friction factor	No friction factor	
96	98	No friction factor	No friction factor	
97	63	0,00881	18,676	
96	97	0,01116	26,595	
98	77	0,00821	22,680	

Branches		**K (kg/m^3)**	**Total Leq (m)**	**R (Ns^2/m^8)**
99	3	0,00881	0,000	
36	99	0,01171	38,421	
37	35	0,00966	13,417	
34	100	0,00966	13,417	
100	37	0,00966	13,417	
102	40	0,00821	46,366	
102	101	No friction factor	No friction factor	
101	103	0,00881	0,000	
103	104	0,00881	0,000	
104	29	0,00881	18,676	
82	111	0,00881	22,412	
111	112	0,00881	18,676	
112	113	0,00881	18,676	
113	114	0,00881	0,000	
114	115	0,00881	20,544	
115	116	0,00881	0,000	
116	117	0,00881	0	
117	118	0,00881	0	
118	119	0,00881	0	
119	14	0,00909	0	
2	99	0,00881	0	

Table 64. Modelling results from fourth configuration.

Branches		**Resistance (N·s^2/m^8)**	**Airflow (m^3/s)**	**Pressure drop (Pa)**
108	106	0,0002	91,91	0
109	86	0,000234	91,91	0
45	105	0,000342	91,91	0
105	106	0,0003422	91,91	0
108	109	0,0023	91,91	0
11	10	0,00056	136,94	10,5
1	2	0,00078	175,43	0
3	4	0,00459	184,2	155,7

Branches		Resistance (N·s²/m⁸)	Airflow (m³/s)	Pressure drop (Pa)
4	5	0,00031	175,62	9,6
5	6	0,00032	175,62	9,9
6	4	250.000	8,58	184
6	7	0,00116	184,2	39,4
7	8	0,0006	184,2	20,4
8	9	0,0006	136,94	11,3
9	11	0,00589	136,94	110,5
10	59	0,00435	128,54	71,9
14	88	0,00029	99,57	2,9
15	16	0,0004	99,57	4
16	17	0,00479	128,54	79,1
17	18	0,0048	136,94	90
18	19	0,00095	136,94	17,8
19	20	0,00563	136,94	105,6
20	21	0,00069	184,2	23,4
21	22	0,00337	184,2	114,3
22	23	0,00104	175,43	32
23	24	0,01145	175,43	352,4
10	25	0,0027	8,41	0,2
25	26	20	8,41	1413
26	17	0,00286	8,41	0,2
27	28	0,00187	26,09	1,3
28	29	184.430	26,09	1255,7
29	16	0,0022	28,97	1,8
8	30	0,00082	47,26	1,8
30	31	0,7854	47,26	1754
31	20	0,00142	47,26	3,2
22	32	0,00068	8,77	0,1
32	38	0,00257	8,77	0,2
2	34	0,00027	22,54	0,1
33	37	0,00083	17,78	0,3
35	36	0,0017	31,31	1,7

Branches		Resistance (N·s^2/m^8)	Airflow (m^3/s)	Pressure drop (Pa)
38	39	500.000	8,77	384,5
39	33	0,00203	8,77	0,2
40	41	0,00014	67,79	0,6
27	96	0,00143	90,78	11,8
41	42	0,00158	67,79	7,3
42	43	0,00006	67,79	0,3
43	44	0,00022	67,79	1
44	45	0,00125	61,2	4,7
45	46	0,00193	-30,71	-1,8
46	47	0,00046	-30,71	-0,4
48	49	0,00083	-30,71	-0,8
49	50	0,00048	-30,71	-0,5
50	51	0,00051	-30,71	-0,5
51	52	0,00022	-30,71	-0,2
52	53	0,00049	-30,71	-0,5
54	53	0,00037	6,6	0
55	54	0,00035	6,6	0
44	55	0,00021	6,6	0
56	33	0,00044	9,01	0
100	56	0,00021	9,01	0
59	27	0,00026	116,87	3,6
59	60	0,00051	11,67	0,1
60	57	0,1236	11,67	16,8
57	58	0,00023	11,67	0
58	61	0,00044	11,67	0,1
61	62	0,00419	11,67	0,6
62	97	0,00025	11,67	0
63	64	0,00077	31,78	0,8
64	65	0,00083	31,78	0,8
65	66	0,00017	31,78	0,2
66	67	0,0001	31,78	0,1
67	68	0,00015	31,78	0,2

Branches		Resistance ($N \cdot s^2/m^8$)	Airflow (m^3/s)	Pressure drop (Pa)
68	69	0,00025	31,78	0,3
69	70	0,00024	31,78	0,2
70	71	0,00022	31,78	0,2
71	72	0,00076	31,78	0,8
72	73	0,00097	31,78	1
73	74	0,00047	31,78	0,5
74	75	0,00032	31,78	0,3
75	76	0,00018	31,78	0,2
77	102	0,00092	70,66	4,6
76	78	0,0003	31,78	0,3
78	79	0,00029	31,78	0,3
79	80	0,0006	31,78	0,6
81	82	0,0006	7,66	0
82	83	0,00049	-24,55	-0,3
83	84	0,00161	-24,55	-1
84	85	0,00093	-24,55	-0,6
85	86	0,00203	-24,55	-1,2
86	87	0,00116	67,36	5,3
87	14	0,0012	67,36	5,4
88	89	0,00089	99,57	8,8
89	90	0,00053	99,57	5,3
90	15	0,00349	99,57	34,6
53	12	0,00069	-24,12	-0,4
12	13	0,00063	-24,12	-0,4
13	91	0,00162	-24,12	-0,9
91	92	0,00043	-24,12	-0,3
92	93	0,00179	-24,12	-1
93	94	0,00057	-24,12	-0,3
94	95	0,00062	24,12	-0,4
95	80	200.000	24,12	-1163,1
96	98	0,231	70,66	1153,5
97	63	0,00041	31,78	0,4

Branches		Resistance (N·s²/m⁸)	Airflow (m³/s)	Pressure drop (Pa)
96	97	0,00559	20,11	2,3
98	77	0,00092	70,66	4,6
99	3	0,00009	184,2	3,1
36	99	0,00028	31,31	0,3
37	35	0,00152	31,31	1,5
34	100	0,00064	22,54	0,3
100	37	0,00172	13,53	0,3
102	40	0,00093	67,79	4,3
101	103	0,00124	2,87	0
103	104	0,00276	2,87	0
104	29	0,00038	2,87	0
82	111	0,00084	32,21	0,9
111	112	0,00044	32,21	0,5
112	113	0,00064	32,21	0,7
113	114	0,00048	32,21	0,5
114	115	0,00046	32,21	0,5
115	116	0,00043	32,21	0,4
116	117	0,00053	32,21	0,5
117	118	0,00205	32,21	2,1
118	119	0,0002	32,21	0,2
119	14	0,00131	32,21	1,4
2	99	0,00018	152,89	4,2
47	48	0	30,71	0
102	101	10	2,87	82,5
80	81	20	7,66	1174,5

5.2.3. Cabanasses

Table 65. Initial data of the model.

Branches		Description	Section (m^2)	Perimeter (m)
1	7	Conveyor belt	34,49	26,22
3	107	Bend 120º	40,06	
4	104	Bend 93º	25,6	20,93
5	4	Parking	40,06	27,5
7	8	Conveyor belt	34,49	26,22
8	9	Conveyor belt and Bend 159º	34,49	26,22
9	12	Conveyor belt	34,49	26,22
10	15	Bend 89º	32,89	27,82
11	10	Conveyor belt	32,89	27,82
12	18	Conveyor belt	32,9	24,57
13	98	Bend 90º	49,71	29,85
13	11	Conveyor belt	32,89	27,82
13	98	Conveyor and bend 90º	49,71	
14	13	Conveyor belt	32,89	27,82
15	16	Bend 100º	31,75	25,43
16	57	Bend 159º	29,99	23,13
17	14	Conveyor belt	32,89	27,82
17	184	Entry and curtain	30,82	
18	20	Conveyor belt	32,9	24,57
19	17	Conveyor and bend 120º	32,89	27,82
20	26	Conveyor belt	32,9	24,57
21	19	Conveyor belt	32,89	27,82
22	164	Bend 155º	28,63	20,92
22	21	Conveyor belt	32,89	27,82
22	164	Entry and bend 155º	28,63	
23	28	Conveyor belt and parking	31,01	22,97
24	23	Conveyor belt	31,01	22,97
25	24	Conveyor belt	31,01	22,97
26	27	Conveyor belt	32,9	24,57
27	36	Conveyor belt	32,9	24,57

Branches		Description	Section (m^2)	Perimeter (m)
28	31	Conveyor belt	31,01	22,97
29	25	Conveyor belt	31,01	22,97
30	45	Conveyor belt	38,3	27,44
31	39	Conveyor belt	31,01	22,97
32	34	Conveyor belt	32,9	24,57
33	29	Conveyor belt	31,01	22,97
33	30	Conveyor belt and parking	34,21	25,42
34	118	Bend 84º	30,6	22,6
34	33	Conveyor belt and bend 110º	32,9	24,57
34	118	Bend 84º	30,6	
35	32	Conveyor belt	32,9	24,57
36	35	Conveyor belt	32,9	24,57
37	22	Conveyor belt and bend 140º	33,03	25,16
38	37	Conveyor belt	33,03	25,16
39	38	Conveyor belt	31,01	22,97
40	91	Bend 129º	27,38	20,72
41	42	Bend 94º	33,04	24,02
41	50	Bend 125º	33,04	24,02
41	42	Conveyor belt	33,04	24,02
43	46	Conveyor belt	38,3	27,44
44	43	Conveyor belt	38,3	27,44
45	44	Conveyor belt	38,3	27,44
46	48	Conveyor belt	38,3	27,44
47	41	Bend 137º	33,04	24,02
47	41	Conveyor belt	33,04	24,02
48	49	Bend 135º	38,3	27,44
48	49	Conveyor belt	38,3	27,44
49	47	Conveyor belt	33,04	24,02
50	114	Bend 64º	33,04	24,02
60	56	Bend 156º	19,69	17,84
64	63	Bend 159º	24,03	19,54
65	67	Bend 36º	24,03	19,54

Branches		Description	Section (m^2)	Perimeter (m)
66	74	Bend 138º	20,78	18,36
67	64	Bend 159º	24,03	19,54
73	68	Bend 133º	23,59	19,63
74	77	Bend 138º	20,78	18,36
84	65	Bend 146º	24,03	19,54
89	87	Bend 150º	27,38	20,72
98	112	Bend 91º	49,75	29,86
100	94	Conveyor belt	25,6	20,93
102	1	Bend 158º	40,06	27,5
103	101	Bend 142º	25,6	20,93
104	100	Conveyor belt	25,6	20,93
106	103	Bend 151º	25,6	20,93
107	106	Bend 160º	25,6	20,93
107	102	Conveyor belt	40,06	27,5
112	113	Bend 95º	49,75	29,86
113	85	Bend 84º	49,71	29,85
114	115	Bend 115º	33,04	24,02
118	125	Conveyor and parking	114	43
147	150	Bend 124º	28,63	20,92
148	147	Bend 158º	28,63	20,92
149	153	Bend 127º	28,63	20,92
150	152	Bend 113º	28,63	20,92
152	154	-	28,63	20,92
153	151	Bend 122º	28,63	20,92
154	113	-	38,29	26,5
154	156	-	28,63	20,92
155	149	Bend 151º	28,63	20,92
156	159	Bend 80º	28,63	20,92
158	155	Bend 129º	28,63	20,92
159	160	Bend 88º	28,63	20,92
160	173	Bend 140º	28,63	20,92
161	160	Bend 109º	28,63	20,92

Branches		Description	Section (m^2)	Perimeter (m)
162	158	Bend 124º	28,63	20,92
163	161	Bend 71º	28,63	20,92
168	169	Bend 128º	28,63	20,92
169	171	Bend 72º	28,63	20,92
173	174	Bend 139º	28,63	20,92
175	176	Bend 80º	30,82	21,65
177	175	Bend 60º	30,82	21,65
178	177	Bend 138º	30,82	21,65
179	178	Bend 101º	30,82	21,65
180	179	Bend 58º	30,82	21,65
181	180	Bend 122º	30,82	21,65
182	181	Bend 146º	30,82	21,65
183	182	Bend 135º	30,82	21,65
187	188	Bend 146º	30,82	21,65
188	189	Bend 87º	30,82	21,65

Table 66. Friction parameters.

Branches		D_h (m)	K (kg/m^3)	Total Leq (m)	R (Ns^2/m^8)
1	7	6,661	No friction factor	R	5
3	107	6,661	0,0078	34,39	
4	104	4,892	0,006	159,01	
5	4	5,262	No friction factor	R	2,5
7	8	5,827	0,0066	24,96	
8	9	5,262	0,0055	35,73	
9	12	5,262	0,0055	24,96	
10	15	4,729	0,0075	66,21	
11	10	4,729	0,0064	20,22	
12	18	5,262	0,0055	25,71	
13	98	6,661	0,0078	53,47	
13	11	4,729	0,0064	265,26	
13	98	4,892	0,006	20,22	

Branches		**D_h (m)**	**K (kg/m³)**	**Total Leq (m)**	**R (Ns²/m⁸)**
14	13	4,729	0,0064	66,42	
15	16	4,994	0,0075	25,76	
16	57	5,186	0,0075	25,71	
17	14	4,729	0,0064	20,22	
17	184	4,729	No friction factor	R	1
18	20	5,262	0,0055	20,22	
19	17	4,729	0,0064	31,3	
20	26	5,356	0,0057	7,82	
21	19	5,251	0,0062	56,7	
22	164	5,474	0,0084	67,91	
22	21	5,251	0,0062	26,12	
23	28	5,4	0,006	26,12	
24	23	5,4	0,006	25,71	
25	24	5,4	0,006	25,71	
26	27	5,356	0,0057	26,12	
27	36	5,356	0,0057	26,12	
28	31	5,4	0,006	23,85	
29	25	5,356	0,006	25,28	
30	45	4,729	0,0064	25,71	
31	39	5,4	0,006	39,62	
32	34	5,356	0,0057	128,52	
33	29	5,356	0,0057	24,42	
33	30	4,729	0,0064	213,58	
34	118	5,416	0,0062	25,71	
34	33	5,356	0,0057	25,71	
35	32	5,356	0,0057	23,08	
36	35	5,356	0,0057	23,08	
37	22	5,4	0,0062	25,28	
38	37	5,4	0,0062	101,72	
39	38	5,4	0,006	160,16	
40	91	5,286	0,0076	15,83	

Branches		**D_h (m)**	**K (kg/m^3)**	**Total Leq (m)**	**R (Ns^2/m^8)**
41	42	5,502	0,0073	21,16	
41	50	5,502	0,0073	21,16	
41	42	5,502	0,0069	21,16	
43	46	5,583	0,0062	19,01	
44	43	5,583	0,0055	129,37	
45	44	5,383	0,0055	128,25	
46	48	5,583	0,0062	21,72	
47	41	5,502	0,0069	32,5	
47	41	5,583	0,0069	50,19	
48	49	5,583	0,0069	8,52	
48	49	5,583	0,0062	8,26	
49	47	5,583	0,0069	85,9	
50	114	5,502	0,0073	80,15	
60	56	4,415	0,0068	6,61	
64	63	4,919	0,0067	5,91	
65	67	4,919	0,0067	42,3	
66	74	4,527	0,0061	87,88	
67	64	4,919	0,0067	16,7	
73	68	4,807	0,008	66,8	
74	77	4,527	0,0061	11,01	
84	65	4,919	0,0067	73,31	
89	87	5,286	0,0073	192,24	
98	112	6,664	0,0078	111,19	
100	94	5,502	0,0073	28,67	
102	1	5,827	0,0061	128,96	
103	101	4,892	0,0066	12,23	
104	100	5,502	0,0069	28,67	
106	103	4,892	0,0066	10,01	
107	106	10,605	0,005	77,84	
107	102	6,664	No friction factor	R	1,5
112	113	6,664	0,0078	139,38	

Branches		**D_h (m)**	**K (kg/m^3)**	**Total Leq (m)**	**R (Ns^2/m^8)**
113	85	6,661	0,0078	110,49	
114	115	5,502	0,0073	22,61	
118	125	10,605	0,005	163,9	
118	125	4,892	0,006	51,32	
147	150	5,474	0,0084	5,87	
148	147	5,474	0,0084	17,11	
149	153	5,474	0,0084	124,64	
150	152	5,474	0,0084	20,53	
152	154	5,474	No friction factor	R	6
153	151	5,474	0,0084	8,8	
154	113	5,474	No friction factor	R	5
154	156	5,474	No friction factor	R	1
155	149	5,474	0,0084	39,1	
156	159	5,474	0,0084	10,75	
158	155	5,474	0,0084	49,85	
159	160	5,474	0,0084	13,69	
160	173	5,474	0,0084	161,29	
161	160	5,474	0,0084	15,88	
162	158	5,474	0,0084	26,88	
163	161	5,474	0,0084	4,89	
168	169	5,474	0,0084	80,65	
169	171	5,474	0,0084	188,11	
173	174	5,474	0,0084	25,42	
175	176	5,694	0,0084	183,03	
177	175	5,694	0,0084	50,33	
178	177	5,694	0,0084	144,9	
179	178	5,694	0,0084	183,03	
180	179	5,694	0,0084	22,88	
181	180	5,694	0,0084	10,17	
182	181	5,694	0,0084	12,2	
183	182	5,694	0,0084	30,5	

Branches		**D_h (m)**	**K (kg/m^3)**	**Total Leq (m)**	**R (Ns^2/m^8)**
187	188	5,694	0,0084	152,52	
188	189	5,694	0,0084	111,85	

Negative airflows in the next table means there is recirculation.

Table 67. Modelling results of Cabanasses.

Branch		**Resistance (N·s^2/m^8)**	**Airflow (m^3/s)**	**Pressure drop (Pa)**
6	5	0,0001	187,35	3,5
5	4	0,00034	208,43	14,8
4	2	0,00034	154,2	8,1
2	105	0,00008	154,2	1,9
3	107	0,00016	154,61	3,8
1	7	0,00104	192,85	38,7
7	8	0,00081	192,85	30,1
8	9	0,00031	192,85	11,5
9	12	0,0004	192,85	14,9
12	18	0,00104	184,57	35,4
18	20	0,00111	184,57	37,8
20	26	0,00064	175,89	19,8
26	27	0,00041	175,89	12,7
27	36	0,00096	175,89	29,7
36	35	0,00088	175,89	27,2
35	32	0,00023	169,73	6,6
32	34	0,00065	169,73	18,7
34	33	0,00093	153,98	22,1
33	29	0,00044	76,77	2,6
29	25	0,00077	76,77	4,5
25	24	0,00096	79,46	6,1
24	23	0,00063	79,46	4
23	28	0,0011	79,46	6,9

Branch		Resistance (N·s^2/m^8)	Airflow (m^3/s)	Pressure drop (Pa)
28	31	0,00023	79,46	1,5
31	39	0,00174	79,46	11
39	38	0,00036	79,46	2,3
38	37	0,0005	96,03	4,6
37	22	0,00213	96,03	19,6
22	21	0,00045	64,93	1,9
21	19	0,00032	64,93	1,3
19	17	0,0023	73,52	12,4
17	14	0,00034	52,33	0,9
14	13	0,00047	52,33	1,3
13	11	0,00042	-4,59	0
11	10	0,00018	-4,59	0
10	15	0,0014	-1,07	0
33	30	0,00059	77,21	3,5
30	45	0,0015	77,21	8,9
45	44	0,00023	80,09	1,5
44	43	0,00022	80,09	1,4
43	46	0,00044	80,09	2,8
46	48	0,00065	80,09	4,2
48	49	0,00059	80,09	3,8
49	47	0,00037	80,09	2,4
47	41	0,00242	80,09	15,5
41	42	0,00124	-3,43	0
15	16	0,00068	-1,07	0
42	40	25	-3,43	-294
51	61	0,00136	208,43	59,1
53	51	0,00493	208,43	214,2
54	53	0,00476	192,85	177
55	54	0,00224	192,85	83,3
56	55	0,0013	192,85	48,4
60	56	0,00314	192,85	116,8

Branch		Resistance (N·s^2/m^8)	Airflow (m^3/s)	Pressure drop (Pa)
62	60	0,00446	184,57	151,9
69	62	0,00245	184,57	83,5
72	69	0,0014	175,89	43,3
75	72	0,00224	175,89	69,3
78	75	0,0017	175,89	52,6
79	78	0,00212	175,89	65,6
77	79	0,00108	169,73	31,1
74	77	0,00209	153,98	49,6
66	74	0,00294	153,98	69,7
68	66	0,00047	76,77	2,8
73	68	0,00512	76,77	30,2
80	73	0,00577	79,46	36,4
83	80	0,0011	79,46	6,9
81	83	0,00039	79,46	2,5
82	81	0,00257	79,46	16,2
76	82	0,00432	96,03	39,8
71	76	0,00185	96,03	17,1
70	71	0,0013	84,91	9,4
59	70	0,00431	93,5	37,7
58	59	20	-4,59	-420,8
57	58	0,00061	-1,07	0
16	57	0,00097	-1,07	0
63	66	0,00041	77,21	2,4
64	63	0,00094	77,21	5,6
67	64	0,00049	77,21	2,9
65	67	0,00137	77,21	8,2
84	65	0,00411	77,21	24,5
86	84	0,00166	77,21	9,9
88	86	0,00016	80,09	1
87	88	0,00025	80,09	1,6
89	87	0,00161	80,09	10,3

Branch		Resistance ($N \cdot s^2/m^8$)	Airflow (m^3/s)	Pressure drop (Pa)
90	89	0,00104	80,09	6,7
91	90	0,00099	80,09	6,4
40	91	0,00461	80,09	29,6
5	108	0,00022	-21,09	-0,1
108	109	0,35	-21,09	-155,6
109	110	0,00013	-21,09	-0,1
110	52	0,00011	-21,09	0
104	100	0,00082	54,23	2,4
94	1	0,006	53,82	17,4
100	94	0,00088	54,23	2,6
94	96	0,00027	0,41	0
96	105	2,5	0,41	0,4
107	106	0,00078	36,46	1
106	103	0,0002	36,46	0,3
103	101	0,00047	36,46	0,6
101	99	0,00017	36,46	0,2
99	102	0,00111	36,46	1,5
102	95	5	15,58	1213,4
95	92	0,00038	15,58	0,1
92	93	0,00066	15,58	0,2
93	97	0,00007	15,58	0
97	111	0,00008	15,58	0
111	53	0,00026	15,58	0,1
12	119	0,00007	8,28	0
119	120	10	8,28	685,7
120	117	0,00035	8,28	0
117	121	0,00012	8,28	0
121	123	0,00008	8,28	0
123	124	0,00011	8,28	0
124	60	0,00004	8,28	0
20	130	5	8,68	377

Branch		Resistance ($N \cdot s^2/m^8$)	Airflow (m^3/s)	Pressure drop (Pa)
130	129	0,00012	8,68	0
129	127	0,00032	8,68	0
127	126	0,00004	8,68	0
126	128	0,00018	8,68	0
128	69	0,00035	8,68	0
35	79	1,5	6,16	56,9
25	73	25	-2,69	-181
38	82	1	-16,58	-274,8
19	70	5	-8,59	-368,6
10	58	0,00034	-3,52	0
45	86	25	-2,88	-206,9
22	164	0,018	31,1	17,4
164	162	0,00011	31,1	0,1
162	158	0,00043	31,1	0,4
158	155	0,00052	31,1	0,5
155	149	0,00051	31,1	0,5
149	153	0,00052	31,1	0,5
153	151	0,00058	31,1	0,6
151	148	0,00031	31,1	0,3
148	147	0,00043	31,1	0,4
147	150	0,00131	31,1	1,3
150	152	0,00148	18	0,5
152	154	0,00073	18	0,2
154	156	0,001	-1,97	0
156	159	0,00143	-1,97	0
159	160	0,0005	-1,97	0
161	160	0,00059	13,1	0,1
163	161	0,00196	13,1	0,3
157	163	0,0008	13,1	0,1
150	157	0,00076	13,1	0,1
171	71	0,00046	11,12	0,1

Branch		Resistance ($N \cdot s^2/m^8$)	Airflow (m^3/s)	Pressure drop (Pa)
169	171	25	11,12	3093,4
168	169	0,00051	11,12	0,1
166	168	0,00064	11,12	0,1
170	166	0,00075	11,12	0,1
174	170	0,00147	11,12	0,2
173	174	0,00089	11,12	0,1
160	173	0,00062	11,12	0,1
17	184	0,02	21,19	9
184	183	0,00018	21,19	0,1
183	182	0,00048	21,19	0,2
182	181	0,00025	21,19	0,1
181	180	0,00098	21,19	0,4
180	179	0,00153	21,19	0,7
179	178	0,00169	21,19	0,8
178	177	0,0006	21,19	0,3
177	175	0,00146	21,19	0,7
175	176	0,00148	21,19	0,7
189	59	0,00118	98,08	11,4
188	189	0,00108	98,08	10,4
187	188	0,00069	98,08	6,6
176	187	0,00073	98,08	7
107	102	0,00026	118,15	3,6
102	1	0,00038	139,03	7,3
105	3	0,00009	154,61	2,2
4	104	0,00155	54,23	4,6
116	6	0,00217	187,35	76,2
52	122	0,00217	187,35	76,2
13	98	0,00096	56,91	3,1
98	112	0,00046	56,91	1,5
112	113	0,00039	56,91	1,3
113	85	0,00034	76,89	2

Branch		**Resistance ($N \cdot s^2/m^8$)**	**Airflow (m^3/s)**	**Pressure drop (Pa)**
85	176	0,00047	76,89	2,8
61	52	0,00193	208,43	83,8
115	40	0,00043	83,52	3
114	115	0,0009	83,52	6,3
50	114	0,00106	83,52	7,4
41	50	0,00081	83,52	5,7
34	118	0,00138	15,75	0,3
118	125	0,00004	15,75	0
125	77	0,00013	15,75	0
154	113	0,00268	19,98	1,1

5.3. Appendix III: ClimSim results from iterations

The following tables display results from the simulations done by means of ClimSim, taking into account the variation of the conditions from each season of the year. The software gives information of temperatures every 20 meters from the initial point to the end.

Table 68. Stretch between points 1-3 January.

Stretch	Dry temperature	Wet temperature	Stretch	Dry temperature	Wet temperature
0	16.00	11.00	**580**	16.70	11.49
20	16.01	11.01	**600**	16.74	11.51
40	16.02	11.02	**620**	16.77	11.53
60	16.03	11.03	**640**	16.80	11.55
80	16.04	11.04	**660**	16.83	11.57
100	16.05	11.05	**680**	16.86	11.59
120	16.06	11.06	**700**	16.90	11.62
140	16.07	11.07	**720**	16.93	11.64
160	16.08	11.08	**740**	16.96	11.66
180	16.09	11.10	**760**	16.99	11.68
200	16.10	11.11	**780**	17.02	11.70
220	16.11	11.12	**800**	17.06	11.72
240	16.14	11.14	**820**	17.09	11.74
260	16.18	11.16	**840**	17.12	11.76
280	16.21	11.18	**860**	17.15	11.78
300	16.24	11.20	**880**	17.18	11.80
320	16.28	11.22	**900**	17.21	11.82
340	16.31	11.24	**920**	17.24	11.84
360	16.34	11.26	**940**	17.28	11.86
380	16.38	11.29	**960**	17.31	11.88
400	16.41	11.31	**980**	17.34	11.90
420	16.44	11.33	**1000**	17.37	11.92
440	16.47	11.35	**1020**	17.40	11.94

Stretch	Dry temperature	Wet temperature	Stretch	Dry temperature	Wet temperature
460	16.51	11.37	**1040**	17.43	11.96
480	16.54	11.39	**1060**	17.46	11.98
500	16.57	11.41	**1080**	17.49	12.00
520	16.61	11.43	**1100**	17.52	12.02
540	16.64	11.45	**1120**	17.55	12.04
560	16.67	11.47	**1140**	17.58	12.06
			1153	17.60	12.07

Table 69. Stretch between points 3-4 January.

Stretch	Dry temperature	Wet temperature	Stretch	Dry temperature	Wet temperature
40	19.08	11.06	**540**	20.04	11.76
60	19.12	11.09	**560**	20.08	11.79
80	19.16	11.12	**580**	20.12	11.82
100	19.20	11.14	**600**	20.15	11.84
120	19.24	11.17	**620**	20.19	11.87
140	19.28	11.20	**640**	20.23	11.90
160	19.32	11.23	**660**	20.26	11.92
180	19.35	11.26	**680**	20.30	11.95
200	19.39	11.29	**700**	20.34	11.98
220	19.43	11.31	**720**	20.37	12.01
240	19.47	11.34	**740**	20.41	12.03
260	19.51	11.37	**760**	20.45	12.06
280	19.55	11.40	**780**	20.48	12.09
300	19.59	11.43	**800**	20.52	12.11
320	19.62	11.46	**820**	20.55	12.14
340	19.66	11.48	**840**	20.59	12.17
360	19.70	11.51	**860**	20.63	12.19
380	19.74	11.54	**880**	20.66	12.22
400	19.78	11.57	**900**	20.70	12.25
420	19.82	11.59	**920**	20.73	12.27

Stretch	**Dry temperature**	**Wet temperature**	**Stretch**	**Dry temperature**	**Wet temperature**
440	19.85	11.62	**940**	20.77	12.30
460	19.89	11.65	**960**	20.81	12.33
480	19.93	11.68	**980**	20.84	12.35
500	19.97	11.71	**1000**	20.88	12.38
520	20.00	11.73	**1011**	20.90	12.40

Table 70. Stretch between points 1-3 April.

Stretch	**Dry temperature**	**Wet temperature**	**Stretch**	**Dry temperature**	**Wet temperature**
0	22.00	15.00	**580**	22.42	15.39
20	22.00	15.01	**600**	22.44	15.41
40	22.00	15.01	**620**	22.46	15.42
60	22.00	15.02	**640**	22.49	15.44
80	21.99	15.03	**660**	22.51	15.46
100	21.99	15.04	**680**	22.53	15.47
120	21.99	15.04	**700**	22.56	15.49
140	21.99	15.05	**720**	22.58	15.51
160	21.99	15.06	**740**	22.60	15.52
180	21.99	15.07	**760**	22.63	15.54
200	21.99	15.07	**780**	22.65	15.56
220	21.99	15.08	**800**	22.67	15.57
240	22.01	15.10	**820**	22.70	15.59
260	22.04	15.12	**840**	22.72	15.61
280	22.06	15.13	**860**	22.74	15.62
300	22.08	15.15	**880**	22.76	15.64
320	22.11	15.17	**900**	22.79	15.66
340	22.13	15.19	**920**	22.81	15.67
360	22.16	15.20	**940**	22.83	15.69
380	22.18	15.22	**960**	22.86	15.71
400	22.20	15.24	**980**	22.88	15.72
420	22.23	15.25	**1000**	22.90	15.74

Stretch	Dry temperature	Wet temperature	Stretch	Dry temperature	Wet temperature
440	22.25	15.27	**1020**	22.92	15.76
460	22.28	15.29	**1040**	22.95	15.77
480	22.30	15.31	**1060**	22.97	15.79
500	22.32	15.32	**1080**	22.99	15.81
520	22.35	15.34	**1100**	23.01	15.82
540	22.37	15.36	**1120**	23.04	15.84
560	22.39	15.37	**1140**	23.06	15.85
			1153	23.07	15.87

Table 71. Stretch between points 3-4 April.

Stretch	Dry temperature	Wet temperature	Stretch	Dry temperature	Wet temperature
0	25.00	18.00	**520**	25.64	18.42
20	25.03	18.02	**540**	25.66	18.44
40	25.05	18.03	**560**	25.68	18.45
60	25.08	18.05	**580**	25.71	18.47
80	25.10	18.07	**600**	25.73	18.48
100	25.13	18.08	**620**	25.75	18.50
120	25.15	18.10	**640**	25.78	18.52
140	25.18	18.11	**660**	25.80	18.53
160	25.20	18.13	**680**	25.82	18.55
180	25.22	18.15	**700**	25.85	18.56
200	25.25	18.16	**720**	25.87	18.58
220	25.27	18.18	**740**	25.89	18.60
240	25.30	18.20	**760**	25.92	18.61
260	25.32	18.21	**780**	25.94	18.63
280	25.35	18.23	**800**	25.96	18.64
300	25.37	18.24	**820**	25.99	18.66
320	25.40	18.26	**840**	26.01	18.67
340	25.42	18.28	**860**	26.03	18.69
360	25.44	18.29	**880**	26.06	18.71

Stretch	Dry temperature	Wet temperature	Stretch	Dry temperature	Wet temperature
380	25.47	18.31	**900**	26.08	18.72
400	25.49	18.33	**920**	26.10	18.74
420	25.52	18.34	**940**	26.12	18.75
440	25.54	18.36	**960**	26.15	18.77
460	25.57	18.37	**980**	26.17	18.78
480	25.59	18.39	**1000**	26.19	18.80
500	25.61	18.41	**1011**	26.20	18.81

Table 72. Stretch between points 1-3 June.

Stretch	Dry temperature	Wet temperature	Stretch	Dry temperature	Wet temperature
80	26.97	20.02	**620**	27.31	20.31
100	26.96	20.02	**640**	27.33	20.32
120	26.96	20.03	**660**	27.35	20.33
140	26.95	20.03	**680**	27.37	20.35
160	26.94	20.04	**700**	27.39	20.36
180	26.94	20.04	**720**	27.41	20.37
200	26.93	20.05	**740**	27.43	20.39
220	26.93	20.05	**760**	27.45	20.40
240	26.95	20.06	**780**	27.46	20.41
260	26.97	20.08	**800**	27.48	20.42
280	26.99	20.09	**820**	27.50	20.44
300	27.01	20.10	**840**	27.52	20.45
320	27.03	20.12	**860**	27.54	20.46
340	27.04	20.13	**880**	27.56	20.47
360	27.06	20.14	**900**	27.58	20.49
380	27.08	20.15	**920**	27.59	20.50
400	27.10	20.17	**940**	27.61	20.51
420	27.12	20.18	**960**	27.63	20.53
440	27.14	20.19	**980**	27.65	20.54
460	27.16	20.21	**1000**	27.67	20.55

Stretch	**Dry temperature**	**Wet temperature**	**Stretch**	**Dry temperature**	**Wet temperature**
480	27.18	20.22	**1020**	27.68	20.56
500	27.20	20.23	**1040**	27.70	20.58
520	27.22	20.25	**1060**	27.72	20.59
540	27.24	20.26	**1080**	27.74	20.60
560	27.26	20.27	**1100**	27.76	20.61
580	27.28	20.28	**1120**	27.78	20.63
600	27.30	20.30	**1140**	27.79	20.64
			1153	27.80	20.65

Table 73. Stretch between points 3-4 June.

Stretch	**Dry temperature**	**Wet temperature**	**Stretch**	**Dry temperature**	**Wet temperature**
0	30.00	22.00	**520**	30.41	22.32
20	30.02	22.01	**540**	30.42	22.34
40	30.03	22.03	**560**	30.44	22.35
60	30.05	22.04	**580**	30.45	22.36
80	30.06	22.05	**600**	30.47	22.37
100	30.08	22.06	**620**	30.48	22.38
120	30.10	22.08	**640**	30.50	22.40
140	30.11	22.09	**660**	30.51	22.41
160	30.13	22.10	**680**	30.53	22.42
180	30.14	22.11	**700**	30.54	22.43
200	30.16	22.13	**720**	30.56	22.45
220	30.17	22.14	**740**	30.57	22.46
240	30.19	22.15	**760**	30.59	22.47
260	30.21	22.16	**780**	30.60	22.48
280	30.22	22.18	**800**	30.62	22.49
300	30.24	22.19	**820**	30.63	22.51
320	30.25	22.20	**840**	30.65	22.52
340	30.27	22.21	**860**	30.66	22.53
360	30.28	22.22	**880**	30.68	22.54

Stretch	Dry temperature	Wet temperature	Stretch	Dry temperature	Wet temperature
380	30.30	22.24	**900**	30.69	22.55
400	30.32	22.25	**920**	30.71	22.57
420	30.33	22.26	**940**	30.72	22.58
440	30.35	22.27	**960**	30.74	22.59
460	30.36	22.29	**980**	30.75	22.60
480	30.38	22.30	**1000**	30.76	22.61
500	30.39	22.31	**1011**	30.77	22.62

Table 74. Stretch between points 1-3 October.

Stretch	Dry temperature	Wet temperature	Stretch	Dry temperature	Wet temperature
0	24.00	17.00	**580**	24.36	17.34
20	24.00	17.01	**600**	24.38	17.36
40	23.99	17.01	**620**	24.40	17.37
60	23.99	17.02	**640**	24.42	17.39
80	23.98	17.02	**660**	24.44	17.40
100	23.98	17.03	**680**	24.46	17.42
120	23.98	17.04	**700**	24.48	17.43
140	23.97	17.04	**720**	24.51	17.45
160	23.97	17.05	**740**	24.53	17.46
180	23.97	17.06	**760**	24.55	17.48
200	23.96	17.06	**780**	24.57	17.49
220	23.96	17.07	**800**	24.59	17.51
240	23.98	17.08	**820**	24.61	17.52
260	24.01	17.10	**840**	24.63	17.54
280	24.03	17.11	**860**	24.65	17.55
300	24.05	17.13	**880**	24.67	17.57
320	24.07	17.15	**900**	24.69	17.58
340	24.10	17.16	**920**	24.71	17.60
360	24.12	17.18	**940**	24.74	17.61
380	24.14	17.19	**960**	24.76	17.63

Stretch	Dry temperature	Wet temperature	Stretch	Dry temperature	Wet temperature
400	24.16	17.21	**980**	24.78	17.64
420	24.18	17.22	**1000**	24.80	17.66
440	24.20	17.24	**1020**	24.82	17.67
460	24.23	17.25	**1040**	24.84	17.68
480	24.25	17.27	**1060**	24.86	17.70
500	24.27	17.28	**1080**	24.88	17.71
520	24.29	17.30	**1100**	24.90	17.73
540	24.31	17.31	**1120**	24.92	17.74
560	24.33	17.33	**1140**	24.94	17.76
			1153	24.95	17.77

Table 75. Stretch between points 3-4 October.

Stretch	Dry temperature	Wet temperature	Stretch	Dry temperature	Wet temperature
0	27.00	19.00	**520**	27.50	19.39
20	27.02	19.02	**540**	27.52	19.40
40	27.04	19.03	**560**	27.54	19.42
60	27.06	19.05	**580**	27.56	19.43
80	27.08	19.06	**600**	27.58	19.45
100	27.10	19.08	**620**	27.60	19.46
120	27.12	19.09	**640**	27.61	19.48
140	27.14	19.11	**660**	27.63	19.49
160	27.16	19.12	**680**	27.65	19.51
180	27.18	19.14	**700**	27.67	19.52
200	27.20	19.15	**720**	27.69	19.54
220	27.22	19.17	**740**	27.71	19.55
240	27.24	19.18	**760**	27.72	19.57
260	27.25	19.20	**780**	27.74	19.58
280	27.27	19.21	**800**	27.76	19.60
300	27.29	19.23	**820**	27.78	19.61
320	27.31	19.24	**840**	27.80	19.62

Stretch	Dry temperature	Wet temperature	Stretch	Dry temperature	Wet temperature
340	27.33	19.26	**860**	27.82	19.64
360	27.35	19.27	**880**	27.83	19.65
380	27.37	19.29	**900**	27.85	19.67
400	27.39	19.30	**920**	27.87	19.68
420	27.41	19.32	**940**	27.89	19.70
440	27.43	19.33	**960**	27.91	19.71
460	27.45	19.35	**980**	27.92	19.73
480	27.46	19.36	**1000**	27.94	19.74
500	27.48	19.38	**1011**	27.95	19.75

ORIGINAL PAPERS

Paper I

Journal: Tunnelling and Underground Space Technology
Status: Published
DOI: 10.1016/j.tust.2015.09.001

Ventilation management system for underground environments

Marc Bascompta Massanés[a,]*, Lluís Sanmiquel Pera[a,b], Josep Oliva Moncunill[b]

[a] Iberpotash Chair in Sustainable Mining, Polytechnic University of Catalonia (UPC), Manresa, Catalonia, Spain.
[b] Department of Mining and Natural Resources, Polytechnic University of Catalonia (UPC), Manresa, Catalonia, Spain.
mbascomptem@gmail.com; sanmi@emrn.upc.edu; josep@emrn.upc.edu

Abstract

The management of the ventilation system is crucial to deal with efficiency, health and safety issues in an underground environment. This paper presents the design of a Geographic Information System –also known as GIS– capable to store, manipulate and extract results from the data collected regarding the ventilation features of an underground mine. The GIS can also be adapted to other types of underground infrastructures or include any additional parameter required.

A database of these parameters, in a case study, has been created taking into account two conditions: the changeable layout of the ventilation system during the evolution of the mine and the location of the control points, so the information can be analysed with the GIS in many different ways and purposes. Therefore, the system can control the underground conditions in the long term and evaluate any change applied to the ventilation circuit.

The study has given insight of the most sensitive parts of a mine in terms of gases, temperature, air velocity and airflow –either from the principal or auxiliary ventilation circuit– finding a relationship among the airflow quantity, gases concentration and effective temperature.

Keywords: Underground ventilation, geographic information system (GIS), health and safety, efficiency.

1 Introduction

Environmental conditions such as effective temperature, gases concentration or airflow have to be controlled and kept within an acceptable range in underground infrastructures where there is a presence of people. These types of space can be found in underground mining, civil infrastructures and tourist mines and caves, being of great concern the implementation of a management system for such purposes (Düzgün et al., 2011; Alfonso et al., 2013).

In general, the most adverse conditions appear in the mining sector, where the control of the underground environment is compulsory. Therefore, it is important the implementation of a methodology for managing this question, otherwise occupational hazards and operating cost rise exponentially either by legal restrictions or by a reduction in the worker’s performance. Thus, the system will have to take into account all the ventilation parameters to deal with efficiency and health and safety issues at the same time. However, their connection is usually overlooked. According to Reddy (2009), up to 60% of the mining operating costs are attributable to mine ventilation, while the relationship among hygienic conditions, accidents and worker’s efficiency has been previously mentioned by García-Herrero et al. (2012).

Many investigations have been focused on occupational health and safety or efficiency (Allen and Keen, 2008; Kurnia et al., 2014), and some of them use a software to optimise or modelling parts of the ventilation system (Hargreaves and Lowndes, 2007; Toraño et al., 2011; Cheng and S. Yang, 2012; Likar and Čadež, 2000). Moreover, the usage of GIS in mining is quite frequent, varying from management (Düzgün et al., 2011) to pollutants emission (Puliafito et al., 2002) or subsidence (Kim et al., 2006) among other applications. However, it is rarely used for the management of ventilation matters (Liu and D. Yang, 2004; Salp, et al., 2009) and not even mentioning the efficiency concept. Despite that, a geographic information system is able to provide the tools, frameworks and understanding of the real situation inside a mine (Saleh and Cummings, 2011) so programs and procedures can be implemented to ensure health and safety objectives (Akcil, 2006) through a database of the underground environment features such as airflow, gases or air pressure drop.

The aim of this paper is to propose a system for managing an underground environment that is able to analyse the real conditions in the long term and provide insight for controlling the current situation and future improvements in terms of working conditions and efficiency of the mine. Its creation will also give a new utility for a GIS. The software fits perfectly with what is demanded in a place that spreads out every day and generates a huge quantity of interconnected spatially referenced information from monitoring a dynamic environment (Gibert et al., 2006). Having the possibility to analyse the data and finally extract conclusions in the form of tables, graphs and even convert the information to other software formats.

2. Case of study: Mine description

The investigation has been focused on a Spanish mine, which is exploiting potassium from the Catalan basin. The resource is exploited by means of a room and pillar system 500 meters below the surface and the connection underground-surface is done through a shaft (intake) and a ramp (return). The main fan is placed at the beginning of the ventilation circuit, leading the airflow by temporary stoppings, curtains and doors. Meanwhile the auxiliary circuit provides clean air to every working face through a duct system. Fig. 1 is a scheme of the mine described above with the most important elements labelled. The image is one of the configurations created using the GIS and it displays the parts of the ventilation system in different colours: the intake is in colour sea blue, the return red, the leakage sky blue and the auxiliary system pink. The airflow direction has also been indicated.

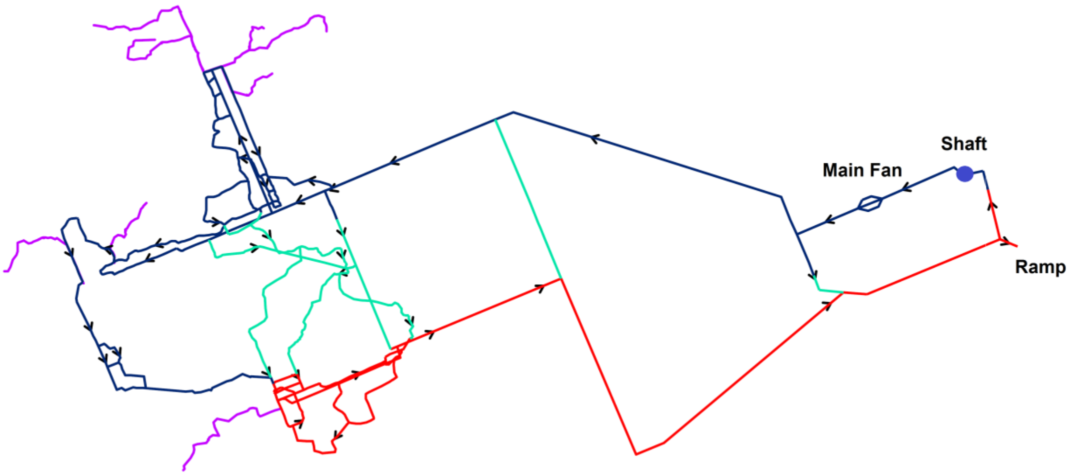

Fig. 1. Scheme of the ventilation circuit.

Initially, the staff of the mine had not stablished the position of the ventilation control points and an adequate analysis of the data collected was almost impossible when the factor time was included in the assessment, being needed a systematic method.

Salp et al. (2009) exposes an interesting approach for managing this type of environments, but it does not take into account all the parameters required for fully control the environmental conditions in this case, so it has been created a GIS based on the factors mentioned by Cheng and Yang (2012) and McPherson (2009) regarding efficiency and safety variables.

3. Methodology and database

Among all the software available, it has been chosen the ArcGIS because of its user-friendly platform, it is widespread in many different sectors and can be employed in any underground space apart from mines. The version used is the 9.3, but anyone would suit.

3.1. Data collection

First, several points standing for the real conditions of the whole ventilation system have been determined based on the following rules:

- Principal circuit: Important places from the intake, return and leakage airways.
- Auxiliary circuit: Variable position corresponding to the continuous miner location in the working faces.

Parameters used in the paper were obtained in situ and measured by conventional methods. They were taken during the same period of time in two consecutive days every month, one for the principal circuit and other for the auxiliary. Overall, 753 points have been stored in an Excel file since April 2009, 594 from the principal and 159 from the auxiliary.

The validity of the analysis depends on the method used for obtaining the data. The lower the reliability of the outcome is, the more difficult it is to detect the effects of an intervention (Lipsey, 1990), typically because of instability in what is measured and variations in the instrument (Shannon et al., 1999). For this reason, the equipment is calibrated regularly and measures are taken twice.

3.2. Data format and characteristics

The initial information consisted of several maps in dxf format (AutoCad) containing the layout of the mine along the time and the database in xls (Excel) with the ventilation parameters. Both files were merged and transformed to a shape file through ArcGIS, connecting the information from the key points with their position in the ventilation layout using the Universal Transverse Mercator projection (UTM) as a reference system. The merger process requires a standardised format for the database, otherwise problems can arise in the pre-processing stage.

3.3 Pre-processing

For the construction of the GIS file, these maps and ventilation data have been divided in different layers regarding two conditions: principal and auxiliary circuit with regard to every ventilation layout. This division makes the database management easier since they have different features and therefore separate analyses are required. Next step was to adequate the database storage from each point, taking into account the division previously described and the calculation of parameters such as airflow or effective temperature by means of the ArcGIS tools, which allow to introduce simple formulas. These equations are indicated in the following section 3.3.1.

3.3.1 Ventilation parameters description

The parameters described below are either measured in situ or calculated using the initial data. 18 parameters concerning the principal ventilation system and 22 in the auxiliary have been chosen to stand for the ventilation conditions. Each parameter is a column in database.

Principal ventilation

- Point: Identification number.
- Coordinates (UTM): Position of the point.
- Date of the measure: Hour, day, month and year.
- Air velocity (m/s): Measured with a rotating vane anemometer.
- Dry and wet temperature (ºC): Using a sling psychrometer.
- Carbon monoxide, CO (ppm), carbon dioxide, CO2 (ppm), nitric oxide, NO (ppm), nitrogen dioxide NO2 (ppm) and oxygen, O2 (%). Determined by a gas detector.
- Section (m2): Calculated with a laser distance measurer.
- Airflow (m3/s): Using the next expression. Airflow = Air velocity x Section.
- Effective temperature (ºC): Through the equation stated by the Spanish law (RGNBSM, itc 04.7.02), $te = 0{,}9 \cdot tw + 0{,}1 \cdot td$. Where te is effective temperature, tw wet temperature and td dry temperature.
- NO + NO2 (ppm): NO and NO2 have to be summarised as the Spanish law requires (RGNBSM, itc 04.7.02) to know if it is below the threshold limit value (TLV-TWA), which is the maximum level that a worker can be exposed day after day without adverse health effects.

Auxiliary ventilation

- Continuous miner: Identification number.
- Miner state: Working or in standby during the measures.
- Coordinates (UTM): Position of the miner.
- Date of the measure: Hour, day, month and year.
- Air velocity (m/s): Measured in front of the entry and exit of the pipeline.
- Pipe section (m2): Provided by the supplier.
- Airflow pipeline entry and exit (m3/s).
- Distance between working face and pipeline entry (m): Using a laser distance measurer.
- Type of fan: Exhausting, forcing or both.
- Other information: Any incident or remarkable situation.
- Dry, wet and effective temperature (ºC).
- CO (ppm), CO2 (ppm), NO (ppm), NO2 (ppm), NO + NO2 (ppm) and O2 (%).

3.4 Database design and management

Fig. 2 shows the structure of the GIS once the data has been properly introduced, organized and calculations are done. Each configuration is a different ventilation layout with the principal and the auxiliary circuits. The principal includes the intake, return, leakages and the points where measures are taken. Meanwhile, the auxiliary contains the continuous miner positions and ventilation ducts. In addition, the mine workings layer stand for all the tunnels exploited along the time.

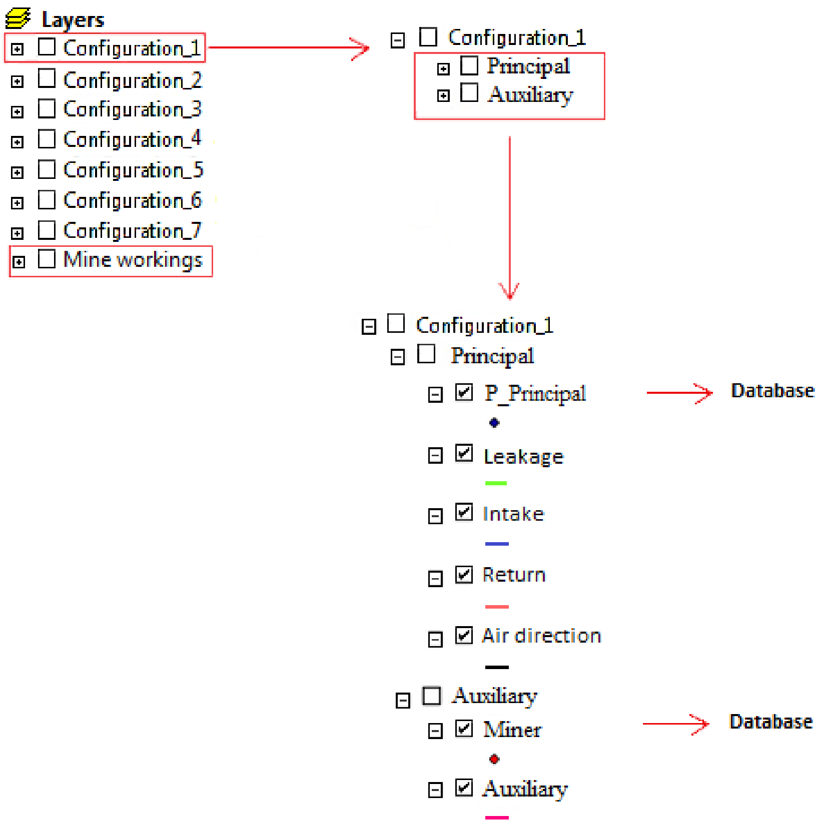

Fig. 2. Internal structure of the geographic information system.

On the other hand, Fig. 3 illustrates the steps followed to create the structure described above. Stages 1, 2 and 3 would be the same in the case of another sort of underground space, varying only the last two stages, 4 and 5, in accordance with its specific characteristics.

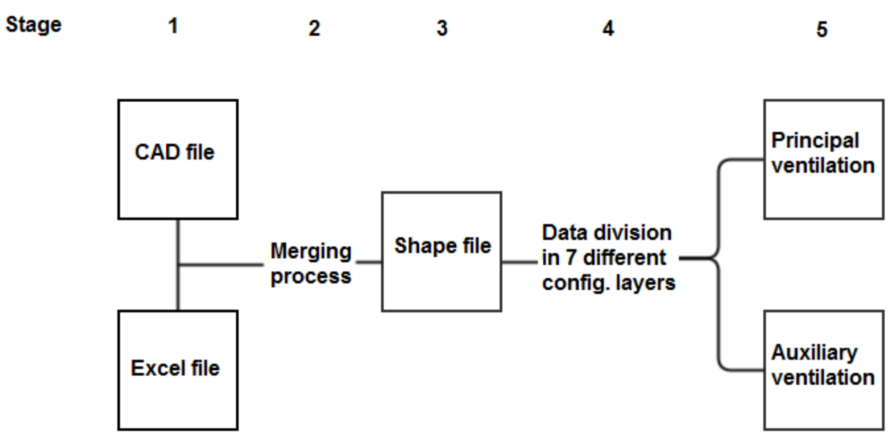

Fig. 3. Scheme of the process followed to create the GIS file.

The process explained is captured in Fig.4, which is one of the configurations with the airflows painted as in Fig. 1. In addition, there are some points that represent the places where measures are taken. The dots called “Mxx” are continuous miners, while the numbers “xx” are control points from the principal circuit.

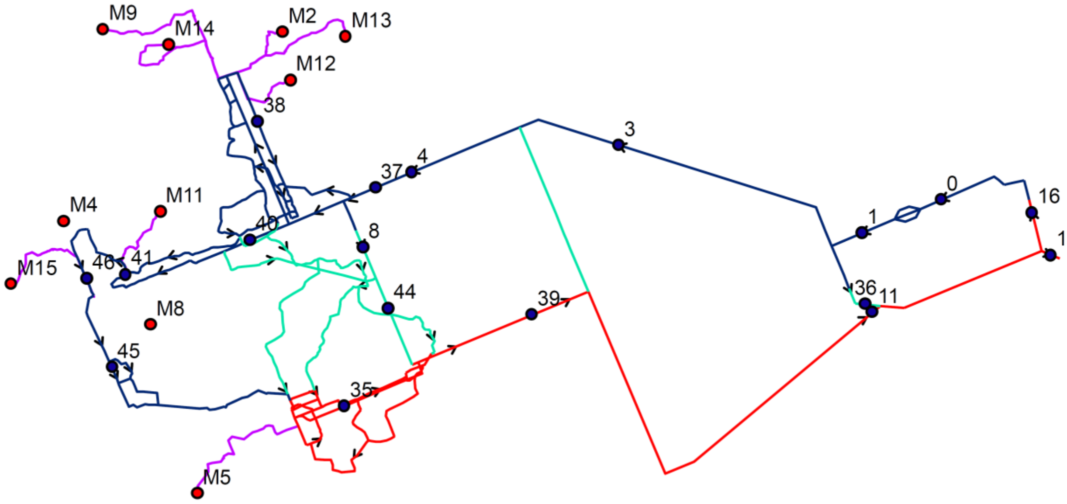

Fig. 4. Ventilation circuit in configuration 7.

Furthermore, Fig. 5 is an image of part of the ventilation circuit and mine workings. Both layers –displayed at the same time– are useful to understand the airflow route and relate the ventilation system with the mine planning.

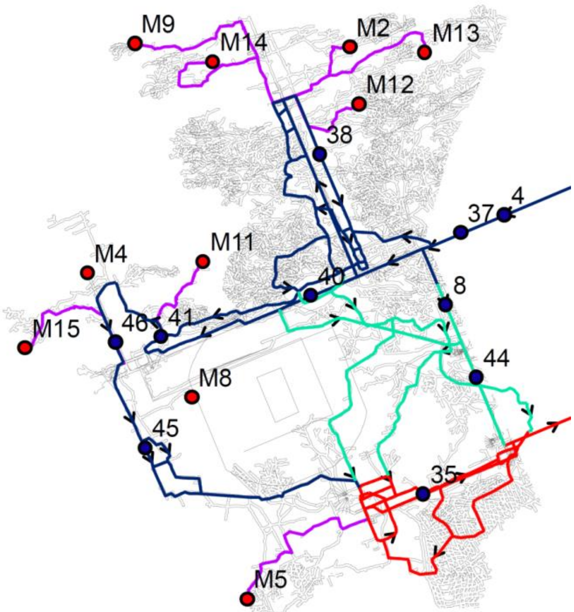

Fig. 5. Part of a ventilation circuit in detail with the mine workings layer activated.

Table 1 shows part of the data stored and how is organized inside the GIS. Once the database is linked to the graphical information, the system can be inquired depending on the necessities of the space and extract results using the GIS tools. The initial excel file can also be linked to the software and update automatically the system with new data introduced, as well as carry out the calculations stated in section 3.3.1.

Table 1. Data from the principal ventilation system in configuration 4.

Point	**X**	**Y**	**Velocity (m/s)**	**Section (m^2)**	**Airflow (m^3/s)**	**Td (ºC)**	**Tw (ºC)**
0	406644	4632795	4,52	40,00	180,80	16	13
1	406299	4632649	5,30	34,54	183,06	22	17
36	406312	4632339	1,20	31,84	38,21	24	17
3	405239	4633032	4,30	34,04	146,37	22	17
4	404338	4632913	4,25	27,86	118,41	27	18
37	404179	4632847	0,40	34,80	13,92	28	23
34	404875	4632946	0,60	28,37	17,02	27	21
7	405059	4632507	0,41	23,86	9,78	31	23
8	404125	4632587	0,41	31,54	12,93	35	22
38	403666	4633134	1,37	32,29	44,24	31	20
35	404044	4631896	3,96	27,83	110,21	38	28
39	404861	4632294	5,08	26,89	136,60	37	25
11	406344	4632305	6,18	24,36	150,54	32	25
13	407122	4632553	4,90	35,96	176,20	33	24
16	407039	4632738	0,45	21,61	9,72	34	24
40	403634	4632619	1,52	31,33	47,62	32	21

Overall, the GIS gives an important connection among visual information, ventilation parameters and evolution of the mine along the time. The fact that all the data is connected and georeferenced in a database provides a very useful tool to control and analyse the reality of an underground environment in a long term and make future research in the field.

4. Further improvements and applications

The system could be automatized instead of taking in situ measures and provide real time operating data, which would help to improve safety aspects and the efficiency of the whole mine (Michell et al., 1986). Currently, there are several software that are able to simulate the environmental conditions of a mine, but the feedback between the simulation and the real situation is quite new. Although some underground facilities start using the software simulator, monitoring the conditions and using the collected data to give feedback between the simulation and the real situation (Ruckman and Prosser, 2010), the GIS could be an intermediate step between the data gathered and the simulation because it is more efficient discriminating the information by means of knowledge and necessities of the technicians.

Moreover, the system proposed can be extrapolated to other spaces instead of a mine, such as tourist caves, confined spaces or any underground infrastructure where environmental conditions have to be controlled.

5. Results and discussion

The following results are obtained from the analysis of the data collected in situ and processed by the GIS, either the principal or the auxiliary ventilation system, giving some approaches of the possible assessments that can be achieved. The most sensitive characteristics of the ventilation system are set out below.

5.1. Principal ventilation system

<u>Air velocity</u>

It is a key parameter for health and safety, operation costs and modelling the airflow necessities of the principal and auxiliary circuit considering the number of workers, gases produced by diesel engines, necessity to remove excessive temperature and maximum air velocity permitted by law. Gas concentrations and temperature increase rapidly without an adequate air supply, worsening the workplace conditions and efficiency rate of the employees. Fig. 6 displays an air velocity evaluation, from data collected in situ, in three different chosen points from the principal circuit.

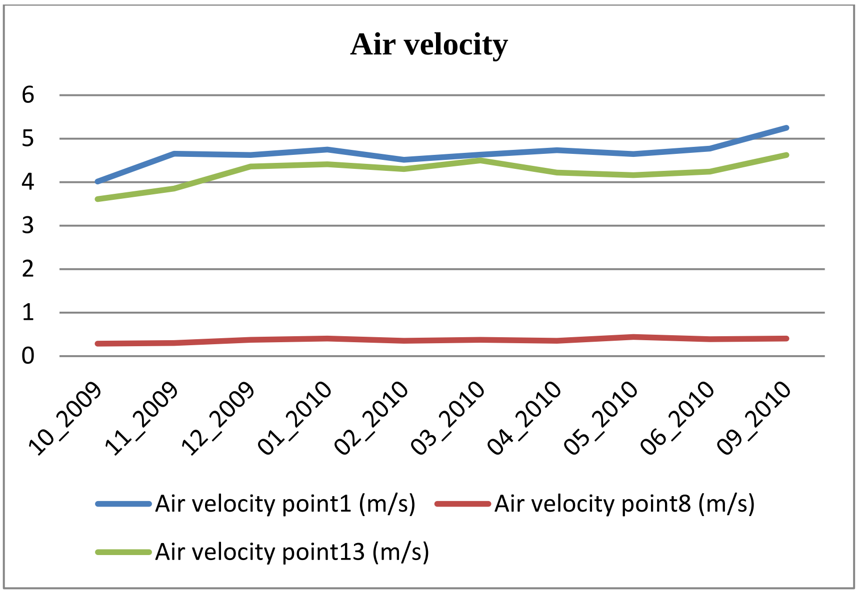

Fig. 6. Air velocity of the points 1, 8, and 13 from configuration 2.

Point 1 is at the beginning of the ventilation circuit after the main fan, while 13 is the last one before the airflow, in the return, flows to the surface. On the other hand, point 8 is in an intermediate position. The system created can assess the air velocity taking into account the different ventilation layouts.

Gases

Points 1 and 13 have been used once more to compare the quantity of gases. Table 2 shows that the first one does not have any concentration of gases, while it is significantly higher in the return. Despite that, values always remain under the TLV specified by the Spanish law, ITC 04.7.02.

Table 2. Gases concentration comparison between points 1 and 13.

Point 1						
Month	**Year**	**Day**	**NO (ppm)**	**NO_2 (ppm)**	**CO (ppm)**	**CO_2 (ppm)**
October	2009	23	0,00	0,00	0,00	0,00
November	2009	26	0,00	0,00	0,00	0,00
December	2009	1	0,00	0,00	0,00	0,00
January	2010	11	0,00	0,00	0,00	0,00
February	2010	25	0,00	0,00	0,00	0,00

March	2010	24	0,00	0,00	0,00	0,00
April	2010	4	0,00	0,00	0,00	0,00
May	2010	17	0,00	0,00	0,00	0,00
June	2010	18	0,00	0,00	0,00	0,00
September	2010	20	0,00	0,00	0,00	0,00
Point 13						
Month	**Year**	**Day**	**NO (ppm)**	**NO_2 (ppm)**	**CO (ppm)**	**CO_2 (ppm)**
October	2009	23	5,00	0,20	8,00	2500,00
November	2009	26	5,00	0,20	8,00	2800,00
December	2009	1	5,00	0,20	9,00	3000,00
January	2010	11	1,00	0,00	0,00	500,00
February	2010	25	2,00	0,00	4,00	1900,00
March	2010	24	0,00	0,00	1,00	1500,00
April	2010	4	0,00	0,20	0,00	800,00
May	2010	17	6,00	0,10	4,00	2100,00
June	2010	18	0,00	0,10	7,00	400,00
September	2010	20	4,00	0,00	0,00	100,00

Additionally, Fig. 7 illustrates the location of the measures taken and used in Table 2. It clarifies the airflow route and gives some clues about where the main sources of gases could be. Therefore, efforts can be focused on the most adverse zones and subsequently control the effectiveness of any remedial action.

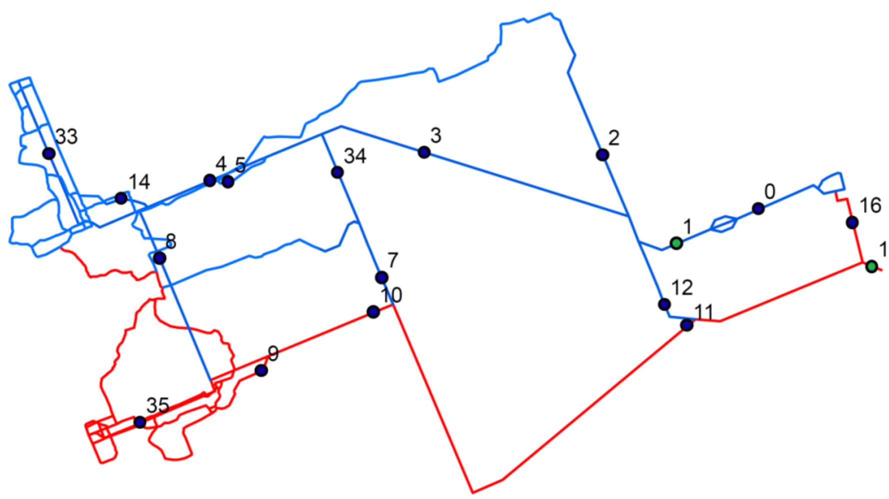

Fig. 7. Principal ventilation circuit with points 1 and 13 selected in green.

5.2. Auxiliary ventilation system

Effective temperature

When temperature is kept below a certain value, the efficiency of the mine increases, because the workforce is able to stay more time in the working faces, according to the law, with a higher mental concentration (García-Herrero et al., 2012). Table 3 comprises a selection, using the GIS tools, of the miners that have been over 30 ºC during 2012, while Fig. 8 displays the location of these miners.

Table 3. Selection of the measures over 30ºC during 2012.

Miner	X	Y	Month	Day	Te (ºC)
M5	403584,3210	4631491,2930	February	21	34,40
M5	403501,3440	4631512,6890	April	21	32,10
M11	403192,3100	4632604,5000	April	21	31,00
M15	402635,8200	4632536,1770	April	21	30,20
M7	403423,8600	4631908,2440	May	23	30,00
M11	403198,0640	4632596,1310	May	23	31,00
M14	403016,5470	4633352,8320	October	19	30,80
M2	404010,7660	4633606,8540	October	19	32,00
M12	403802,5090	4633316,2760	October	19	32,50
M6	404061,2650	4631677,4540	October	19	31,80
M5	403500,6710	4631509,1540	October	19	33,80
M7	403521,0480	4631717,8980	October	19	30,00
M5	403403,1010	4631515,7260	November	22	30,00
M11	403243,7040	4632742,6100	November	22	31,10

As it can be seen, only 14 in 156 measures from 2012 have exceeded the conditions imposed. Using the GIS, it is possible to detect adverse conditions more easily and quickly. Knowing when it has happened, how many times and which parts are the most negative with regard to health and safety.

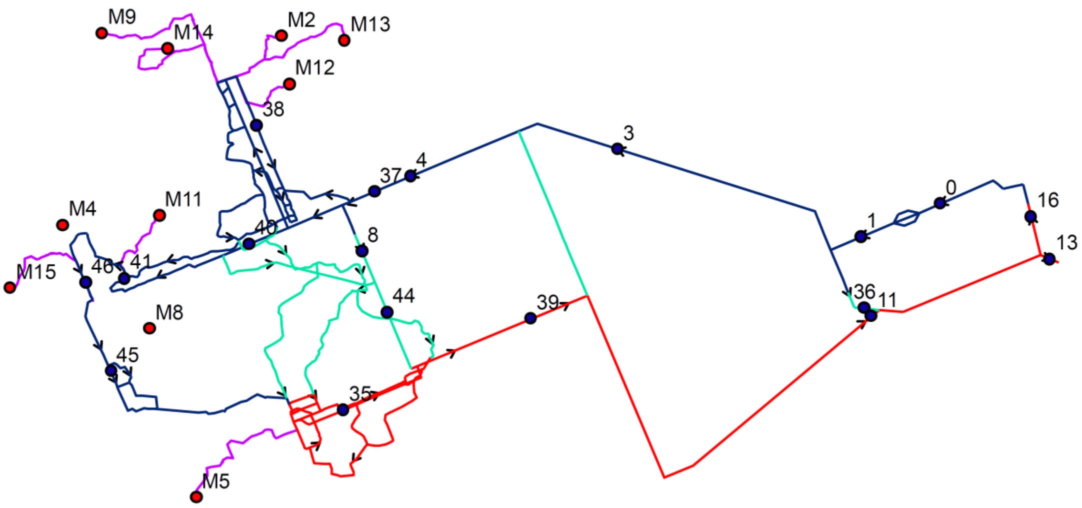

Fig. 8. Principal and auxiliary ventilation system with the control points and miners position (configuration 7).

Relationship temperature-gases-airflow

Several features can also be studied together. Fig. 9 relates all the data collected concerning temperature, gases and airflow from the auxiliary circuit (159 measures in total). Unfortunately, there is a short period without CO and airflow measures. The concentration of the CO_2 (in ppm) has been divided per 100 to get a more visual chart.

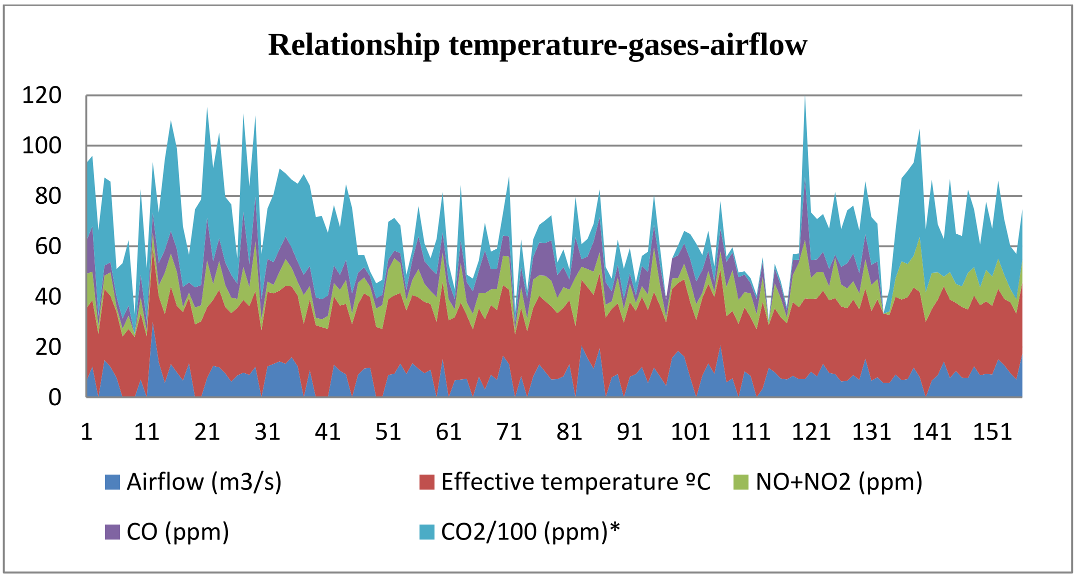

Fig. 9. Values of temperature, gases and airflow from the auxiliary ventilation system.

As it can be seen, there is a correlation between temperature, gases and airflow. The larger the airflow is, the higher the temperature and the gases concentration are. The air, supposedly clean, flows from a working face to another, carrying part of the gases from the previous miner and so on. This approach can be useful to assess any change in the auxiliary system and to find unwanted local airflow recirculation.

5.3. Other possible outcomes

Although the core issues of the case study have already been treated, the capabilities of the GIS could be focused on other aspects depending on the underground space and its specific necessities.

6. Conclusions

The GIS created has been confirmed as a powerful tool to provide a safer and healthier work environment and improve the efficiency of the ventilation system. The connection of both concepts is crucial to make any decision that concerns applying changes to the ventilation system and the use of the geographic information system can be helpful for such purpose. In addition, the possibility to complement the GIS with other software and include other factors when it is necessary gives an enormous flexibility to control an underground environment.

In this case, the system has given insight of the most sensitive parts concerning gases, temperature, air velocity and airflow in the principal and auxiliary ventilation circuits. The factors have been assessed individual and collectively. Specifically, the variations of velocity and gases concentration along the principal circuit have been obtained using all the historical data. Meanwhile, the most adverse working faces in terms of effective temperatures and gases concentration have also been studied. In the auxiliary system, a pattern among airflow, gases concentration and effective temperature has also been found.

Acknowledgements

This research has been carried out by the Iberpotash Chair in mining sustainability in collaboration with ICL-Iberia. The authors would like to thank the staff of the mine for their willingness as well as the postgraduate students A. Galera and D. Flores for important contributions to create the database.

References

Akcil, A. (2006). Managing cyanide: health, safety and risk management practices at Turkey's Ovacik gold–silver mine. Journal of Cleaner Production, 14(8), 727–735.

Alfonso Abella, M. P., Sanmiquel Pera, Ll., Vintro Sanchez , C., Parcerisa Duocastella, D., Oliva Moncunill, J., Freijo Alvarez, M., Mata Perelló, J. M. (2013). Development of an integrated monitoring system for touristic mines and caves. International Conference on Sustainable Tourism and Cultural Heritage, 303-307.

Allen, C., Inco, V., Keen, B. (2008). Ventilation on demand (VOD) project – Vale Inco Ltd . Coleman Mine. 12th North American Mine Ventilation Symposium 2008, 45–50.

Cheng, J., Yang, S. (2012). Data mining applications in evaluating mine ventilation system. Safety Science, 50(4), 918–922.

Düzgün, Ş., Künzer, C., Özgen Karacan, C. (2011). Applications of remote sensing and GIS for monitoring of coal fires, mine subsidence, environmental impacts of coal-mine closure and reclamation. International Journal of Coal Geology, 86(1), 1–2.

E. Puliafito, M. Guevara, C. P. (2002). Characterization of urban air quality using GIS as a management system. Environmental Pollution.

Garcia-Herrero, S., Mariscal M.A., García-Rodríguez J., Ritzel D. O. (2012). Working conditions psychological physical symptoms and occupational accidents. Bayesian network models. Safety Science, 50, 1760-1774.

Gibert, K., Sànchez-Marrè, M., Rodríguez-Roda, I. (2006). GESCONDA: An intelligent data analysis system for knowledge discovery and management in environmental databases. Environmental Modelling & Software, 21(1), 115–120.

Hargreaves, D. M., Lowndes, I. S. (2007). The computational modelling of the ventilation flows within a rapid development drivage. Tunnelling and Underground Space Technology, 22, 150–160.

Kim, K.-D., Lee, S., Oh, H.-J., Choi, J.-K., Won, J.-S. (2006). Assessment of ground subsidence hazard near an abandoned underground coal mine using GIS. Environmental Geology, 50(8), 1183–1191.

Kurnia, J. C., Sasmito, A. P., Mujumdar, A. S. (2014). Simulation of a novel intermittent ventilation system for underground mines. Tunnelling and Underground Space Technology, 42, 206–215.

Likar, J., Čadež, J. (2000). Ventilation Design of Enclosed Underground Structures. Tunnelling and Underground Space Technology, 15(4), 477–480.

Lipsey, M.W. (1990). Design Sensitivity. Sage Publications, Newbury Park, California.

Liu, H., Yang, D., City, H. (2004). GIS-Based Mine Ventilation Network and Safety Analysis. IEEE International Geoscience and Remote Sensing Symposium Proceedings, 5, 2945–2948.

Ministerio de industria y energía (1994). ITC 04.7.02 and ITC 04.7.05. In: Ministerio de industria y energía (Ed.). Reglamento General de Normas Básicas de Seguridad Minera. Centro de publicaciones. Madrid. ISBN: 8474747481.

McPherson, M. J. (2009). Subsurface Ventilation and Environmental Engineering. California, USA, ISBN: 978-0-692.00024-3.

Mitchell, J., Eros, L., King, R. (1986). Deserado Mine Computer Monitoring and Control System. Proceedings of the Eighth WVU Mining Electro Technology Conference.

Reddy, A.C. (2009). Development of a Coal Reserve GIS Model and Estimation of the Recoverability and Extraction Costs. Master of Science Thesis, Department of Mining Engineering, West Virginia University.

Ruckman, R., Prosser, B. (2010). Integrating ventilation monitoring sensor data with ventilation computer simulation software at the Waste Isolation Pilot Plant facility. 13th United States/North American Mine Ventilation Symposium, (96), 237–242.

Şalap, S., Karslıoğlu, M. O., Demirel, N. (2009). Development of a GIS-based monitoring and management system for underground coal mining safety. International Journal of Coal Geology, 80(2), 105–112.

Saleh, J. H., Cummings, A. M. (2011). Safety in the mining industry and the unfinished legacy of mining accidents: Safety levers and defense-in-depth for addressing mining hazards. Safety Science, 49(6), 764–777.

Shannon, H. S., Robson, L. S., Guastello, S. J. (1999). Methodological criteria for evaluating occupational safety intervention research. Safety Science, 31, 161–179.

Toraño, J., Torno, S., Menéndez, M., Gent, M. (2011). Auxiliary ventilation in mining roadways driven with roadheaders : Validated CFD modelling of dust behaviour. Tunnelling and Underground Space Technology, 26, 201–210.

Paper II

Journal: Journal of Mining Science

Status: Published

DOI: 10.1134/S1062739114050159

Determination of the Friction Factors in Potash Mines

Marc Bascompta Massanés, Lluís Sanmiquel Pera and Josep Oliva Moncunill

Polytechnic University of Catalonia (UPC),
Av. Bases de Manresa, 61-73 08242, Manresa, Spain
e-mail: mbascomptem@gmai.com; sanmi@emrn.upc.edu; josep@emrn.upc.edu

Abstract

The friction factor is an essential parameter to take into account for modelling the ventilation system. One of the principal features that define the friction factor is the roughness, which not only does it have influence on the airway resistance, but it has also a direct bearing on the rate of heat transfer between the rock and the airstream. In this paper, the characteristic friction factors of a potash mine exploited using a room and pillar method has been determined by means of the Chezy–Darcy and Atkinson equations. The results give an impulse to achieve standardized friction factor values in potash mines very useful for future mining ventilation surveys.

Keywords: Mining ventilation, friction factor, potash mine, room and pillar exploitation method.

Introduction

The knowledge of the ventilation system and the parameters that define its behaviour is crucial for modelling it [1]. Among all of them, one of the most important aspects to take into account is the friction factor, which will be basically affected by the exploitation method, geometric characteristics of the tunnels and physic conditions of the mine [2].These factors have a huge influence to the resistance against the flow of the air through the airways [3]. However, there is little information about potash exploitations, being mainly focused on coal and metal mines.

This paper give insight of the friction factors in an underground potash mine that uses continuous mining machines to exploit the mineral and carrying it to the surface through a conveyor belt system. These kinds of mines are very deformable due to the pressure from the surrounding rock, producing a considerable roughness in the surface of the galleries. This roughness can also be caused for the exploitation method, the temperature and the humidity grade.

One of the first studies concerning friction factors in mining was done by McElroy [4], which was based on data of the pressure loss collected from coal and metal mines. Many subsequent related studies adding data and determining new values have been published [5–11], even with the goal to standardise the friction factors [12], but there is still a lack of data for other exploitations than metal and coal mines.

1. Ventilation theory

Frictional pressure drop is an essential parameter to know the ventilation conditions in an underground mine. It can be obtained using the equation below, which is a form of the Chezy–Darcy expression:

$$p = f\mathrm{L}\frac{\mathrm{Per}}{\mathrm{A}}\rho\frac{u^2}{2} \text{ (Pa)},$$

where f is the dimensionless coefficient of friction; Per is the airway perimeter, m; A is the area, m^2; ρ is the air density, kg/m^3; u is the air velocity, m/s; L is the length of the airway, m.

Later on, it was adapted by Atkinson to the well-known Atkinson equation, expressed in frictional pressure drop:

$$p = \mathrm{kL}\frac{\mathrm{Per}}{\mathrm{A}}u^2 \text{ (Pa)},$$

where k is the friction factor, kg/m^3.

The same equation can also be showed in terms of resistance, using the square law, and taking into account any other air density inside the mine due to pressure or temperature factors [13, 14]:

$$R = \frac{\mathrm{p}}{\mathrm{Q}^2} = \mathrm{kL}\frac{\mathrm{Per}}{\mathrm{A}^{\mathrm{S}}}\frac{\rho}{1.2} \text{ (Ns}^2\text{/m}^8\text{)},$$

The Atkinson friction factor is not a constant value, it varies with the Reynolds Number. However, the flow of the air in the vast majority of underground places is turbulent in nature except in few cases such as behind the stopings [15]. The Von Kármán equation gives a relationship with the friction factor from the Atkinson expression for turbulent flows. The equation is applicable to circular and non-circular airway, by means of the hydraulic mean diameter calculated with the following relationship $Dh = 4$ A/Per:

$$f = \frac{2\mathrm{k}}{\rho} = \frac{1}{4\left[2\log_{10(\frac{Dh}{e})+1.14}\right]^2} \text{ (Dimentionless)},$$

where Dh is the hydraulic mean diameter of the tunnel, m; e is the height of the roughening, m.

In addition, the airflow also suffers shock losses due to obstacles in the ventilation circuit like direction changes, machines, conveyors, etc. All these elements are independent of the roughness and it is not possible to include it in the friction factor. However, it can be used the equivalent length concept:

$$\mathrm{Leq} = \frac{0.15X}{\mathrm{k}} Dh,$$

where Leq is the equivalen length, m; *X* is the shock loss factor.

The shock loss factor *X* is experimentally determined [4, 8, 14], adding an equivalent increase in the length of the tunnel where the air flows [17]. The length increase will vary depending on the type of obstacle [18], obtaining a corrected Atkinson equation:

$$R = \mathrm{k}(\mathrm{L} + \mathrm{Leq})\frac{\mathrm{Per}}{\mathrm{A}^3}\frac{\rho}{1.2}\ (\mathrm{Ns}^2/\mathrm{m}^8).$$

3. Methodology

Achieving a proper ventilation system planning not only does it need a good knowledge of the ventilation laws, but it is also necessary an updated database of the ventilation features [17]. For this reason, 18 key points that stand for the principal ventilation circuit have been selected, collecting the main ventilation parameters every month from 2008 to 2013, which are detailed below. Figure 1 displays an example of the points used to obtain the friction factors.

—Geometric features of the galleries: section, perimeter, length, roughness and any permanent obstacles in the ventilation circuit.
—Dry and wet temperatures: used to control and link airway roughness and surface climate conditions
—Air velocity: knowing the section, it is possible to calculate de airflow.

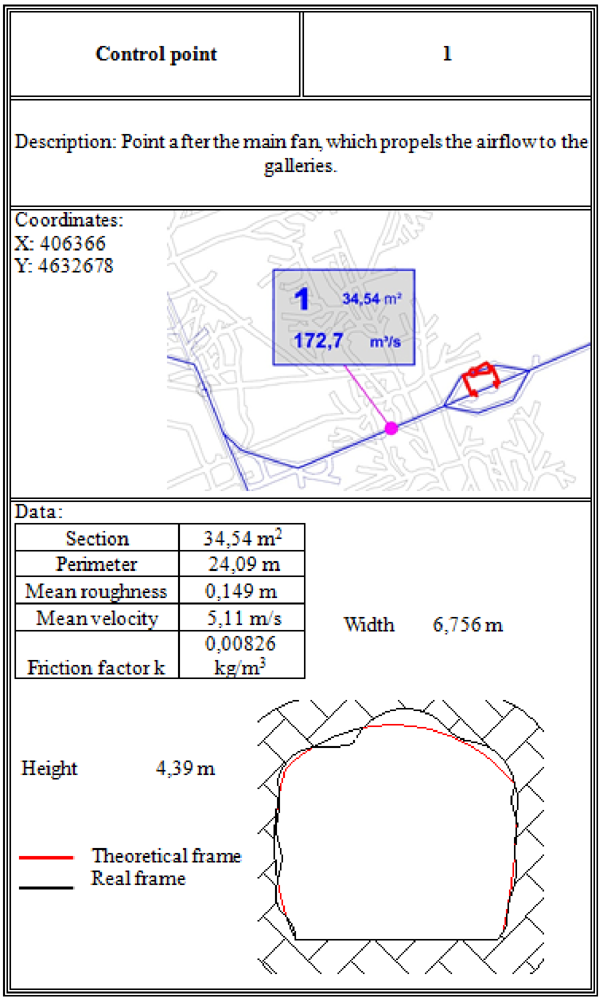

Fig. 1. Description of one of the control points.

Two important aspects in the process of calculating the friction factors have been taken into account in this paper, the Reynolds number and the hydraulic diameter. The first one is necessary to know the fluid rate and so use the proper equation and the second one to adapt the noncircular diameter of the galleries to the equations.

Once all the information detailed above has been collected, the fiction factors have been calculated for each key point four times, corresponding the four seasons of the year, because airflow and temperatures suffer an important variation during the year, affecting the friction factor result. Finally, the mean friction for each point has been obtained.

3. Results

Table 1 shows the mean parameters used to calculate the friction factors. They have been either measured in situ or calculated with the data collected from 2008 to 2013.
The values displayed in table 2 correspond to the mean friction factors per season and the general value per point, taking into account the four seasons values in each key point, as well as the standard deviation [19].

The current bibliography details the friction factor values for coal and metal mines. Tables 3 and 4 compare the results obtained in this paper with the published data among different types of airways. Despite the survey is focused on a potash mine, not on coal or metal mines, it is possible to get a rough idea of the reliability of the results.

Table 1. Parameters used to calculate the friction factor

Point	A, m^2	Per, m	*Dh*, m	*V*, m/s	*e*, m	*f*
0	40.00	24.60	6.50	4.42	0.36300	0.01880
1	34.54	24.09	5.74	5.11	0.14900	0.01345
2	31.84	22.60	5.64	0.94	0.14390	0.01336
3	34.04	23.22	5.86	4.33	0.13260	0.01273
4	27.86	21.85	5.10	4.36	0.11000	0.01250
5	34.80	23.24	5.99	0.52	0.14170	0.01296
6	28.37	21.50	5.28	0.81	0.23330	0.01687
7	23.86	17.50	5.45	0.43	0.23750	0.01676
8	31.54	25.00	5.05	0.38	0.11910	0.01295
9	32.29	23.09	5.59	1.71	0.30000	0.01845
10	27.83	22.03	5.05	4.07	0.18240	0.01543
11	26.89	20.73	5.19	5.62	0.11440	0.01261
12	24.36	18.00	5.41	6.40	0.10000	0.01178
13	35.96	26.28	5.47	4.70	0.12000	0.01258
14	21.61	20.00	4.32	0.46	0.17480	0.01622
15	31.33	19.34	6.48	1.58	0.17480	0.01366
A	29.82	21.89	5.45	0.91	0.30000	0.01868
D	33.40	23.00	5.81	0.71	0.23750	0.01630

Table 2. Mean friction factor and standard deviation for each point

Point	Spring k, kg/m^3	Summer k, kg/m^3	Autumn k, kg/m^3	Winter k, kg/m^3	General value k, kg/m^3	Standard deviation
0	0.01163	0.01134	0.01168	0.01184	0.01162	0.00021
1	0.00821	0.00801	0.00822	0.00838	0.00820	0.00015
2	0.00835	0.00848	0.00835	0.00853	0.00843	0.00009
3	0.00794	0.00778	0.00787	0.00802	0.00790	0.00010
4	0.00781	0.00796	0.00781	0.00796	0.00788	0.00009
5	0.00743	0.00701	0.00750	0.00739	0.00733	0.00022
6	0.00876	0.00872	0.00875	0.00933	0.00889	0.00029
7	0.00860	0.00856	0.00857	0.00856	0.00857	0.00002
8	0.00894	0.01014	0.00900	0.00940	0.00937	0.00055
9	0.00947	0.00787	0.00952	0.00900	0.00896	0.00077
10	0.00890	0.00890	0.00900	0.00893	0.00893	0.00005
11	0.00735	0.00729	0.00738	0.00732	0.00733	0.00004
12	0.00690	0.00686	0.00677	0.00677	0.00682	0.00007
13	0.00798	0.00855	0.00803	0.00821	0.00819	0.00026
14	0.00956	0.00956	0.00963	0.00956	0.00958	0.00003
15	0.00758	0.00694	0.00821	0.00759	0.00758	0.00052
A	0.01081	-	0.01207	0.01088	0.01125	0.00071
D	0.00956	-	0.00972	0.00960	0.00963	0.00009

Table 3. Comparison between published data and values from the paper

Airway type	Prosser and Wallace (2002)	McPherson (1993)	Hartman et al. (1997)	Paper values
Rectangular Airway–Clean Airway (Coal and soft rocks)	0.0075	0.0090	0.0080	0.0073
Rectangular Airway–Some Irregularities (Coal and soft rocks)	0.0087	0.0090	0.0091	0.0084
Metal Mine Drift	0.0088	0.0120	0.0269	0.0115

Metal Mine Ramp	0.0116	-	0.0297	0.0082

Table 4. Percentage difference between paper and bibliographic values

Airway type	Paper values	Difference, %		
		Prosser and Wallace (2002)	McPherson (1993)	Hartman et al. (1997)
Rectangular Airway–Clean Airway	0.0073	2.32	22.78	9.14
Rectangular Airway–Some Irregularities	0.0084	3.20	6.76	7.95
Potash Mine Drift	0.0115	23.68	4.08	133.30
Potash Mine Ramp	0.0082	40.95	-	260.87

Conclusions

The characteristic friction factors in a potash mine using a room and pillar method have been determined. Despite each mine has its own characteristics, it has been achieved a framework for future studies related to mine ventilation in this type of exploitations.

The Chezy–Darcy and Atkinson equations have been employed to calculate the friction factor k, using the parameters measured in the control points. Roughness of the airways is due to, basically, the exploitation method and the nature of the de deposit, which has a certain deformable properties that define the shape of the tunnels.

Acknowledgments

This work was supported by the Iberpotash Chair in mining sustainability from the Polytechnic University of Catalonia (UPC). The authors would like to thank the staff of Iberpotash S.A. for their willingness as well as postgraduate student Hernan Francisco Anticoi for important contributions.

References

Shalimov, A.V., Numerical Modeling of Air Flows in Mines under Emergency State Ventilation, *J. Min. Sci.*, 2011, vol. 47, no. 6, pp. 807–813.

Duckworth, I., and Prosser, B., Analysis of the Data Obtained from Ventilation Studies of Longwall Panels, Proc. 6th Int. Mine Ventilation Congress, 1997, pp. 223-229.

Alymenko, N.I., Aerodynamic Parameters of Ventilating Passages Joined-Up with the Main Mine Fan, J. Min. Sci., 2012, vol. 47, no. 6, pp. 814–823.

McElroy, G., Engineering Factors in the Ventilation of Metal Mines, Bureau of Mines, U.S. Deparment of Interior, Washington, 1935.

Duckworth, I. J., Loomis, I., and Prosser, B., Fifteen Years of Resistance Data Collected at Freeport Indonesia, Proc. 14th U.S./North American Mine Ventilation Symposium, 2012, pp. 161–166.

Fytas, K., and Gagnon, C., A Database of Ventilation Friction Factors for Quebec Underground Mines, Proc. 14th U.S./North American Mine Ventilation Symposium, 2008, pp. 615- 622.

Hall, C.J., Mine Ventilation Engineering, The Society for Mining, Metallurgy, and Exploration, Inc., 1981.

Hartman, H., Mutmansky, J., Ramani, R., and Wang, Y, Mine Ventilation and Air Conditioning, 3rd Edition, Vancouver: John Wiley and Sons, 1997.

Kharkar, R., Stefanko, R., and Ramani, R.V., Analysis of Leakage and Friction Factors in Coal Mine Ventilation Systems, Special Research Report No. SR-99, Pennsylvania Department of Commerce, 1974.

Prosser, B.S., and Wallace, K.G., Practical Values of Friction Factors, Proc. 8th US Mine Ventilation Symposium, 1999, pp 691-696.

Wala, A.M., Studies of Friction Factor for Kentucky's Coal Mines, Proc. 5th U.S. Mine Ventilation Symposium, 1991, pp. 675- 684.

Prosser, B., and Wallace, K., Practical Values of Friction Factors, Mine Ventilation Service, Inc., California, USA 2002.

Diego, I., Torno, S., Toraño, J., Menéndez, M., and Gent, M., A Practical Use of CDF for Ventilation of Underground Works, Tunnelling and Underground Space Technology, 2011, pp. 189- 200.

Montecinos, C., and Wallace, K., Equivalent Roughness for Pressure Drop Calculations in Mine Ventilation, Proc. 13th U.S./North American Mine Ventilation Symposium, 2010, pp. 225- 230.

McPherson, M.J., Subsurface Ventilation and Environmental Engineering, Mine Ventilation Services, Inc., California, USA, 2009.

Hurtado, J.P., Díaz, N., Acuña, E.I., and Fernández, J., Shock Losses Characterization of Ventilation Circuits for Block Caving Production Levels, Tunnelling and Underground Space Technology, 2014, vol. 41, pp. 88–94.

Meyer, C., Determining the Friction Factors for Underground Colliery Board and Pillar Working, Safety in Mines Research Advisory Committee, 1998.

Carrasco Galan, J., Manual de ventilación de minas y obrassubterráneas (Please give English translation here), Aitemin Centro Tecnológico, Espanya, Madrid, 2011.

Box, G.E.P., Hunter J.S. and Hunter, W.G., Statistics for Experiments. Design, Innovation and Discovery, New Jersey: Wiley & Sons, 2005.

Paper III

Journal: Journal of environmental management
Status: Under review

Ventilation layout influence to the environmental conditions in an underground mine and managing proposal

Marc Bascompta[a],*, Ana María Castañón[b], Lluís Sanmiquel[a], Josep Oliva[a]

a Department of Mining and Natural Resources, Polytechnic University of Catalonia (UPC), Manresa (Barcelona) Spain. Av. Bases de Manresa, 61-73, 08242
b Department of Mining, Topography and Structures, University of León (ESTIM), León Spain. Campus de Vegazana, s.n, 24071.
marc.bascompta@emrn.upc.edu; amcasg@unileon.es; sanmi@emrn.upc.edu; josep@emrn.upc.edu

Abstract

Gases such as CO, CO_2 or NO_x are constantly generated in any underground mine by the equipment and the ventilation layout has a very important influence to their concentrations in the working faces. Hence, a method able to control the workplace environment in a long term is crucial. This paper proposes a geographical information system (GIS) for such goal. The system created provides the necessary tools to manage and analyse an underground environment connecting the pollutant generated and the ventilation characteristics along the time.

Data concerning the ventilation system in the case study has been taken every month since 2009 and integrated into the management system, which has quantified the gasses concentration along the mine due to the characteristics and evolution of the ventilation layout. Three different zones concerning CO, CO_2, NO_x and effective temperature have been found as well as some variations among the workplaces within the same zone due to local airflow recirculation.

Keywords: Underground environment; pollutants management; safer workplace; ventilation layout.

1. Introduction

A safe underground environment is crucial for the running of a mine and the sake of its employees. The issue has been deeply studied, taking different approaches such as controlling airflow leakages (Widiatmojo, et al., 2014), focused on underground gases and finding out more efficient ventilation designs (Kurnia et al., 2014) or improving the underground environment conditions in coal mines reducing the level of dust and methane (Su et al., 2008; Xi et al., 2014; Zhang et al., 2015).

One of the main functions of a ventilation system is to remove and dilute gases to keep a workplace safe and fulfil the national regulations. Unfortunately, it becomes more difficult as the mine spreads out and the ventilation circuit gains complexity. The origin of gases generated in a mine can be a consequence of the mineralization exploited or exploitation method (mining equipment, blasting, etc.). In potash mining, carbon monoxide and dioxide can also be spontaneously released in some particular geological conditions (Carrasco et al., 2011; Hedlund, 2012).

The importance of controlling the concentration levels is because they affect the health of the employees in short and long them, being toxics and even some of them cancerous (Rundell et al., 1996). For this reason, it is very important to provide the tools to design a proper underground ventilation system able to control gas concentrations and keep the environmental conditions below the maximum allowable levels. Several investigations have been carried out in this field, especially in coal mining (Cheng et al., 2015; Noack, 1998; Sasmito et al., 2013). Despite that, the relationship between ventilation layout and gas concentrations has not been thoroughly analysed. This paper gives insight to the affection of airflow recirculation to the level of pollutants and effective temperature in the working faces and proposes a system, by means of a geographical information system (GIS), to manage and analyse the data collected in the long term. This method can provide the adequate tools, frameworks and understanding of the real situation inside a mine (Saleh and Cummings, 2011). The objectives of the study are as follows:

- To create a system able to manage, store and manipulate ventilation data to assess the ventilation circuit.
- To evaluate the relationship among gas concentrations, effective temperature and airflow in the working faces depending on the ventilation layout.

1.1. Safety and health impact of the underground environment

Although the origin of the gases is diverse, diesel combustion is the main factor of generation in the case analysed. Table 1 details the gases studied by the mining activity as well as their threshold limit values (TLV), either the time weighted average (TWA) or the short-term exposure limit (STEL), according to the Spanish legislation (Royal Decree 863/1985).

Table 1. Origin and effects of the gases.

Gas	Physical risk	Hygienic risk	Principal origin	TLV TWA (ppm)	TLV STEAL (ppm)
CO	Explosive Inflammable	Asphyxiating Toxic	Engine combustion Strata emissions	50	100
CO_2		Asphyxiating	Engine combustion Strata emissions	5000	12500
NO_x		Toxic	Engine combustion	10	25

2. Data collection

The mine uses a room and pillar exploitation method, extracting the mineral by means of continuous mining machines and carried to a conveyor system by trucks and loaders. As the most adverse locations, in terms of environmental conditions, are in the working faces, where the continuous machines are placed, a control point has been stablished in each one to monitor these conditions. The system is fed with measures taken regularly. 265 measures have been collected and gathered between 2009 and 2014. The equipment is calibrated regularly to keep the accuracy of the data.

The list below details the parameters measured in the workshops based on the mine particular exploitation characteristics, Spanish law (Royal Decree 863/1985) and bibliographic references (McPherson, 1993; Carrasco et al., 2011):

- Control point: Coordinates of points.
- Date: Day and hour of the measure.
- Air velocity (m/s): Measured with a rotating vane anemometer.
- Dry and wet temperature (ºC): Using a sling psychrometer.
- Carbon monoxide (CO), carbon dioxide (CO_2), nitric oxide (NO) and nitrogen dioxide (NO_2) in ppm. Measured with a gas detector.
- Cross section (m^2): Using a laser distance measurer.

Once the parameters previously stated have been obtained, airflow has been calculated by means of the GIS following the well-known equation.

$$Q = u \cdot A \qquad (1)$$

Where, Q= Airflow (m^3/s), u= air velocity (m/s), A= cross section (m2). According to the Spanish law, the temperature analysis has to done by means of the following expression.

$$te = 0{,}9 \cdot tw + 0{,}1 \cdot td \qquad (2)$$

Where, te= effective temperature (ºC), tw= wet temperature (ºC), td= dry temperature (ºC). On the other hand, nitric oxide and nitrogen dioxide have to be summarized and analysed together (NO_x) to see if it is below the threshold limit value according to the law.

3. Management system

3.1. GIS creation

All the data described in the section 2 have been stored in a GIS created to manage the ventilation parameters together with the different ventilation layouts of the mine along the years. This connection will allow better assessments of the ventilation system and the knowledge of any variation in the environmental conditions. The ArcGIS software has been chosen because of its user-friendly platform. Fig. 1 displays the steps followed to create the GIS file. Starting with the ventilation layouts, in CAD format, and the data collected, which have been merged in a single file that connects both types of information by means of the ArcGIS tools. This creation gives the possibility to connect graphical and numerical information about the ventilation system taking into account its evolution along the time.

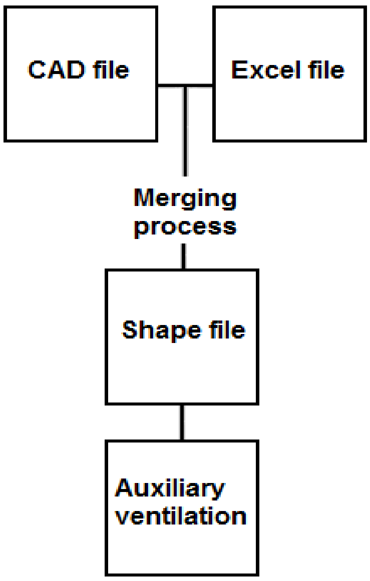

Fig. 1. Scheme of the process followed to create the GIS file.

Fig. 2 stands for different ventilation layouts regarding the period of time and evolution of the auxiliary ventilation system. On the other hand, the layer called mine workings helps to obtain an easier understanding of the mine development. Each configuration can be analysed and inquired concerning gases, temperature and airflow.

Fig 2. Auxiliary ventilation layers.

3.2. Case study description

Fig. 3 details part of the ventilation circuit with the groups regarding the working faces and their environmental conditions after storing the data with the GIS. As there is a continuous miner in each working face, it will be simply referred as miner henceforth. The number of these miners in each group varies depending on the configuration.

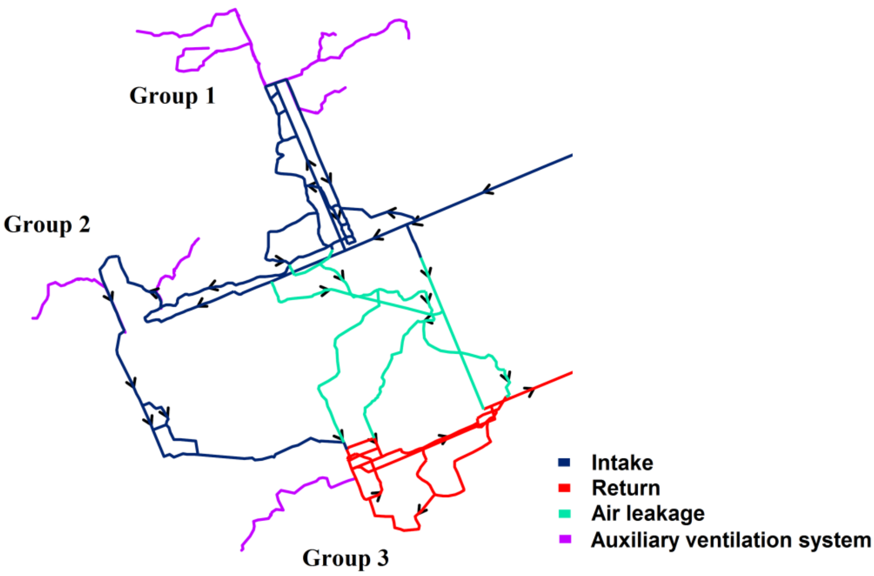

Fig. 3. Scheme of the ventilation circuit in the case study.

The mine uses a partial recirculation ventilation system in which a controlled fraction of the air returning from a working face goes back into the intake. This method has the advantage to be more economical, but the airflow has to be monitored to control that the gas concentrations are below a certain value in the short term. As it can be seen in Fig.

3, there are three groups regarding the clearness of the air arriving to the working faces, each one will have different environmental conditions.

- Group 1: Provided with clean air.
- Group 2: Partially provided with clean air.
- Group 3: Mainly provided with recirculated air.

3.3. Data processing

Data have been analysed by group and working face. First, all measures have been split in groups based on their ventilation characteristics by means of the GIS, having each group 126, 70 and 69 measurements respectively. Afterwards, mean values of airflow, effective temperature, CO, CO_2, NO and NO_2 of each group and working face have been calculated. These distinctions will allow analysing the situation by group and individually.

Fig. 4 shows an example of one of the workplaces, called M8, and the evolution of its position between April 2009 and September 2010, changing from group 1 to group 2, thus this variation has to be taken into account to analyse the environment conditions, moving from a clean air to a partially recirculated situation.

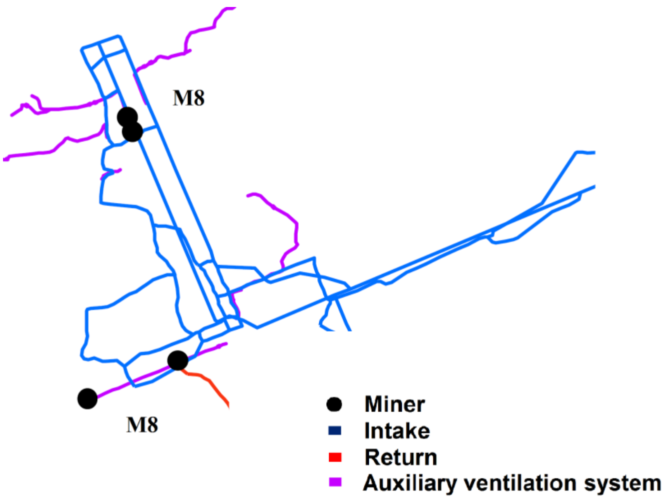

Fig. 4. Position evolution of the continuous miner M8.

Without the usage of the GIS it would have been more difficult to discriminate this information in the three groups proposed. Especially when the data collected is from a long time ago.

4. Results and discussion

The following outcomes show some possibilities of the system created to control the working conditions in an underground mine and evaluate the layout variations along the time with the capabilities of the software. The data from next tables and figures have been processed using the GIS.

Mean values of airflow, effective temperature, CO, CO_2 and NO_x are gathered in Table 2, while Table 3 compares the percentage variation in the different underground conditions.

Table 2. Mean values from the different groups.

	Airflow (m^3/s)	**Effective temperature (ºC)**	**CO (ppm)**	**CO_2 (ppm)**	**NO_x (ppm)**
Group 1	10,59	27,99	6,18	1819,27	7,974
Group 2	10,03	28,17	5,81	1641,62	8,28
Group 3	11,32	29,19	8,43	1883,53	9,306

Table 3. Percentage variation using group 1 as reference.

	Airflow (%)	**Effective temperature (%)**	**CO (%)**	**CO_2 (%)**	**NO_x (%)**
Group 1	0,00	0,00	0,00	0,00	0,00
Group 2	-5,29	0,64	-5,99	-9,76	3,84
Group 3	6,89	4,29	36,41	3,53	16,70

As it can be seen, there is an increase in pollutants concentration and effective temperatures comparing group 1 and 3 despite similar airflows, specially in CO and NO_x values. However, the comparison between group 1 and 2 provides mixed results, probably because there is air recirculation within the same group (group 1) as it can be seen examining the position of the miners and the ventilation layout.

The individual analysis by miner is displayed in the next Tables and Figures, where each miner stands for a row in Table 4 and a bar in Fig. 5 to 9. However, the same miner has changed from one group to another in some cases, such as miners 2 and 3 from group 1, which are physically the same as miners 2 and 3 from group 2, because at some point they were changed to another part of the mine. Therefore, they are considered as different miners for the study of the environmental factors. However, their identification names will be very important for managing the database in the GIS. In addition, Table 5 compares the minimum and maximum values of the parameters analysed among the miners.

Table 4. Name and number of measures from each miner.

	Name of the miner	**Number of measures**
Group 1	1	21
	2	15
	3	17
	4	27
	5	21
	6	23
Group 2	1	17
	2	21
	3	14
	4	18
Group 3	1	24
	2	27
	3	18

The percentage variation of the conditions showed in Table 5 has been linked to the information from Table 4 by the last column, called Group-miner, which identify the group and then the miner having the maximum and minimum value of each condition respectively.

Table 5. Difference between maximum and minimum values in the working faces.

	Maximum Value	Minimum value	Difference (%)	Group-miner
Airflow (m^3/s)	12,92	9,74	32,65	3.2-2.4
Effective temperature (ºC)	29,75	26,74	11,26	3.1-1.1
CO (ppm)	8,96	5,60	60,00	3.2-2.2
CO_2 (ppm)	2400,00	1291,88	85,78	1.3-2.1
NO_x (ppm)	10,94	7,39	48,04	3.1-1.1

Meanwhile, Fig. 5 to 9 show the individual mean values of each miner, distinguishing the three groups in different coloured bars depending on the airflow conditions: clean air, partially recirculated or recirculated. As it can be seen, the quantity of continuous miners per group is different; having groups 1, 2 and 3 a quantity of 6, 4 and 3 miners respectively. The difference in the number of miners is just a matter of mine planning.

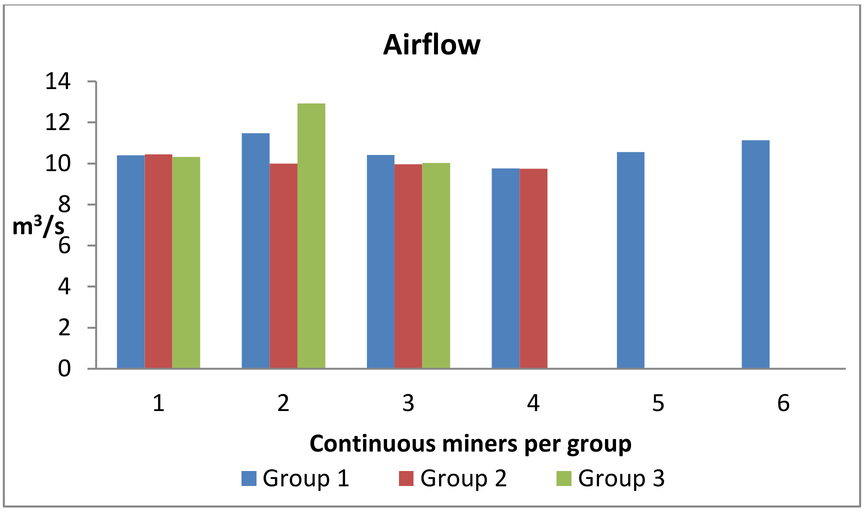

Fig. 5. Airflow per continuous miner, distinguishing each group.

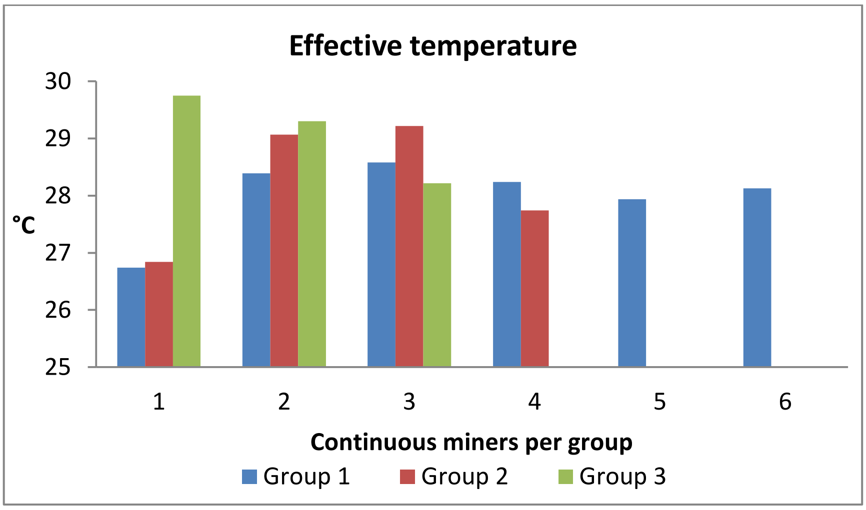

Fig. 6. Effective temperature in each continuous miner.

The airflow per continuous miner fluctuates around 10 m^3/s. All miners have a similar quantity of air regardless the ventilation layout and the presence of recirculation. Therefore, the variation in the workplace conditions is not caused by the airflow supply. Analysing the effective temperature, all the mean values are between almost 27 and 30 ºC, having the highest difference, 11,26%, between miner 1 from Group 1 and miner 1 from Group 3 according to Table 6. In accordance with the groups of clean and recirculated airflow respectively. In addition, when both miners are individually examined with the GIS, it can be appreciated that the one with the lowest effective temperature is placed very close to the service tunnels, having less heat input to the ventilation system than the other miners.

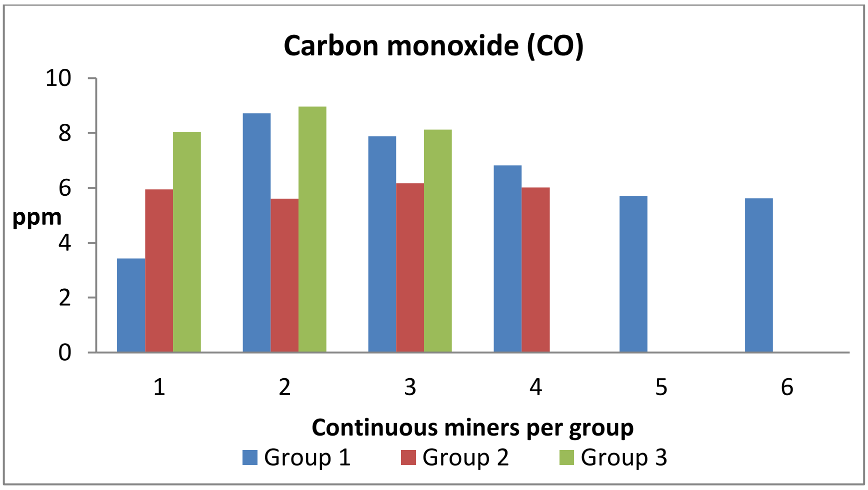

Fig. 7. Carbon monoxide concentration per continuous miner.

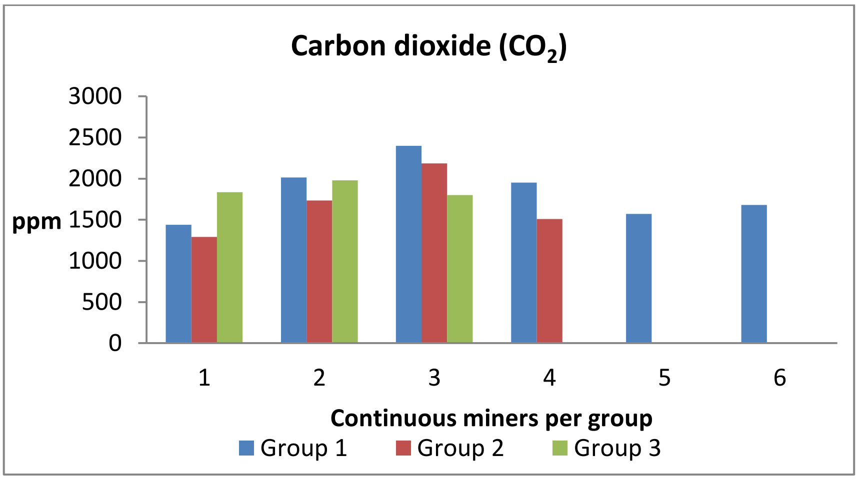

Fig. 8. Carbon dioxide concentration per continuous miner.

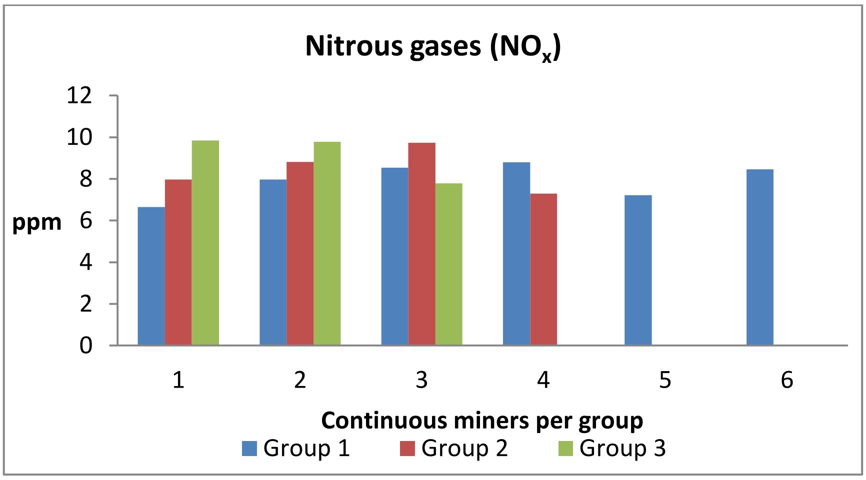

Fig. 9. Nitrous gases concentration per continuous miner.

Carbon monoxide values from Group 3 show a trend of higher concentrations. However, there is not any clear variation in CO levels between group 1 and 2. Moreover, there is an important difference between the highest and lowest concentration level within group 1, reaching a variation of 56,47%.

In the case of carbon dioxide, the trend is not clear either. This parameter should be analysed thoroughly because it cannot be obtained any conclusion from individual and group values.

Regarding nitrous gases, group 3 displays higher concentrations, but the trend is not as clear as the mean values.

If graphs are analysed together, it can be pointed out that the environmental conditions vary considerably despite having the same airflow within each group. However, if the ventilation circuit is assessed it does not explain this phenomenon, which is probably caused by local uncontrolled airflow recirculation due to an unappropriated auxiliary circuit.

The mine uses an exhausting system to renew the air in the working faces, leading the pollutants and heat throw a duct to the main circuit. The information related to these ducts has be included in the GIS such as position, leakages, layout of the auxiliary fans and distance from the entry of the duct and the working face. In addition, information regarding the discharge zone of the duct has to be included as well, so that tunnels with potential recirculation can be taken into account.

5. Conclusions

The geographical information system has been proved as a proper tool to manage and control the environmental conditions of an underground mine in medium and long term as well as inquiring the data in many different ways to take decisions concerning the ventilation circuit.

On the other hand, individual and general results extracted from the GIS have given insight of the gasses and temperature evolution throughout the mine and the influence of the airflow recirculation to the underground environmental conditions.

Although all the working faces comply with the current Spanish legislation, group 3 displays a considerable increasing in terms of temperature and pollutants compared to the situation with clean air, there is an increase of around 36% in CO, 4% CO2, 17% NOx and 4%. Whereas the conditions are acceptable if the airflow is only partially recirculated. Hence, it would be advisable to partially change the ventilation layout in the working faces from group 3 to provide air with less gases and heat.

Moreover, local airflow recirculation within each group has been found out with the GIS created. The knowledge of their specific characteristics would help to plan better auxiliary ventilation circuits, which would impact positively on the efficiency rates of the employees.

Acknowledgements

The authors would like to thank ICL-Iberia and the Iberpotash Chair in Sustainable Mining from the Polytechnic University of Catalonia (UPC).

References

Carrasco Galán J., Alarcón Rojas D., Albuerne Pérez J., Fernández Bustillo E., Fernández Vilas E., García García L., Madera García J., 2011. Manual de ventilación de minas y obras subterráneas. Aitemin Centro Tecnológico, Madrid, Spain, ISBN 978-84-615-0941-6.

Cheng, J., Wu, Y., Xu, H., Liu, J., Yang, Y., Deng, H., Wang, Y., 2015. Comprehensive and Integrated Mine Ventilation Consultation Model – CIMVCM. Tunnelling and Underground Space Technology, 45, 166–180.

Hedlund, F. H. (2012). The extreme carbon dioxide outburst at the Menzengraben potash mine 7 July 1953. Safety Science, 50(3), 537–553.

Kurnia, J. C., Sasmito, A. P., Wong, W. Y., Mujumdar, A. S., 2014. Prediction and innovative control strategies for oxygen and hazardous gases from diesel emission in underground mines. The Science of the total environment. 481. 317–334.

McPherson, M.J., 1993. Subsurface ventilation engineering. Springer, USA. ISBN: 978-94-010-4677-0.

Noack, K., 1998. Control of gas emissions in underground coal mines. International Journal of Coal Geology. 35. 57–82.

Rundell, B., Ledin, M. C., Hammarström, U., Stjernberg, N., Lundback, B., Sandstrom, T. (1996). Effects on symptoms and lung function in humans experimentally exposed to diesel exhaust. Occupational Environmental Medicine, 53, 658-662.

Saleh, J. H., Cummings, A. M., 2011. Safety in the mining industry and the unfinished legacy of mining accidents: Safety levers and defense-in-depth for addressing mining hazards. Safety Science. 49 (6). 764–777.

Sasmito, A.P., Birgersson, E., Ly, H.C., Mujumdar, A. S., 2013. Some approaches to improve ventilation system in underground coal mines environment – A computational fluid dynamic study. Tunnelling and Underground Space Technology. 34. 82–95.

Su, S., Chen, H., Teakle, P., and Xue, S. 2008. Characteristics of coal mine ventilation air flows. Journal of Environmental Management, 86, 44–62.

Widiatmojo, A., Sasaki, K., Sugai, Y., Suzuki, Y., Tanaka, H., Uchida, K., Matsumoto, H., 2015. Assessment of air dispersion characteristic in underground mine ventilation: Field measurement and numerical evaluation. Process Safety and Environmental Protection, 93, 173–181.

Xi, Z., Jiang, M., Yang, J., Tu, X., 2014. Experimental study on advantages of foam–sol in coal dust control. Process Safety and Environmental Protection. 92 (6). 637–644.

Zhang, H., Sanmiquel Pera, L., Zhao, Y., Vintro Sánchez, C., 2015. Researches and applications on geostatistical simulation and laboratory modeling of mine ventilation network and gas drainage zone. Process Safety and Environmental Protection. 94. 55–64.

Paper IV

Journal: DYNA
Status: Under review

Heat flow assessment of the equipment in an underground mine and approach to improve the environmental conditions

Marc Bascompta[a,*], Ana María Castañón[a], Lluís Sanmiquel[b], Josep Oliva[b]

a Department of Mining and Natural Resources, Polytechnic University of Catalonia (UPC), Manresa (Barcelona) Spain. Av. Bases de Manresa, 61-73, 08242
b Department of Mining, Topography and Structures, University of León (ESTIM), León Spain. Campus de Vegazana, s.n, 24071.
mbascomptem@gmail.com; amcasg@unileon.es; sanmi@emrn.upc.edu; josep@emrn.upc.edu

Abstract

The generation of heat in underground spaces due to working activities is a factor that has influence to the production and productivity rates. This paper analyses the heat generation in an underground mine and some approaches to enhance the ventilation conditions using electrical instead of diesel machines. This assessment has been carried out by means of theoretical equations and modelling software. Investigations prove that sensible and latent heat would be reduced around 50% and 84% respectively if the change were applied in the case study. This reduction on heat input to the ventilation system would improve the workplace environment because of lower effective temperatures and gas concentrations, which would result in better safety conditions and efficiency of the employees.

Keywords: Mine ventilation, safety and health, efficiency, heat, mining equipment.

1. Introduction

Heat flow is an important aspect in underground mine ventilation and mining equipment has a significant impact on it. As workings go deeper and mine evolves, factors such as temperature and humidity become crucial to keep acceptable environmental conditions and fulfil the legal requirements. Efficiency rates and safety levels are also influenced by this factor. Many studies have been carried out regarding gases generated by diesel engines [1] and the incidence of temperature in underground mines [2, 3, 4].

The reduction of heat flow in these cases is usually focused on optimising the efficiency of the refrigeration system and cutting down its operating costs through an improvement of the current systems [5, 6, 7, 8, 9], but this important issue has not been approached trying to change the mining equipment. Diesel equipment have an overall efficiency about one third of the electrical units. Hence, the usage of fuel will produce approximately three times as much heat as electrical machines for the same mechanical work output [10]. Moreover, the combustion process generates harmful pollutants that have to be controlled, not only in the underground mining sector, but it is also crucial in indoor placements and buildings [11], where the renewal of air depends on artificial facilities like fans.

Apart from the type of energy source, there are other important factors that affect the underground air temperature, for instance the outer climate, geological factors of the zone or mineral exploitation method [12].

This paper determines these different heat inputs in an underground potash mine by means of empirical equations and modelling software. Afterwards, heat flow contribution of electrical and diesel equipment is compared with the idea to expose an alternative to improve the environmental conditions in an underground infrastructure. The procedure followed is:

- To determine the heat contribution of each source in the case study.
- To compare the situation using electrical energy instead of diesel trucks and loaders.

2. Methodology to measure the heat inputs

Data used in theoretical equations and modelling software have been provided by the staff of the mine, measured in situ, between 2008 and 2014, or extracted from bibliography in the case of the initial iterations with the software. The equipment features have been obtained from the manufacturer's data.

First, the airflow behaviour has been determined using Vnet. These initial results will be used to know the climatic conditions of the airways and the heat sources (strata heat, equipment and fragmented rock).

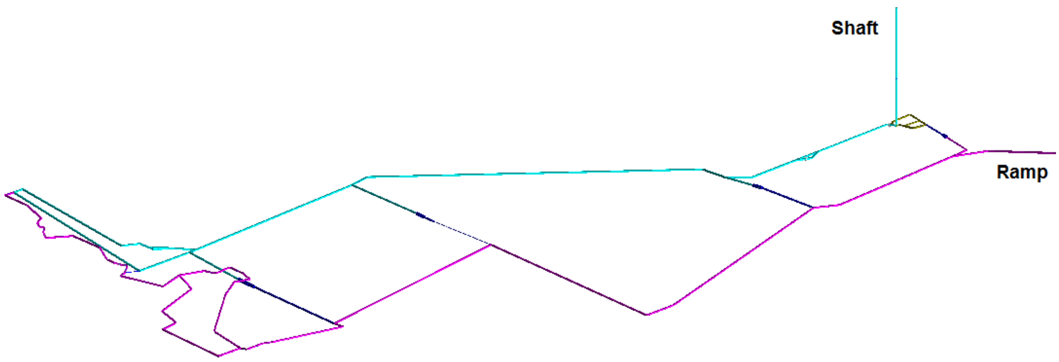

Figure 1 Modelling scheme of the mine using Vnet.

2.1. Strata heat

Heat emission from the strata is function of the type of rock, exploitation method and depth and length of the airways. However, the amount of heat transmitted decrease over the time, being the working faces where there is more transmission. Sometimes, strata heat can be obtained by empirical methods based on other similar mines [10]. Unfortunately, there is not such information in this case and equations and software have to be applied.

The equations method defines two expressions depending on the time since the tunnel was opened. If it has been opened for more than 30 days, eq. (1) is used to determine the radial heat flow.

$$q = 3{,}35 \cdot L \cdot k^{0{,}854} \cdot (VRT - \theta d) \quad (1)$$

Where q is heat flow from the strata (W); L is length of the tunnel (m); K is thermal conductivity of the rock (W/m·ºC); VRT is virgin rock temperature (ºC); θd is mean dry bulb temperature (ºC). Meanwhile eq. (2) is applied if the advancing has been done in the last 30 days.

$$q = 6 \cdot k \cdot (L + (4 \cdot DFA)) \cdot (VRT - \theta d) \quad (2)$$

Where L is length of the advancing end of the heading (m), which cannot be greater than the length advanced in the last month; DFA is daily face advance (m). The main problem from eq. (1) is to find out the period that heat is transferred from the strata to the air until thermal equilibrium is achieved. This setback has been solved modelling the strata behaviour with ClimSim. The software takes into account the heat flow transferred to the air by radiation and convection methods, determining the heat flow of a circular tunnel for a certain homogenous rock. Heat flow determination is based on the radial heat conduction equation, expressed in polar cylindrical coordinates (W/m^2).

$$k[\frac{r\partial^2\theta}{\partial r^2} + \left(\frac{\partial\theta}{dr}\right) + \frac{1}{r}\left(\frac{\partial^2\theta}{\partial\emptyset^2}\right) + r\,\frac{\partial^2\theta}{\partial z^2}] = r\rho C\,\frac{\partial\theta}{\partial t} \quad (3)$$

Heat transfer can be either from the strata to the air or from the air to the strata depending on where temperature is higher, happening until there is a thermal equilibrium. When airways have been opened for a long time, a phenomenon called “thermal flywheel” could arise, transferring heat from the air to the strata during the day and the opposite at night [13].

Figure 2 explains the ClimSim functioning. First, the climatic variables have to be calculated or measured. Once the initial model is built, it has to be compared with real measures to validate it, applying iterations as many times as necessary to achieve a proper model.

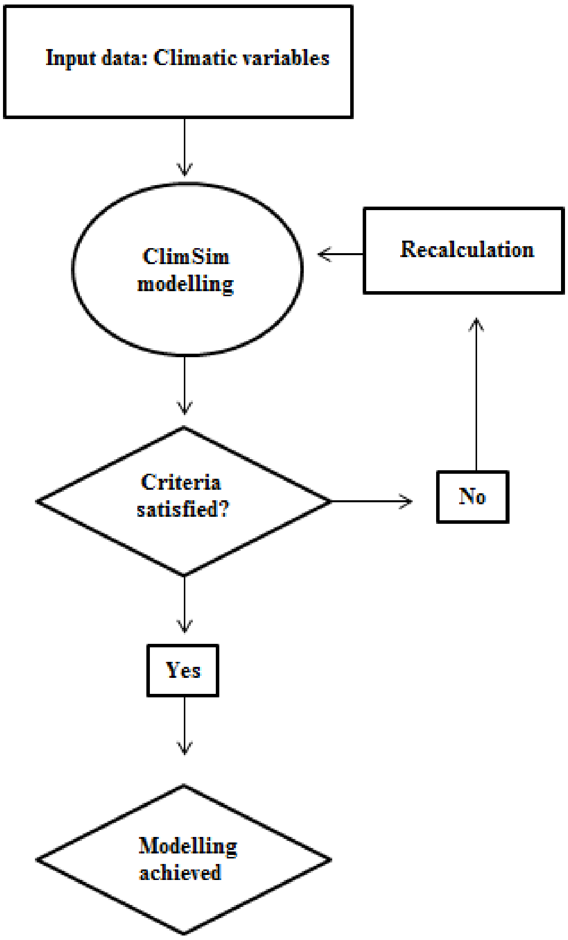

Figure 2 Scheme of the ClimSim functioning based on the user's manual explanation.

After several iterations, the rock conductivity and diffusivity were obtained, 6 W/mºC and 5,55 $m^2/s \cdot 10^{-6}$ respectively. According to the manual, values are considered acceptable when there is a difference around ±1 ºC between modelled and measured mean values, between 2008 and 2014 in this case. Moreover, the iterations have carried out in two different zones and four periods of the year in order to achieve more reliable results. Table 1 displays the temperature difference once the modelling is correctly adjusted.

Table 1 Temperature comparison of two points from the ventilation layout.

Point 1						
Period	**Dry bulb temperature ºC**			**Wet bulb temperature ºC**		
	Measured	**ClimSim**	**Difference**	**Measured**	**ClimSim**	**Difference**
Overall	24	21,62	2,38	17	15,96	1,04
January	19	17,6	1,4	11	12,07	-1,07

April	25	23,07	1,93	18	15,87	2,13
June	30	27,8	2,2	22	20,65	1,35
October	27	24,95	2,05	19	17,77	1,23
Point 2						
Overall	26	25,45	0,55	17	17,93	-0,93
January	26	20,9	5,1	14	12,4	1,6
April	28	26,2	1,8	18	18,81	-0,81
June	31	30,7	0,3	23	22,62	0,38
October	31	27,95	3,05	21	19,75	1,25

On the other hand, Figure 3 details the effective temperatures, calculated according to the Spanish law (RGNBSM, itc 04.7.02), te = 0,9·tw + 0,1·td, where te is effective temperature, tw wet temperature and td dry temperature.

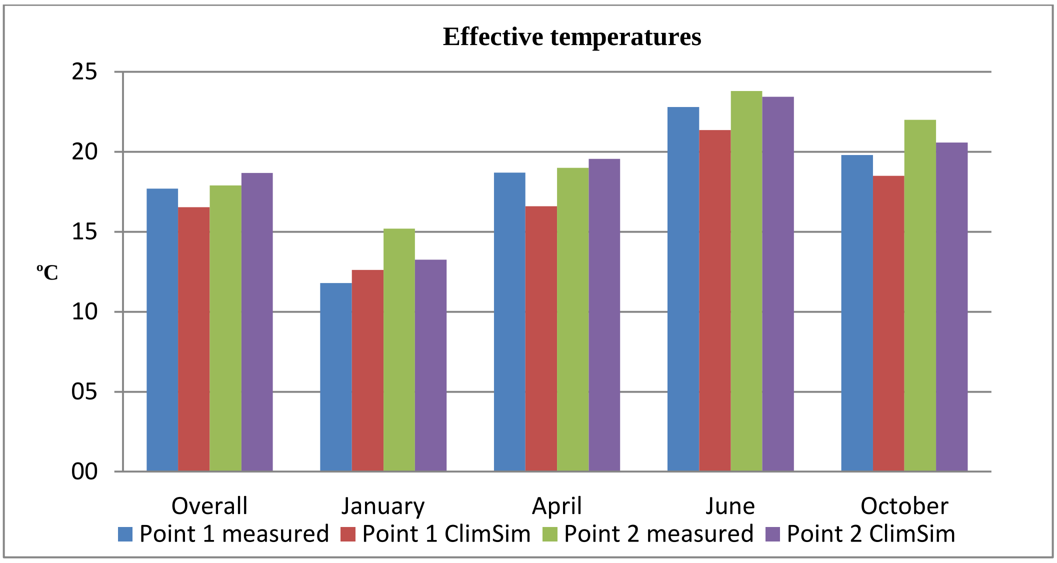

Figure 3 Comparison of the effective temperatures modelled and measured in situ.

Subsequently, the base modelling has been used to calculate the length of the tunnels giving heat to the airways changing some variables within the software called "age in" and "age out", which takes into account the time since the tunnel was opened, until the sensible heat reaches a value of zero. In this case, the contribution of sensible heat to the airways is near zero after approximately one year.

After that, it has been calculated theoretically to corroborate the modelled values, giving an average variation of only 9.97% between both ways. Table 2 and Figure 4 detail the behaviour of the strata heat using ClimSim.

Table 2 Behaviour of the strata modelled by means of ClimSim.

Age in (days)	Age out (days)	Sensible heat (kW)	Latent heat (kW)	Months with the tunnel opened
30	0	17,93	33,72	1
90	60	6	27,28	3
182	152	2,64	25,97	6
365	335	0,13	25,08	12
730	700	-1,85	24,43	24

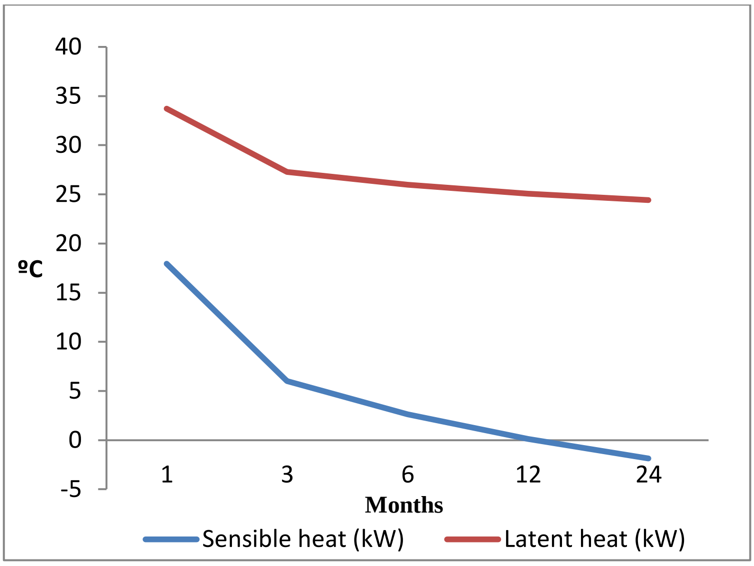

Figure 4 Behaviour of the strata heat, either sensible or latent.

2.2. Mechanized equipment

The exploitation method determines the heat contribution from the equipment into the ventilation system, having a huge difference in terms of heat generation between the usage of diesel and electrical energy. Figure 5 describes the steps to determine the heat input generated by electrical machines.

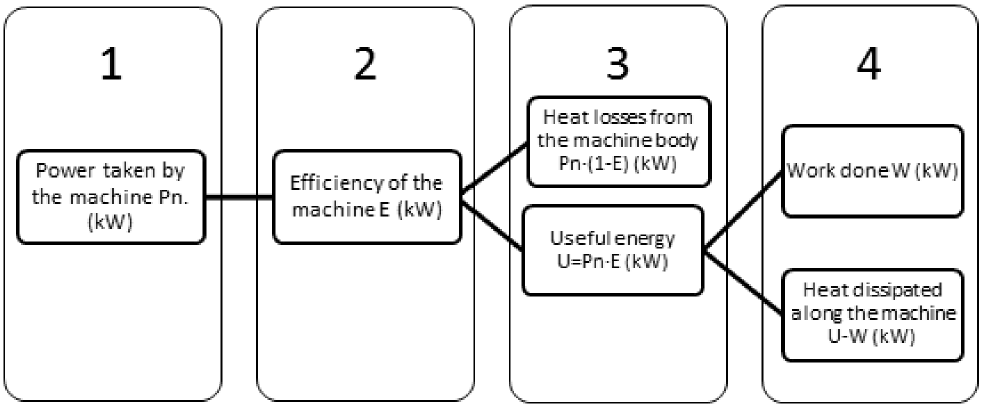

Figure 5 Scheme of the heat generated by electrical machines.

On the other hand, the efficiency of diesel machines is, approximately, 1/3 of the electrical equipment and produces either sensible or latent heat, whereas the electrical equipment only sensible. The three main heat sources are: 1) radiator and body of the machine, 2) combustion gases and 3) movement and friction due to the usage of the machine [10]. Its quantification can be achieved considering a ratio of 0.3 litres of diesel per 1 kW per hour, with a calorific value of 34000 kJ/litre, and giving a heat generation of 2.83 kJ/s for each kilowatt of mechanical output.

Each litre of fuel consumed will produce around 1.1 litres of water due to the combustion gases [14]. However, this value could be several times higher because of the refrigeration system. Some in situ analysis have pointed out that this ratio could vary from 3 to 10 litres per litre of fuel consumed, depending on the power and maintenance [15]. The following equation determines the total heat generated, which comprises latent and sensible heat.

$$qc = c \cdot \frac{Ec}{100} \cdot PC \qquad (4)$$

Where qc is heat emitted by the combustion (kW); c: combustible (l/s); Ec: combustion efficiency (%); PC: combustible calorific value (kJ/l). McPherson [10] gives some references for combustion efficiency, 95%, and the rate of liquid equivalent per litre of fuel, 5. Last parameter is necessary to calculate the quantity of water generated by the combustion.

$$W = c \cdot \frac{Ec}{100} \cdot r \qquad (5)$$

Where W is water generated (l); r is rate of liquid equivalent. After determining the water generated, latent heat is obtained taking into account a standard value of the water latent vaporization heat, 2450 kJ/kg, and an equivalency 1:1 litre-kilogram of water.

$$ql = \lambda\text{w} \cdot W \qquad (6)$$

Where ql is latent heat (kW); λw is water latent vaporization heat (kJ/kg). Finally, sensible heat can be obtained deducting latent heat from the result in eq. 4.

2.3. Fragmented rock

When fragmented rock is exposed to the ventilation airstream and there is a difference between rock and air temperature, heat transference is generated.

$$q_{fr} = m \cdot C \cdot (\theta_1 - \theta_2) \qquad (7)$$

Where qfr is heat load due to rock fragmentation (kW); m is mass flow of the mineral exploited (Kg/s); C is specific heat of the rock (kJ/kgºC); θ_1 is temperature of the rock immediately after fragmentation (ºC); θ_2 is temperature of the fragmented rock at the exit of the ventilation system (ºC). Temperature θ_1 can be considered equivalent to the virgin rock temperature with accuracy enough according to McPherson [10].

3. Mining equipment

Tables 3 and 4 detail the current mining equipment in the case study and the features needed to determine the heat input.

Table 3 Diesel equipment characteristics.

Type	Quantity	Nominal power (CV)	Nominal power (kW)	Consumption (l/h)
Truck	22	400	294	67
Loader	12	300	221	58
Car	64	100	74	14
Jumbo	3	90	66	14
Auxiliary equipment	6	88	65	14

Table 4 Electrical equipment characteristics.

Type	Nominal power (kW)	Quantity
Continuous haulage machine	165	1
	180	1
	220	5
Conveyors	56	2
	110	1
	180	1
	200	2
	400	3
	600	6
Continuous miner	529	10

The electrical trucks and loaders chosen have very similar characteristics compared to the diesel ones regarding size and capacity. The models used have been the Scooptram ST1030 and Scooptram EST1030 for the diesel and electrical loader respectively and the MT 436B and EMT35 for the trucks.

4. Results and discussion

Heat input described above are gathered in Tables 5 and 6 regarding latent and sensible heat contribution of each source as well as the percentage contribution of heat added to the whole system using internal combustion engine loaders and trucks or electrical ones.

Table 5 Heat input using diesel trucks and loaders.

Source of heat	Sensible heat(kW)	Latent heat (kW)	(%)
Machines	11093	6248	73,8
Conveyors	1072		4,6
Continuous haulage machine	145		0,6
Miners	1455		6,2
Fragmented rock	297		1,3
Strata	1102	2072	13,5
Total	**15163**	**8320**	**100,0**

Table 6 Heat input using electrical trucks and loaders.

Source of heat	Sensible heat (kW)	Latent heat (kW)	(%)
Machines	5609	987	51,8
Conveyors	1072		8,4
Continuous haulage machine	145		1,1
Miners	1455		11,4
Fragmented rock	297		2,3
Strata	1102	2072	24,9
Total	**9679**	**3059**	**100,0**

As it can be deduced from tables above and Figure 6, the main source of heat is due to the machinery with regard to sensible or latent heat. Overall, the change of the loaders and trucks would reduce the contribution of the mining equipment by 23%, meanwhile assessing the sensible and latent heat, they would decrease about 36% and 63% respectively.

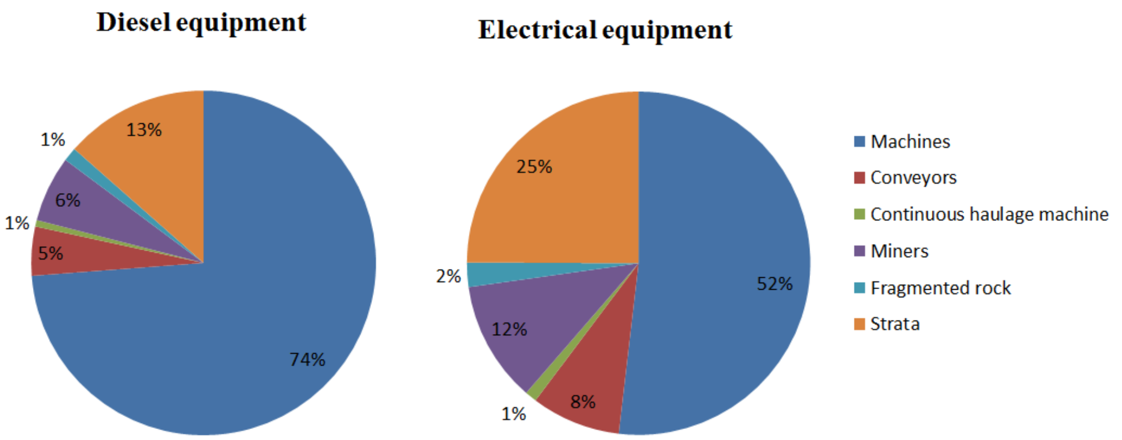

Figure 6 Percentage variation of the different heat inputs using electrical or diesel equipment.

Furthermore, Table 7 exposes the current fleet of vehicles using diesel and the proposal, together with their heat generation and the percentage variation of both options.

Table 7 Summary of the heat generated by the vehicles.

Type	Unit heat (kW)		Total sensible heat (kW)		Difference of sensible heat (%)	Total latent heat (kW)		Difference of latent heat (%)
	Dies.	Elec.	Dies.	Elec.		Dies.	Elec.	
Truck	450,9	90	6345	1984	68,7	3574	0	-
Loader	390,3	156	2996	1873	37,5	1687	0	-
Car	39,3	-	1607	[1]	-	905	[2]	-
Jumbo	25,1	-	48	[1]	-	27	[2]	-
Auxiliary equipment	25,1	-	96	[1]	-	54	[2]	-
Total			**11093**	**5608**	**49,4**	**6248**	**986**	**84,2**

[1] Only loaders and trucks are changed. Thus, other equipment using diesel is added to the total sensible heat input after applying the proposal.

The unit heat per machine is considerably reduced using the electrical equipment. Results above show a huge difference in terms of heat generation. Besides, as consumption of fuel would be cut down, the generation of pollutants such as NOx, CO or CO2 would also decrease. Taking a ratio of 1:1 quantity of pollutants-litres of diesel burned, the generation would be minimized by 88% based on the data used.

Despite the considerable improvements of the hypothetical change, it has to be pointed out that these machines need a trolley or a cable in the majority of the cases to match the power required, especially in the case of trucks, reducing the flexibility of the vehicle fleet. Thus, it could be necessary a mix of both types of equipment. On the other hand, more investigations to achieve suitable batteries have to be undertaken.

5. Conclusions

The usage of electrical loaders and trucks decreases the generation of sensible heat by 49.4% and latent heat 84.2%. Overall, the contribution of heat from machines plummeted from 73.8% to 51.85%. In addition, the modelling by ClimSim has permitted to know the behaviour of strata heat in a potash mine, finding out the trend of sensible and latent heat in the airways.

Apart from higher energy efficiency of the electrical engines, less consumption of diesel would mean a drop in temperature and pollutants concentration. Therefore, ventilation requirements would be reduced and it could be achieved a better workplace environment, which leads to higher productivity and production rates. The usage of electrical equipment can also help to reduce the uncertainty in the future mining activity regarding the oil price variations and more restrictive legal requirements.

6. Acknowledgements

The authors would like to thank the staff of ICL-Iberia for their willingness and the Iberpotash Chair in Sustainable Mining from the Polytechnic University of Catalonia (UPC).

7. References

Kurnia J C, Sasmito A P, Wong W Y, Mujumdar A S. Prediction and innovative control strategies for oxygen and hazardous gases from diesel emission in underground mines. Science of the Total Environment, 2014, 481: 317--334.

Payne T, Mitra R. A review of heat issues in underground metalliferous mines. 12th U.S./North American Mine Ventilation Symposium, 2008, 197--202.

Garcia-Herrero S, Mariscal M A, García-Rodríguez J, Ritzel D O. Working conditions psychological physical symptoms and occupational accidents. Bayesian network models. Safety Science, 2012, 50: 1760--1774.

Bluhm S, Moreby R, Von Glehn F, Pascoe C. Life-of-mine ventilation and refrigeration planning for Resolution Copper Mine. The Journal of the Southern African Institute of Mining and Metallurgy, 2014, 114: 497--503.

Del Castillo D. Air cycle refrigeration system for cooling deep mines. International journal of refrigeration, 1988, 11(2): 87--91.

Swart C. Optimising the operation of underground mine refrigeration plants and ventilation fans for minimum electricity cost. Dissertation for Doctoral Degree. USA: North-West University, 2003.

Hardcastle S, Kocsis C, Li G. Analyzing ventilation requirements and the utilization efficiency of the Kidd Creek mine ventilation system. 12th U.S./North American Mine Ventilation Symposium, 2008, 27--36.

Vosloo J, Liebenberg L, Velleman D. Case study: Energy savings for a deep-mine water reticulation system. Applied Energy, 2012, 92: 328--35.

Edgar G, Plessis D, Liebenberg L, Mathews E H, Nicolaas J. A versatile energy management system for large integrated cooling systems. Energy Conversion and Management, 2013, 66: 312--325.

McPherson M J. Subsurface ventilation engineering. USA: Springer, 1993, ISBN: 978-94-010-4677-0.

Zhang Y, Li X, Wang X, Deng W, Qian K. (2006). Spatial flow influence factor: A novel concept for indoor air pollutant control. Science in China Technological Sciences, 2006, 49(1): 115--128.

Xiaojie Y, Qiaoyun H, Jiewen P, Xiaowei S, Dinggui H, Chao L. Progress of heat-hazard treatment in deep mines. Mining Science and Technology (China), 2011, 21(2): 295--299.

Stroh R. A note on the downcast shaft as a thermal flywheel. Journal of the Mine Ventilation Society of South Africa, 1979, 32: 77--80.

Kibble J D. Some notes on mining diesels. Mining Technology, 1978, 393--400.

McPherson M J. The analysis and simulation of heat flow into underground airways. International Journal of Mining and Geological Engineering, 1986, 4: 165--196.